3
2007

LIBRARY
Michigan State
University

This is to certify that the
dissertation entitled

SYNTHESIS AND SOLUTION PROPERTIES OF LINEAR-DENDRIMER DIBLOCK COPOLYMERS

presented by

LESLIE MICHELE PASSENO

has been accepted towards fulfillment
of the requirements for the

Ph. D. degree in Chemistry

Major Professor's Signature

9 May 2006

Date

MSU is an Affirmative Action/Equal Opportunity Institution

PLACE IN RETURN BOX to remove this checkout from your record.
TO AVOID FINES return on or before date due.
MAY BE RECALLED with earlier due date if requested.

DATE DUE	DATE DUE	DATE DUE

2/05 p:/CIRC/DateDue.indd-p.1

SYNTHESIS AND SOLUTION PROPERTIES OF DENDRIMERS AND LINEAR-DENDRIMER DIBLOCK COPOLYMERS

By

Leslie Michele Passeno

A DISSERTATION

Submitted to
Michigan State University
in partial fulfillment of the requirements
for the degree of

DOCTOR OF PHILOSOPHY

Chemistry

2006

ABSTRACT

SYNTHESIS AND SOLUTION PROPERTIES OF DENDRIMERS AND LINEAR-DENDRIMER DIBLOCK COPOLYMERS

By

Leslie Michele Passeno

Dendrimer – linear diblock copolymers have potential applications as molecular sensor and drug delivery vehicles, among other uses, by manipulation of the dendrimer block's size and conformation. We synthesized and investigated the conformation of these diblocks in solution, with particular emphasis on probing the location of the linear chain with respect to the dendrimer in a variety of environmental conditions.

Neutron scattering from a poly(styrene)-poly(benzyl ether) (PS PBE) linear-dendrimer diblock revealed the system underwent a single molecule phase transition. The dendrimer expelled the linear polymer from its cavities to the surrounding solvent and changed shape as the molecular weight of the linear polymer increased. This unusual behavior demonstrates the potential for this class of architecturally asymmetric molecules to perform as molecular machines. Since we believe it is the relative size of the linear polymer to the dendron that is responsible for this transition a second system was studied to test this hypothesis.

We investigated a poly(ethylene oxide)-poly(amido amine) (PEO-PAMAM) linear - dendrimer diblock since the PAMAM dendrimer can undergo a significant size change that depends on solvent environment and molecular weight (generation number). The PAMAM dendron was synthesized from a 2-methoxyethylamine core by exhaustive Michael addition with methyl acrylate followed by amidation with ethylene-diamine to

create the first generation. These steps were repeated until the desired generation was obtained. Small angle neutron scattering experiments of PAMAM solutions revealed that the fourth generation dendrimer had the greatest volume change as expected from a simple scaling theory. In addition, fluorescence measurements of dansyl-cored PAMAM di-dendrons reveal a change in morphology at generation 4 from an extended to a globular morphology. This generation is anticipated to have the most utility as a molecular machine and was the target for the synthesis of PEO-PAMAM linear dendrimer diblocks. Dynamic light scattering of the PEO-PAMAM hybrids in water demonstrates that the hydrodynamic radius (R_h) goes through a transition as the molecular weight of the PEO chain increases. At low hybrid molecular weights the R_h is smaller than a PEO chain with analogous molecular weight. When the molecular weight of the linear PEO chain is increased the R_h of the hybrid is equal to that of an analogous PEO chain. This transition parallels that of the PS-PBE system, demonstrating that the relative molecular weight of the linear and dendrimer blocks, along with the dendrimers' ability to change morphology in response to its surrounding environment, allows the hybrid systems to change conformation.

ACKNOWLEDGEMENTS

I had a lot of help over the years all of which is very much appreciated. I am very grateful for Dr. Baker's patience and guidance, who taught me when I didn't know I was learning and helped me think in an innovative way. Thanks to Dr. Mackay who gave me an appreciation of learning new things, including everything I know about neutron scattering, and also being there to answer all of my questions. Thanks to my guidance committee, Dr. Bruening and Dr. Maleczka for helping me throughout this process.

Thanks to all of my group members, Bao, Ying, Ping, Erin V., Xuwei, Feng, DJ, Sampa, Anish, Krishnan, Erin P., Tiffany, Melissa, Dave and Qin for opening bottles, showing me how to fix things, answering questions and most importantly making this fun.

I am very grateful for my family for their support and encouragement. Thank you mom for answering millions of questions I had growing up. Thanks sister (Liz) for making me laugh and being my roommate. Thanks Papa and Jojo for always being supportive. Thanks Tom for the endless patience you have with me.

TABLE OF CONTENTS

LIST OF TABLES vii

LIST OF FIGURES viii

LIST OF SCHEMES xvi

ABBREVIATIONS xvii

CHAPTER ONE: Introduction 1
Anatomy of a Dendrimer 1
A Brief History of Dendrimers 3
Iterative Growth of Dendrimers 5
Applications of Dendrimers 11
Motivation of work 16
References 17

CHAPTER TWO: Scattering Theory 20
Small Angle Neutron Scattering (SANS) 21
Dynamic Light Scattering 28
References 30

CHAPTER THREE: Conformation of Poly(styrene)-Poly(benzyl ether) Linear-Dendrimer Diblock Copolymers in Dilute Solution 32
Introduction 32
Experimental 37
Materials. 37
SANS. 37
Dynamic Light Scattering (DLS). 40
Results and Discussion 41
Conformation of PBE Dendrimer 41
Conformation of Dendrimer Block 45
Conformation of Linear Block 57
Conclusion 63
References 64

CHAPTER FOUR: Synthesis and Solution Behavior of PAMAM di-dendrons 67
Introduction 67
Experimental 75
Materials. 75
PAMAM Synthesis 75
SANS. 77
Dynamic Light Scattering (DLS). 79
Results and Discussion 80
Synthesis of MEA dendrons 80

Size of MEA G3.0-G5.0 Dendrons in D_2O 81
Effect of Solvent Quality on the Dimensions of MEA-G4.0 in Solution 89
Comparison of the Solution Behavior of MEA G4.0 and MEA G5.0 95
Influence of Core-Functionality on the Behavior of PAMAM Dendrimers in Solution 97
Effect of Ionic Strength on the Morphology and Solution Behavior of MEA Dendrons 101
Conclusion 104
References 106

CHAPTER FIVE: Synthesis and Characterization of Dansyl-Cored PAMAM Di- 109
Dendrons 109
Introduction 109
Experimental 116
Materials. 116
Dansyl-PAMAM Synthesis 116
Fluorescence Measurements. 120
Results and Discussion 120
Solvent Dependence of the Emission Spectra of (Dansyl-EDA) (2) 120
Fluorescence of Dansyl-PAMAM 124
Conclusion 143
References 145

CHAPTER SIX: Synthesis and Solution Properties of PEO-PAMAM Linear-Dendrimer Diblock Copolymer 147
Introduction 147
Experimental 152
Materials 152
Synthesis of PEO-NH_2 (2 kDa) 153
Synthesis for PEO-NH_2 (Mw = 750 Da, 5 kDa, 9 kDa, 20 kDa) 154
Dynamic Light Scattering (DLS). 161
Results and Discussion 162
Synthesis of PEO-PAMAM 162
Dynamic Light Scattering 165
Conclusion 176
References 177

APPENDICIES 179

APPENDIX A 180

APPENDIX B 201

APPENDIX C 221

LIST OF TABLES

Table 3.1. Sample codes and number average molecular mass (M) of compounds used in this study[a] 38

Table 3.2. Values for R_g and R_c determined from Guinier analyses described in the text at a concentration of 50 mg/mL. 43

Table 3.3. Experimental QI(0) values were set equal to the numerical prefactor of the Guinier expression for a finite sized cone, eq 3.5, with various R values representing the radius of the cone's base. 57

Table 4.1. Sample codes and theoretical molecular mass (M) of MEA compounds..... 78

Table 4.2. R_g values for MEA G3.0-G5.0 determined from the Guinier analysis described in the text at a concentration of 4 mg/mL..... 86

Table 4.3. R_g values for MEA G4.0 and G5.0 in $D(CD_2)_mOD$ determined from the Guinier analysis described in the text at a concentration of 4 mg/mL..... 94

Table 4.4. R_g values for Tetra G4.0 in D_2O and d^{10}-butanol determined from the Guinier analysis described in the text at a concentration of 4 mg/mL..... 100

Table 5.1. Theoretical molecular mass (M) of the dansyl-cored PAMAM dendrimers. 114

Table 5.2. Solvents and their dielectric constants (ε) used in this study. 121

Table 5.3. λ_{max} (nm) data for dansyl-PAMAM dendrimers..... 127

Table 6.1. Sample codes and number average molecular mass (M) of compounds used in this study[a] 166

Table 6.2. Hydrodyamic radii (nm) of PEO and PEO-PAMAM samples..... 166

LIST OF FIGURES

Figure 1.1. Anatomy of a dendrimer. 1

Figure 1.2. Elements of a generation 2, poly(amido amine) (PAMAM) dendrimer. 2

Figure 1.3. Flory's branched polymer architecture created by the reaction of AB_2 type monomers. 4

Figure 1.4. Example of a divergent synthesis of a dendrimer with a 1→2 branching scheme and a tri-functional core. 6

Figure 1.5. The synthesis of poly(propylene imine) dendrimers. 7

Figure 1.6. Possible defects and imperfections that can result during the divergent synthesis of a poly(amido amine) dendrimer. 8

Figure 1.7. Example of a convergent synthesis of a dendrimer with 1→2 branching scheme and a di-functional core. 9

Figure 1.8. A linear-dendrimer diblock copolymer (hybrid) where a poly(L-lysine) linear chain is covalently attached to the focal point of a carboxylic acid terminated PAMAM dendrimer. 14

Figure 1.9. A dendronized polymer consisting of a fourth generation hydroxyl terminated polyester dendrimer attached to the repeat unit of poly(L-lysine). 15

Figure 2.1. Schematic of a small angle neutron scattering experiment. 22

Figure 2.2. Cartoon representing information that can be obtained from a series of contrast match experiments. 26

Figure 2.3. Set-up of a dynamic light scattering experiment. 30

Figure 3.1. Three potential conformational states of linear-dendrimer diblocks in solution: a. knitted coil b. encapsulated dendrimer c. random coil. 35

Figure 3.2. Guinier analysis for PBE G4 dendrons in d^6-benzene and d^8-THF at a concentration of 50 mg/mL, data fit for a compact (sphere-like) object. 42

Figure 3.3. Guinier analysis for PBE-dPS 20kDa system in d^8-THF. 46

Figure 3.4. Rod-like Guinier analysis for PBE-dPS 45kDa hybrid in d^8-THF at a concentration of 50 mg/mL. 48

Figure 3.5. Rod-like Guinier analysis for PBE-dPS 100kDa hybrid in d^8-THF at 50mg/mL. 49

Figure 3.6. Holtzer plot (QI vs. Q) of G4-PBE in d^6-benzene at 50 mg/mL. 51

Figure 3.7. Holtzer plot (QI vs. Q) of G4-PBE in d^8-THF at 50 mg/mL. 52

Figure 3.8. Holtzer plot (QI vs. Q) of G4-dPS-20 kDa in d^8-THF at 50 mg/mL 53

Figure 3.9. Holtzer (QI vs. Q) plot of G4-dPS-45 kDa in d^8-THF at 50 mg/mL 54

Figure 3.10. Holtzer (QI vs. Q) plot of G4-dPS-100 kDa in d^8-THF at 50 mg/mL 55

Figure 3.11. A plot of radius of gyration versus molecular weight for both the dPSblock of the hybrids and dPS in 79:21 h^6:d^6 benzene at 4 mg/mL. 59

Figure 3.12. A plot of radius of gyration versus molecular weight for G4-PBE-PS hybrids and PS in d^8-THF at a concentration of 4 mg/mL. 60

Figure 3.13. A plot of hydrodynamic radius versus molecular weight for G4-PBE-PS hybrids and PS in THF at a concentration of 4 mg/mL. 61

Figure 4.1.SANS data for MEA G 3.0 dendrons in D_2O. 82

Figure 4.2. SANS data for MEA G 3.5 dendrons in D_2O. 82

Figure 4.3. SANS data for MEA G 4.0 dendrons in D_2O. 83

Figure 4.4. SANS data for MEA G 4.5 dendrons in D_2O 83

Figure 4.5. SANS data for MEA G 5.0 dendrons in D_2O. 84

Figure 4.6. R_g and volume of MEA dendrons in D_2O. 85

Figure 4.7. Radius of gyration vs. molecular weight for the MEA dendrons G 3.0-G 5.0 in D_2O at a concentration of 4 mg/mL. 89

Figure 4.8. SANS of MEA G4.0 dendrons in d^4-methanol. 91

Figure 4.9. SANS of MEA G4.0 dendrons in d^6-ethanol 91

Figure 4.10. SANS of MEA G4.0 dendrons in d^{10}-butanol. 92

Figure 4.11. R_g of MEA G4 vs. solvent type (m) of $D(CD2)_mOD$. 92

Figure 4.12. SANS of MEA G5.0 in d^{10}-butanol 96

Figure 4.13. SANS of Tetra G 4.0 dendrons in D_2O. 98

Figure 4.14. SANS of Tetra G 4.0 in d^{10}-butanol. 99

Figure 4.15. Percent mass vs. hydrodynamic radius for a MEA G4.0 dendron in 1 M HCl. 102

Figure 4.16. I(Q) vs. Q for MEA G4.0 in D_2O at a concentration of 25 mg/mL 103

Figure 4.17. Percent mass vs. hydrodynamic radius of an MEA G4.0 dendron in 1 M HCl and 0.100 M NaCl at a concentration of 4 mg/mL. 104

Figure 5.1. Normalized fluorescence emission spectra of (2-aminoethyl)-dansylamide. 122

Figure 5.2. λ_{max} vs. dielectric constant for dansyl-EDA. 123

Figure 5.3. Normalized emission spectra of dansyl-PAMAM full generations (G1-G5) in methanol 125

Figure 5.4. Normalized fluorescence emission spectra of dansyl-PAMAM half generations in methanol. 126

Figure 5.5. λ_{max} vs. generation for dansyl-cored PAMAM dendrimer in methanol. 127

Figure 5.6. Normalized fluorescence emission spectra of full generation dansyl-PAMAM dendrimers in ethanol 130

Figure 5.7. Normalized fluorescence emission spectra of dansyl-PAMAM half generation dendrimers in ethanol 131

Figure 5.8. λ_{max} vs. generation for dansyl-cored PAMAM dendrimer in ethanol. 132

Figure 5.9. Normalized fluorescence emission spectra of dansyl-PAMAM full generations, G1-G4, in butanol. 133

Figure 5.10. Normalized fluorescence emission spectra of dansyl-PAMAM half generation dendrimers in butanol 134

Figure 5.11. λ_{max} vs. generation for dansyl-cored PAMAM dendrimer in butanol. 135

Figure 5.12. Normalized fluorescence emission spectra of dansyl-PAMAM full generation dendrimers in chloroform 136

Figure 5.13. Normalized fluorescence emission spectra of dansyl-PAMAM half generation dendrimers in chloroform 137

Figure 5.14. λ_{max} vs. generation for dansyl-cored PAMAM dendrimer in chloroform.. 138

Figure 5.15. Normalized fluorescence emission spectra of dansyl-PAMAM full generations in acetonitrile. 140

Figure 5.16. Normalized fluorescence emission spectra of dansyl-PAMAM half generations in acetonitrile. 141

Figure 5.17. λ_{max} vs. generation for dansyl-cored PAMAM dendrimer in acetonitrile. 142

Figure 6.1. Cartoon showing the conformational changes of a linear-dendrimer diblock copolymer. 151

Figure 6.2. Dynamic light scattering results for PEO 750 Da-G4 in Milli Q water. 166

Figure 6.3. Dynamic light scattering results for PEO 2 kDa-G4 in Milli Q water. 167

Figure 6.4. Dynamic light scattering results for PEO 5 kDa-G4 in Milli Q water. 167

Figure 6.5. Dynamic light scattering results for PEO 9 kDa-G4 in Milli Q water. 168

Figure 6.6. Dynamic light scattering results for PEO 20 kDa-G4 in Milli Q water. 168

Figure 6.7. Dynamic light scattering results for PEO 2 kDa in Milli Q water. 169

Figure 6.8. Dynamic light scattering results for PEO 5 kDa in Milli Q water. 170

Figure 6.9. Dynamic light scattering results for PEO 8 kDa in Milli Q water. 170

Figure 6.10. Dynamic light scattering results for PEO 20 kDa in Milli Q water. 171

Figure 6.11. Dynamic light scattering results for PEO 36 kDa in Milli Q water. 171

Figure 6.12. Hydrodynamic radius vs. molecular weight of PEO and PEO-PAMAM hybrids in Milli Q water at concentrations of 10 mg/mL. 172

Figure 6.13. Dynamic light scattering results for G4 in Milli Q water..... 174

Figure A.1. ^{1}H NMR MEA G0.5 181

Figure A.2. ^{13}C NMR MEA G0.5 182

Figure A.3. ^{1}H NMR MEA G1.0 183

Figure A.4. ^{13}C NMR MEA G1.0 184

Figure A.5. ^{1}H NMR MEA G1.5 185

Figure A.6. ^{13}C NMR MEA G1.5 186

Figure A.7. ^{1}H NMR MEA G2.0 187

Figure A.8. ^{13}C NMR MEA G2.0 188

Figure A.9. ^{1}H NMR MEA G2.5 189

Figure A.10. ^{13}C NMR MEA G2.5 190

Figure A.11. ^{1}H NMR MEA G3.0 191

Figure A.12. ^{13}C NMR MEA G3.0 192

Figure A.13. ^{1}H NMR MEA G3.5 193

Figure A.14. ^{13}C NMR MEA G3.5 194

Figure A.15. ^{1}H NMR MEA G4.0 195

Figure A.16. ^{13}C NMR MEA G4.0 196

Figure A.17. ^{1}H NMR MEA G4.5 197

Figure A.18. ^{13}C NMR MEA G4.5 198

Figure A.19. ^{1}H NMR MEA G5.0 199

Figure A.20. ^{13}C NMR MEA G5.0 200

Figure B.1. ^{1}H NMR Dansyl EDA 202

Figure B.2. ^{1}H NMR Dansyl G0.5 203

Figure B.3. ^{13}C NMR Dansyl G0.5 204

Figure B.4. ^{1}H NMR Dansyl 1.0 205

Figure B.5. ^{13}C NMR Dansyl G1.0 206

Figure B.6. ^{1}H NMR Dansyl G1.5 207

Figure B.7. ^{13}C NMR Dansyl G1.5 208

Figure B.8. ^{1}H NMR Dansyl G2.0 209

Figure B.9. ^{13}C NMR Dansyl G2.0 210

Figure B.10. ^{1}H NMR Dansyl G2.5 211

Figure B.11. ^{13}C NMR Dansyl G2.5 212

Figure B.12. ^{1}H NMR Dansyl G3.0 213

Figure B.13. ^{13}C NMR Dansyl G3.0 214

Figure B.14. ^{1}H NMR Dansyl G3.5 215

Figure B.15. ^{13}C NMR Dansyl G3.5 216

Figure B.16. ^{1}H NMR Dansyl G4.0 217

Figure B.17. ^{13}C NMR Dansyl G4.0 218

Figure B.18. ^{1}H NMR Dansyl G4.5 219

Figure B.19. ^{13}C NMR Dansyl G4.5 220

Figure C.1. ^{1}H NMR PEO 750 Da OMs 222

Figure C.2. ^{1}H NMR PEO 750 Da phth 223

Figure C.3. ^{1}H NMR PEO 750 Da NH_2 224

Figure C.4. ^{1}H NMR PEO 750 G0.5 225

Figure C.5. ^{1}H NMR PEO 750 Da G1.0 226

Figure C.6. ^{1}H NMR PEO 750 Da G1.5 227

Figure C.7. ^{1}H NMR PEO 750 Da G2.0 228

Figure C.8. ^{1}H NMR PEO 750 Da G2.5 229

Figure C.9. ^{1}H NMR PEO 750 Da G3.0 230

Figure C.10. ^{1}H NMR PEO 750 Da G3.5 231

Figure C.11. ^{1}H NMR PEO 2 kDa OMs 232

Figure C.12. ^{1}H NMR PEO 2 kDa phth 233

Figure C.13. ^{1}H NMR PEO 2 kDa NH_2 234

Figure C.14. ^{1}H NMR PEO 2 kDa G0.5 235

Figure C.15. ^{1}H NMR PEO 2 kDa G1.0 236

Figure C.16. ^{1}H NMR PEO 2 kDa G1.5 237

Figure C.17. ^{1}H NMR PEO 2 kDa G2.0 238

Figure C.18. ^{1}H NMR PEO 2 kDa G2.5 239

Figure C.19. ^{1}H NMR PEO 2 kDa G3.0 240

Figure C.20. ^{1}H NMR PEO 2 kDa G3.5 241

Figure C.21. ^{1}H NMR PEO 2 kDa G4.0 242

Figure C.22. ^{1}H NMR PEO 5 kDa OMs 243

Figure C.23. ^{1}H NMR PEO 5 kDa phth 244

Figure C.24. ^{1}H NMR PEO 5 kDa NH_2 245

Figure C.25. ^{1}H NMR PEO 5 kDa G0.5 246

Figure C.26. ^{1}H NMR PEO 5 kDa G1.0 247

Figure C.27. ^{1}H NMR PEO 5 kDa G1.5 248

Figure C.28. ^{1}H NMR PEO 5 kDa G2.0 249

Figure C.29. ^{1}H NMR PEO 5 kDa G2.5 250

Figure C.30. ^{1}H NMR PEO 5 kDa G 3.0 251

Figure C. 31. ^{1}H NMR PEO 5 kDa G3.5 252

Figure C.32. ^{1}H NMR PEO 5 kDa G4.0 253

Figure C.33. ^{1}H NMR PEO 9 kDa OMs 254

Figure C.34. ^{1}H NMR PEO 9 kDa phth 255

Figure C.35. ^{1}H NMR PEO 9 kDa NH_2 256

Figure C.36. ^{1}H NMR PEO 9 kDa G0.5 257

Figure C.37. ^{1}H NMR PEO 9 kDa G1.0 258

Figure C.38. ^{1}H NMR PEO 9 kDa G1.5 259

Figure C.39. ^{1}H NMR PEO 9 kDa G2.0 260

Figure C.40. ^{1}H NMR PEO 9 kDa G2.5 261

Figure C.41. ^{1}H NMR PEO 9 kDa G3.0 262

Figure C.42. ^{1}H NMR PEO 9 kDa G3.5 263

Figure C.43. ^{1}H NMR PEO 9 kDa G4.0 264

Figure C.44. ^{1}H NMR PEO 20 kDa OMs 265

Figure C.45. ^{1}H NMR PEO 20 kDa NH_2 266

Figure C.46. ^{1}H NMR PEO 20 kDa G0.5 267

Figure C.47. ^{1}H NMR PEO 20 kDa G1.0 268

Figure C.48. ^{1}H NMR PEO 20 kDa G1.5 269

Figure C.49. ^{1}H NMR PEO 20 kDa G2.0 270

Figure C.50. ^{1}H NMR PEO 20 kDa G2.5 271

Figure C.51. ^{1}H NMR PEO 20 kDa G3.0 272

Figure C.52. ^{1}H NMR PEO 20 kDa G3.5 273

Figure C.53. ^{1}H NMR PEO 20 kDa G4.0 274

LIST OF SCHEMES

Scheme 3.1. PBE-G4-PS dendrimer-linear diblock copolymer..... 36

Scheme 4.1. Synthesis of MEA-PAMAM dendrons. 73

Scheme 4.2. MEA-G4.0. 74

Scheme 5.1. Synthesis of dansyl-cored PAMAM dendrimer. 114

Scheme 5.2. Generation 4 dansyl-cored PAMAM dendrimer. 115

Scheme 6.1. Synthesis of methoxy-amine terminated poly(ethylene oxide). 163

Scheme 6.2. Synthesis of PEO-PAMAM diblock copolymers..... 164

ABBREVIATIONS

$\Delta\,\Omega$	solid angle element defined by the size of a detector pixel
$(\Delta\rho)^2$	the square of the difference of the solvent and the scatterer SLD
$\Sigma\partial/\delta\Omega$	differential scanning cross-section
a	effective Stokes radius of a sphere
A	area of the particle
A_s	spectral amplitude
B	background signal
b_i	coherent neutron scattering length of nucleus *i*
B_l	baseline
$C(\delta t)$	correlation function
δ	bulk density of the molecule,
D	diffusion coefficient
dansyl-EDA	preparation of (2-aminoethyl)-dansylamide
DLS	dynamic light scattering
dPS	deuterated poly(styrene)
$\Delta\rho$	difference in scattering length density of the sample and medium
ϕ	volume fraction of scattering centers
f_{bu}	multiplicity of the branching units
f_c	core functionality
η_d	detector efficiency
η	viscosity of the solvent
I(0)	intensity at zero wave vector
I(t)	intensity fluctuations
I_0	incident flux of neutrons
k	magnitude of the scattering vector
k_B	Boltzmann's constant
$\mathbf{k_i}$	incident wavevector
$\mathbf{k_s}$	scattered wavevector
λ	wavelength
L	rod length
L_{sd}	distance between sample and detector in SANS
M	molecular weight of the molecule
MEA	2-methoxyethylamine
N	number concentration of scattering centers
N_A	Avogadro's number
P(Q)	form factor

PAMAM	poly(amido amine)
PBE	poly(benzyl ether) dendrimer
PEO	poly(ethylene oxide)
PS	poly(styrene)
$\|\mathbf{Q}\|$ or Q	modulus of **Q**, independent variable in SANS
Q	scattering vector
θ	mass fraction of solvent within the scatterer
ρ	scattering length density
R	homogeneous sphere radius
R_c	root-mean-square of the distances of all of the atoms in a cross-section of R_r
r_{det}	radial distance between sample and scattered neutrons
R_g	radius of gyration
R_h	hydrodynamic radius
R_η	visciometric radius
ρ_{dend}	scattering length density of the dendrimer
ρ_{scatt}	scattering length density of the scatterers
ρ_{solv}	scattering length density of the solvent
S(Q)	structure factor
SAND	small-angle neutron diffractometer
SLD	scattering length density
SPCM	Single Photon Counting Module
T	neutron transmission of the sample
τ	time for the diffusion step to occur
T	duration of a dynamic light scattering experiment
T_a	absolute temperature
Tetra – G4.0	Tetra-functional PAMAM G4.0
THF	tetrahydrofuran
T_s	sheet thickness
V	volume of one scattering center
V	volume
V_{hc}	hard-core volume
V_s	volume of each scattering center
V_{vdw}	van der Waals volume

CHAPTER ONE: Introduction

Anatomy of a Dendrimer

Dendrimers are globular, nano-sized macromolecules synthesized in a controlled manner to result in a highly branched structure with three distinct regions: (i) a central focal point, core, which is a single atom or an atomic group with at least two identical chemical moieties, (ii) branches emanating from the focal point, consisting of repeat units that have at least one branch junction or split resulting in a series of radially concentric layers called generations and (iii) multiple end groups that have identical functionality (Figure 1.1). A segment of a dendrimer, a dendron, is shown in Figure 1.1 along with the basic anatomy of a dendrimer, with the parts of the dendrimer labeled. An example of a second generation poly(amido amine) (PAMAM) dendrimer is displayed in Figure 1.2 where the focal point is tri-functional, a tri-dendron, meaning it has three sites of reactivity for dendrimer growth.

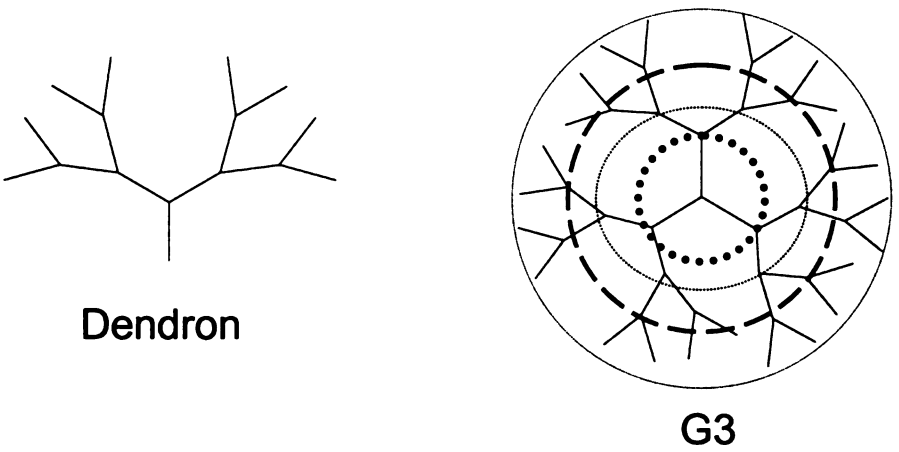

Figure 1.1. Anatomy of a dendrimer.

Dendron and dendrimer are represented by the solid lines.
The broken lines beginning from the center of the generation three dendrimer represent the core, first, second and third generations respectively.

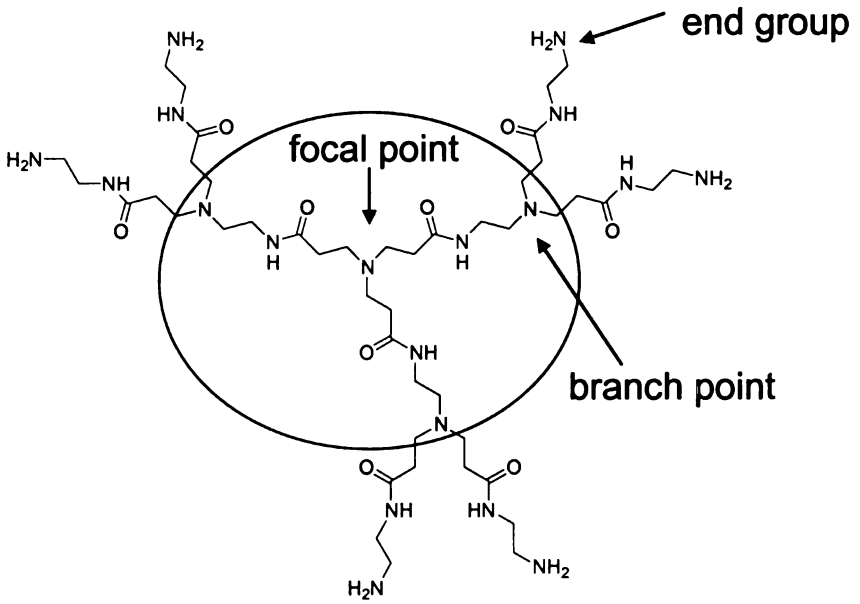

Figure 1.2. Elements of a generation 2, poly(amido amine) (PAMAM) dendrimer.

The constituents of generation one are circled.

These three elements of a dendrimer are critical to the morphology of these molecules in solution, and altering any element has a direct influence on their properties. For example modifying the functionality of the core, i.e. how many dendrons emanate from the focal point, directly affects the steric bulk of the growing dendrimer as well the number of end groups at each generation. The flexibility of the branching units plays a key role in the dynamics of the dendrimers in solution. Rigid dendrimers have been synthesized with a highly conjugated branching system and have different properties than those synthesized with more flexible connecting groups. In addition, the chemical functionality of the end groups greatly influences the interaction of these molecules both with themselves and their surrounding medium. The properties of dendrimers are also controlled by the interaction of the different dendritic elements, i.e. hydrogen bonding.

A Brief History of Dendrimers

The evolution of the construction of macromolecules possessing a branched architecture has three general eras.[1] The first period was from the late 1860's to the early 1940's when branched impurities were thought to be the insoluble byproducts formed in polymerization reactions, however purification and separation techniques were too primitive at the time to prove the structures of these impurities. In the second period of dendrimer history, from the early 1940's to the late 1970's, branched polymer structures were considered mostly from the view of polymer physicists who were developing theory that described the behavior of macromolecules and branched species. The synthesis of these branched structures was attempted using differentiated monomers in a traditional one-pot synthesis used for the preparation of linear polymer chains. Flory noted in the 1950's,[2] "The breadth of the distribution coupled with the impossibility of selectively

fractionating 'branching' and 'molecular weight' separately make this approach impractical. Attempts to investigate 'branching by such means consequently have been notably fruitless." However, he did examine the scaling properties of branched polymers where he envisioned a branched system synthesized with an AB_2 type monomer resulting in a 1→ 2 branching system (Figure 1.3). It wasn't until the late 1970's and early 1980's when dendrimers were successfully synthesized using a controlled iterative method of growth. The first example of this approach was reported by Vögtel,[3] who named the process a "cascade synthesis." Soon after, Denkewalter and Kolc[4] published a series of US patents describing the synthesis of L-lysine-based dendrimers made by an iterative controlled growth, however little characterization of theses molecules was reported.

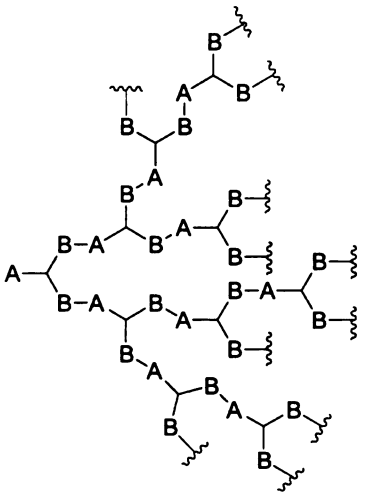

Figure 1.3. Flory's branched polymer architecture created by the reaction of AB_2 type monomers.

Iterative Growth of Dendrimers

Two distinct approaches for iterative growth have been developed for the synthesis of dendrimers: a divergent approach to make "starburst" and "arboral" structures by Tomalia[5, 6] and Newkome[7] respectively, and the convergent approach characterized by the synthesis of poly(benzyl ether) dendrons by Fréchet.[8, 9] Later, Moore's group[10-12] convergently produced phenylacetylene dendrimers. The main difference between the two methods is the site of reactivity. For the divergent scheme the end groups are the reactive species, whereas for the convergent approach, the focal point is the site of reactivity. Both methods require the same number of theoretical steps to produce each generation.

The divergent approach (Figure 1.4) begins with a core or focal point and via sequential monomer addition, extends the branches from the focal point towards the periphery of the molecule. Since numerous reactions are being done on the same molecule, each reaction has to be very selective and proceed to high conversion to ensure the integrity of the final product. For example, there are 64 end groups in a fifth generation poly(propylene imine) dendrimer requiring 248 reactions to occur on one molecule to achieve a perfect dendrimer.[13] If the average selectivity of each reaction is 99.5% the yield of defect-free dendrimer produced is only $0.995^{248} = 29\%$. Since every new generation is very difficult to purify, the presence of a small number of statistical defects cannot be avoided (Figure 1.5). The divergent synthesis of poly(amido amine) dendrimers may lead to structural defects including ring formation and incomplete growth of dendritic arms (Figure 1.6) The number of such defects is minimized by controlling the reaction conditions and stoichiometry.[14] The purity of the molecules

produced by the divergent method is controlled by statistics and thus it is virtually impossible to produce perfect dendrimers beyond generation five or six. [15]

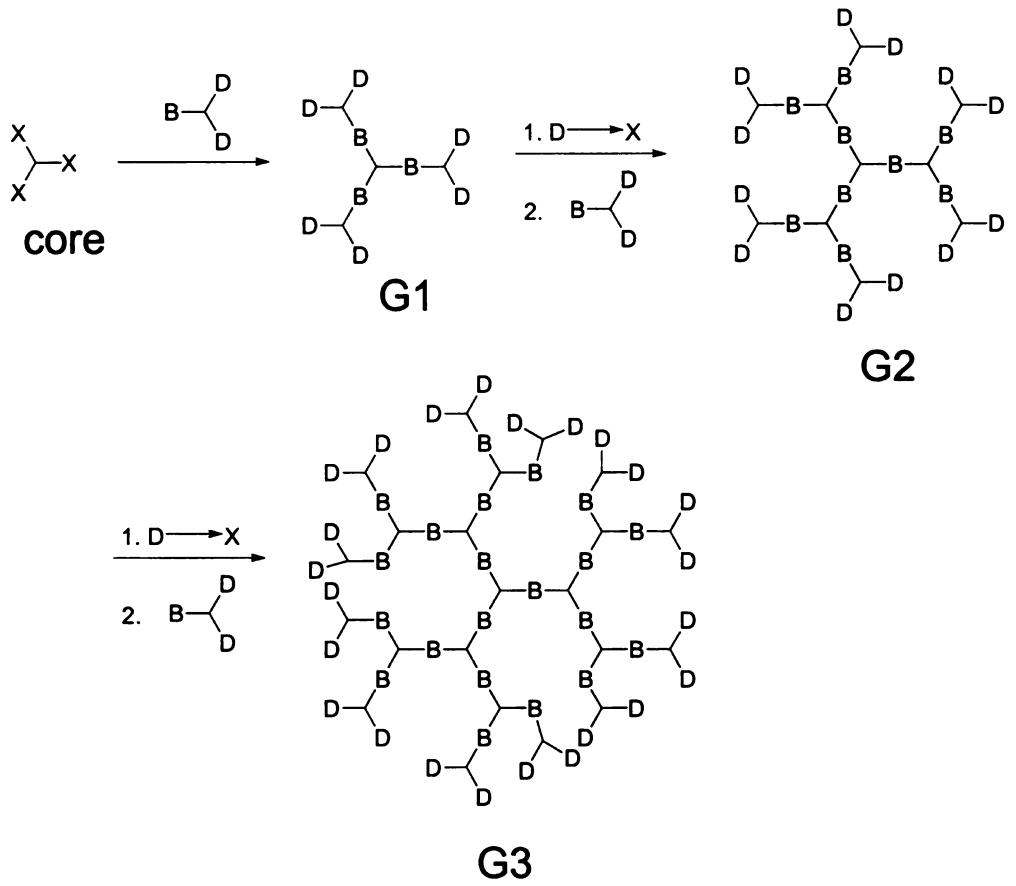

Figure 1.4. Example of a divergent synthesis of a dendrimer with a 1→2 branching scheme and a tri-functional core.

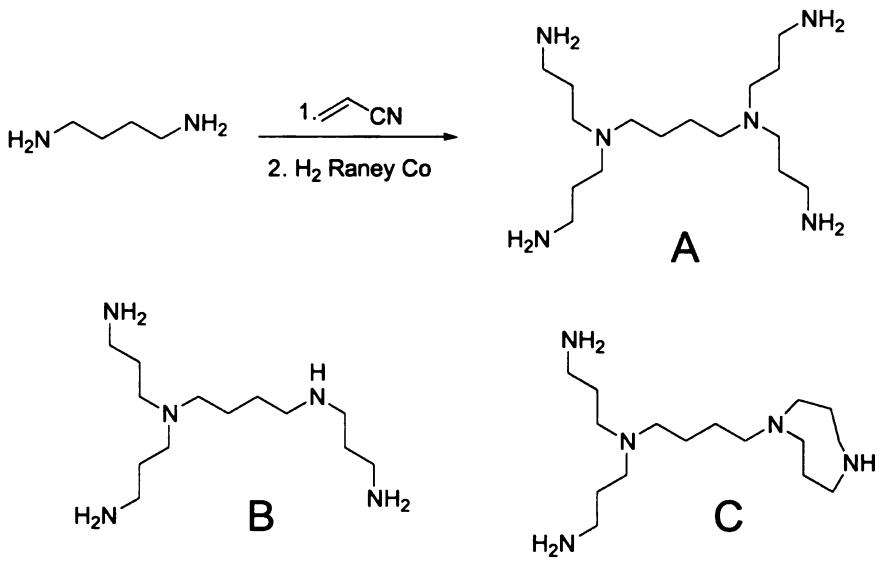

Figure 1.5. The synthesis of poly(propylene imine) dendrimers.

Product A is the desired first generation and products B and C are unwanted impurities. B results from incomplete Michael addition or a retro-Michael reaction and C is the result of an undesired cyclization reaction. Both impurities have properties similar to the desired product, thus complicating purification.

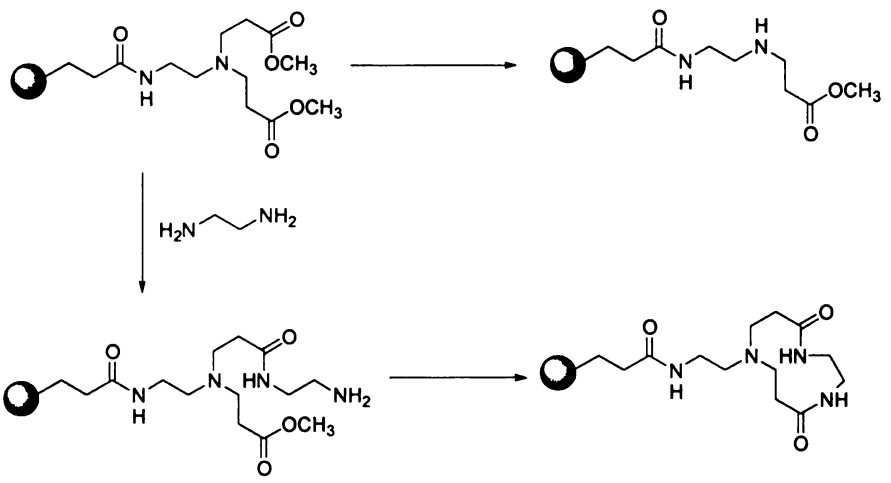

Figure 1.6. Possible defects and imperfections that can result during the divergent synthesis of a poly(amido amine) dendrimer.

Both ring formation and retro-Michael reactions can be avoided by controlling the reaction conditions.

The convergent approach (Figure 1.7) entails synthesizing the branches of the dendrimers and attaching them to core and is often called the "outside-in" approach (Figure 1.3). It begins by attaching two terminal units, each containing one reactive group, X, to one monomer possessing a protected functionality Z, resulting in the first generation (G1). The protected focal point, Z, is converted to functionality X, and then reacted with 0.5 equivalents of the monomer to obtain G2. The reactivity point in the convergent approach is the focal point of the dendron and thus there is increased steric crowding at the site of reactivity with each subsequent generation and this results in a synthesis that is increasingly challenging with increasing generation. Dendrimers synthesized by the convergent approach can be nearly pure, and mass spectroscopy data on Fréchet-type dendrimers[16, 17] and Moore's phenylacetylene dendrimers[18] display limited amounts of impurities.

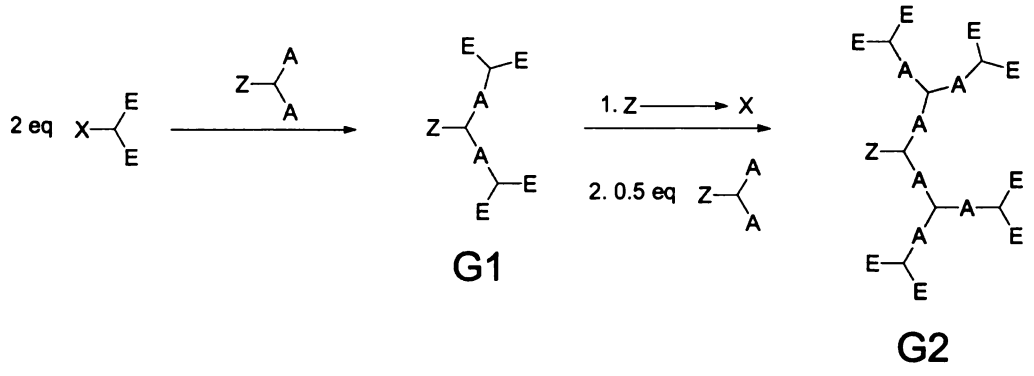

Figure 1.7. Example of a convergent synthesis of a dendrimer with 1→2 branching scheme and a di-functional core.

Both synthetic methods provide the unique highly symmetric branched architecture, characteristic of dendrimers. The number of end groups (N_e) of a dendrimer is defined as[19]

$$N_e = f_c(f_{bu} - 1)^g \tag{1.1}$$

where f_c is the functionality of the core, f_{bu} is the functionality of the branching unit and g is the generation number. Similarly, the molecular mass of a dendrimer is[19]

$$M_g = M_c + f_c\left[M_{bu}\left(\frac{f_{bu}^g - 1}{f_{bu} - 1}\right)\right] + M_t + f_{bu}^g \tag{1.2}$$

where M_c, M_{bu} and M_t are the molecular weights of the core, branching unit and terminal group respectfully. Simplifying eq 1.2, demonstrates the molecular mass scales as

$$M \sim f_c(f_{bu} - 1)^g \tag{1.3}$$

The PAMAM and poly(benzyl ether) (PBE) dendrimers studied here both have a multiplicity at the branch junction points (f_{bu}) of 2 and both are di-dendrons, giving a value of f_c=2. Thus molecular mass scales as

$$M \sim 2^g \tag{1.4}$$

The volume of dendrimers (V) is approximated as

$$V \sim g^3 \tag{1.5}$$

which is quite different from the volume growth of linear chains which follow the trend

$$V \sim RU^{3/2} \tag{1.6}$$

where RU is the number of repeat units. The growth properties of dendrimers determine their solution properties and will be discussed in greater detail in Chapter 3, where the

solution properties of a di-functional PAMAM dendrimer were measured with small angle neutron scattering (SANS) and dynamic light scattering (DLS). It should be noted that the solution properties of dendrimers are a direct consequence of their molecular architecture, which results in the occupied volume of a single molecule to increase cubically with generation, whereas its mass increases exponentially. This makes their solution properties deviate from linear polymers, especially at higher generations. Unlike linear polymers, whose intrinsic viscosity increases with increasing molecular weight, the intrinsic viscosity of dendrimers reaches a maximum at a certain dendrimer generation, which is determined by the functionality of the core and branching units.

Applications of Dendrimers

The ability to control the chemical functionality at the focal point, branching units and end groups of dendrimers enhances the diversity of their material properties and thus a wide array of applications of these molecules has appeared in the literature over the past 25 years. Groups have fine tuned the properties of dendrimers for uses such as drug delivery,[20-23] reaction catalysis,[24, 25] transfection agents,[26] process additives,[27] calibration standards,[28] electrokinetic chromatography[29] and light harvesting.[30] Medicinal application of dendrimers has gained recent attention with researchers taking advantage of the numerous functional groups of these molecules as well as their ability to sequester guests. Dendrimers have advantages over linear chains for polymer therapeutics since drug manufacturers desire a drug to be composed of a single, defined species, whose identity (and impurities) can be specified using validated techniques and whose pharmacokinetics and therapeutic index (activity and toxicity) can be precisely defined. The heterogeneity of linear polymers and their conjugates has a profound effect on the

biological activity of pharmaceuticals. While it has been possible to define acceptable product specifications using linear polymers in therapies methods are being sought to minimize the polymer heterogeneity thereby simplifying the process of bringing polymer-drug conjugates to market.

Dendrimers have potential as drug delivery vehicles, since their chemistry can be altered to create water soluble compounds with targeting peripheral groups and shielding branching units. The determining factor for the commercialization of dendrimers will be the cost-effectiveness of their complex synthesis as well as their challenging characterization. Despite these challenges, many researchers have developed promising dendrimer-drug conjugates. Glycodendrimers with an L-lysine cores were synthesized by Roy et al.[31, 32] with various carbohydrates at the end groups. Compared to a monofunctional compound they show an enhanced binding capability in a direct enzyme-linked lectin assay. Tam et al.[33, 34] coupled peptides to a dendritic core to be used as multiple antigen peptides. When injected into mice or rabbits, the immunoresponse was greater than for conventional peptide carrier conjugates, and was attributed to the high antigen content of the modified dendrimers. More recently, Qualmann et al.[35, 36] have introduced antigen selectivity in boron neutron capture therapy,[37] a cancer treatment where cytotoxic and energetic products from nuclear fission reactions of low-energy neutrons and ^{10}B nuclei are used to destroy malignant cells. Coupling a lysine-based boronated dendrimer to antibody fragments leads to better stability compared to borate coated polystyrene beads.

To expand the range of applications of dendrimers many groups have synthesized and characterized dendrimer-linear conjugates. Three distinct classes of these adducts

include (i) attachment of linear chains to the end groups of dendrimers, (ii) placement of a linear chain at the focal point of a dendrimer, resulting in a linear-dendrimer diblock (hybrid) and (iii) attachment of a dendron to the repeat unit of a linear polymer (dendronized polymer). Combining the properties of a linear chain to that of a dendrimer greatly increases the diversity of the material properties of these systems.

Harada et al. recently published the synthesis and polycation behavior of a linear-dendrimer diblock copolymer where a poly(L-lysine) (PLL) linear chain is covalently attached to the focal point of a carboxylic acid terminated PAMAM dendrimer (Figure 1.8).[38] The hybrid was synthesized by polymerization from the focal point of the PAMAM dendrimer where the resulting diblock showed a 10^2 fold higher transfection efficiency to cells compared to the PLL alone. Fréchet and Lee[39] recently synthesized a dendronized polymer based on a poly(L-lysine) backbone with a fourth generation polyester dendrimer (Figure 1.9). The dendronized polypeptide backbones are helical at lower generations, but upon increasing dendon size undergo a conformation change from α-helical to disordered as observed by scanning force microscopy. The dendrons encapsulate the linear chain and because of the unique backbone conformation are the first known macromolecules to behave as single molecule glasses.[40]

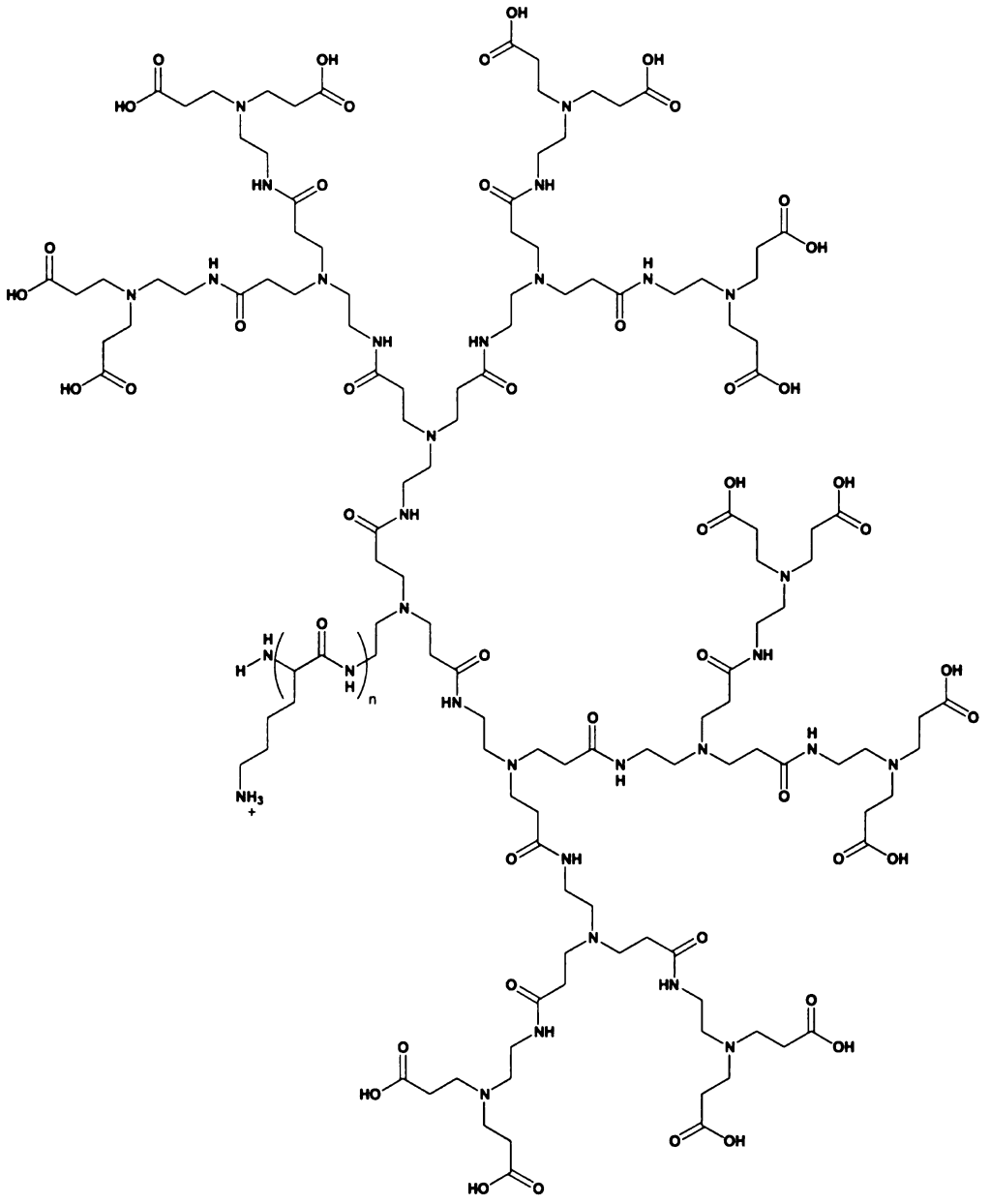

Figure 1.8. A linear-dendrimer diblock copolymer (hybrid) where a poly(L-lysine) linear chain is covalently attached to the focal point of a carboxylic acid terminated PAMAM dendrimer.

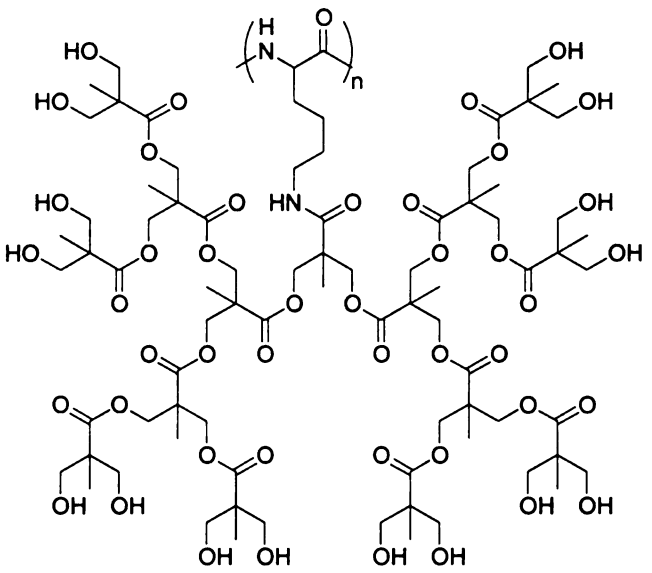

Figure 1.9. A dendronized polymer consisting of a fourth generation hydroxyl terminated polyester dendrimer attached to the repeat unit of poly(L-lysine).

Motivation of work

This dissertation will focus on the properties of linear-dendrimer diblock copolymers where a linear polymer chain is covalently bonded to the focal point of a dendron. We have studied two different systems where the first consists of a Fréchet-type PBE dendron with a poly(styrene) (PS) chain connected to its focal point. Extensive SANS experiments on partially deuterated molecules were conducted to determine the relative location of the linear chain and dendrimer block and will be discussed in Chapter 3. The ability of the dendrimer block to change size and shape will also be discussed. The second system is water soluble and consists of a linear poly(ethylene oxide) (PEO) chain connected to the focal point of a PAMAM di-dendron. The morphology of this system in dilute solution is discussed in Chapter 6. The properties of the dendrimer block of this system are discussed in Chapter 4, where we describe the synthesis of a dendrimer as well as its solution properties. We used SANS and DLS experiments to investigate the dynamics of PAMAM dendrimers with respect to solvent quality and found that functionality of the core as well as chemistry of the end groups greatly influences the dimensions of these molecules in solution. To further look at the morphology of the dendrimer block of the PEO-PAMAM system, we synthesized a di-functional PAMAM dendron with a solvatochromic probe at its focal point. The behavior of the fluorescence of this molecule as a function of generation and solvent is discussed in Chapter 5. The chapters are organized in order of the thought process I used to answer the questions (1) How can the morphology of linear-dendrimer diblock copolymers be probed and proven? (2) What factors of the dendrimer block, if any, influence the behavior of these molecularly asymmetric molecules in solution?

References

1. Newkome, G. R.; Moorefield, C. N.; Vögtle, F., *Dendritic Molecules: Concepts, Syntheses, Perspectives*. John Wiley & Sons: New York, 1996.

2. Flory, P. J., *J. Am. Chem. Soc.* **1952,** *74*, 2718.

3. Buhleier, E. W.; Wehner, W.; Vögtle, F., *Synthesis* **1978,** 155.

4. Denkewalter, R. G.; Kolc, J. U. S. Pat. 4-410,688, Oct 18 1983.

5. Tomalia, D.; Baker, H.; Dewald, J.; Hall, M.; Kallos, G.; Martin, S.; Roeck, J.; Ryder, J.; Smith, P., *Poly. J.* **1985,** *17*, 117-132.

6. Tomalia, D. A. B., H.; Martin, S.; J.; Hall, M.; Kallos, G.; Roeck, J.; Ryder, J.; Smith, P., *Macromolecules* **1986,** 2466.

7. Newkome, G. R.; Yao, Z.; Baker, G. R.; Gupta, V. K., *J. Org. Chem.* **1985,** *50*, 2004.

8. Hawker, C. J.; Fréchet, J. M. J., *J. Am. Chem. Soc.* **1990,** *112*, 7638-7647.

9. Hawker, C. J.; Frechet, J. M. J., *J. Chem. Soc., Chem. Commun.* **1990,** *15*, 1010.

10. Moore, J. S.; Xu, Z., *Macromolecules* **1991,** *24*, 5893-5894.

11. Xu, Z.; Moore, J. S., *Angew. Chem. Int. Ed. Eng.* **1993,** *32*, 246-248.

12. Kawaguchi, T.; Walker, K. L.; Wilkins, C. L.; Moore, J. S., *J. Am. Chem. Soc.* **1995,** *117*, 2159-2165.

13. Bosman, A. W.; Janssen, H. M.; Meijer, E. W., *Chem. Rev.* **1999,** *99*, 1665-1688.

14. Tomalia, D. A.; Smith, P. B.; Hall, M. J.; Martin, S. J., *A Characterization of the Structure and Synthetic Reactions of Polyamidoamine "Starburst" Polymers*. Hanser: Munich, 1987.

15. Bosman, A. W.; Janssen, H. M.; Meijer, E. W., *Chem. Rev.* **1999,** *99*, 1665-1688.

16. Leon, J. W. F., J. M. J., *Polym. Bull.* **1995,** *35*, 449-455.

17. Pollak, K. W.; Sanford, E. M.; Frechet, J. M. J., *Mater. Chem* **1998,** *8*, 519-527.

18. Walker, K. L.; Kahr, M. S.; Wilkins, C. L.; Xu, Z.; Moore, J. S., *J. Am. Mass. Spectrom.* **1994,** *5*, 731-739.

19. Tomalia, D. A.; Naylor, A. M.; Goddard, W. A., *Angew. Chem. Int. Ed. Engl.* **1990,** *29*, 138-175.

20. Ihre, H. R.; De-Jesus, O. L.; Francis, C. S., Jr.; Frechet, J. M. J., *Bioconj. Chem.* **2002,** *13*, 443-452.

21. Dhanikula, R. S.; Hildgen, P., *Bioconj. Chem.* **2006,** *17*, 29-41.

22. Majoros, I. J.; Myc, A.; Thomas, T.; Mehta, C. B.; Baker, J. R., *Biomacromolecules* **2006,** *7*, 572-579.

23. Majoros, I. J.; Thomas, T. P.; Mehta, C. B.; Baker, J. R., *J. Med. Chem.* **2005,** *48*, 5892-5899.

24. Mak, C. C.; Chow, H.-F., *Macromolecules* **1997,** *30*, 1228-1230.

25. Knapen, J. W. J.; van der Made, A. W.; de Wilde, J. C.; van Leeuwen, P. W. M.; Wijkens, P., *Nature* **1994,** *372*, 659-663.

26. DeLong, R.; Stephenson, K.; Loftus, T.; Fisher, M.; Alahari, S.; Nolting, A.; Juliano, R. L., *J. Pharm. Sci.* **1997,** *86*, 762-764.

27. Mackay, M. E.; Hong, Y.; Hong, S.; Russell, T. P.; Hawker, C. J.; Vestberg, R.; Douglas, J., *Langmuir* **2002,** *18*, 1877-1882.

28. Dubin, P. L.; Edwards, S. L.; Kaplan, J. I.; Mehta, M. S.; Tomalia, D. A.; Xia, J., *Anal. Chem.* **1992,** *64*, 2344.

29. Tanaka, N.; Fukutome, T.; Tanigawa, T.; Hosoya, K.; Kimata, K.; Araki, T.; Unger, K. K., *J. Chromatogr. A* **1995,** *669*, 331.

30. Tyson, D. S.; Luman, C. R.; Castellano, F. N., *Inorg. Chem.* **2002,** *41*, 3578-3586.

31. Roy, R.; Zanini, D.; Meunier, S. J.; Romanowska, A., *J. Chem. Soc., Chem. Commun.* **1992,** 1869-1872.

32. Zanini, D.; Roy, R., *Bioconj. Chem.* **1997,** *8*, 187-192.

33. Posnett, D. N.; McGrath, H.; Tam, J. P., *J. Biol. Chem.* **1988,** *263*, 1719-1725.

34. Rao, C.; Tam, J. P., *J. Amer. Chem. Soc.* **1994,** *116*, 6975-6976.

35. Qualmann, B.; Kessels, M. M.; Musiol, H.-J.; Sierralta, W. D.; Jungblut, P. W.; Moroder, L., *Angew. Chem. Int. Ed. Engl.* **1996,** *35*, 909-911.

36. Qualmann, B.; Kessels, M. M.; Klobasa, F.; Jungblut, P. W.; Sierralta, W. D., *J. Micros.* **1996,** *183*, 69-77.

37. Hawthorne, M. F., *Angew. Chem. Int. Ed. Eng.* **1993,** *32*, 950-984.

38. Harada, A.; Kawamura, M.; Matsuo, T.; Takahashi, T.; Kono, K., *Bioconj. Chem.* **2006,** *17*, 3-5.

39. Frechet, J. M. J.; Lee, C. C., *Macromolecules* **2006,** *39*, 476-481.

40. Das, J.; Yoshida, M.; Fresco, Z. M.; Choi, T. L.; Frechet, J. M. J., *J. Phys. Chem. B.* **2005,** *109*, 6535-6543.

CHAPTER TWO: Scattering Theory

The size of polymers in solution can be probed with light, neutron or x-ray scattering experiments. It has become increasingly popular in polymer characterization to not only be concerned with molecular weight, but also with the dimensions of macromolecules and how environmental factors can alter their morphology. There are two basic types of scattering experiments, static (elastic) scattering and dynamic (quasi-elastic) scattering. Elastic scattering experiments provide information such as molecular weight, and with collection of the time-averaged intensity over a range of wave vector (Q), can provide us the radius of gyration (R_g) and second virial coefficient.[1-3] Quasi-elastic scattering experiments monitor the random (Brownian) motion of polymers in solution by collecting a time average change in intensity to obtain a diffusion coefficient, which can be used to determine the size and shape of polymers via the Stokes Einstein equation.[4]

I have used both neutron and light scattering experiments to analyze dendrimers and their copolymers in solution. Small angle neutron scattering experiments (SANS) were conducted to determine the R_g of linear polymers, dendrimers and linear-dendrimer diblock copolymers in dilute solution. The hydrodynamic radius (R_h) of samples was determined from quasi-elastic light scattering, also known as dynamic light scattering (DLS) or photon correlation spectroscopy. The field of polymer characterization using SANS and DLS has increased in popularity over the years and implementation of both DLS[4-6] and SANS[3, 7-11] have been discussed in great detail elsewhere. Here only a brief outline of the two methods is presented.

Small Angle Neutron Scattering (SANS)

Small Angle Neutron Scattering is a technique that enables one to probe the size and shape of molecules and their assemblies both in solution and in the bulk. It is comparable to other diffraction techniques, such as Small Angle X-Ray scattering (SAXS) and static light scattering, and while often the same information can be drawn from all three techniques, a key advantage of SANS for the polymer chemist is that hydrogen and deuterium scatter differently, thus allowing interrogation of selected parts of macromolecules by deuterium labeling chemistry.[2]

SANS uses slow (long-wavelength) neutrons that range from 0.15 to 2.5 nm. Neutrons leave the radiation source and are collimated to an appropriate size and shape through the use of neutron-absorbing material. This is analogous to focusing a beam of light. The neutrons hit the sample and are scattered with equal intensity in all directions. The lack of angular dependence of intensity is due to the wavelength of the neutrons being orders of magnitude larger than the size of the nucleus from which they are being scattered, thus in neutron scattering, nuclei may be considered as 'point scatters.' This is contrary to scattered light and X-ray radiation where there is pronounced angular dependence in intensity due to the radiation being scattered by electrons surrounding the nucleus and the wavelength of radiation is closer in size to the scatterer.

The geometry of a SANS experiment is shown in Figure 2.1 where neutrons with a wavelength, λ, are scattered by the nuclei of the sample at an angle, θ. The scattered neutrons hit a detector at a distance, L_{sd}, from the sample. The scattering vector, $\mathbf{Q}$, describes the relationship between the incident, $\mathbf{k_i}$, and scattered, $\mathbf{k_s}$, wavevectors, where

$\mathbf{Q} = \mathbf{k}_i - \mathbf{k}_s$. The modulus of $\mathbf{Q}$, $|\mathbf{Q}|$, is the independent variable in a SANS experiment and has dimensions of (length)$^{-1}$.[2]

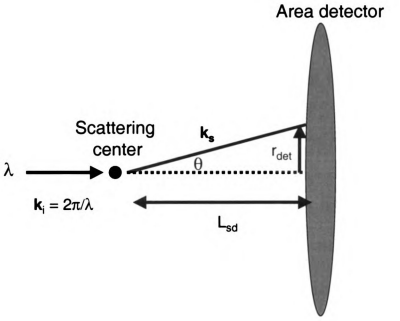

Figure 2.1. Schematic of a small angle neutron scattering experiment.

There are two main types of SANS instruments that differ based on the neutron source. At a reactor source a fixed-wavelength instrument is most common, whereas at a spallation source a fixed-geometry instrument is used. Use of the fixed-wavelength instrument entails choosing a value of λ, and varying the Q range by changing the sample-detector distance, L_{sd}. A fixed-geometry instrument has set values of L_{sd} and r_{det}. The Q range is varied by the range of wavelengths hitting the detector and the range in wavelength sets the Q range of the experiment.

The dependent variable in SANS is the differential scanning cross-section $(\partial\Sigma/d\Omega)$ (Q), which typically has units of cm^{-1} and gives information about the size and shape of the sample. A common misinterpretation of $(\partial\Sigma/\partial\Omega)$ (Q) is that it is the same as the intensity of scattering, I(Q). $(\partial\Sigma/\partial\Omega)$ (Q) is determined from the intensity of scattering given by[2]

$$I(Q) = I_0(\lambda)\Delta\ \Omega\ \eta_d(\lambda)\ T(\lambda)\ V_s\ (\partial\Sigma/\partial\Omega)\ (Q) \qquad (2.1)$$

where I_0 is the incident flux of neutrons, $\Delta\ \Omega$ is the solid angle element defined by the size of a detector pixel, η_d is the detector efficiency, T is the neutron transmission of the sample and V_s is the volume of the sample illuminated by the neutron beam. The incident flux, solid angle element and detector efficiency are all instrument specific and typically determined by the instrument scientist. The transmission is sample specific and is measured before each scattering run. The volume of sample is known, thus leaving only the differential scanning cross section to be determined during data reduction.

The differential scanning cross section is then used to determine the structural features of the sample by[2]

$$(\partial\Sigma/\partial\Omega) = nV^2(\Delta\rho)^2 P(Q)S(Q) + B \quad (2.2)$$

where N is the number concentration of scattering centers, V is the volume of one scattering center, $(\Delta\rho)^2$ is the contrast between the sample and the solvent/medium, P(Q) is the form factor, S(Q) is the structure factor and B is the background signal.

The contrast between the sample and the solvent, $(\Delta\rho)^2$, allows a SANS experiment to take place. Here, ρ represents scattering length density and $\Delta\rho$ is the difference between the scattering length density of the sample and the solvent. The scattering length density typically has the units 10^{10} cm^{-2} or 10^{-6} Å^{-2} and can be found by[2]

$$\rho = N \cdot \sum_i b_i = \frac{\delta N_A}{M} \cdot \sum_i b_i \quad (2.3)$$

where δ is the bulk density of the molecule, N_A is Avogadro's number, M is the molecular weight of the molecule and b_i is the coherent neutron scattering length of nucleus *i*. It is important to note that only coherently scattered neutrons, where phase is conserved, carry any structural information about the sample.

Scattering length density (SLD) varies irregularly between atoms. The magnitude of scattering length is determined by the quantum mechanics of the neutron-nucleus interaction. The bulk density of the sample has a great influence on the scattering length density of a sample. For polymers, the scattering length density is calculated by using the molecular formula of the monomer, since the monomer represents a scattering center. The contrast, $(\Delta\rho)^2$, is the square of the difference between the sample and the solvent/medium. When the SLD of the solvent matches that of the sample, no scattering will occur and this is called a contrast match. Contrast matching ideally allows one to

look at a specific portion of a two component system. For a diblock copolymer where one of the blocks is deuterated, the solvent can be matched to the deuterated portion of the molecule and scattering that occurs will be representative of the hydrogenated portion of the molecule.

An example of a contrast match experiment is shown in Figure 2.2, where a linear chain (gray in color) has a different SLD than the dendrimer diblock (black in color). Three different experiments can be conducted; the first allows the size and shape of the entire molecule to be obtained by placing the linear-dendrimer diblock in a solvent that has a SLD different from both blocks. Information on the dimensions of the linear block is obtained by a second experiment where the scattering length density of the solvent matches that of the dendrimer, thus the neutrons only scatter off the linear chain. Thirdly, conformational information regarding the dendrimer block is obtained by placing the system in a solvent that has a scattering length density equal to that of the linear chain.

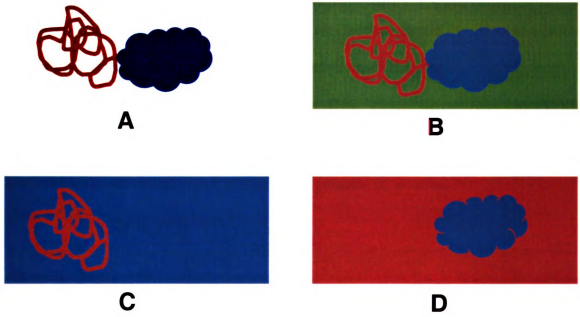

Figure 2.2. Cartoon representing information that can be obtained from a series of contrast match experiments.

A. A linear-dendrimer diblock copolymer where the linear block, red in color, has a different scattering length density than the blue colored dendrimer block. B. The solvent has a different scattering length density than both the linear and dendrimer block and neutrons scatter off the entire molecule. C. The scattering length density of the solvent matches that of the dendrimer block, thus size and shape information of the linear block is obtained from SANS. D. The scattering length density of the solvent matches that of the linear chain, thus neutrons only scatter from the dendrimer. Images in this dissertation are presented in color.

In addition to the contrast, the differential scanning cross section is related to the form factor, P(Q). P(Q) is a dimensionless function that describes how the differential scanning cross section, more commonly referred to as the intensity of scattering, is changed by neutrons scattered from different parts within the same molecule. This makes P(Q) a function of the size and shape of the molecule. Many common shapes have analytical expressions for the form factor. The two most important form factors used by a polymer chemist is the homogeneous sphere with a radius R, given by

$$P(Q) = \left[\frac{3(\sin(QR) - QR\cos(QR))}{(QR)^3} \right]^2 \tag{2.4}$$

and a Gaussian coil characterized by a radius of gyration, R_g given by

$$P(Q) = \frac{2(\exp(-Q^2R_g^2) + Q^2R_g^2 - 1)}{(Q^2R_g^2)^2} \tag{2.5}$$

where P(Q) deals with the scattering of neutrons from the same molecule, S(Q), the structure factor, describes how neutrons are scattered by different molecules within the sample. S(Q) is a dimensionless function which is dependent on the local organization within a sample and the interaction between two molecules in a sample. As a sample becomes more dilute and the probability of two molecules interacting with one another decreases, the structure factor goes to unity and is given by

$$S(Q) = 1 + \frac{4\pi N}{QV_s} \int_0^\infty [g(r) - 1] r \sin(Qr) dr \tag{2.6}$$

Here, g(r) is a density distribution function related to the radial distribution function in statistical mechanics and is usually a damped oscillatory function whose maxima

corresponds to a distance, r, of each nearest-neighbor coordination shell. The structure factor is calculated from eq 2.2, by scattering at two different concentrations, assuming that the form factor is not concentration dependent.

Dynamic Light Scattering

Dynamic light scattering, also referred to as quasielastic light scattering or photon correlation spectroscopy, is a noninvasive probe of diffusion in complex fluids.[4, 6] DLS measures the diffusion coefficient and when applied to dilute monodisperse solutions it is used to estimate the size of the molecules in solution. In a light scattering experiment, light from a laser passes through a polarizer and then through the sample. The electric field of the light induces an oscillating polarization of the electrons in the molecules. The molecules then scatter the light in a way that is characteristic of their size and shape. The basic geometry of the dynamic light scattering experiment I conducted is displayed in Figure 2.3, where light from a laser is passed though a polarizer and hits the sample. The light scattered at 90° is guided via a fiber optic cable to an actively quenched, solid state Single Photon Counting Module (SPCM). The photons are then converted to electrical pulses and correlated. Light is scattered from a homogeneous solution due to Brownian motion, which moves the solute molecules in a semi-random manner. When the solute molecules move, the light paths and phases of the waves change. These changes are directly related to the diffusion of the solute. To obtain constructive scattering, two particles need to diffuse far enough that light paths differ by about half a light wavelength. This distance is called a diffusion step and the time for the diffusion step to take place is called τ ,equal to[6]

$$\tau^{-1} = DQ^2 \qquad (2.7)$$

where τ is the time scale for the experiment, D is the diffusion coefficient of the solute species and Q is the magnitude of the scattering vector. The time scale of the experiment is important. Due to the random movement of the solute particles, the intensity at the detector is also changing randomly. Therefore intensity may either decrease or increase for small changes in time. To obtain an accurate recording of the intensity, the intensity data is subjected to the correlation function,

$$C(\delta t) = \int_0^T dt I(t) I(t + \delta t) \tag{2.8}$$

where T is the duration of the experiment and C(δt) is the correlation function. The intensity fluctuations, I(t), are sent to a digital correlator which produces the correlation function for that sample, C(t), given by

$$C(t) = A_s \exp(-2Dk^2 t) + B_l \tag{2.9}$$

where A_s is the spectral amplitude, D is the diffusion coefficient, k is the magnitude of the scattering vector and B_l is the baseline. The diffusion coefficient can be related to the size of the solute via the Stokes-Einstein equation

$$D = \frac{k_B T_a}{6\pi\eta\alpha} \tag{2.10}$$

D is the translational diffusion coefficient, k_B is Boltzmann's constant, T_a is the absolute temperature, η is the viscosity of the solvent and α is the effective Stokes radius of a sphere.

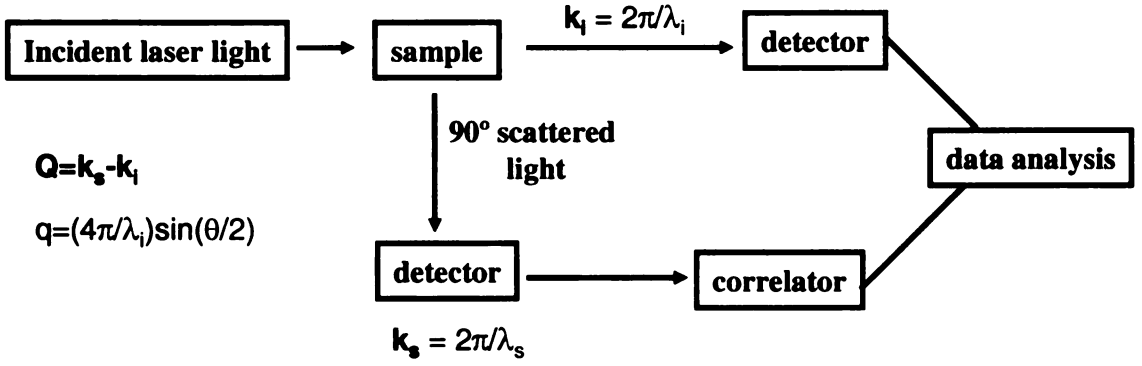

Figure 2.3. Set-up of a dynamic light scattering experiment.

References

1. Dawkins, J. V., *Developments in Polymer Characterization*. 5 ed.; Elsevier Science: New York, 1986; p 1-94.

2. King, S. M., Small-angle neutron scattering. In *Modern Techniques for Polymer Characterization*, Pethrick, R. A.; Dawkins, J. V., Eds. John Wiley & Sons: New York, 1999.

3. Higgins, J. S.; Benoît, H. C., *Polymers and Neutron Scattering*. Clarendon Press: Oxford, 2002.

4. Berne, B. J.; Pecoria, R., *Dynamic Light Scattering*. John Wiley & Sons, Inc.: New York, 1976.

5. Dahneke, B. E., *Measurement of Suspended Particles by QuasiElastic Light Scattering*. Wiley-Interscience: New York, 1983.

6. Phillies, G. D. J., *Anal. Chem.* **1990,** *62*, 1049A-1057A.

7. Arrighi, V.; Higgins, J. S., *Plastics Rubber and Composites* **2004,** *33*, 313-329.

8. Oberthur, R. C., *Revue Phys. Appl.* **1984,** *19*, 663-670.

9. Richards, R., *Adv. Poly. Sci.* **1985,** *71*, 1-39.

10. Richards, R., *J. Macrom. Sci. Chem.* **1989,** *26*, 787-815.

11. Feigin, L. A.; Svergun, D. I., *Structure Analysis by Small-Angle X-ray and Neutron Scattering*. Plenum Press: New York, 1987; p 335.

CHAPTER THREE: Conformation of Poly(styrene)-Poly(benzyl ether) Linear-Dendrimer Diblock Copolymers in Dilute Solution

Introduction

Dendrimers or dendrons are a unique class of macromolecules that have a specific molecular weight, large number of terminal groups and well-defined architecture consisting of branched units emanating from a focal point. [1-3] These unique characteristics have triggered numerous studies to use dendrimers in applications such as drug delivery,[4] light harvesting[5] and reaction catalysis.[6] It is clear that the dendrimer molecular architecture dictates its physical properties and thus enables such diverse applications to be explored. In addition, synthetic modification of dendrimers at both the focal point[7, 8] and the end group[9-11] has proven successful in expanding their utility. Further, block copolymers consisting of a linear polymer attached to the focal point[12-21] have promising applications due to their architectural asymmetry.[12-15]

In order to take full advantage of the properties of linear-dendrimer diblock copolymers their conformation in both solution and the bulk must be understood. In prior studies, the phase behavior of these molecules in the bulk has been proven to be different from traditional linear-linear diblock copolymers due to the architectural differences between each block.[12-21] It was found that both the generation number as well as the molecular weight of the linear chain dictated which morphology the hybrid diblock copolymer adopted.

The solution behavior of these diblocks has also been shown to be unique and significantly affected by the molecular asymmetry between the two blocks. For example, Gitsov and Fréchet[19] have investigated the solution properties of poly(benzyl ether) (PBE)-poly(ethylene oxide) (PEO) diblocks which are dominated by this molecular

asymmetry. Since the dendrimer and linear blocks have different solubility parameters, they examined how the solvent quality affected the intrinsic viscosity and solubility of the system as compared to linear PEO analogs. The solution behavior of a generation 4 (G4) PBE dendrimer - PEO chain was reported to be a function of the PEO molecular weight, and for PEO molecular weights of 26kDa and 46kDa, the intrinsic viscosity values were lower than that of pure PEO when in THF. This is a marginal solvent for PEO and a good solvent for the dendrimer, thus indicating the entire molecule was in a collapsed state compared to the linear chain. When the system was placed in a methanol/water solution, a good solvent for the linear block and a poor solvent for the dendrimer block, the solubility of the diblocks was dependent on the molecular weight of the linear chain being large enough to allow unimolecular micelle formation. These results indicate that the hybrids' conformations are a function of both the chain molecular weight and dendrimer generation.

A hybrid system containing a PBE dendron block was studied via intrinsic viscosity by Jeong et al.[22] Here, a G4 PBE dendrimer with a linear chain attached to its focal point was investigated and showed interesting behavior with an increase of the PS chain molecular weight. In particular, when compared to the intrinsic viscosity of linear PS, the smaller molecular weight hybrids had an intrinsic viscosity lower than a PS chain of equal molecular weight. However, a sudden intrinsic viscosity increase was observed for the hybrids between molecular weights of 60 kDa and 80 kDa to that of linear PS having molecular weights greater than 80 kDa. This suggests the overall molecular conformation of the hybrid changes with respect to the relative molecular weight of the two blocks.

While the intrinsic viscosity studies hint that the PBE-PS hybrids are capable of a conformational transformation, it is difficult to infer if one or both of the blocks changes conformation. All studies of linear-dendrimer diblock copolymers in solution thus far have focused on the conformation of the entire system.[17, 19, 22] A full understanding of the system necessitates pinpointing the relative locations and morphology of each block. Figure 3.1 illustrates three possible linear-dendrimer diblock conformational states in solution for a system where the linear and dendrimer blocks are compatible with each other. Each conformational state pertains to different relative locations of the two blocks.[23] The first state is a knitted coil, where the linear chain weaves in and out of the dendrimer, thus the dendrimer shields or partially shields the linear polymer from the surrounding environment. For this to occur, the dendrimer must have enough free volume to accommodate the linear block. A second hybrid conformation consists of the linear chain wrapping itself around the dendrimer, thus shielding the dendrimer from the surroundings and forming a unimolecular micelle. This encapsulated dendrimer state would occur when the linear block is compatible with the surrounding medium and the dendrimer less compatible, resulting in a core-shell morphology. A third potential molecular arrangement consists of the linear chain completely expelled from the cavities within the dendrimer. This could occur if there is not enough free volume within the dendrimer to contain the entire linear chain and each component has similar solubility in the solvent.[22]

Figure 3.1. Three potential conformational states of linear-dendrimer diblocks in solution: a. knitted coil b. encapsulated dendrimer c. random coil.

Distinguishing between these three states requires knowledge of the relative block locations, which was performed for the G4-PBE-PS hybrid, Scheme 3.1, in the present work. We studied three different molecular weight hybrids, 20kDa, 45kDa and 100kDa, which include the G4 PBE dendrimer (M = 3288g/mol) and linear chain molecular weights, and thus the only difference between the three hybrids is the molecular weight of the linear block. The PS chain was also deuterated (dPS) to allow small angle neutron scattering (SANS) to individually visualize each block though a series of contrast matching experiments.[24] This information can be used to ascertain the architectural structure of the two blocks.

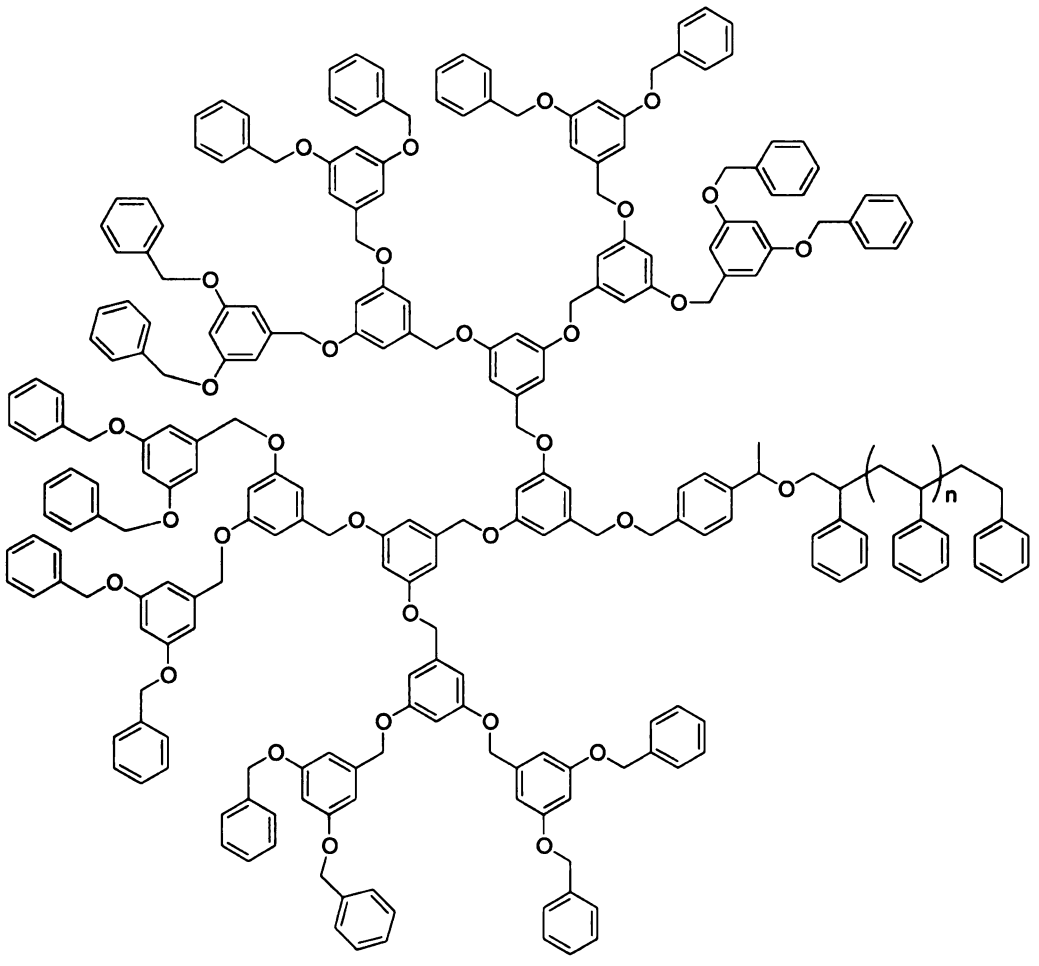

Scheme 3.1. PBE-G4-PS dendrimer-linear diblock copolymer.

Experimental

Materials. Poly (benzyl ether) dendrimers were prepared according to a previous procedure.[2] The third generation (G3) bromides were coupled with a 3,5-dihydroxylbenzyl-functionalized alkoxyamine initiator.[25] The purified fourth generation (G4) dendritic initiators were then used to prepare the hybrid dendrimer-linear diblock copolymers by standard living free radical conditions. The linear polystyrene block degree of polymerization is controlled by the molar ratio of dendritic initiator to monomer. Deuterated solvents were purchased from Aldrich Chemical Co. (St. Louis, MO) and used as received.

SANS. Measurements were taken at the small-angle neutron diffractometer (SAND) at Argonne's Intense Pulsed Neutron Source. A sample to area detector distance of 2.0 m was used. The radiation had a wavelength range of 1-14 Å making the total wave vector (Q) range covered 0.0034-0.6 $Å^{-1}$, where $Q = 4\pi\sin(\theta/2)/\lambda$ with θ and λ defined as the scattering angle and radiation wavelength, respectively. Measurements were taken at room temperature. Low concentrations were used for each sample to generate sufficient scattering in the allotted time while minimizing intermolecular scattering effects.[24] Hence consistent power laws were not observed for plots of radius versus molecular mass due to concentration effects, particularly for the higher molecular weight samples. Note the effect of concentration on the size of polymers has been extensively studied before, [26-28] here the radius was compared at a particular (low) concentration. Samples were filtered through a 0.1μm Whatman Anodisc 13 filter and sonicated for 20 minutes and placed in a hermetically sealed quartz cell for the scattering experiments. A list of samples is given in Table 3.1.

Table 3.1. Sample codes and number average molecular mass (M) of compounds used in this study[a]

Sample code	M-dendrimer(Da) /M-polystyrene (kDa)/M (kDa)	PDI[b]	Sample code	M-dendrimer(Da) /M-polystyrene (kDa)/M (kDa)	PDI[b]
G4	3288/0/3288	~1	dPS-156k	0/156/156	1.19
G4-dPS-20k	3288/16.7/20	1.06	G4-PS-46k	3288/42.7/46	1.09
G4-dPS-45k	3288/41.7/45	1.08	G4-PS-70k	3288/66.7/46	1.11
G4-dPS-100k	3288/96.7/100	1.12	G4-PS-91k	3288/87.7/91	1.15
dPS-21k	0/21/21	1.04	PS-44k	0/44.1/44.1	1.07
dPS-63.5k	0/63.5/63.5	1.10	PS-75k	0/75.2/75.2	1.17
dPS-83k	0/83/83	1.16	PS-115	0/115.3/115.3	1.08

[a] M-dendrimer represents the mass of the dendrimer, M-polystyrene, the mass of the polystyrene and M, the total mass. [b] The polydispersity index, PDI, is defined as the weight to number-average molecular mass ratio.

When the scattering length density (SLD) of the solvent matches that of the scatterer, there is a contrast match, and no coherent scattering occurs. Deuterating the linear chain makes the two blocks' SLD quite different, with the dendrimer block having a SLD of 2.03×10^{-6} Å $^{-2}$ and the dPS, a SLD of 6.42×10^{-6} Å $^{-2}$. When the G4-dPS hybrid is placed in d^8-THF (SLD = 6.35×10^{-6} Å^{-2}) the dPS chain is essentially contrast matched with the solvent and scattering only occurs from the dendrimer block. The linear block was investigated using a solvent combination of 79:21 h^6 benzene:d^6 benzene (SLD of 2.07×10^{-6} Å $^{-2}$) which provides a contrast match to the G4 PBE dendrimer and thus scattering only occurs from the linear block. Performing both of these contrast match experiments on the three molecular weight hybrids and comparing the behavior of each block to that of a native PBE dendrimer or dPS chain in the same solvent, allowed the conformation of each block to be determined as well as the overall conformation of the diblock.

Neutron scattering data for hybrids were analyzed in the Guinier regime.[29] This analysis allowed for quick determination of the shape and size of the dendrimer as models for compact-objects, rods, and sheets were applied to all samples. The scattering intensity, I(Q), in the low Q regime was evaluated using the expression for compact ('sphere-like') objects with a given radius of gyration (R_g),[30]

$$I(Q) \approx \phi V_s (\Delta\rho)^2 \exp\left(-\frac{Q^2 R_g^2}{3}\right) \equiv I(0)\exp\left(-\frac{Q^2 R_g^2}{3}\right) \qquad (3.1)$$

where ϕ is volume fraction of scattering centers, V_s, the volume of each scattering center, $(\Delta\rho)^2$, the square of the difference of the solvent and the scatterer SLD and I(0), the intensity at zero wave vector. The slope resulting from a plot of ln(I(Q)) versus Q^2 in the region where $QR_g \cong 1$ allows R_g to be obtained. The radius of a homogeneous, constant density sphere is determined from the R_g by $R = 0.775 \times R_g$.

A modified Guinier analysis for rod-like objects approximates the scattering intensity in the low Q regime by[30]

$$QI(Q) \approx \frac{\pi\phi V (\Delta\rho)^2}{L} \exp\left(\frac{-Q^2 R_c^2}{2}\right) \equiv QI(0)\exp\left(\frac{-Q^2 R_c^2}{2}\right) \qquad (3.2)$$

where L is the rod length and R_c is the root-mean-square of the distances of all of the atoms in a cross-section of the rod to the centroid of this cross-section determined from the slope in a plot of ln(Q(I(Q)) versus Q^2, in the region of Q where $QR_c \cong 1$. The radius of the rod (R_r) is obtained by $R_c\sqrt{2}$. A sheet-like particle, which is much smaller in one dimension than the other two, has, [30]

$$Q^2 I(Q) \approx \frac{2\pi\phi V(\Delta\rho)^2}{A} \exp\left(\frac{-Q^2 T_s^{\,2}}{12}\right) \equiv Q^2 I(0) \exp\left(\frac{-Q^2 T_s^{\,2}}{12}\right) \quad (3.3)$$

where A is the area of the particle and T_s, the sheet thickness and is valid when $QT_s < \sqrt{12}$.

To determine the goodness of each Guinier fit, the experimental value of I(0) or QI(0) was used to determine the amount of solvent within each sample and check that the mass density of the swollen dendrimer is reasonable. The numerical prefactors of equations 3.1 and 3.2 were set equal to the experimental value of I(0) and QI(0) respectively and then solved for $(\Delta\rho)^2$. Using this value of $(\Delta\rho)^2$ and the scattering length density of the solvent (ρ_{solv}) we calculated the scattering length density of the scatterers (ρ_{scat}), which includes solvent and dendrimer. We calculated the amount of solvent within the dendrimer by,

$$(\rho_{scat}) = [\rho_{solv}]\times\theta + [1-\theta]\times\rho_{sample}] \quad (3.4)$$

where θ is the mass fraction of solvent within the scatterer and ρ_{sample} is the scattering length density of the dendrimer.

Neutron scattering data was also analyzed by fitting I vs Q to the form factor of a solid sphere or Gaussian coil when appropriate. We also used Holtzer plots[31] to reveal coil-like and rod-like behavior.

Dynamic Light Scattering (DLS). Measurements were performed with a Protein Solutions Dyna Pro-MS/X system with temperature control. All samples were filtered as described above and allowed to equilibrate in the instrument for 25 minutes at 25 °C before measurements were taken resulting in calculation of the hydrodynamic radius (R_h). The sample is illuminated by a semi-conductor laser with ~ 830 nm wavelength. The light scattered at an angle of 90° is collected and guided via a fiber optic cable to an

actively quenched, solid state Single Photon Counting Module (SPCM), where the photons are converted to electrical pulses and correlated. Autocorrelation is used to analyze the time scale of the scattered light intensity fluctuations. The uniformity of the sample sizes is determined by a monomodal curve fit, cumulants, which assumes a single particle size with a Gaussian distribution.

Results and Discussion

Conformation of PBE Dendrimer

The molecular morphology of the G4-PBE dendron samples was investigated in both d^6-benzene and d^8-THF using the three Guinier analyses mentioned above to determine the influence of solvent on the size and shape of the dendrimer block. The dendrimers behave as sphere-like objects in both d^6-benzene and d^8-THF due to the observed negatively sloped straight line in the Guinier plots for compact objects (Figure 3.2). It is evident from the Guinier fits in Figure 3.2 that the dendrimer is larger in d^6-benzene than in d^8-THF, with radii values of 1.73 ± 0.03 nm and 1.35 ± 0.04 nm, respectively. These sizes agree reasonably well with radii values reported by Tande et al.[12] of 1.93 ± 0.1 nm and 1.50 ± 0.1 nm in d^6-benzene and d^8-THF, respectively. Using the experimental value of I(0) (Table 3.2) the mass fraction of solvent (θ) within the dendrimer was calculated by eq 3.4 as described above and found to be 0.45 and 0.51 for d^8-THF and d^6-benzene, respectively.

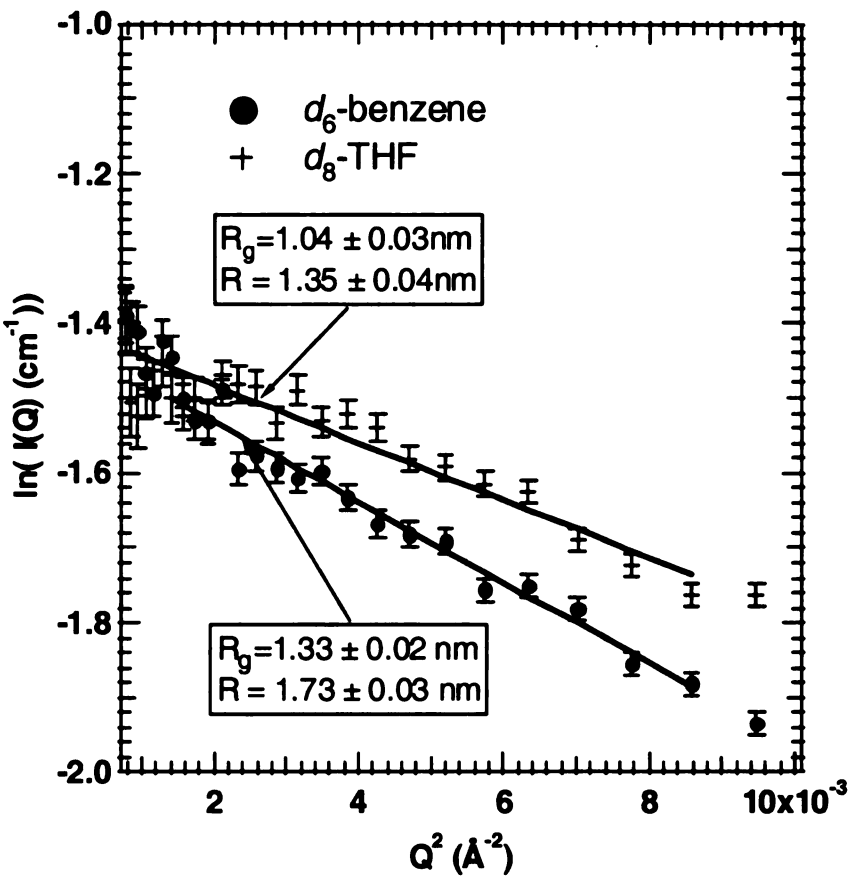

Figure 3.2. Guinier analysis for PBE G4 dendrons in d^6-benzene and d^8-THF at a concentration of 50 mg/mL, data fit for a compact (sphere-like) object.

Table 3.2. Values for R_g and R_c determined from Guinier analyses described in the text at a concentration of 50 mg/mL.

Symbols are explained in the text while Q_{max} is the maximum Q-value used in the regression.

Sample code →	**G4**	**G4**	**G4-dPS-20k**	**G4-dPS-45k**	**G4-dPS-100k**
solvent	d^8-THF	d^6-benzene	d^8-THF	d^8-THF	d^8-THF
scattering from	dendrimer	dendrimer	dendrimer	dendrimer	dendrimer
R_g (nm)[a]	1.04 ± 0.03	1.33 ± 0.02	1.40 ± 0.01	na[b]	na
$I(0)_{exp}$[c] **(cm^{-1})**	0.241 ± 0.002	0.245 ± 0.002	0.062 ± 0.003	na	na
$Q_{max}*R_g$	0.919	1.13	1.35	na	na
R_c (nm)[d]	na[e]	na	na	2.70±0.28	2.62±0.29
$QI(0)_{exp}$[f] **($Å^{-1}cm^{-1}$)**	na	na	na	(2.50±0.4) $\times 10^{-3}$	(3.7±2.0) $\times 10^{-3}$
$Q_{max}*R_c$	na	na	na	1.006	0.976
θ[g]	0.45	0.51	0.56	0.82	0.78

[a] Radius of gyration for a sphere-like object. [b] Attempts to fit data to a sphere-like object failed for these samples. [c] Experimental value of I(0) from a sphere-like object Gunier plot (eq1). [d] Cross sectional radius for a rod. [e] Attempts to fit data to a rod-like object failed for these samples. [f] Experimental value of QI(0) from a rod-like object Gunier fit (eq 3.2). [g] θ is the mass fraction of solvent within the scatterers.

The G4 PBE dendrimer is larger than its minimum solution radius, 1.09 nm in chloroform, which is close to the value expected if the dendrimer collapses to its bulk density,[22] indicating the dendrimer is in an expanded state in both d^6-benzene and d^8-THF. A solvent dependence on size is a well known property of linear polymers and has been previously observed in dendrimers.[22] While the dendrimer size has changed with solvent quality, the shape has remained 'sphere-like.' Further contrast variation studies of the dendrons need be conducted to determine the overall segment distribution and whether this distribution changes with solvent.[32-34]

These structural changes may be delineated in part by measuring the hydrodynamic radius, R_h, of the G4-PBE dendrimers in both d^6-benzene and d^8-THF. An R_h of 1.70 ± 0.02 nm was obtained in both solvents making the ratio of R_g/R_h = 0.79 ± 0.03 for d^8-THF and 1.02 ± 0.03 for d^6-benzene. This ratio is a quantitative indicator of molecular conformation,[35] where an R_g/R_h ratio of $\sqrt{(3/5)} \approx 0.775$ indicates a constant density, homogeneous sphere, 1.50 describes a monodisperse Gaussian coil in a theta solvent and 1.78 represents linear polymers in a good solvent[36, 37] although experiments show values of 1.16 and 1.27 for linear polymers in theta solvents.[37, 38] The R_g/R_h ratios for the dendrimer suggest a more spherical nature in both d^8-THF and d^6-benzene indicating a significantly different structure in solution as compared to random-coil linear polymers under analogous conditions. The ratio also suggests that the dendron behaves as a constant density (expanded) sphere in d^8-THF implying backfolding of end groups.[39, 40] It should be noted that this effect is not due to poor dendrimer-solvent interactions as the solubility parameter of the dendrimer has been found to be similar to that of benzene and

THF while the radius of the dendrimer is larger in both solvents than the minimum possible value of 1.09 nm. [22]

Conformation of Dendrimer Block

The dendrimer block conformation within the hybrid block copolymers was determined by dissolving the G4-PBE-dPS diblocks in d^8-THF, which is a contrast match for the dPS block. Two different concentrations were analyzed, 4 mg/mL and 50 mg/mL, for the hybrids with molecular weights of 20kDa, 45kDa and 100kDa, noting there are insignificant differences observed for the dendrimer block size at these two concentrations.

By fitting the scattering data of the G4-PBE-dPS 20kDa hybrid in d^8-THF at a concentration of 50 mg/mL with a Guinier analysis for compact objects (eq. 3.1), Figure 3.3, a radius of 1.82 ± 0.01 nm for the dendrimer block was found, which is appreciably larger that the radius of the 'free' dendrimer in the same solvent, 1.35 ± 0.04 nm. The mass fraction of solvent and dPS within the dendrimer is 0.56 (Table 3.2), which is higher than the value for the corresponding free dendrimer in d^8-THF, 0.45. Since the hybrids' dendrimer block is more swollen than the corresponding free dendrimer, there is more mass, i.e. linear dPS block and solvent, occupying the free volume within the dendrimer. Attempts to fit scattering data for the dendron as a rod-like object (eq 3.2) failed as shown in the inset of Figure 3.3. The sheet-like architecture (eq 3.3) also did not represent the scattering data for any of the samples and will not be mentioned further.

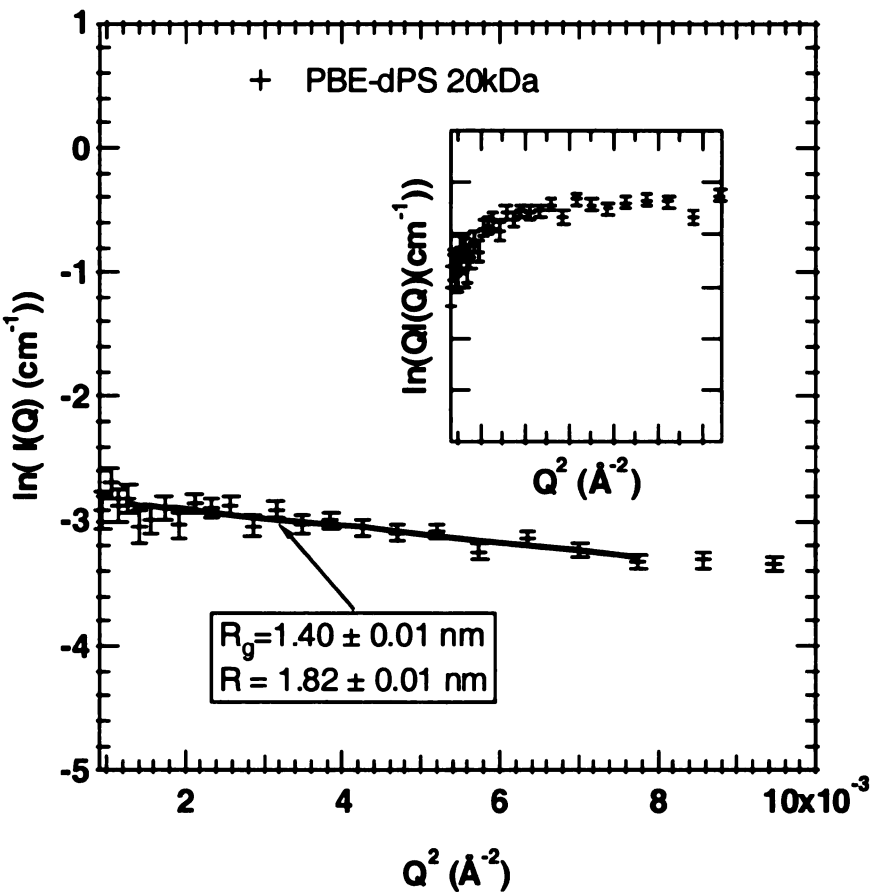

Figure 3.3. Guinier analysis for PBE-dPS 20kDa system in d^8-THF.

Dendrimer block is scattering as a sphere-like object. Inset is a modified Guinier analysis for a rod-like object, which does not represent the data.

The dendrimer block of the next higher molecular weight G4-PBE-dPS hybrid (45kDa) was subsequently studied in d^8-THF at a concentration of 50 mg/mL using a Guinier analysis for compact objects, see Figure 3.4. Attempts to make a linear fit with the 'sphere-like' morphology failed, as evidenced by the non-linear behavior at small Q as displayed in the inset of Figure 3.4. The Guinier analysis for rod-like objects (eq 3.2) proved successful, Figure 3.4, with a substantial increase in the dendron size and an R_c value of 3.81 ± 0.39 nm, which is comparable to the maximum possible radius of ~3.6 nm and corresponding to the dendrons in an a fully extended state. This is a much larger dendrimer radius as compared to both the 'free' dendrimer radius, 1.35 ± 0.04 nm, and the dendrimer block of the 20kDa hybrid, 1.82 ± 0.01 nm, and will be discussed in greater detail below.

We performed a Guinier analysis for the G4-PBE-dPS 100kDa hybrid in d^8-THF at a concentration of 50 mg/mL and found that the dendrimer block behaves analogously to that of the 45kDa system, scattering as a rod-like object as opposed to a sphere, Figure 3.5. The model fit results in a dendrimer radius of 3.40 ± 0.38 nm, which matches the size of the 45kDa dendrimer block considering experimental error. As for the 45kDa system, attempts to fit the 100kDa hybrid's data to a Guinier analysis for a sphere failed due to non-linear behavior at small values of Q, inset of Figure 3.5.

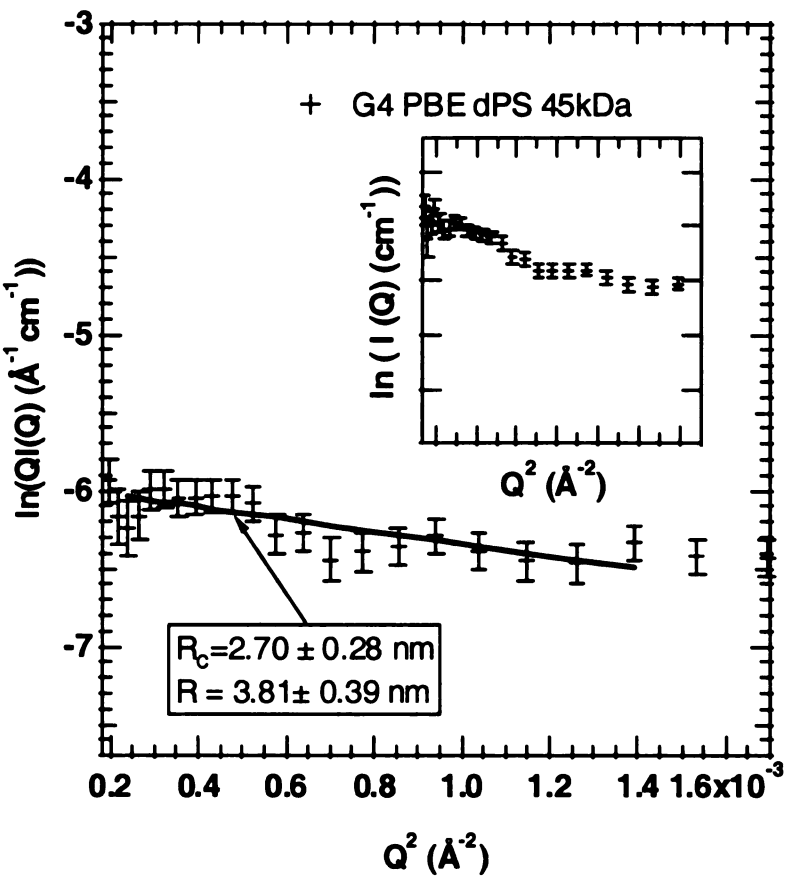

Figure 3.4. Rod-like Guinier analysis for PBE-dPS 45kDa hybrid in d^8-THF at a concentration of 50 mg/mL.

Inset shows the attempted representation of data to Guinier fit for compact object.

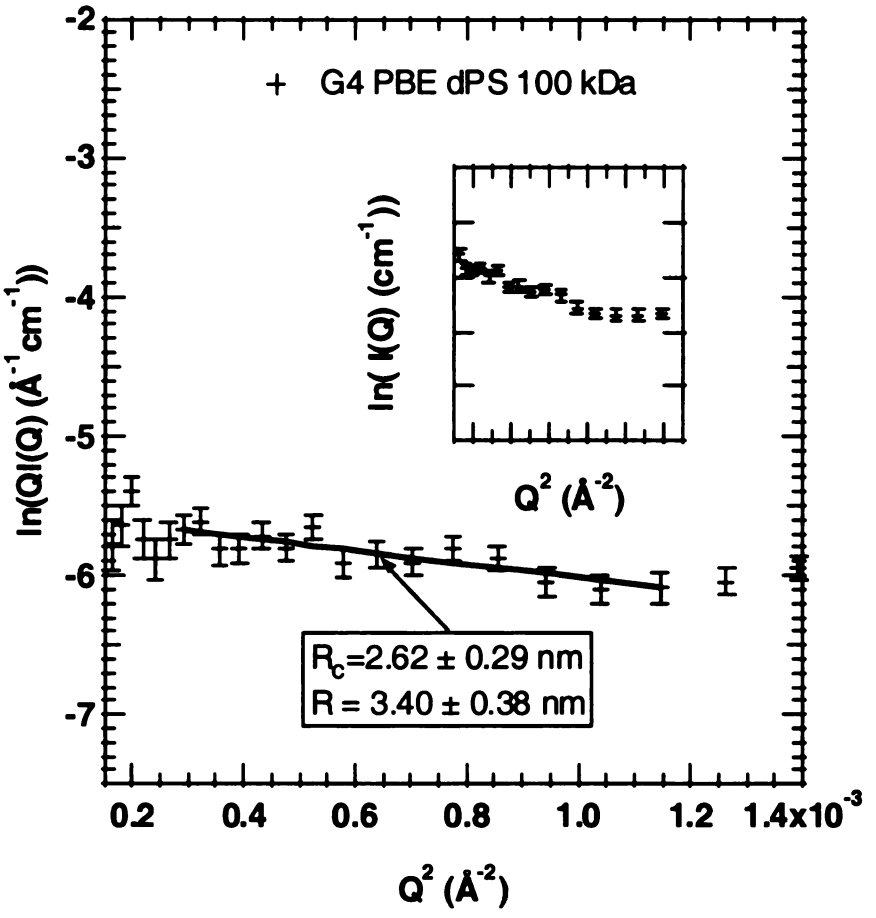

Figure 3.5. Rod-like Guinier analysis for PBE-dPS 100kDa hybrid in d^8-THF at 50mg/mL.
Inset is the Guinier analysis for compact-object, which is a poor fit due to curvature.

These contrast match experiments revealed that the dendrimer block's size and shape is dependent upon the linear block molecular weight. The G4-PBE-dPS-20kDa hybrid has a dendrimer block where the branches adopt a 'sphere-like' shape, Figure 3.3, just as the free dendrimer in solution, Figure 3.2, yet the size of this sphere is approximately 35% larger in the hybrid system (> 2× change in volume). The difference in size between the hybrid's dendrimer block and the free dendrimer in solution is probably due to the linear chain occupying space within the dendrimer, resulting in swelling and possible development of the knitted coil morphology shown in Figure 3.1. The two higher molecular weight systems, G4-PBE-dPS 45kDa, Figure 3.4, and G4-PBE-dPS 100kDa, Figure 3.5, did not show the expanded sphere-like morphology and instead these two systems have dendrimer blocks that are 'rod-like' in shape (eq 3.2). According to the model, the cylinder radius for the 45kDa and 100kDa systems has values of 3.81 ± 0.39 nm and 3.40 ± 0.38 nm, respectively, making the cylinder length of order 0.1 nm suggesting a disc-like morphology. Fitting the I vs. Q data with the disc form factor, similar in form to eq 3.3, was unsuccessful.

Evidence of the dendrimer's change in structure from a sphere-like object to a more expanded 'rod-like' structure is supported by fitting the scattering data to a Holtzer plot,[31] a plot of Q × I vs. Q where a peak in this plot indicates a coil or sphere and a plateau indicates a rod-like object or a more expanded structure. Holtzer plots of the G4-PBE dendron in both d^6-benzene (Figure 3.6) and d^8-THF (Figure 3.7) result in a peak indicating a more compact coil-like structure, which agrees with the Guinier analyses that shows these dendrimers are spherical. The Holtzer plot of G4-PBE-dPS 20kDa in d^8-THF (Figure 3.8), which is only scattering from dendrimer, also shows a peak and agrees

with the Guinier analysis that the dendrimer block is a sphere-like object. The Holtzer plots of the G4-PBE-dPS 45kDa and G4-PBE-dPS 100kDa in d^8-THF, Figures 3.9 and 3.10 respectively show no peak, indicating the dendrimer blocks of these hybrids are in a more expanded state.

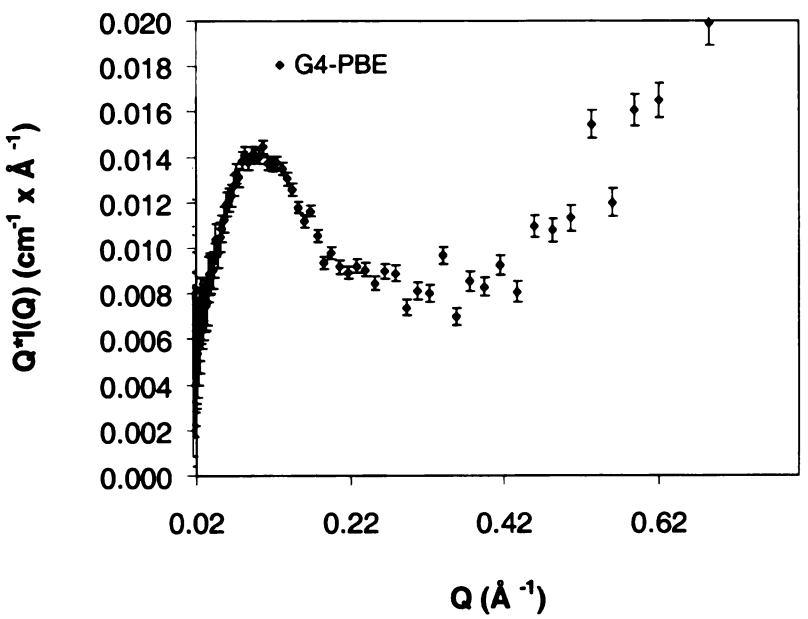

Figure 3.6. Holtzer plot (QI vs. Q) of G4-PBE in d^6-benzene at 50 mg/mL. A peak indicates that the dendrimer is in a coil-like or sphere-like state.

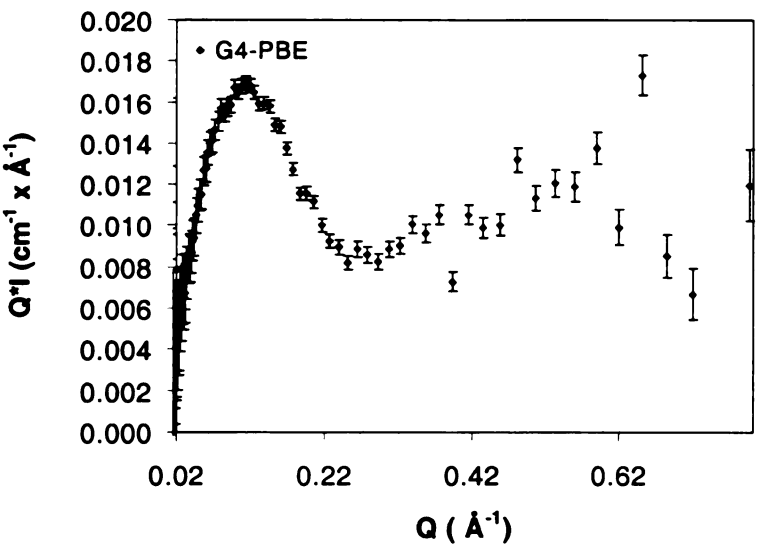

Figure 3.7. Holtzer plot (QI vs. Q) of G4-PBE in d^8-THF at 50 mg/mL. A peak indicates that the dendrimer is in a coil-like or sphere-like state.

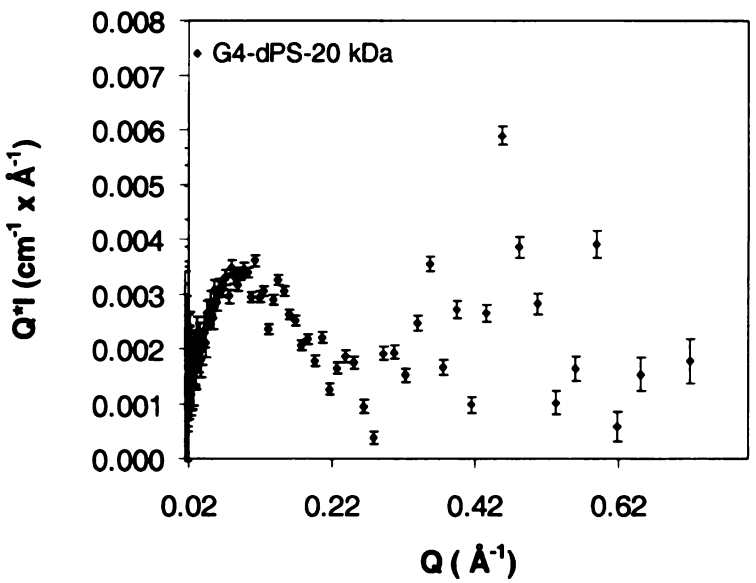

Figure 3.8. Holtzer plot (QI vs. Q) of G4-dPS-20 kDa in d^8-THF at 50 mg/mL. A peak indicates that the dendrimer is in a coil-like or sphere-like state.

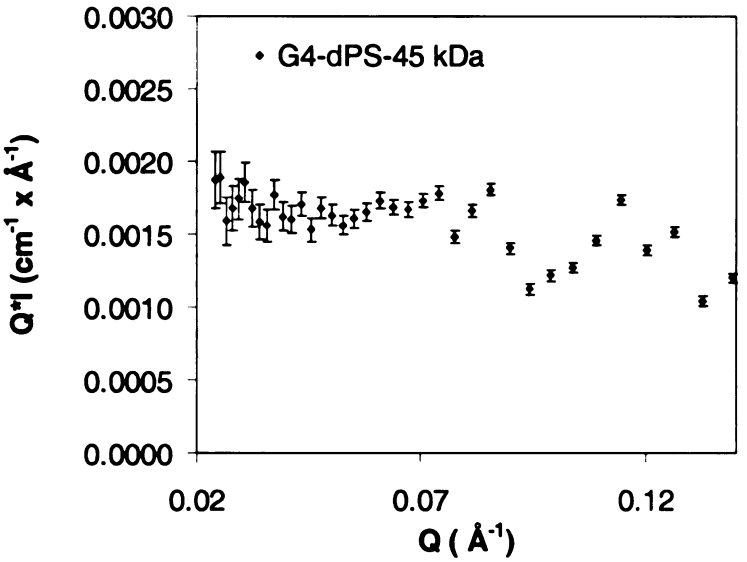

Figure 3.9. Holtzer (QI vs. Q) plot of G4-dPS-45 kDa in d^8-THF at 50 mg/mL. There is no peak in this plot indicating the dendrimer block of the hybrid is in a more expanded or stretched out state as opposed to a coil or sphere.

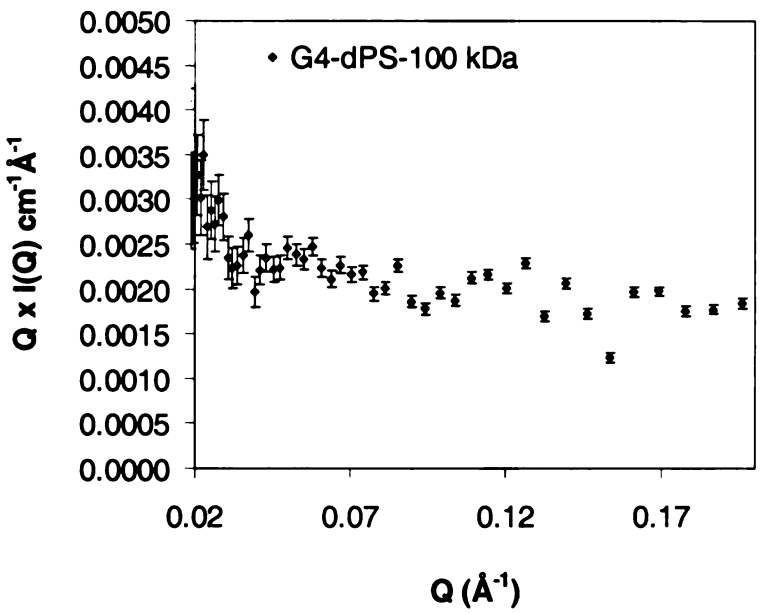

Figure 3.10. Holtzer (QI vs. Q) plot of G4-dPS-100 kDa in d^8-THF at 50 mg/mL. There is no peak in the plot indicating the dendrimer block of the hybrid is in a more expanded or stretched out state as opposed to a coil or sphere.

Further, due to the large solvent mass fractions of 0.82 and 0.78 calculated from the rod-like Guinier fit of the dendron blocks of the 45kDa and 100kDa systems respectively, see Table 3.2, the dendrimer molecule it is not expected to adopt a rod-like conformation. Rather, it is believed that the actual conformation of the dendrimer block for the 45kDa and 100kDa hybrids is that of a distorted wedge or "ice-cream cone." This molecular arrangement explains why a Guinier analysis for sheet-like objects failed and morphological equivalence between the cone and rod is expected to follow eq 3.2. In fact the results given by Hjelm[41] show the Guinier expression for a finite size cone should follow (see Hjelm's eq 19)

$$QI(Q) \approx 0.2\phi R^2 (\Delta\rho)^2 \exp\left(\frac{-Q^2[R_c^2]}{2}\right) \tag{3.5}$$

for Q < 1/L and where R is the radius of the cone's base and $[R_c^2]$ represents a "weight" average radius. The numerical prefactor in eq 3.5 reduces the value of QI(0) to numbers of order 10^{-3} $Å^{-1}cm^{-1}$ in better agreement with the experimental values than those given in Table 3.2 for a true rod. To justify the cone-shaped dendrimer block, we set the experimental values of QI(0) equal to the numerical prefactor of eq 3.5 by using known values of ϕ and estimated value of R to find $(\Delta\rho)^2$ and θ, listed in Table 3.3. The resulting θ values are more reasonable than those from the rod-like fit (Table 3.2) indicating the dendrimer block is more cone-like. While the exact dendron shape is difficult to fully ascertain, the data support the conclusion that the shape of the free dendrimer and 20kDa hybrid's dendron block is quite different from that of the 45 and 100 kDa hybrid's dendrimer block.

Table 3.3. Experimental QI(0) values were set equal to the numerical prefactor of the Guinier expression for a finite sized cone, eq 3.5, with various R values representing the radius of the cone's base.

Sample Code ↓	R (nm)[a]	$(\Delta\rho)^2$ (cm^{-4})[b]	θ[c]
G4-dPS-45k[d]	2	8.68×10^{13}	0.32
	2.5	5.56×10^{13}	0.45
	3	3.86×10^{13}	0.55
G4-dPS -100k[d]	2	1.28×10^{13}	0.17
	2.5	8.22×10^{13}	0.34
	3	5.71×10^{13}	0.45

[a] Radius of cone's base, various values tried. [b]Experimental value of the difference in scattering length density between the scatterer and the solvent found by equating experimental QI(0) values to numerical prefactor in eq 3.5. [c] Mass fraction of solvent and possibly linear dPS within dendrimer, eq 3.4.

Conformation of Linear Block

It is apparent that the relative molecular weights of the linear and dendrimer blocks play a key role in the subsequent morphology of the dendrimer block, yet complete information on the location of the two blocks in solution cannot be made without characterizing the linear block of the hybrids. This was done by placing the G4-PBE-dPS hybrids in a solution of 79:21 h^6-benzene: d^6-benzene, which is a contrast match for the dendrimer. The concentration used for these experiments was 4 mg/mL and the radius of gyration of the linear block was obtained by plotting I(Q) versus (Q) and fitting the profile to the form factor of a Gaussian coil.[32] To compare the behavior of the linear block to that of 'free' dPS in the same solvent, we ran scattering experiments on dPS with molecular weights of 18kDa, 63kDa, 83kDa and 155kDa under the same

conditions with similar data interpretation. A plot of the radius of gyration versus molecular weight was used to compare the size difference between the linear block of the hybrids to that of a free dPS chain of comparable molecular weight. Figure 3.11 shows that the two lower molecular weight hybrids, 20kDa and 45kDa, have a linear block that falls below the size of the analogous 'free' dPS chain, indicating the dPS block of the hybrid is in a more compact state for these two systems. The 100kDa hybrid's linear block is approximately the same size as the 'free' linear chain, suggesting that it expands in solution to the size of the corresponding dPS chain. These results match the intrinsic viscosity data of Jeong et al.[22] who studied the analogous non-deuterated forms of the hybrids in benzene.

To verify that the observations from the contrast match experiments are independent of solvent type and deuteration effects we performed two additional series of experiments. First, the size of G4-PBE-PS hybrids with molecular weights of 46 kDa, 70 kDa and 91 kDa in d^8-THF was compared to PS in d^8-THF, all solutions were at a concentration of 4 mg/mL, see Figure 3.12. The radius of gyration for the G4-PBE-PS hybrid and the 'free' linear PS was again found by fitting the I(Q) – Q data to the form factor for a Gaussian coil.[32] This value is similar to that found by using a compact sphere Gunier analysis. As seen in the figure the 46 kDa hybrid has a smaller R_g than a PS chain of an equal molecular weight, indicating that the hybrid is in a collapsed state. The 70 kDa and 91 kDa hybrids have a R_g that is equal to or greater than its corresponding "free" PS chain. These results agree with those in Figure 3.11. Both indicate that hybrids below a molecular weight of ~ 45 kDa are more collapsed than those above ~ 70 kDa, and this

collapsed state transition correlates with the transition in dendron block conformation. Further, the two solvents do not affect the transition for these systems.

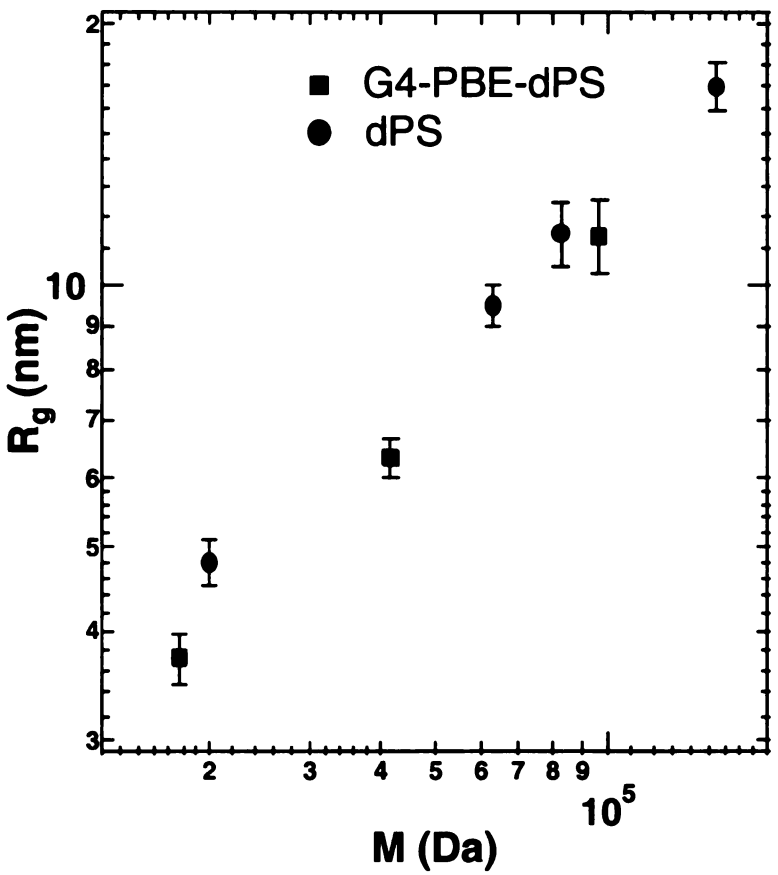

Figure 3.11. A plot of radius of gyration versus molecular weight for both the dPSblock of the hybrids and dPS in 79:21 h^6:d^6 benzene at 4 mg/mL.
The two lower molecular weight hybrids fall below the size of the corresponding dPS linear chains, indicating a collapsed state for the two hybrids' linear block.

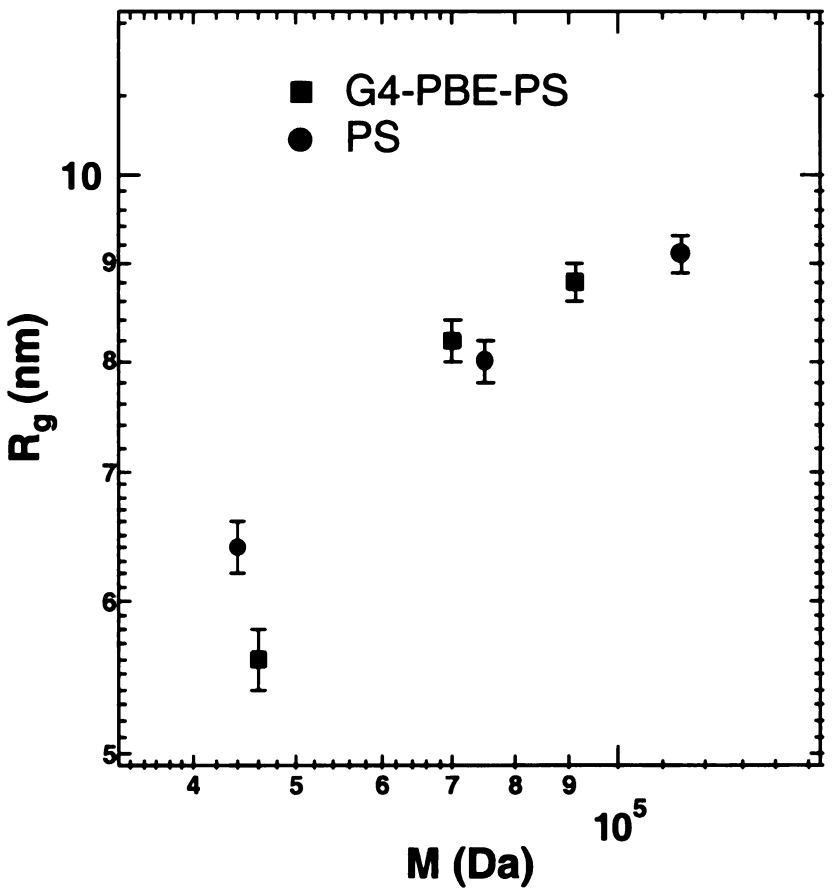

Figure 3.12. A plot of radius of gyration versus molecular weight for G4-PBE-PS hybrids and PS in d^8-THF at a concentration of 4 mg/mL.
The 46 kDa G4-PBE-PS hybrid's size is below that of the corresponding PS linear chain, indicating a collapsed state. The R_g's of the 70 kDa and 91 kDa G4-PBE-PS hybridsare approximately equal to that of a corresponding linear PS chain indicating a non-collapsed state for these systems.

To rule out the possibility of deuteration effects between the linear block and the solvent, we studied G4-PBE-PS hybrids and linear PS in THF at a concentration of 4 mg/mL via DLS to determine R_h, see Figure 3.13. The 46 kDa hybrid has a smaller R_h than a corresponding PS chain, again demonstrating it is in a collapsed state. The 70 kDa and 91 kDa hybrids have an R_h that is larger than the corresponding PS chain similar to the R_g results for the deuterated material.

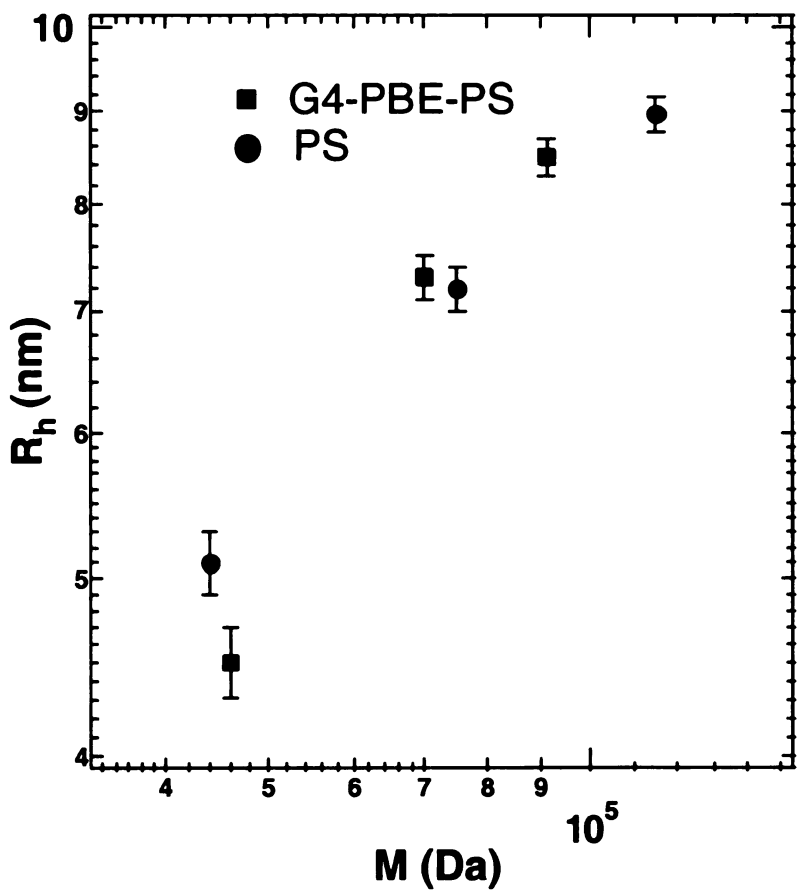

Figure 3.13. A plot of hydrodynamic radius versus molecular weight for G4-PBE-PS hybrids and PS in THF at a concentration of 4 mg/mL.
The 46 kDa G4-PBE-PS hybrid's size is below that of the corresponding PS linear chain, indicating a collapsed state. The 70 kDa and 91 kDa G4-PBE-PS hybrids' R_h is larger than the corresponding linear PS chain.

We hypothesized that the 20kDa hybrid has the conformation of a knitted coil for the conditions studied (Figure 3.1). This hypothesis is supported by data that show the dendrimer block is a spherical object with a radius about 1 nm larger that the corresponding 'free' dendrimer, as well as a linear block that is more contracted than its native PS chain. A more contracted linear block potentially indicates that the linear chain is weaving in and out of the dendrimer free volume, thus occupying a smaller space than if it were a free chain in solution. Comparing the size of the linear block, 3.75 ± 0.25 nm, to the size of the dendrimer block, 1.82 ± 0.01 nm, shows that some of the linear block can be shielded by the dendrimer. Our data for this system do not support an encapsulated dendrimer conformation since attempts to fit the SANS data of this system to a core-shell morphology failed.

In the 45kDa system, the linear block is in a more compact form than a free dPS chain, similar to the 20 kDa system. However, the dendrimer has adopted an extended form rather than a sphere. Further, the 100kDa hybrid adopted a form where the linear block is essentially equivalent to an unattached linear molecule with a cone-like dendrimer attached to it. We believe that the increase in molecular weight triggered a change from the spherical to an extended/cone-like morphology allowing the linear chain to maximize the system entropy. This is the hypothesis advanced by Jeong et al.[22] following the ideas of Skvortsov et al.[42] Basically, a chain tethered in a high energy region (dendrimer) next to a lower energy one (free solvent) will adopt a random walk if its tethered far from the interface and is of small molecular weight. However, increasing the molecular mass allows greater sampling of the lower energy region until the chain straightens within the high energy space and adopts a random walk in the low energy

region. This appears to be similar to what we observe except the dendrimer (high energy region) is flexible and changes shape to minimize contact with the linear macromolecule. Skvortsov et al. [42] clearly demonstrate that the key to this transition is the relative size of the chain to tethering distance and so it is expected that the dendrimer generation will influence the molecular weight at which the morphological change occurs.

Conclusion

The conformation of linear-dendrimer diblock copolymers in solution can be probed by deuterating one block and performing a series of SANS contrast match experiments. It was found for the G4-PBE-dPS system that there is a transition from a knitted to random coil conformation upon increasing the relative molecular weight of the linear block to the dendrimer block. Further, the dendron changes shape from spherical to an extended, cone-like structure. This unexpected transition is expected to be driven by the linear chain maximizing its entropy at the expense of the dendrons. We believe this shape change, if triggered through external stimuli, can be exploited in the design of a range of advanced materials ranging from sensors to molecular machines. Future research will examine these issues and the development of a viable system.

References

1. Newkome, G. R.; Moorefield, C. N.; Vögtle, F., *Dendritic Molecules: Concepts, Syntheses, Perspectives*. John Wiley & Sons: New York, 1996.

2. Hawker, C. J.; Fréchet, J. M. J., *J. Am. Chem. Soc.* **1990,** *112*, 7638-7647.

3. Tomalia, D.; Baker, H.; Dewald, J.; Hall, M.; Kallos, G.; Martin, S.; Roeck, J.; Ryder, J.; Smith, P., *Poly. J.* **1985,** *17*, 117-132.

4. Chen, H.; Neerman, M. F.; Parrish, A. R.; Simanek, E. E., *J. Am. Chem. Soc.* **2004,** *126*, 10044-10048.

5. Hahn, U.; Gorka, M.; Vogtle, F.; Vicinelli, V.; Ceroni, P.; Maestri, M.; Balzani, V., *Angew. Chem. Int. Ed.* **2002,** *41*, 3595-3598.

6. Murugan, E.; Sherman, R. L.; Spivey, H. O.; Ford, W. T., *Langmuir* **2004,** *20*, 8307-8312.

7. Vestberg, R.; Nilsson, C.; Lopes, C.; Lind, P.; Eliasson, B.; Malmstrom, E., *J. Polym. Sci. A: Polym Chem.* **2004,** *42*, 2784.

8. Chiba, H.; Tsuruta, M.; Shiki, S.; Higuchi, M.; Yamamoto, K., *Nature* **2002,** *415*, 509-511.

9. Barbera, J.; Donnini, B.; Gimenez, R.; Guillon, D., *J. Mat. Chem* **2001,** *2001*, 2808-2813.

10. Sashiwa, H.; Shigemasa, Y.; Roy, R., *Macromolecules* **2001,** *24*, 3211-3214.

11. Percec, V.; Chow, W.; Ungor, G., *J. Am. Chem. Soc.* **2000,** *122*, 10273-10281.

12. Tande, B. M.; Wagner, N. J.; Mackay, M. E.; Hawker, C. J.; Vestberg, R.; Jeong, M., *Macromolecules* **2001,** *34*, 8580-8585.

13. Chapman, T. M.; Hillyer, G. L.; Mahan, E. J.; Schaffer, K. A., *J. Am. Chem. Soc.* **1994,** *116*, 11195-11196.

14. Cho, B. K.; Jain, A.; Gruner, S. M.; Wiesner, U., *Science* **2004,** *305*, 1598-1601.

15. Pochan, D. J.; Pakstis, L.; Huang, E.; Hawker, C.; Vestberg, R.; Pople, J., *Macromolecules* **2002,** *35*, 9239-9242.

16. vanHest, J. C. M.; Delnoye, D. A. P.; Baars, M. W. P. L.; vanGenderen, M. H. P.; Meijer, E. W., *Science* **1995,** *268*, 1592-1595.

17. Santini, C. M. B.; Johnson, M. A.; Boedicker, J. Q.; Hatton, T. A.; Hammond, P. T., *J. Polym. Sci. A: Polym. Chem.* **2004,** *42*, 2784-2814.

18. Aoi, K.; Motoda, A.; Okada, M.; Imae, T., *Macromol. Rapid. Comm.* **1997,** *18*, 945-952.

19. Gitsov, I.; Fréchet, J. M. J., *Macromolecules* **1993,** *26*, 6536-6537.

20. Frechet, J. M. J.; Dao, J.; Hawker, C. J.; Leduc, M. R., *J. Am. Chem. Soc.* **1996,** *118*, 11111-11118.

21. Mackay, M. E.; Jeong, M.; Hong, Y.; Hong, S.; Gido, S. P.; Tande, B.; Wagner, N. J.; Hawker, C. J.; Vestberg, R., *Macromolecules* **2002,** *35*, 8391 -8399.

22. Jeong, M.; Mackay, M. E.; Hawker, C. J.; Vestberg, R., *Macromolecules* **2001,** *34*, 4927-4936.

23. Tande, B. M.; Wagner, N. J.; Mackay, M. E., *Comptes Rendus Chimie* **2003,** *6*, 853-864.

24. King, S. M., Small-angle neutron scattering. In *Modern Techniques for Polymer Characterization*, Pethrick, R. A.; Dawkins, J. V., Eds. John Wiley & Sons: New York, 1999.

25. Benoit, D.; Chaplinski, V.; Braslau, R.; Hawker, C. J., *J. Am. Chem. Soc.* **1999,** *121*, 3904-3392.

26. de Gennes, P. G., *Scaling Properties in Polymer Physics*. Cornell University Press: Cornell, 1979.

27. Akcasu, A. Z.; Hammouda, B., *Macromolecules* **1983,** *16*, 951-956.

28. Takahashi, Y.; Matsumota, N.; Iio, S.; Kondo, H.; Noda, I.; Imai, M.; Matsushita, Y., *Langmuir* **1999,** *15*, 4120-4122.

29. Guinier, A. F., G, *Small Angle Scattering of X-Rays*. John Wiley & Sons, Ltd: New York, 1955.

30. Gallas, J. M.; Littrell, K. C.; Seifert, S.; Zajac, G. W.; Thiyagarajan, P., *Biophys. J.* **1999,** *77*, 1135-1142.

31. Holtzer, A., *J. Poly. Sci.* **1955,** *17*, 432-434.

32. Higgins, J. S.; Benoit, H. C., *Polymers and Neutron Scattering*. Clarendon Press: Oxford, 1994.

33. Potschke, D.; Ballauff, M.; Lindner, P.; Fischer, M.; Vogtle, F., *Macromolecules* **1999,** *32*, 4079-4087.

34. Likos, C. N.; Ballauff, M.; Dingenouts, N.; Rosenfeldt, S.; Vogtle, F.; Werner, N.; Linder, P., *J. Chem. Phys.* **2002,** *117*, 1869-1877.

35. Burchard, W., *Adv. Polym. Sci.* **1999,** *143*, 113-195.

36. Schmidt, M.; Burchard, W., *Macromolecules* **1999,** *14*, 210.

37. Schmidt, M.; Burchard, W., *Macromolecules* **1981,** *14*, 210-211.

38. Termeer, H. U.; Burchard, W.; Wunderlich, W., *Coll. Poly. Sci.* **1980,** *258*, 675-684.

39. Mansfield, M. L.; Jeong, M., *Macromolecules* **2002,** *35*, 9794-9798.

40. Mansfield, M. L., *Macromolecules* **2000,** *33*, 8043-8049.

41. Hjelm, R. P., *J. Appl. Crystal.* **1985,** *18*, 452-460.

42. Skvortsov, A. M.; Klushin, L. I.; vanMale, J.; Leermakers, F. A. M., *J. Chem. Phys.* **2001,** *115*, 1586-1595.

CHAPTER FOUR: Synthesis and Solution Behavior of PAMAM Di-dendrons

Introduction

Dendrimers are a distinctive class of macromolecules consisting of branches emanating from a focal point to a precise number of end groups.[1] They differ from hyperbranched polymers in that they are synthesized in a controlled manner resulting in molecules that have a specific molecular weight and a well defined architecture.[2, 3] Applications of dendrimers are often dependent on the knowledge of the internal segment density of their branches and if certain environmental factors can govern this density distribution. Of particular interest is the design of smart materials that are capable of delivering a drug or signaling a disease, which would occur by a system conformational change. Meijer's dendritic box[4] has shown the capability of dendrimers to sequester small molecules within their core, which implies potential applications to drug delivery.

Most work done on the behavior of dendrimers in solution has focused on generations five and larger with tri-functional and tetra-functional cores where results on the morphology varies vastly between systems. Theoretical and experimental work investigated the morphology of dendrimers with respect to generation number as well as solvent quality. One of the earliest theoretical investigations of dendrimers in solution was performed by de Gennes and Hervet,[5] who used self-consistent field analysis. They assumed the monomers of each generation lie in a concentric shell and that the end groups lie at the surface of the molecule, a dense shell morphology. These assumptions resulted in a maximum generation limit due to steric crowding of the end groups, however no other theoretical results have matched this theory to date.

Experimental evidence supporting the 'dense-shell' theory of de Gennes and Hervet[5] was shown by Topp et al.[6] who used small angle neutron scattering (SANS) to study the spatial distribution of the terminal groups of poly(amido amine) (PAMAM) dendrimers by labeling the end groups with deuterium. They found that the radius of gyration (R_g) of the deuterated end groups of generation seven (G7.0) is nearly 0.5 nm larger than that of the entire dendrimer, and from this concluded that the end groups are located at the periphery of the molecule. Since then it has been shown that making such a conclusion on R_g results alone is invalid.[7]

Muthukumar and Lesanec[8] published the first theory to contradict the work of deGennes,[5] where they presented a kinetic growth model of a starburst dendrimer with tri-functional branch points and flexible spacers between pairs of the branch points. From an algorithm that allowed the molecule to grow in a self-avoiding walk, they concluded that the end groups of the dendrimer are not at the surface of the molecule but rather buried within the cavities of the dendrimer, causing the focal point to have the highest molecular density which decays monotonically to the edge of the molecule. This theory also predicted the scaling of the radius of gyration with respect to molecular weight to be $R_g \propto M^{0.5}$ for G3.0 and lower, whereas for higher generations (G = 5.0-7.0) $R_g \propto M^{0.02 \pm 0.02}$ was proposed.

Experimental evidence has been published showing that the end groups of dendrimers are capable of back-folding to the interior of the molecule, supporting the dense-core model. Wooley et al.[9] used rotational-echo double-resonance NMR on poly(benzyl ether) dendrimers containing isotope labels of ^{13}C at the end groups and ^{19}F at the focal point. The intramolecular distances between the focal point and end group were found by the

^{13}C-^{19}F dipolar coupling and were approximately 1.2 nm for generations 3-5. They found decreased interpenetration of the end groups towards the focal point for larger generations, which is consistent with the geometric constraints of the larger generations. Ballauff et al.[10] used contrast variation studies on fourth generation urea-functionalized poly(propyleneamine) dendrimers and showed that the end groups are dispersed throughout the dendrimer with a broad maximum located at a radial distance that is approximately half of the overall size of the molecule.

In addition to the earlier work of Muthukumar and Lesanec,[8] theoretical calculations have shown that dendrimer end groups are capable of 'back-folding' into the interior of the molecule. Mansfield and Klushin[11] allowed PAMAM-type dendrimers to come into equilibrium using Monte Carlo calculations and discovered that for generations greater than four, the end groups of the dendrimer are back-folded towards the focal point. They concluded that crowding in the outer layers for the larger generations forces the density to go through a minimum near the core of the molecule, resulting in a slight hollowness or lower density near the dendrimer's core, which is in agreement with the results of Ballauff et al.[10] For low generations, the density was greatest near the center of the molecule and decreased monotonically to the periphery, demonstrating the change in morphology of theses molecules as a function of generation.

Murat and Grest[12] did theoretical studies on PAMAM type dendrimers and showed an increase in internal segment density when the dendrimer is in a poor solvent, which resulted in a ~45% decrease in size. They also concluded that lower generations have stretched out branches, causing a lower density near the core. Welch and Muthukumar[13] did Monte Carlo simulations on the effect of ionic strength and pH on the size of

dendrimers and found that the size can increase by as much as 180% as the ionic concentration and pH are changed. The variance in size of the molecule occurred with a new density distribution where the maximum density changed from the core to the periphery as the solvent conditions were altered. More recently, Goddard et al.[14] modeled the behavior of tetrafunctional PAMAM dendrimers at various protonation levels in a good solvent and found the molecular dimensions of the dendrimer varying up to 16% from high to low pH. Goddard and coworkers expanded on this work by adding Cl^- counterions for neutral and low pH conditions, which neutralizes the charge of the dendrimer.[15] They found the presence of the counterions causes the dendrimer to swell in size, particularly at high protonation levels.

In addition to the theoretical studies on the effect of solvent on the dimensions of dendrimers, experimental investigations have shown radii changes, varying from 30% to no change, depending on the system studied. SANS studies of tetrafunctional PAMAM dendrimers were done by Amis et al.[16] in dilute solutions of $D(CH_2)_mOD$ (with m=0, 1, 2, 4). PAMAM G5.0 dendrimers decreased in size by ~10% when the solvent was changed from D_2O to d^{10}-butanol. A greater transformation of the radius was observed by Eimer and Stechmesser[17] who used holographic relation spectroscopy to determine the hydrodynamic radius of a tetrafunctional PAMAM dendrimer in both butanol and water. A nearly 30% reduction in size was observed for G6.0 upon changing from a good solvent, water, to a poor solvent, butanol. The influence of solution ionic strength on the dimensions of a PAMAM G4.0 dendrimer with an ammonia core was studied via intrinsic viscosity by Tomalia et al.[18] who found a 15% reduction in visciometric radius (R_η) when changing from H_2O to a 1M HCl aqueous solution. The smaller R_η when the

dendrimer is in acid was attributed to protonation of the amines that disturbs the intermolecular hydrogen bonding, and thus decreasing the viscosity and R_η. Nisato et al.[19] used SANS to study a tetrafunctional PAMAM G8.0 dendrimer and found contrary results; the ionic strength of the solution had no effect on the size of the molecule. In this study the pH was lowered to 4.7 without the dendrimer changing size, yet Tomalia et al.[18] demonstrated that no change in size occurs until the pH is below 2, which is required for protonation of the internal tertiary amines. However, earlier SANS studies by Topp et al. on PAMAM G5.0 dendrimers showed that the addition of acid to dendrimer solutions in D_2O resulted in liquid-like ordering which were attributed to interparticle interactions that increase ionization of the terminal amine moieties.[20] When NaCl was added to the solutions, the charges of the amine groups were screened resulting in the elimination of local ordering of the molecules. The difference in these two studies is the generation of dendrimer used. The lower generations are less sterically hindered and more capable of changing size. However the G8.0 system used to study the size change was too large to exhibit significant variation in dimensions with respect to solvent type.

Extensive experimental studies have shown that as the generation number increases the morphology of the dendrimer transforms from an extended to a globular morphology. Evidence of this transformation has been shown by the intrinsic viscosity of poly(benzyl ether) dendrimers as a function of generation, which goes through a transition at generation 4. The intrinsic viscosity of the early generations increases with molecular weight, which is also typical of linear polymers.[21, 22] A decrease in viscosity is observed for higher generations due to increased steric crowding of the dendritic arms

and the adoption of a more globular shape. A maximum in intrinsic viscosity was also reported for PAMAM tri-dendrons near generation four.[23, 24]

Globular transition of dendrimers with increasing generation has been shown via other experimental methods. Hawker et al.[25] studied the microenvironment of Fréchet-type dendrimers containing a polarity sensitive solvatochromic probe at its focal point, which is sensitive to the polarity of the surroundings, and found a discontinuity in the emission λ_{max} when going from G3.0 to G 4.0, suggesting the transition from an extended to a globular state. We have observed a similar transition in λ_{max} for a PAMAM dendron with a dansyl group attached at the focal point (see Chapter 5). This result is also analogous to those of Tomalia et al.,[26] who used photoinduced electron-transfer to detect a transition in PAMAM structure from extended to globular between G3.0 and G4.0. Earlier work by Tomalia et al.[27] established that the amount of solvent within tri-functional PAMAM dendrimers reaches a maximum at generations 5 and greater suggesting a dendrimer structure that changes with increasing generation and reaches a constant morphology at large generations. Prosa et al.[28] used small angle X-ray scattering to investigate tetra-functional cored PAMAM dendrimers from G3.0-G10.0 and found that generations 5 and higher have a more dense structure, with nearly uniform internal segment densities.

In this study, we used SANS and dynamic light scattering (DLS) experiments to investigate the effect of solvent quality on the molecular dimensions of PAMAM dendrons, G3.0-G5.0, with a di-functional core. Solvents used for the neutron scattering experiments include d^{10}-butanol, d^{6}-ethanol and d^{4}-methanol and D_2O. PAMAM dendrons were synthesized by exhaustive Michael addition of a 2-methoxyethylamine

(MEA) core to methyl acrylate followed by transamidation with ethylenediamine to result in G1.0, Scheme 4.1. These steps were repeated until G5.0 was reached with thorough characterization and purification of each intermediate generation. We also investigated the impact of the functionality of the core on the behavior of PAMAM dendrons in solution, where we used SANS and DLS to characterize tetra-functional cored G4.0 PAMAM dendrons (Tetra-G4.0) in D_2O and d^{10}-butanol. In addition we looked at the effect of ionic strength on the size of a di-functional, 2-methoxyethylamine cored generation 4 (MEA G4.0) via DLS experiments.

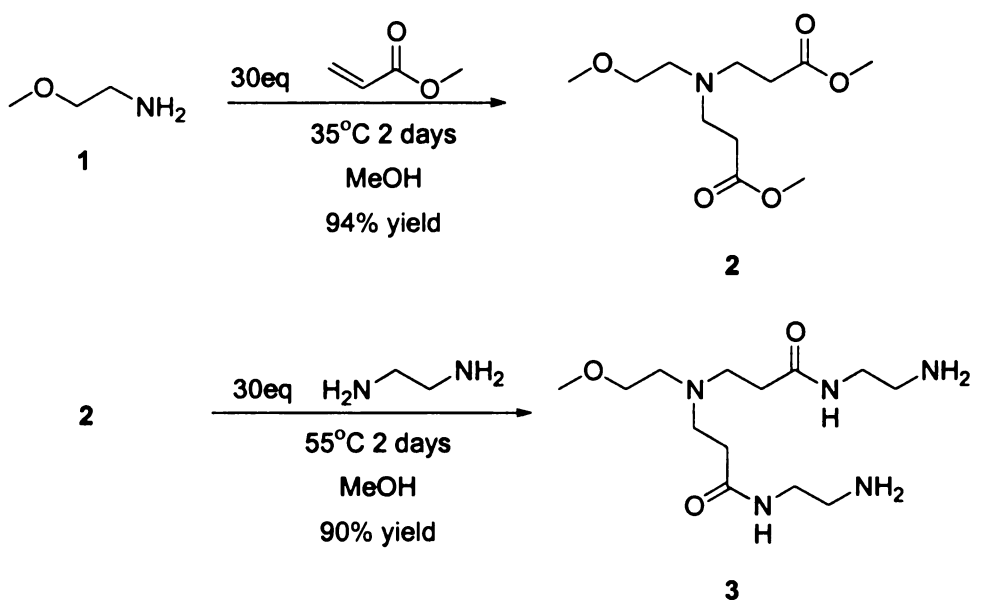

Scheme 4.1. Synthesis of MEA-PAMAM dendrons.

Experimental

Materials. All chemicals were purchased from Aldrich Chemical Co., Saint Louis, MO. Tetra-functional PAMAM G4.0, (ethylenediamine core) was donated by Dow Chemical Co., Midland, MI. Ethylenediamine and 2-methoxyethylamine were distilled under nitrogen prior to use. Methyl acrylate was distilled from KOH to remove the inhibitor. ^{1}H NMR and ^{13}C NMR spectra were obtained using a Varian 300 or 500 MHz instrument, as indicated, using the residual proton signals from the solvent was as the reference peak.

PAMAM Synthesis

2-Methoxyethylamine-PAMAM (MEA-PAMAM) G0.5 (2): A solution of 1.00g (0.013 mol) of 2-methoxyethylamine (MEA) in 25 mL of methanol was slowly dripped into 34.3g (0.400 mol) of uninhibited methyl acrylate. The reaction was stirred for two days at 35 °C under nitrogen. Methanol and unreacted methyl acrylate was removed in vacuo, resulting in 3.14 g of **2** as a clear oil (98% yield). ^{1}H NMR ($CDCl_3$, 300 MHz) δ: 3.46 (s, 6H), 3.23 (t, 2H, J = 6.0 Hz), 3.13 (s, 2H), 2.63 (t, 4H, J = 7.2 Hz), 2.45 (t, 2H, J = 6.0 Hz), 2.26 (t, 4H, J = 7.2 Hz) ^{13}C NMR ($CDCl_3$, 300 MHz) 173.2, 71.0, 59.0, 51.2, 49.9, 32.1.

MEA-PAMAM G 1.0 (3): A solution of 0.97g (3.8 mmol) of **2** in 20 mL methanol was slowly dripped into 6.85g (0.114 mol) of freshly distilled ethylenediamine. The reaction was stirred at 55 °C for two days. Methanol and unreacted ethylenediamine was removed under vacuum. The remaining residue was dissolved in octanol (100 mL) and stirred under vacuum (5 mTorr) at 40 °C for 2 days to remove residual amounts of ethylenediamine. The octanol mixture was washed with 200 mL solution of 50:50

hexane:water. The water layer was collected and washed with hexanes (3 × 100 mL), then concentrated and dried under vacuum (5 mTorr) at 40 °C, resulting in 1.03 g of **3** as a clear oil, (90% yield). ^{1}H NMR ($CDCl_3$, 300MHz); δ 7.4 (br s, 2H), 3.4 (t, 2H, J = 5.4 Hz), 3.25 (s, 3H), 3.10 (quartet, 4H, J = 6.3 Hz), 2.80-2.60 (m, 8H), 2.54 (t, 2H, J = 5.4 Hz), 2.70 (t, 4H, J = 6.6 Hz), 2.14 (s, 4H). ^{13}C NMR ($CDCl_3$, 300 MHz) δ 172.4, 70.2, 58.6, 53.1, 50.1, 42.0, 41.1, 34.0

General Procedure for synthesizing MEA-PAMAM dendron

Conditions for the formation of subsequent half and whole generations were identical to that for the formation of **2** and **3** respectively. To avoid impurities, it is imperative to remove all residual monomer before proceeding to the next step.

MEA-PAMAM G 1.5: ^{1}H NMR (300 MHz, $CDCl_3$) δ: 3.64 (s, 12H), 3.50 (t, 2H, J = 6.0 Hz), 3.21 (s, 3H), 3.07 (t, 4H, J = 5.7 Hz), 2.80 (m, 12H), 2.72 (t, 2H, J = 6.0 Hz), 2.51 (t, 4H, J = 5.7 Hz), 2.45 (t, 8H, J = 7.2 Hz), and 2.41 (t, 4H, J = 7.2 Hz). ^{13}C NMR (300 MHz, $CDCl_3$) δ: 174.6, 172.6, 70.4, 58.7, 52.7, 52.6, 51.6, 50.3, 49.9, 49.1, 37.0, 32.5.

MEA-PAMAM G2.0: ^{1}H NMR (300 MHz, d^4-methanol) δ: 3.49 (t, 2H, J = 5.4 Hz), 3.24 (s, 3H), 3.17 (t, 12H, J = 6.6 Hz), 2.86-2.60 (m, 22H), 2.54 (t, 4H, J = 6.6 Hz), and 2.32 (t, 12H, J = 6.6 Hz). ^{13}C NMR (300 MHz, d^4-methanol) δ: 175.2, 175.0, 72.0, 60.0, 53.8, 53.2, 51.2, 49.9, 43.0, 42.0, 38.7, 35.0, 34.5.

MEA-PAMAM G2.5 ^{1}H NMR (500 MHz, $CDCl_3$) δ: 3.50 (s, 24H), 3.29 (t, 2H, J = 5.4 Hz), 3.15 (s, 3H), 3.10 (q, 12H, J = 6.0 Hz), 2.63 (t, 12H, J = 7.0 Hz), 2.58 (t, 16H, J = 7.0 Hz), 2.51 (t, 2H, J = 5.4 Hz), 2.42-2.36 (m, 12H), 2.27 (t, 16H, J = 7.0 Hz), and 2.19 (t, 12H, J = 7.0 Hz). ^{13}C NMR (500 MHz, $CDCl_3$) δ: 172.8, 172.4, 172.3, 70.0, 59.0, 52.4, 52.2, 51.3, 49.8, 48.8, 37.9, 37.0, 34.0, 33.5, 32.1.

MEA-PAMAM G3.0 ^{1}H NMR (500 MHz, $CDCl_3$) δ: 8.05 (t, 4H, J = 7.8 Hz), 7.98 (t, 2H, J = 7.8 Hz), 7.75 (t, 8H, J = 7.8 Hz), 3.41 (t, 2H, J = 5.4 Hz), 3.28 (s, 28H), 3.26-3.16 (m, 28H), 2.54-2.40 (m, 42H), 2.40-2.20 (m, 12H), and 2.40-2.20 (m, 28H). ^{13}C NMR (500 MHz, $CDCl_3$) δ: 175.1, 174.9, 72.0, 59.9, 53.5, 51.2, 49.9, 43.0, 42.0, 37.2, 34.9, 34.7.

MEA-PAMAM G3.5 ^{1}H NMR (500 MHz, $CDCl_3$) δ: 3.60 (s, 48H), 3.36 (t, 2H, J = 5.4 Hz), 3.20 (m, 31H), 2.80-2.64 (m, 62H), 2.60-2.45 (m, 28H), and 2.40-2.25 (m, 60H). ^{13}C NMR (500 MHz, $CDCl_3$) δ:172.9, 172.3, 172.1, 74.0, 59.1, 53.7, 53.5, 53.4, 51.8, 50.4, 50.1, 49.9, 49.7.

MEA-PAMAM G4.0 ^{1}H NMR (500 MHz, d^4-methanol) δ: 3.50 (t, 2H, J = 5.4 Hz), 3.37 (s, 3H), 3.34-3.10 (m, 60H), 2.90-2.66 (m, 92H), 2.62 (m, 26H), and 2.48-2.20 (m, 60H). ^{13}C NMR (500 MHz, d^4-methanol) δ: 173.1, 172.6, 67.0, 59.0, 52.6, 52.4, 52.1, 50.3, 42.1, 41.2, 37.8, 37.6, 34.2, 33.8.

MEA-PAMAM G4.5 ^{1}H NMR (500 MHz, $CDCl_3$) δ: 3.42 (s, 96H), 3.20 (t, 2H, J = 5.4 Hz), 3.12 (s, 3H), 3.10-2.90 (m, 60H), 2.60-2.50 (m, 124H), 2.37-2.28 (m, 60H), 2.20 (t, 64H, J = 7.0 Hz), and 2.10-1.90 (m, 60H). ^{13}C NMR (500 MHz, $CDCl_3$) δ: 172.4, 171.82, 171.75, 70.0, 57.6, 52.3, 52.0, 51.8, 51.0, 49.5, 49.3, 48.5, 37.0, 36.7, 33.2, 32.1.

MEA-PAMAM G5.0 ^{1}H NMR (500 MHz, d^4-methanol) δ: 3.42 (t, 2H, J 5.4 Hz), 3.36 (s, 3H), 3.30-3.10 (m, 124H), 2.82-2.64 (m, 188H), 2.60-2.50 (m, 60H), and 2.40-2.20 (m, 128H). ^{13}C NMR (500 MHz, d^4-methanol) δ: 175.2, 174.9, 70.0, 59.9, 54.4, 54.2, 53.9, 51.5, 42.3, 41.9, 38.4, 34.5.

SANS. Measurements were taken at the small-angle neutron diffractometer (SAND) at Argonne's Intense Pulsed Neutron Source. A sample to area detector distance of 2.0 m

was used. The radiation had a wavelength range of 1-14 Å making the total wave vector (Q) range covered 0.0034-0.6 $Å^{-1}$, where $Q = 4\pi\sin(\theta/2)/\lambda$ with θ and λ defined as the scattering angle and radiation wavelength, respectively. Measurements were taken at room temperature. Low concentrations were used for each sample to generate sufficient scattering in the allotted time while minimizing intermolecular scattering effects. Samples were filtered through a 0.1μm Whatman Anodisc 13 filter and sonicated for 20 minutes and placed in a hermetically sealed quartz cell for the scattering experiments. A list of samples is given in Table 4.1.

Table 4.1. Sample codes and theoretical molecular mass (M) of MEA compounds.

Sample Code	M (Da)	# end groups	end group functionality
MEA G3.0	1671	8	1° amine
MEA G3.5	3047	16	methyl ester
MEA G4.0	3261	16	1° amine
MEA G4.5	6247	32	methyl ester
MEA G5.0	7143	32	1° amine
Tetra G4.0	6872	32	1° amine

Neutron scattering data for dendrons was analyzed in the Guinier regime.[29] This analysis allowed for quick determination of the shape and size of the dendrimer, with all samples in this study fitting to the compact-objects (sphere) model. The scattering intensity, I(Q), in the low Q regime was evaluated using the expression for compact ('sphere-like') objects with a given radius of gyration (R_g),[30]

$$I(Q) \approx \phi V(\Delta\rho)^2 \exp\left(-\frac{Q^2 R_g^2}{3}\right) \equiv I(0)\exp\left(-\frac{Q^2 R_g^2}{3}\right) \qquad (4.1)$$

where ϕ is volume fraction of scattering centers, V, the volume of each scattering center, $(\Delta\rho)^2$, the square of the difference of the solvent and the scatterer scattering length density (SLD) and I(0), the intensity at zero wave vector. The slope resulting from a plot of ln(I(Q)) versus Q^2 in the region where $QR_g \cong 1$ allows R_g to be obtained. The radius of a homogeneous, constant density sphere is determined from the R_g by $R = R_g/0.775$. We also analyzed the scattering data of the dendrons in the Guinier regime using the Guinier approximation for both rods and sheet-like objects, however neither of these approximations resulted in a good fit indicating the dendrons are always sphere-like for our experimental conditions.

To determine the goodness of each Guinier fit, the experimental value of I(0) was used to determine the amount of solvent within each sample and check that the mass density of the swollen dendrimer is reasonable. The numerical prefactor of eq 4.1 was set equal to the experimental value of I(0) and then solved for $(\Delta\rho)^2$. Using this value of $(\Delta\rho)^2$ and the scattering length density of the solvent (ρ_{solv}); we calculated the scattering length density of the scatterers (ρ_{scat}), which includes solvent and dendrimer. We calculated the amount of solvent within the dendrimer by,

$$(\rho_{scat}) = [\rho_{solv}]\times\theta + [1-\theta]\times\rho_{sample} \qquad (4.2)$$

where θ is the mass fraction of solvent within the scatterer and ρ_{sample} is the scattering length density of the dendrimer.

Dynamic Light Scattering (DLS). Measurements were performed with a Protein Solutions Dyna Pro-MS/X system with temperature control. All samples were filtered as described above and allowed to equilibrate in the instrument for 25 minutes at 25 °C

before measurements were taken that resulted in calculation of the hydrodynamic radius (R_h). Samples for agglomeration studies were pre-equilibrated at 25 °C before filtering. The sample is illuminated by a semi-conductor laser with ~ 830 nm wavelength. The light scattered at an angle of 90° is collected and guided via a fiber optic cable to an actively quenched, solid state Single Photon Counting Module (SPCM), where the photons are converted to electrical pulses and correlated. Autocorrelation is used to analyze the time scale of the scattered light intensity fluctuations. The uniformity of the sample sizes is determined by a monomodal curve fit, cumulants, which assumes a single particle size with a Gaussian distribution.

Results and Discussion

Synthesis of MEA dendrons

Dendrons were synthesized from a 2-methoxyethylamine core, **1**, via exhaustive Michael addition to methyl acrylate resulting in methyl-ester terminated MEA-PAMAM G0.5 (MEA G0.5), **2** (Scheme 4.1). Excess methyl acrylate was used to ensure di-alkylation of the primary amine moiety and was removed after the reaction was complete by stirring under vacuum (5 mTorr) at 40 °C for 24 hours, resulting in a clear oil. We used ^{1}H and ^{13}C NMR to characterize purity of dendrons. ^{13}C NMR has been shown by Tomalia et al. to be a useful technique to detect dendron impurities.[18] Detailed NMR spectra are in Appendix A. MEA G0.5 was reacted with excess ethylenediamine to afford primary amine terminated MEA G1.0, **3**. After thorough removal of excess diamine, the primary amine end groups of the full generation allow for these two steps to be repeated to obtain MEA G2.0. We continued the synthesis to MEA G5.0. Scheme 4.2 displays the MEA G4.0 dendron, which has 16 primary amine end groups. The number of

dendron end groups and the molecular weight of these dendrons doubles with each successive full generation, Table 4.1.

Size of MEA G3.0-G5.0 Dendrons in D_2O

The molecular morphology of MEA dendrons G3.0-G5.0 was studied using the Guinier analysis of a compact object, sphere, mentioned above,[29] to determine their size and shape as a function of generation. SANS experiments on 4 mg/mL dendron solutions in D_2O showed that all generations studied behave as sphere-like objects due to the negatively sloped straight line obtained from a Guinier fit, Figures 4.1a-4.5a. The intensity of scattering as a function of Q (Figures 4.1b-4.5b) is shown to demonstrate the valid Q range used for the Guinier analyses. The full generation dendrons, which have primary amine end groups show an increase in R_g with increasing generation, with R_g values of 1.28 ± 0.03 nm for MEA G3.0, 2.59 ± 0.13 nm for MEA G4.0 and 3.18± 0.05 nm for MEA G5.0. The methyl-ester terminated half generation dendrons, MEA G3.5 and MEA G4.5, have R_g values of 0.563 ± 0.04 nm and 0.736 ± 0.012nm respectively.

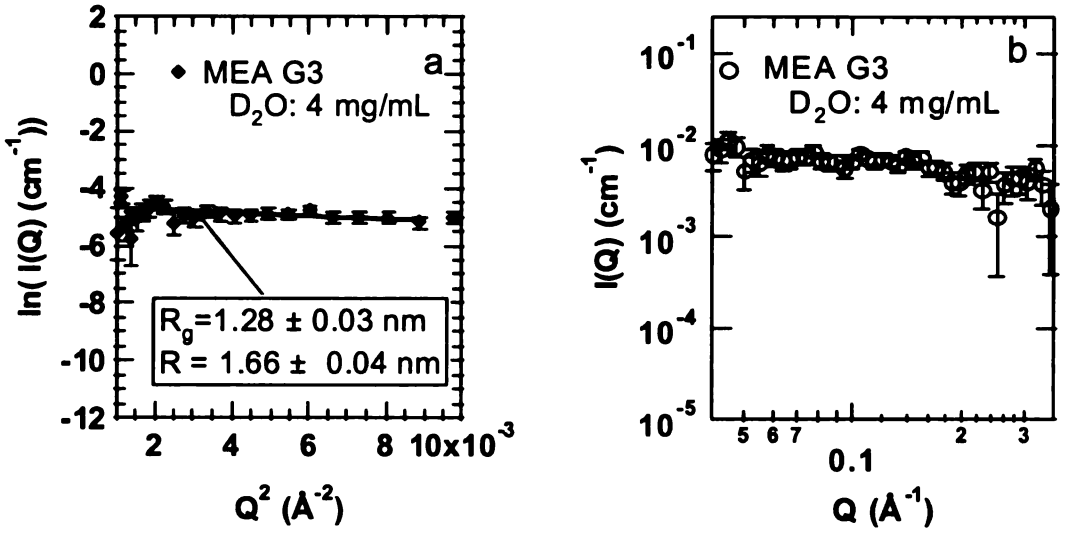

Figure 4.1.SANS data for MEA G 3.0 dendrons in D_2O.

a. Guinier analysis for MEA G3 dendrons in D_2O at a concentration of 4 mg/mL, data fit for a compact (sphere-like) object. b. I vs Q plot of MEA G3 dendrons in D_2O at a concentration of 4 mg/mL.

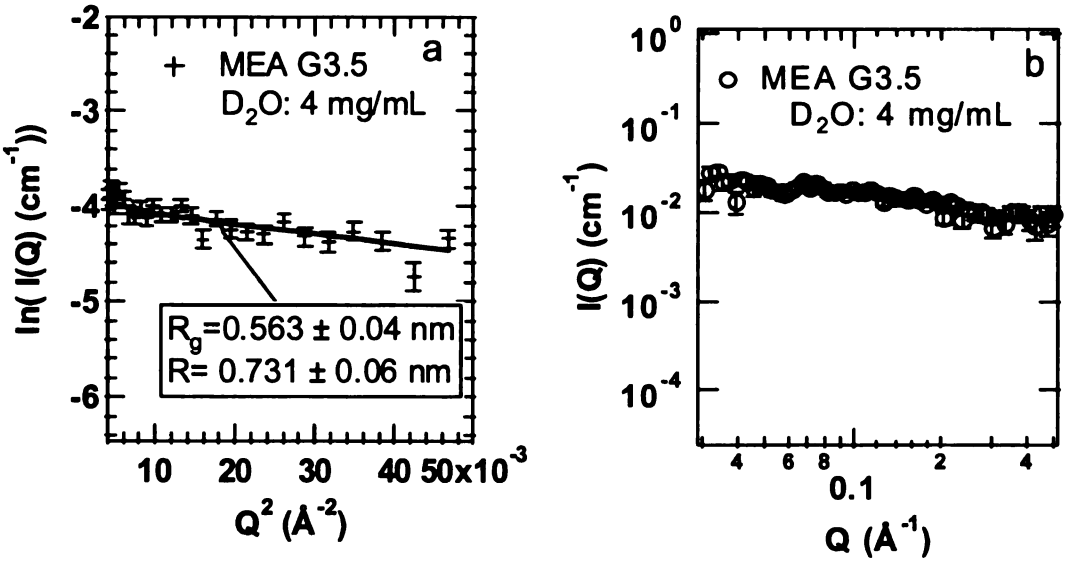

Figure 4.2. SANS data for MEA G 3.5 dendrons in D_2O.

a. Guinier analysis for MEA G3.5 dendrons in D_2O at a concentration of 4 mg/mL, data fit for a compact (sphere-like) object. b. I vs Q plot of MEA G3.5 dendrons in D_2O at a concentration of 4 mg/mL.

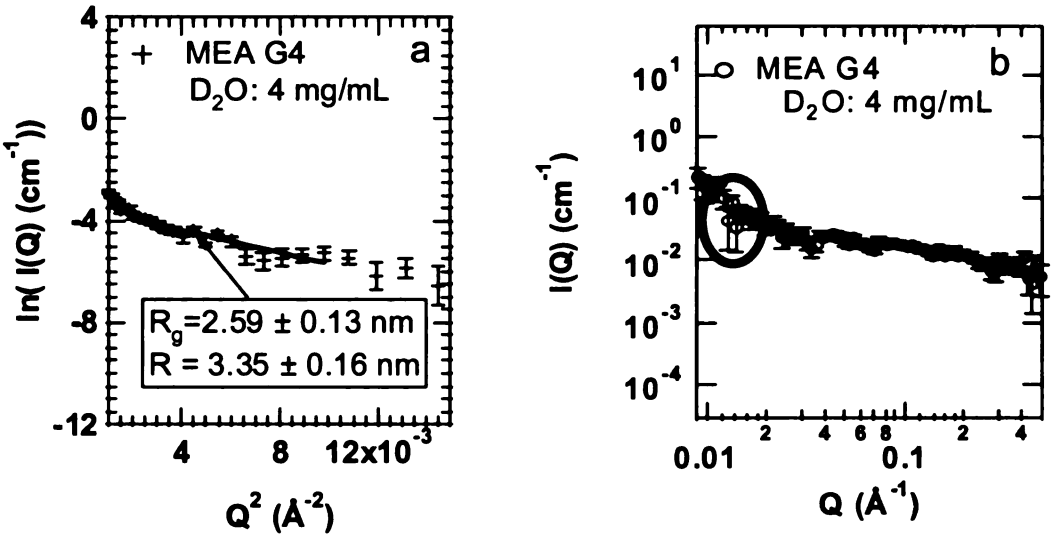

Figure 4.3. SANS data for MEA G 4.0 dendrons in D_2O.

a. Guinier analysis for MEA G4.0 dendrons in D_2O at a concentration of 4 mg/mL, data fit for a compact (sphere-like) object. b. I vs Q plot of MEA G4.0 dendrons in D_2O at a concentration of 4 mg/mL, where the circled region indicates agglomeration, thus low Q-regime was not used in the Guinier approximation.

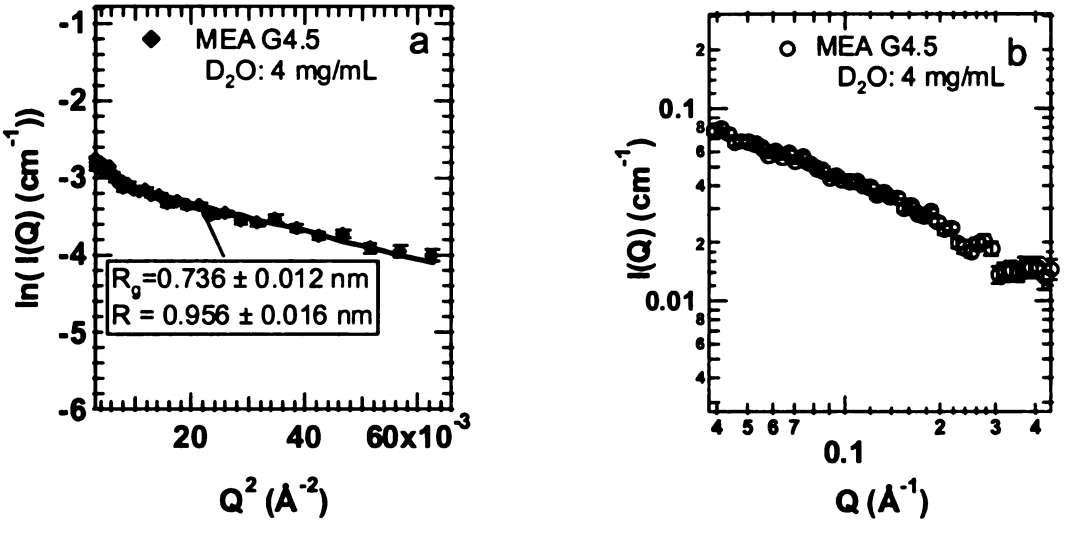

Figure 4.4. SANS data for MEA G 4.5 dendrons in D_2O.

a. Guinier analysis for MEA G4.5 dendrons in D_2O at a concentration of 4 mg/mL, data fit for a compact (sphere-like) object. b. I vs Q plot of MEA G4.5 dendrons in D_2O at a concentration of 4 mg/mL.

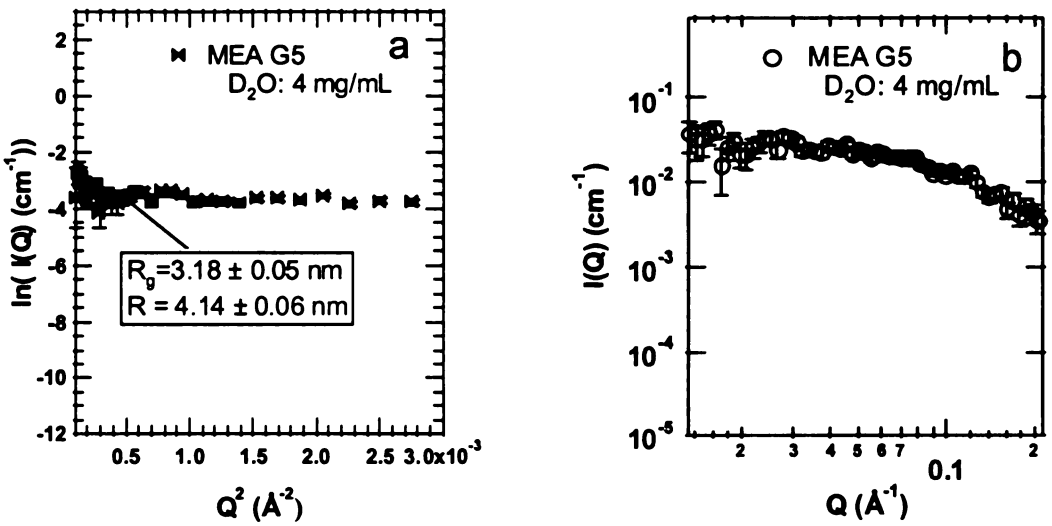

Figure 4.5. SANS data for MEA G 5.0 dendrons in D_2O.

a. Guinier analysis for MEA G5.0 dendrons in D_2O at a concentration of 4 mg/mL, data fit for a compact (sphere-like) object. b. I vs Q plot of MEA G5.0 dendrons in D_2O at a concentration of 4 mg/mL.

The size of the dendrons as a function of generation is displayed in Figure 4.6a. The half generation dendrons have significantly smaller dimensions in solution compared to the full generations. Despite the nearly two-fold increase in molecular weight between MEA G3.0 and MEA G3.5, the R_g of the molecule has decreased from 1.28 ± 0.03 nm for MEA G3.0 to 0.568 ± 0.06 nm for MEA G3.5. The same trend is observed for MEA G4.0 and MEA G4.5, with R_g decreasing from 2.59 ± 0.13 nm for MEA G4.0 to 0.736 ± 0.012 nm for MEA G4.5. The full generation dendrons have primary amine end groups that can act as both hydrogen bond donors and acceptors, whereas the half generation dendrons have methyl ester end groups which are less polar and cannot act as hydrogen bond donors. The decrease in size for the half generations is due to the poor interaction of the end groups with the solvent, D_2O, demonstrating that the functionality of the end-group is critical to the behavior of the PAMAM di-dendrons in solution.

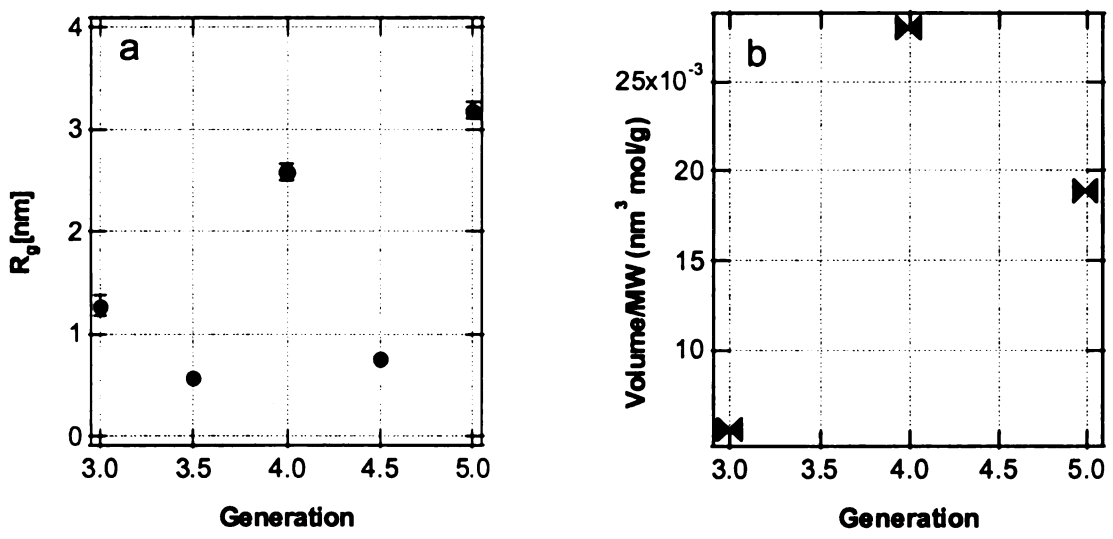

Figure 4.6. R_g and volume of MEA dendrons in D_2O.
a. R_g vs. generation for MEA dendrons in D_2O at a concentration of 4 mg/mL. b. Volume/MW vs. generation for full generation, amine terminated, MEA dendrons in D_2O at a concentration of 4 mg/mL, where volume was calculated using the volume of a sphere and R_g as the radius.

Using the experimental value of I(0) (Table 4.2) the mass fraction of solvent (θ) within the dendrimer was calculated using eq 4.2 as described above and was 0.28 and 0.30 for MEA G3.5 and MEA G4.5, respectively. The θ values for the full generations were 0.38 for MEA G3.0, 0.64 for MEA G4.0 and 0.61 for MEA G5.0. The large increase in the amount of solvent contained within the dendrimer from MEA G3.0 to MEA G4.0 can be explained by the system transitioning from an extended to a globular structure as the steric requirements of the dendritic branches increase. Similar transitions have been observed for poly(benzyl ether) dendrons via intrinsic viscosity [21, 22, 25] and solvatochromism[25] studies as well as for carboxylate-terminated starburst dendrons via photo-induced electron transfer measurements.[26]

Table 4.2. R_g values for MEA G3.0-G5.0 determined from the Guinier analysis described in the text at a concentration of 4 mg/mL. Symbols are explained in the text while Q_{max} is the maximum Q-value used in the regression.

Sample	MEA G3.0	MEA G3.5	MEA G4.0	MEA G4.5	MEA G5.0
solvent	D_2O	D_2O	D_2O	D_2O	D_2O
R_g(nm) [a]	1.28±0.03	0.563±0.04	2.59±0.13	0.736±0.01	3.18±0.05
$I(0)_{exp}$ [b] (cm^{-1})	0.009±.001	0.010±0.0011	0.028±0.0015	0.051±0.017	0.052±0.005
Q_{max}*R_g	1.211	1.228	1.42	1.703	1.180
θ [c]	0.38	0.28	0.64	0.30	0.61
R_h(nm) [d]	0.90±0.05 [e]	0.80±0.05 [e]	1.90±0.05	1.40±0.05	2.30±0.10
R_g/R_h	1.42±.0.08	0.70±0.05	1.36±0.04	0.53±0.02	1.38±0.06

[a] Radius of gyration for a sphere-like object. [b] Experimental value of I(0) from a sphere-like object Gunier plot (eq 1). [c] θ is the mass fraction of solvent within the scatterers. [d] Hydrodynamic radius of dendrons determined from dynamic light scattering. [e] This value is on the lower edge of the instruments size detection limit, 1 nm.

Dynamic light scattering experiments were performed for MEA G3.0-G5.0 in Milli Q water at a concentration of 4 mg/mL to determine the hydrodynamic radius (R_h). Values of R_h are reported in Table 4.2. Information on the internal segment density of the dendrons in solution can be gained from the ratio of R_g/R_h (Table 4.2).[31] An R_g/R_h ratio of $\sqrt{(3/5)} \approx 0.775$ is indicative of a constant density, homogeneous sphere. A value of 1.50 is descriptive of a monodisperse Gaussian coil in a theta solvent and 1.78 represents linear polymers in a good solvent,[31] although experiments show values of 1.16 and 1.27 for linear polymers in theta solvents.[32, 33]

The half generation dendrons, MEA G3.5 and MEA G4.5 have R_g/R_h ratios of 0.70 ± 0.05 and 0.53 ± 0.02 respectively. These values are lower than expected for a constant density sphere indicating the segmental distribution of the branches is not

uniform from the center to the edge of the molecule. A sphere whose maximum density is at the center and decreases linearly to outer radius has a theoretical R_g/R_h ratio of $\sqrt{(2/5)} = 0.63$. A sphere whose minimum density is at the center and increases linearly to the outer radius has a theoretical R_g/R_h ratio of $\sqrt{(22/35)} = 0.80$. The R_g/R_h values for the half generation MEA dendrons indicate the maximum density is neither at the center nor at the edge of the molecule, which matches theoretical calculations[11, 12] as well as experimental results.[10]

The full generation dendrons have R_g/R_h ratios that are higher than the half generations, demonstrating they have a different segment distribution in solution. The lowest generation studied, MEA G3.0, has an R_g/R_h ratio of 1.42 ± 0.04, which is within experimental error of the R_g/R_h ratios of MEA G4.0 and MEA G5.0, 1.36 ± 0.04 and 1.45 ± 0.06 respectively. None of the full generation dendrons adopt the morphology of a constant density sphere when in D_2O, but rather are in a more expanded state. Within the sensitivity of our experiments, the segmental distribution of dendritic arms of the full generations does not change with generation.

A plot of V/M vs. generation of the full generation dendrons is shown in Figure 4.6b. This graph displays a maximum at generation 4.0, corresponding to a minimum in density, which has been observed previously for poly(benzyl ether) dendrons[21, 34] and PAMAM tri-dendrons.[3, 23] This maximum at generation 4 can be explained by the difference in growth of the molecular weight and volume of dendrimers in solution. The molecular mass scales as

$$M \sim f_c\left(f_{bu} - 1\right)^g \tag{4.3}$$

Where f_c is the core functionality and f_{bu} is the multiplicity of the branching units. MEA dendrimers have multiplicity of 2 at the branch junction points (f_{bu}) and a core functionality of 2 (f_c=2). Thus molecular mass scales as

$$M \sim 2^g \tag{4.4}$$

We assume the dendrimers are sphere-like, which is appropriate according to our SANS results, and each generation contributes linearly to the radius resulting in a volume that scales as g^3. This model predicts a maximum in theV/M ratio at a $g=3/\ln(f_c(f_{bu}-1))$ or between the fourth and fifth generations for the MEA-PAMAM system. A linear increase in radius with increasing generation assumes the dendrimer is in a good solvent. Tomalia et al.[23] studied PAMAM tri-dendrons and found a linear increase in radius for generations three and greater. The plot of R_g vs. generation (Figure 4.6a) shows an approximately linear increase in the size of the full generation dendrons with increasing generation, confirming the assumption is valid for our system. The maximum V/M ratio for G4.0 indicates that MEA G4.0 has the greatest potential for changing size in solution.

Using the theoretical molecular weights listed in Table 4.1 and the R_g values in Table 4.2, a log-log plot, Figure 4.7, demonstrates that the scaling of the MEA dendron with respect to molecular weight is non linear between MEA G3.0 and G5.0 As the dendrimer becomes larger, the mass increases at a rate faster than the size, corresponding to the maximum in intrinsic viscosity found for both poly(benzyl ether)[21, 22] and trifunctional cored PAMAM dendrimers.[23, 24] While more data are needed to thoroughly explain the scaling behavior of these molecules, it is clear that the radius increases at a decreasing rate with respect to generation number, agreeing with theoretical work of

Muthukumar and Lesance[8] as well as more recent results of Scheler and Fritzinger[35] who studied the scaling behavior of carboxylate terminated tetra-functional cored PAMAM dendrons in solutions of methanol.

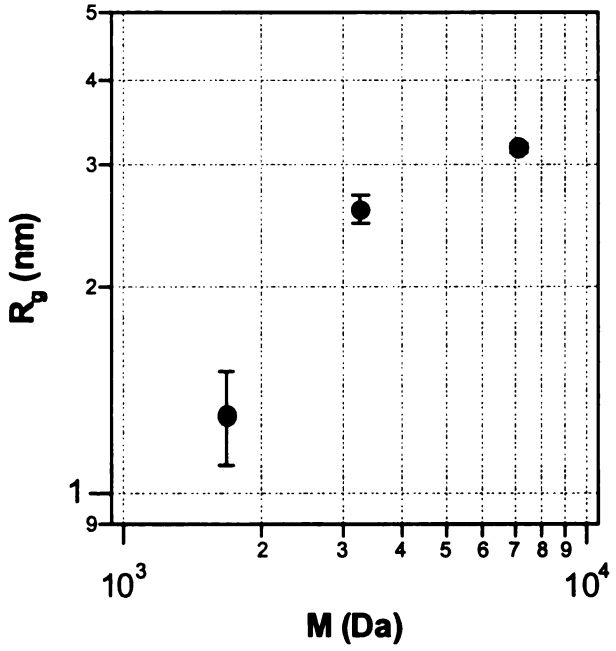

Figure 4.7. Radius of gyration vs. molecular weight for the MEA dendrons G 3.0-G 5.0 in D_2O at a concentration of 4 mg/mL.

Effect of Solvent Quality on the Dimensions of MEA-G4.0 in Solution

The magnitude of size change for MEA G4.0, Scheme 4.2, in solution was determined by performing SANS experiments in a series of solvents, $D(CD_2)_mOD$, with m = 1, 2, and 4. The scattering data were fit to a Guinier analysis for compact objects, spheres, to determine the R_g for each system (Figures 4.8a-4.10a). The graphs of intensity of scattering as a function of wave vector (Figures 4.8b-4.10b) were used to determine the valid Q range for the Guinier analysis.

The R_g of MEA G4.0 dendrons is sensitive to the solvent quality, as shown in a plot of R_g versus m, from m=0 (D_2O) to m=4 (d^{10}-butanol), Figure 4.10. The values of R_g are also reported in Tables 4.2 and 4.3. The size of the MEA G4.0 dendrons decreases as the polarity of the solvent decreases. The dendron radius shrinks from 2.59 ± 0.13 nm to 0.91 ± 0.06 nm when the solvent is changed from D_2O to d^{10}-butanol, a 67% decrease in radius, that corresponds to a nearly 96% decrease in volume (Figure 4.11). These results contradict those obtained by Amis et al.,[16] who observed only a 10% reduction in the size of a G8.0 PAMAM tetra-dendron when changing the solvent from D_2O to d^{10}-butanol. The greater size change of the MEA G4.0 system compared to the G8.0 tetra-dendrons can be attributed to the disparity in functionality of the core; MEA G4.0 has a di-functional core which is less sterically hindered than the tetra-functional core of the system studied by Amis et al.[16] Also our results (Figure 4.6b) indicate that G4.0 has the largest volume:molecular mass ratio and thus the greatest potential for changing size in solution.

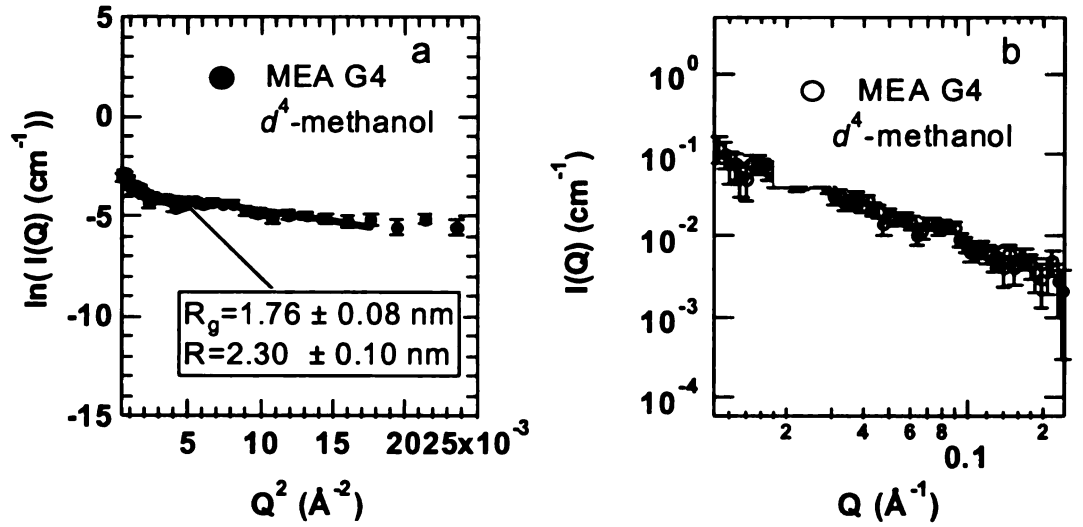

Figure 4.8. SANS of MEA G4.0 dendrons in d^4-methanol.

a. Guinier analysis for MEA G4.0 dendrons in d^4-methanol at a concentration of 4 mg/mL, data fit for a compact (sphere-like) object. b. I vs Q plot of MEA 4.0 dendrons in d^4-methanol at a concentration of 4 mg/mL.

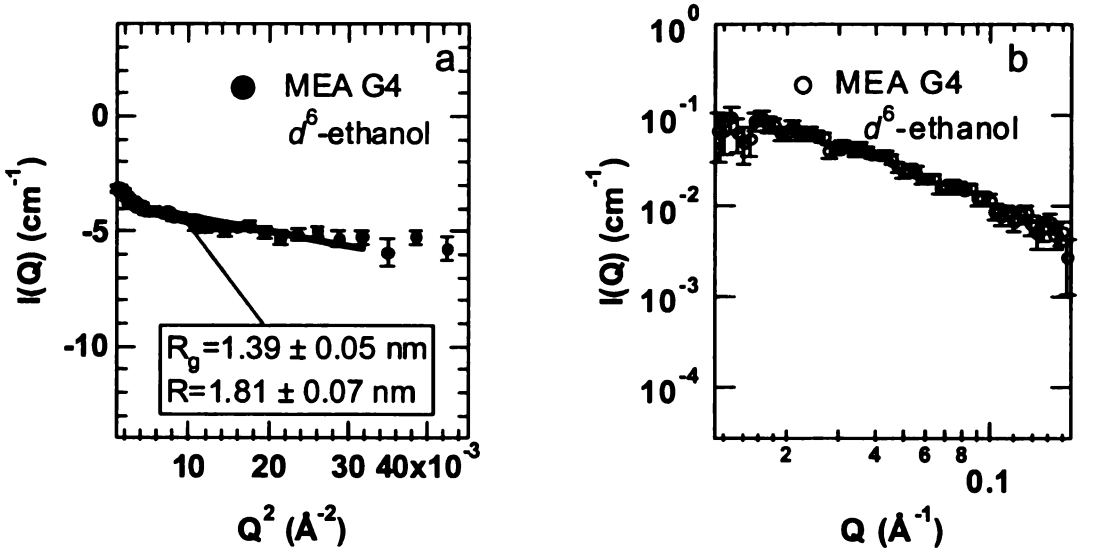

Figure 4.9. SANS of MEA G4.0 dendrons in d^6-ethanol.

a. Guinier analysis for MEA G4.0 dendrons in d^6-ethanol at a concentration of 4 mg/mL, data fit for a compact (sphere-like) object. b. I vs Q plot of MEA 4.0 dendrons in d^6-ethanol at a concentration of 4 mg/mL.

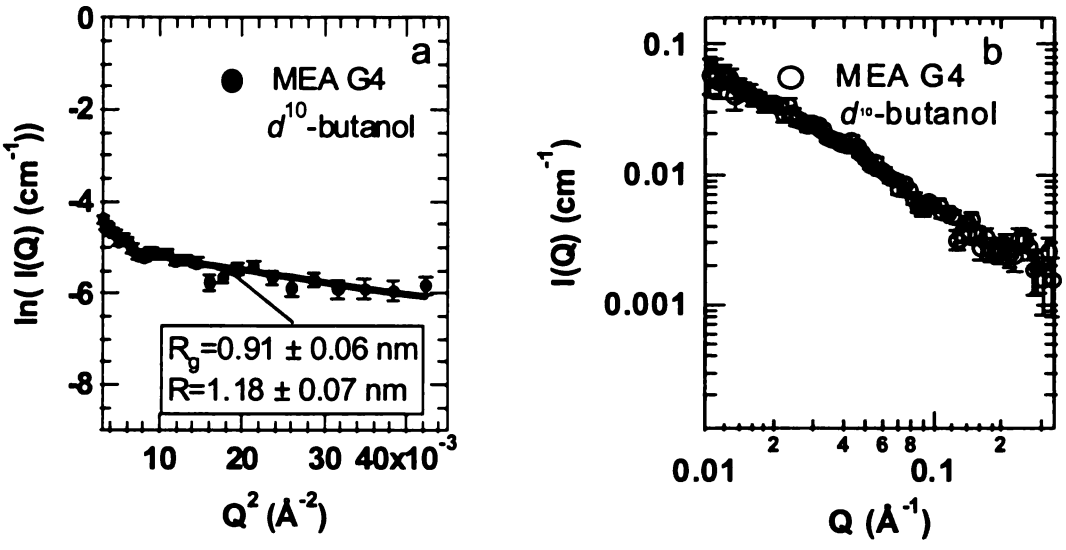

Figure 4.10. SANS of MEA G4.0 dendrons in d^{10}-butanol.

a. Guinier analysis for MEA G4.0 dendrons in d^{10}-butanol at a concentration of 4 mg/mL, data fit for a compact (sphere-like) object. b. I vs Q plot of MEA 4.0 dendrons in d^{10}-butanol at a concentration of 4 mg/mL.

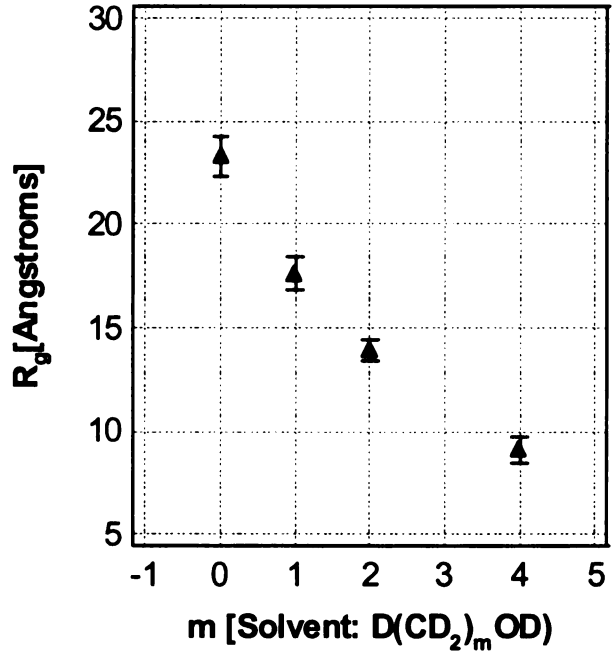

Figure 4.11. R_g of MEA G4 vs. solvent type (m) of D(CD2)$_m$OD.

All solutions were at a concentration of 4 mg/mL.

To ensure that the MEA G4.0 dendron is capable of collapsing to the size measured in d^{10}-butanol, R_g = 0.91 ± 0.06 nm, R_h = 1.40 ± 0.05 nm, we calculated the radius of a MEA G4.0 dendron in the bulk state. The reported bulk density (δ) of these dendrons is 1.22 g/cm^3.[16] Using this value for the density and the molecular weight of the G4.0 dendron, (Table 4.1) the minimum volume was calculated from V=M/δ. The minimum radius was found to be ~1 nm, close to the hydrodynamic radius of the MEA G4.0 dendron in butanol, 1.40 ± 0.05 nm.

The mass fraction of solvent, θ, contained within the MEA G4.0 dendrimer as a function of solvent quality was extracted from the experimental value of I(0) using equation 4.2 as described above; these values are listed in Table 4.3. As the quality of the solvent decreases the amount of solvent located within the dendrimer also decreases with θ values of 0.46, 0.45 and 0.40 for MEA G4.0 in d^4-methanol, d^6-ethanol and d^{10}-butanol respectively. These values are all smaller than the value for MEA G4.0 in D_2O, 0.64.

We performed DLS experiments on the MEA G4.0 dendrons in methanol, ethanol and butanol at a concentration of 4 mg/mL to obtain R_h as a function of solvent quality, Table 4.3. The MEA G4.0 dendron has an R_h in methanol of 1.50 ± 0.05 nm and 1.40 ± 0.05 nm when in either ethanol or butanol. To gain more information about the conformational changes of the MEA dendrons as a function of solvent quality, the ratio of R_g/R_h was calculated and these values are listed in Table 4.3. This ratio decreases from 1.17 ± 0.04 in d^4-methanol to 0.99 ± 0.04 in d^6-ethanol to 0.65 ± 0.03 in d^{10}-butanol, indicating the dendron segmental distribution is largely influenced by the quality of solvent. All of these values are larger than 1.36 ± 0.04, which is the R_g/R_h value for the

MEA G4.0 dendron in water. We observed no difference in R_h values for dendrons in D_2O and H_2O, indicating negligible deuteration effects for this system. When in d^6-ethanol and d^{10}-butanol, the dendrimer is in a compact state, and the R_g/R_h values are similar to those found for poly(benzyl ether) G4.0 dendron in solution.[36] The large differences in the R_g/R_h ratios for dendrons placed in different polarity environments demonstrate that MEA dendrons are capable of changing both size and internal segment distribution.

Table 4.3. R_g values for MEA G4.0 and G5.0 in $D(CD_2)_mOD$ determined from the Guinier analysis described in the text at a concentration of 4 mg/mL. Symbols are explained in the text while Q_{max} is the maximum Q value used in the regression

Sample Code →	**MEA G4.0**	**MEA G4.0**	**MEA G4.0**	**MEA G5.0**
solvent	d^4-methanol	d^6-ethanol	d^{10}-butanol	d^{10}-butanol
R_g(nm) [a]	1.76±0.08	1.39±0.05	0.91±0.06	1.23±0.02
$I(0)_{exp}$ [b] **(cm^{-1})**	0.025±0.002	0.0242±0.00	0.034±0.001	0.065±0.0006
Q_{max}*R_g	2.34	2.47	1.87	2.44
θ [c]	0.46	0.45	0.40	0.52
R_h(nm) [d]	1.50±.05	1.40±.05	1.40±.05	2.00±.05
R_g/R_h	1.17±.04	0.99±.04	0.65±.03	0.61±.02

[a] Radius of gyration for a sphere-like object. [b] Experimental value of I(0) from a sphere-like object Gunier plot (eq 1). [c] θ is the mass fraction of solvent within the scatterers. [d] Hydrodynamic radius of dendrons determined from dynamic light scattering.

Comparison of the Solution Behavior of MEA G4.0 and MEA G5.0

Since the MEA G4.0 dendron has a morphology that undergoes substantial changes as a result of its interactions with the surrounding medium, we wanted to confirm that MEA G4.0 is more dynamic in solution than MEA G5.0 as suggested by the maximum V/M ratio displayed in Figure 4.6b. We used SANS and DLS to study the MEA G5.0 dendron in 4mg/mL solutions of D_2O and d^{10}-butanol. The radius of gyration was determined from the Guinier approximation for compact objects, eq 4.1. The Guinier plots of the MEA G5.0 dendron in D_2O and d^{10}-butanol are displayed in Figures 4.5a and 4.12a respectively and indicate that the dendrons are sphere-like due to the negatively sloped straight line. The plots of the intensity of scattering as a function of wave vector for both the D_2O and d^{10}-butanol system (Figures 4.5b and 4.12b) were used to determine the valid Q range to use in the Guinier approximation.

The MEA G5.0 dendron has an R_g value of 3.18 ± 0.05 nm in D_2O (Table 4.2), which decreases to 1.23 ± 0.20 nm when the dendron is in d^{10}-butanol (Table 4.3). This 61% decrease in radius is smaller than the 67% change in radius observed for the MEA G4.0 system going through the same solvent change. This confirms that the generation 4 has the greatest potential to change size. Despite MEA G5.0 dendron having twice the molecular weight and number of end groups of MEA G4.0 still changes size with respect to its surroundings.

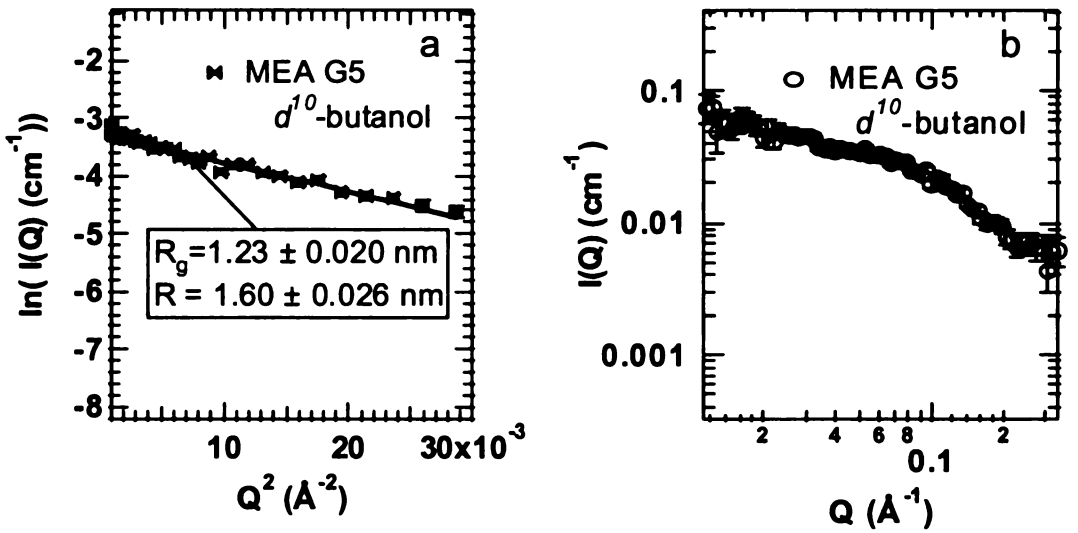

Figure 4.12. SANS of MEA G5.0 in d^{10}-butanol.

a. Guinier analysis for MEA G5.0 dendrons in d^{10}-butanol at a concentration of 4 mg/mL, data fit for a compact (sphere-like) object. b. I vs Q plot of MEA 5.0 dendrons in d^{10}-butanol at a concentration of 4 mg/mL.

The mass fraction of solvent contained within the MEA G5.0 dendrimer was calculated from the experimental I(0) value, eq 4.2, was 0.61 in D_2O and 0.52 in d^{10}-butanol. There is less solvent within the dendrimer when it is in d^{10}-butanol, since the dendrimer has smaller dimensions and is more contracted. This reduction in the mass fraction of solvent (θ) within the dendrimer was also observed for the MEA G4.0 system, where θ decreased from 0.64 for D_2O (Table 4.2) to 0.40 when in d^{10}-butanol (Table 4.3). The lower generation can collapse to a more compact state as indicated by the smaller θ value of 0.40 when in d^{10}-butanol. The MEA G4.0 dendron has a slightly larger amount of solvent within its cavities compared to MEA G5.0, suggesting it has more potential to change size in solution.

We used DLS to determine the hydrodynamic radius of the MEA G5.0 dendron in water and butanol and found values of 2.30 ± 0.10 and 2.00 ± 0.05 nm respectively (Tables 4.2 and 4.3). The R_g/R_h ratio for the MEA G5.0 dendron in water is 1.38 ± 0.06 and 0.61 ± 0.02 when in butanol, where both of these values within experimental error of the R_g/R_h ratios of the MEA G4.0 systems. The change in R_g/R_h with solvent type, also observed for the MEA G4.0 system, is a quantitative indicator that the segmental distribution is a function of the surrounding medium. The matching R_g/R_h ratios for the MEA G4.0 and MEA G5.0 dendrons point to similar spatial arrangements of the dendritic arms of the MEA G4.0 and MEA G5.0 molecules, despite the approximate two-fold difference in molecular weight. This suggests that the density distribution of the molecule is not generation dependent, but rather a function of the interaction of the dendrimers with their surrounding environment for the systems we studied, however further experiments are necessary to verify these results. Despite the similarities in the molecular arrangement of MEA G4.0 and MEA G5.0 it is important to point out that MEA G4.0 has the most potential to change size as shown in Figure 4.6b and discussed above.

Influence of Core-Functionality on the Behavior of PAMAM Dendrimers in Solution

Thus far, all dendrons studied in this work have di-functional cores, which differ from the tri and tetra-functional cores studied by Tomalia,[18] Topp et al.[16, 37] and Nisato et al.[20, 38] To investigate how the functionality of the core dictates the behavior of PAMAM dendrons in solution, we studied a tetra-functional cored PAMAM G4.0 dendron in 4 mg/mL solutions of both D_2O and d^{10}-butanol. This molecule has four dendritic wedges

connected to the focal point and is substantially more sterically hindered than the di-functional MEA dendrons.

The SANS data were analyzed using the Guinier analysis for compact spheres resulting in an R_g of 2.14 ± 0.04 nm and 1.79 ± 0.03 for the Tetra G4.0 dendrimers in D_2O and d^{10}-butanol respectively, Figures 4.13a and 4.14a. This is only a 16% difference in size which is much smaller than the 67% difference we observed for the MEA G4.0 dendrons undergoing the same solvent change. It is clear from these results that the functionality of the core has a substantial impact on the ability of the dendrons to alter dimension in solution, as it determines how the mass scales with generation, eq 4.3.

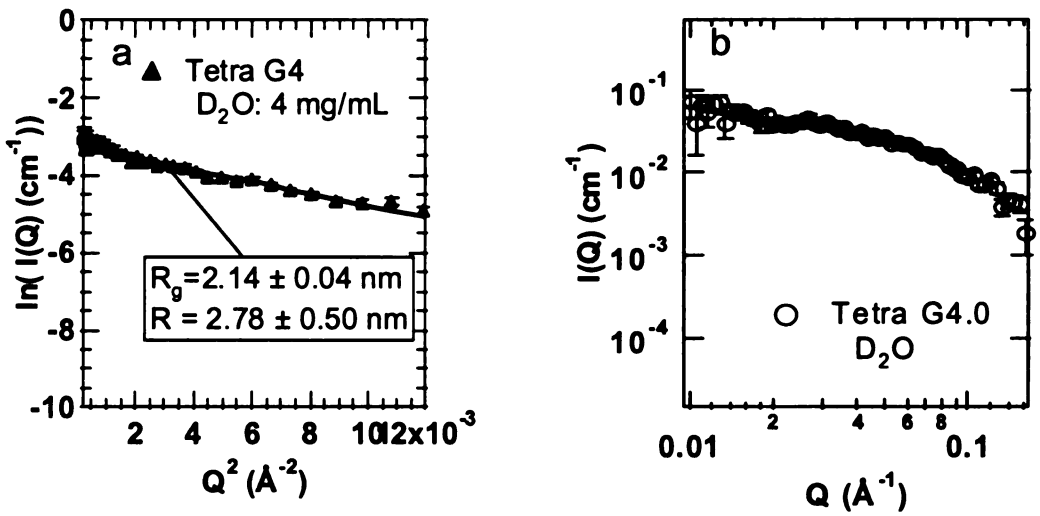

Figure 4.13. SANS of Tetra G 4.0 dendrons in D_2O.

a. Guinier analysis for Tetra G4.0 dendrons in D_2O at a concentration of 4 mg/mL, data fit for a compact (sphere-like) object. b. I vs Q plot of Tetra 4.0 dendrons in D_2O at a concentration of 4 mg/mL.

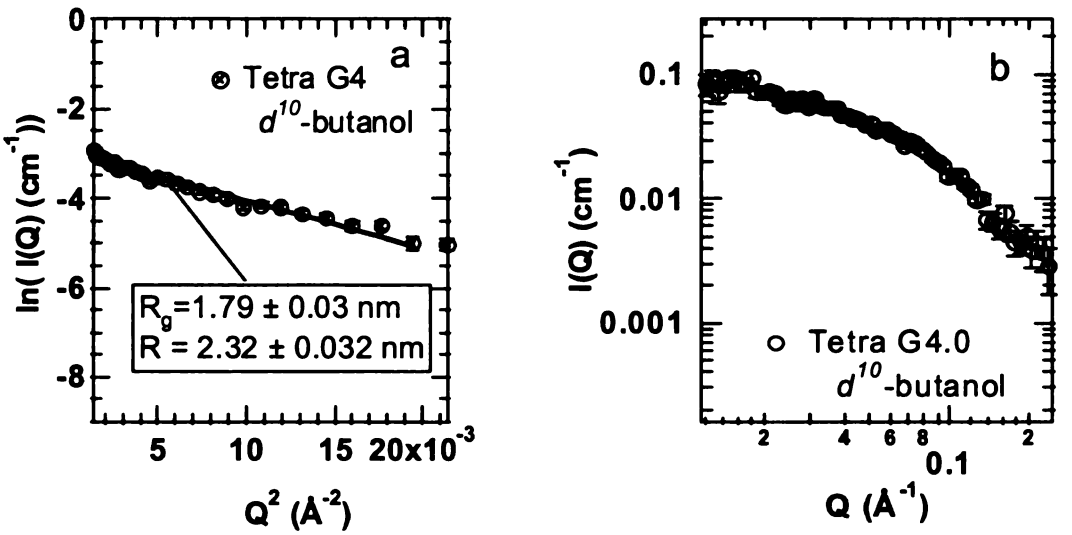

Figure 4.14. SANS of Tetra G 4.0 in d^{10}-butanol.

a. Guinier analysis for Tetra G4.0 dendrons in d^{10}-butanol at a concentration of 4 mg/mL, data fit for a compact (sphere-like) object. b. I vs Q plot of Tetra 4.0 dendrons in d^{10}-butanol at a concentration of 4 mg/mL.

We measured the hydrodynamic radius of the Teta-G4.0 dendrimers using dynamic light scattering and found R_h values of 2.00 ± 0.05 nm and 1.80 ± 0.05 nm when in water and butanol, respectively (Table 4.4). The R_g/R_h ratios for the Tetra-G4.0 dendrons are 1.07 ± 0.03 when in water and 0.99 ± 0.04 in butanol, which are equivalent within experimental error. The Tetra G4.0 dendrimers segmental distribution in solution is less sensitive to the surrounding environment than the MEA G4.0 dendron, where the R_g/R_h ratio changed from 1.36 ± 0.04 to 0.65 ± 0.03 from butanol to water. The steric hindrance of the tetra-functional cored system increases the difficulty of the dendritic arms to adapt to the surrounding medium, explaining the equal R_g/R_h ratio for the butanol and water systems. The segmental distribution of tetra-functional PAMAMs is similar to

that of di-functional cored poly(benzyl ether) in benzene, where an R_g/R_h ratio of 1.02 ± 0.03 was reported in d^6-benzene.[36]

Table 4.4. R_g values for Tetra G4.0 in D_2O and d^{10}-butanol determined from the Guinier analysis described in the text at a concentration of 4 mg/mL. Symbols are explained in the text while Q_{max} is the maximum Q-value used in the regression

Sample Code→	**Tetra**	**Tetra**
solvent	D_2O	d^{10}-butanol
R_g(nm) [a]	2.14±0.04	1.78±0.03
$I(0)_{exp}$ [b] **(cm^{-1})**	0.038	0.050±0.001
$Q_{max}*R_g$	2.34	2.49
θ [c]	0.47	0.43
R_h(nm) [d]	2.00±.0.05	1.80±.0.05
R_g/R_h	1.07±0.03	0.99±.0.04

[a] Radius of gyration for a sphere-like object. [b] Experimental value of I(0) from a sphere-like object Gunier plot (eq 1). [c] θ is the mass fraction of solvent within the scatterers.

Due to the inability of the Tetra-G4.0 dendrimer to alter its morphology in solution, there is little change in the mass fraction of solvent contained within the dendrimer when the solvent is changed from D_2O to d^{10}-butanol (Table 4.4). Using the experimental value of I(0), eq 4.2, θ was calculated as described above to be 0.47 and 0.43 for D_2O and d^{10}-butanol respectively. This contrasts with the change in θ for MEA G4.0 from 0.65 when in D_2O to 0.40 in d^{10}-butanol, and emphasizes the importance of the core functionality on the ability of the dendritic arms to hold guest molecules. The Tetra-G4.0 system is only capable of altering its conformation in solution by small amounts, as opposed to the di-functional cored MEA G4.0 dendrons.

Effect of Ionic Strength on the Morphology and Solution Behavior of MEA Dendrons

To determine the effect of ionic strength on the behavior of MEA dendrons in solution, we conducted dynamic light scattering experiments on MEA G4.0 dendrons in solutions of 1 M HCl, and 1 M HCl with 0.100 M NaCl at concentrations of 4 mg/mL. For the acidic solution with no salt added, the primary and tertiary amine groups of the dendrons are protonated and charged.[39] The hydrodynamic radius of the MEA G4.0 dendron in 1 M HCl is 1.70 ± 0.05 nm, 10% smaller than when the dendron is in water, 1.90 ± 0.05 nm. This size change parallelsthe results of Tomalia et al.[18]

A decrease in size with decreasing pH was also observed by Newkome et al. for amine terminated cascade polymers.[40] Figure 4.15a shows a graph of percent mass vs. R_h of MEA G4.0 in 1 M HCl measured 5 minutes after preparing the sample. Agglomeration of the sample occurs, with a second peak of particle size ~30 nm, appearing 25 minutes after preparing the sample, Figure 4.15b. Attempts were made to conduct further measurements, but the scattering intensity was too high to analyze without risking damage to the detector. We observed evidence of agglomeration of the MEA dendrons in aqueous salt-free solutions via SANS experiments as well, with Figures 4.3b and 4.16 showing I(Q) vs. Q for the MEA G4.0 in D_2O at concentrations of 4 mg/mL and 25 mg/mL respectively. In both graphs, there is a sharp upward change in I(Q) for Q values lower than 0.02 $Å^{-1}$. It appears that the entire sample does not agglomerate at the concentrations studied allowing the data to be analyzed in the Q region greater than 0.02 $Å^{-1}$.

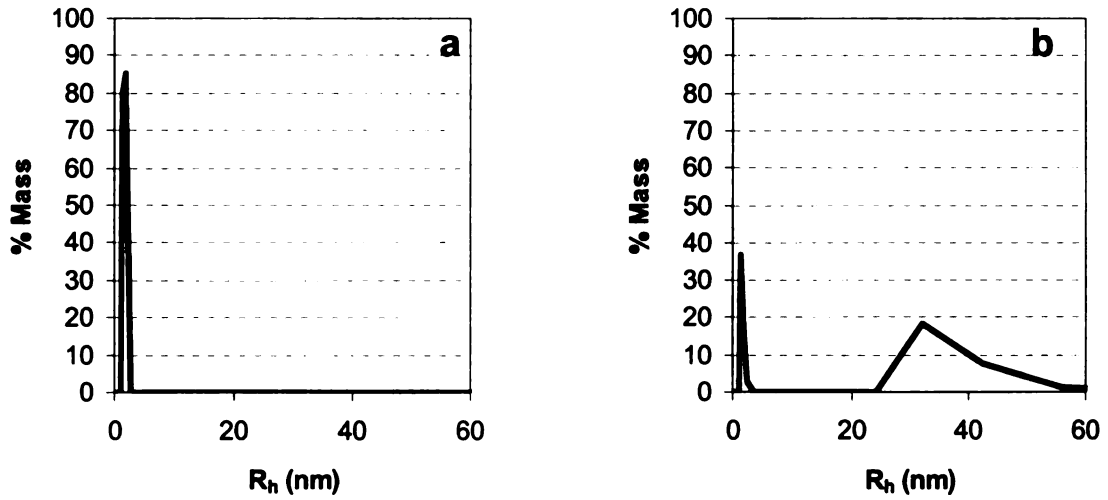

Figure 4.15. Percent mass vs. hydrodynamic radius for a MEA G4.0 dendron in 1 M HCl.

a. Measurements were taken 5 minutes after the 4 mg/mL.
sample was prepared, the peak corresponds to an R_h of 1.70 ± 0.05 nm. b. Percent mass vs. hydrodynamic radius for a MEA G 4.0 dendron in 1 M HCl at a concentration of 4 mg/mL. This measurement was taken 25 minutes after the sample was prepared and shows agglomeration.

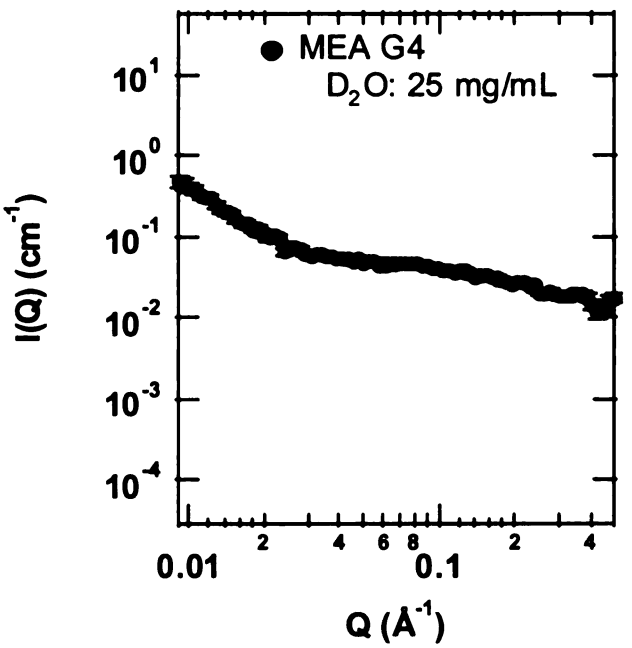

Figure 4.16. I(Q) vs. Q for MEA G4.0 in D_2O at a concentration of 25 mg/mL. The negatively sloped line at Q values below 0.02 $Å^{-1}$ indicates significant agglomeration of the dendrons in salt free conditions.

To determine the cause of agglomeration, we added NaCl to the solutions to eliminate the electrostatic interactions of the protonated amines and conducted DLS experiments on the solutions to determine R_h. The graph of percent mass vs. R_h (Figure 4.17a) shows the size of the dendron is 4.10 ± 0.05 nm when the salt is introduced to the acidic solution, a greater than two-fold increase compared to the salt free conditions. We saw no signs of agglomeration in the salt solution, as shown by Figure 4.17b, which was taken approximately 36 hours after the sample was made. Our results are comparable to those of Russo et al.[41] who showed R_h values of tri-functional cored PAMAMs to increase with increased salt concentration before reaching a plateau at ~75 mM NaCl.

They also observed R_h values that were greatly dependent on the salt concentration at low salt levels at neutral pH.

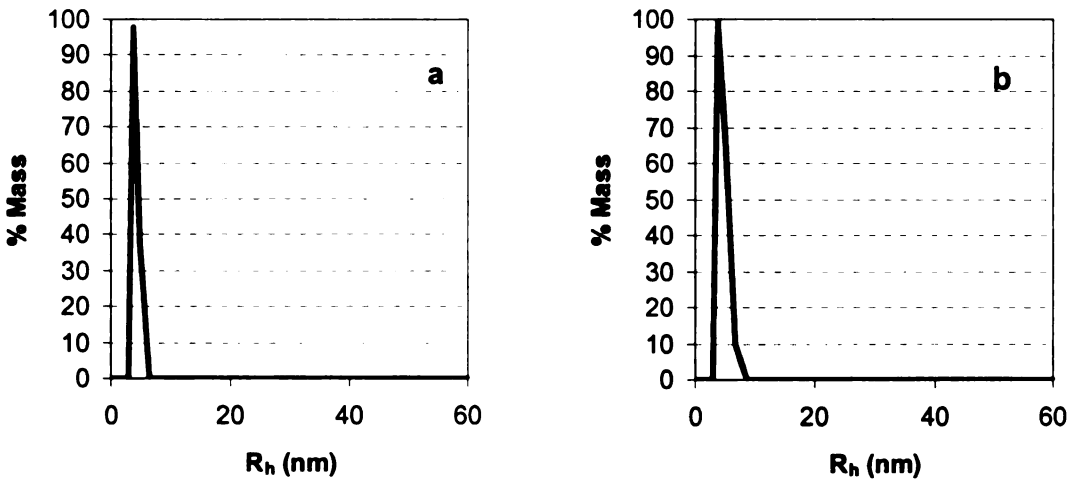

Figure 4.17. Percent mass vs. hydrodynamic radius of an MEA G4.0 dendron in 1 M HCl and 0.100 M NaCl at a concentration of 4 mg/mL.

a. Measurement taken 25 minutes after the sample was made; the peak corresponds to an R_h of 4.10 ± 0.05 nm. b. Measurement taken 36 hours after the sample was made. The addition of salt prevents agglomeration of dendrons in solution.

Agglomeration of the MEA dendrons is eliminated by shielding the electrostatic interactions of the amine groups. At the same time the size of the molecule increases as the ionic strength increases, suggesting an increase in solvent quality. The unique intermolecular hydrogen bonding capabilities of the PAMAM dendron serves as a handle to control their morphology and apply them to unique materials.

Conclusion

A generation 4 MEA dendron has the largest volume:molecular weight ratio, which demonstrates it is most capable of changing size as a function of the surrounding medium. We used SANS and DLS experiments to demonstrate that the size of di-functional MEA dendrons is a function of the quality and ionic strength of the solvent.

These molecules are dynamic in solution and can change size, with the smallest size in d^{10}-butanol and the largest size in a solution of 1 M HCl with 0.100 M NaCl. The functionality of the core strongly governs the change in size and density distribution of dendrimers in solution. A tetra-functional PAMAM dendrimer only decreases in size by 16% when going from D_2O to d^{10}-butanol, whereas the size of a di-functional MEA dendron decreases by 67%. The steric constraints caused by the increased functionality of the core decreases the ability of the molecules to change size in solution at a given generation. PAMAM dendrons have potential to be used for novel "smart" materials since their molecular dimensions are sensitive to the surrounding environment.

References

1. Newkome, G. R.; Moorefield, C. N.; Vögtle, F., *Dendritic Molecules: Concepts, Syntheses, Perspectives*. John Wiley & Sons: New York, 1996.

2. Hawker, C. J.; Fréchet, J. M. J., *J. Am. Chem. Soc.* **1990,** *112*, 7638-7647.

3. Tomalia, D.; Baker, H.; Dewald, J.; Hall, M.; Kallos, G.; Martin, S.; Roeck, J.; Ryder, J.; Smith, P., *Poly. J.* **1985,** *17*, 117-132.

4. Jansen, J. F. G. A.; Meijer, E. W.; de Brabander-van den Berg, E., *Science* **1994,** *266*, 1266-1229.

5. deGennes, P. G.; Hervet, H., *J. Phys. Let.* **1983,** *44*, L351-L360.

6. Topp, A.; Bauer, B. J.; Klimash, J. W.; Spindler, R.; Tomalia, D. A.; Amis, E. J., *Macromolecules* **1999,** *32*, 7226-7231.

7. Lyulin, A. V.; Davies, G. R.; Adolf, D. B., *Macromolecules* **2000,** *33*, 6899.

8. Lescance, R. L.; Muthukumar, M., *Macromolecules* **1990,** *23*, 2280-2289.

9. Wooley, K. L.; Klug, C. A.; Tasaki, K.; Schaefer, J., *J. Am. Chem. Soc.* **1997,** *119*, 53-58.

10. Ballauff, M.; Rosenfeldt, S.; Dingenouts, N.; Werner, N.; Vogtle, F.; Lindner, P., *Macromolecules* **2002,** *35*, 8089-8105.

11. Mansfield, M. L.; Klushin, L. I., *Macromolecules* **1993,** *26*, 4262-4268.

12. Murat, M.; Grest, G. S., *Macromolecules* **1996,** *29*, 1278-1285.

13. Welch, P.; Muthukumar, M., *Macromolecules* **1998,** *31*, 5892-5897.

14. Maiti, P. K.; Cagin, T.; Wang, G.; Goddard, W. A., III, *Macromolecules* **2004,** *37*, 6236-6254.

15. Maiti, P. K.; Cagin, T.; Lin, S. T.; Goddard, W. A., *Macromolecules* **2005,** *38*, 979-991.

16. Topp, A.; Bauer, B.; Tomalia, D.; Amis, E., *Macromolecules* **1999,** *32*, 7232-7237.

17. Stechemesser, S.; Eimer, W., *Macromolecules* **1997,** *30*, 2204-2206.

18. Tomalia, D. A.; Smith, P. B.; Hall, M. J.; Martin, S. J., *A Characterization of the Structure and Synthetic Reactions of Polyamidoamine "Starburst" Polymers*. Hanser: Munich, 1987.

19. Nisato, G.; Ivkov, R.; Amis, E., *Macromolecules* **2000,** *33*, 4172-4176.

20. Nisato, G.; Ivkov, R.; Amis, E. J., *Macromolecules* **1999,** *32*, 5895-5900.

21. Mourey, T. H.; Turner, S. R.; Rubenstein, M.; Frechet, J. M. J.; Hawker, C. J.; Wooley, K. L., *Macromolecules* **1992,** *25*, 2401-2406.

22. Jeong, M.; Mackay, M. E.; Vestberg, R.; Hawker, C. J., *Macromolecules* **2001,** *34*, 4927-4936.

23. Tomalia, D. A.; Naylor, A. M.; Goddard, W. A., *Angew. Chem. Int. Ed. Engl.* **1990,** *29*, 138-175.

24. Tomalia, D. A.; Hedstrand, D. M.; Wilson, L. R., *Enclylopedia of Polymer Science and Engineering*. 2 ed.; Wiley: New York, 1990; p 69-75.

25. Hawker, C. J.; Wooley, K. L.; Frechet, J. M. J., *J. Am. Chem. Soc.* **1993,** *115*, 4375-4376.

26. Moreno-Bondi; M. A.; Orellana; G.; Turro, N. J.; Tomalia, D. A., *Macromolecules* **1990,** *23*, 912.

27. Tomalia, D. A.; Hall, M.; Hedstrand, D. M., *J. Am. Chem. Soc.* **1987,** *109*, 1601-1603.

28. Prosa, T. J.; Bauer, B. J.; Amis, E. J.; Tomalia, D. A.; Scherrenberg, R., *J. Polym. Sci. B: Polym. Phys.* **1997,** *35*, 2913-2924.

29. Guinier, A. F., G, *Small Angle Scattering of X-Rays*. John Wiley & Sons, Ltd: New York, 1955.

30. Gallas, J. M.; Littrell, K. C.; Seifert, S.; Zajac, G. W.; Thiyagarajan, P., *Biophys. J.* **1999,** *77*, 1135-1142.

31. Burchard, W., *Adv. Polym. Sci.* **1999,** *143*, 113-195.

32. Schmidt, M.; Burchard, W., *Macromolecules* **1981,** *14*, 210-211.

33. Termeer, H. U.; Burchard, W.; Wunderlich, W., *Coll. Poly. Sci.* **1980,** *258*, 675-684.

34. Jeong, M.; Mackay, M. E.; Hawker, C. J.; Vestberg, R., *Macromolecules* **2001,** *34*, 4927-4936.

35. Fritzinger, B.; Scheler, U., *Macrom. Chem. Phys.* **2005,** *206*, 1288-1291.

36. Passeno, L. M.; Mackay, M. E.; Baker, G. L.; Vestberg, R.; Hawker, C. J., *Macromolecules* **2006,** *39*, 740-746.

37. Topp, A.; Bauer, B. J.; Klimash, J. W.; Spindler, R.; Tomalia, D. A.; Amis, E. J., *Macromolecules* **1999,** *32*, 7226-7231.

38. Nisato, G.; Ivkov, R.; Amis, E. J., *Macromolecules* **2000,** *33*, 4172-4176.

39. Niu, Y.; Sun, L.; Crooks, R. M., *Macromolecules* **2003,** *36*, 5725-5731.

40. Young, J. K.; Baker, G. R.; Newkome, G. R.; Morris, K. F.; Johnson, C. S., *Macromolecules* **1994,** *27*, 3464-3471.

41. Yu, K.; Russo, P. S., *J. Polym. Sci. B: Polym. Phys.* **1996,** *34*, 1467-1475.

CHAPTER FIVE: Synthesis and Characterization of Dansyl-Cored PAMAM Di-Dendrons

Introduction

Cascade molecules,[1] more commonly known as dendrimers[2, 3] are a unique type of macromolecule whose branched molecular architecture provides the diversity of functionalization either at the focal point, the branching units or the periphery. The chemical modification of dendrimers is a rapidly growing field aimed to understand both the fundamental properties of these molecules as well as their potential technological applications. Implementation of dendrimers in molecular sensing and drug delivery schemes requires a thorough understanding of the behavior of these molecules in solution, in the bulk or at an interface.

The polarity of microenvironments within a dendrimer can be probed using solvatochromic compounds, whose absorption and emission spectra vary with solvent polarity. There have been several studies of dendrimers with fluorescent probes located at either the periphery or the focal point of the molecule. One of the first examples of functionalization of a dendrimer with a solvatochromic compound was done by Hawker et al.[4] who covalently linked 4-(N, N-dimethylamino)-1-nitrobenzene to the focal point of a poly(benzyl ether) dendrimer. They observed a discontinuity in the shifting of λ_{max} for the chromophore from generation 3 to generation 4, which they explained by the conversion of the dendrimer architecture from an extended to a globular state. More recently Bright and coworkers[5, 6] investigated dendrimers with a fluorescent dansyl group at the focal point to determine its host-guest relationships and molecular sensing properties. They placed a dansyl group at the focal point of a carboxylic acid terminated dendrimer and via photophysical measurements, showed that the dansyl residue is

progressively shielded from the solvent as the dendrimer generation increases.[5] They also showed that access to the dansyl moiety at the core is impeded with increasing dendrimer generation by determining the equilibrium binding constant of β-cyclodextrin to dansyl as a function of generation. In further work, Bright and coworkers[6] attached a pyrene residue to the tertiary amine at the focal point of asymmetric poly(amido) dendrimers with carboxylate end groups and investigated the accessibility of the core to a series of neutral and ionic (iodide and cupric ions) quenchers. They found that the approach of neutral and ionic quenching agents is increasingly hindered as the generation of the dendrimer increases.

Similar ion detection schemes were reported by Baker and coworkers[7] who placed a pyrene moiety at the focal point of carboxylate terminated poly(amido) dendrons to detect the permeability of Pb^{2+} to the core of the molecule as a function of pH and generation. For aqueous solutions near neutral pH, the dendrimer-pyrene scheme has a detection limit below the level defined by the World Health Organization for safe drinking water, 10 ppb, which is encouraging for the utility of dendrimers as sensing devices. Gawley et al.[8] placed a fluorescent dansyl moiety at the core of Newkome-type dendrimers and attached a portion of the dendrons' carboxylic end groups to the amine functionality on a solid-phase protein synthesis bead. The unreacted end groups were then covalently bound to rhodamine dye, and the ability of the dye to penetrate through the dendrimer was signaled by the dansyl group.

Numerous groups have attached fluorescent chromophores to the end groups of dendrimers. Wei and coworkers[9] attached phenyl, naphthyl, pyrenyl and dansyl chromophores to the periphery of poly(amido amine) (PAMAM) dendrimers to study the

self-organization of these materials in aqueous solutions. Using fluorescence spectroscopy, they found aggregates form for G1 to G3 where the size and aggregation number of the vesicles decreases with increasing generation. The PAMAM dendrimers G0-G5 showed a broad structure less fluorescence peak at 468 nm, which was attributed to the $\pi-\pi$ interaction between adjacent parallel-oriented pyrene chromophores.[9] The excimer emission increased from G0 to G3, suggesting that higher generations favor parallel alignment of the pyrene rings, yet upon reaching G4 the emission intensity decreased indicating the rings are no longer able to adopt such an arrangement. This implies that the dendritic arms for G4 and G5 are more sterically crowded and the molecular arrangement of the dendron changes from G3 to G4 preventing pyrene alignment. For the dendrimer functionalized with dansyl groups at the periphery, the λ_{max} emission shifted from 445 nm for G2 to 512 nm for G3.[9] This shift is due to transforming the dansyl chromophore from a locally excited state (coplanar) to an intramolecular charge transfer excited state (twisted)[10] due to the changes in the dendritic architecture.[9] Wei et al. [11] functionalized PAMAM tetra-dendrons end groups with 1-(naphthalenyl)-2-phenyldiazene to study the aggregation behavior with respect to generation number. They found organized aggregates to occur in a predictable fashion for G3 and lower, but generations higher than 4 did not self-assemble into ordered structures. The lack of self assembly at higher generations illustrates the change in dendrimer morphology between G3 and G4 from an extended to a globular state.

Schluter and coworkers[12] designed a targeting drug delivery device by modifing a 2,3,-D/L-diaminopropionic acid dendrimer, placing dansyl groups on a certain number of the end groups and a cleavable peptide spacer on the remaining end groups. The peptide

chain was used as the spacer between the fluorescent dendrimer and potentially a cleavable anti-cancer drug. Fluorescence microscopy displayed the rapid uptake of dendrimers into human HeLa cells and a localized dendrimer concentration next to the cell nucleus after 18 hours of incubation.

Balzani and coworkers[13, 14, 15] chemically linked dansyl groups to the periphery of poly(propylene amine) dendrimers and measured fluorescence quenching as a function of Co^{2+} ion concentration. They showed that metal ions coordinate to the interior of the dendrimers in a fully reversible fashion. An increase in the fluorescence quenching efficiency with increasing dendrimer size leads to strong amplification of the signal and thus an increased sensitivity of the sensor.

The host-guest behavior of poly(lysine) dendrimers and lanthanide ions was studied by Vögtle et al.[16] using dansyl terminated poly(lysine) dendrimers and measuring the fluorescent quenching as a function of ion concentration. Formation of metal complexes accompanies quenching of the fluorescent excited state of the dansyl units. This effect is very large for Nd^{3+} and Eu^{3+} and may be exploited for a variety of applications from sensors to fluoroimmunoassays. Using a similar system, Vögtle and coworkers[17] studied the host-guest properties of a dansyl terminated poly(propylene amine) dendrimer and eosin dye molecules. The ability of the dye to penetrate into dendritic cavities is dependent on the size of the dendrimer, since the number of dye molecules capable that can be held by the dendrimer increases with increasing generation. Vögtle et al.[18] synthesized a dendrimer with a cyclam metal ligand core and naphthyl terminal groups to further study the ability of dendrimers to sequester metal cations. Complexation of the cyclam core with Zn^{2+} was shown by an increased i the

naphthyl fluorescence intensity. They found that two cyclam-cored dendrons coordinate with one zinc cation and suggested the ability of the dendrimer to coordinate in a controlled fashion with Zn^{2+} may play an important role in catalysis and medical diagnosis.

Work where dendrimers were modified a dendrimer with a fluorophore was motivated by the dendron acting as a molecular sensor, with little emphasis on the actual morphology of the dendrimer as a function of environment or generation. Understanding the dendritic morphology should simplify the design of such systems and enhance the efficiency of sensing devices. Depending on the application, it may be desirable to have either an accessible or more hidden probe, which would alter its selectivity. To investigate the molecular domains or solvent penetrability near the focal point of a PAMAM dendrimer, we synthesized a PAMAM di-dendron that contains a solvatochromic dansyl moiety at its focal point, Scheme 4.1. The synthesis was continued to G5.0 and the theoretical molecular weight of each generation is listed in Table 5.1. The fluorescence emission of the dansyl moiety was measured as a function of generation number and solvent conditions to determine how the solvent quality influences the behavior of these molecules in solution.

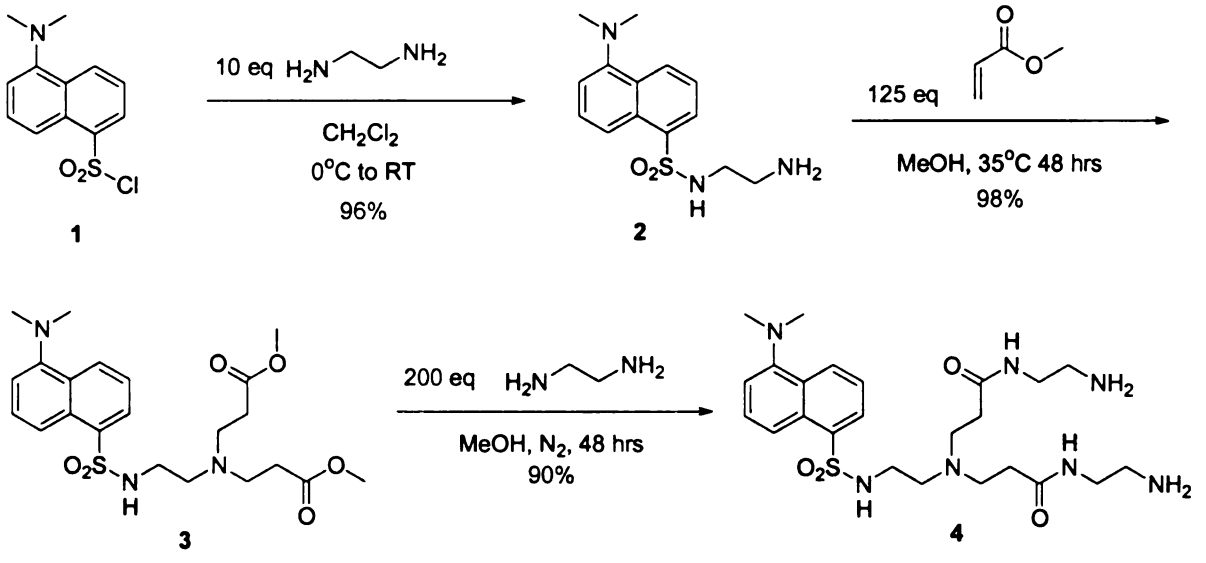

Scheme 5.1. Synthesis of dansyl-cored PAMAM dendrimer.

Table 5.1. Theoretical molecular mass (M) of the dansyl-cored PAMAM dendrimers.

Sample Code	M (Da)	Sample Code	M (Da)
dansyl G0.5	465	dansyl G3.0	1889
dansyl G1.0	521	dansyl G3.5	3265
dansyl G1.5	865	dansyl G4.0	3713
dansyl G2.0	977	dansyl G4.5	6465
dansyl G2.5	1665	dansyl G5.0	7361

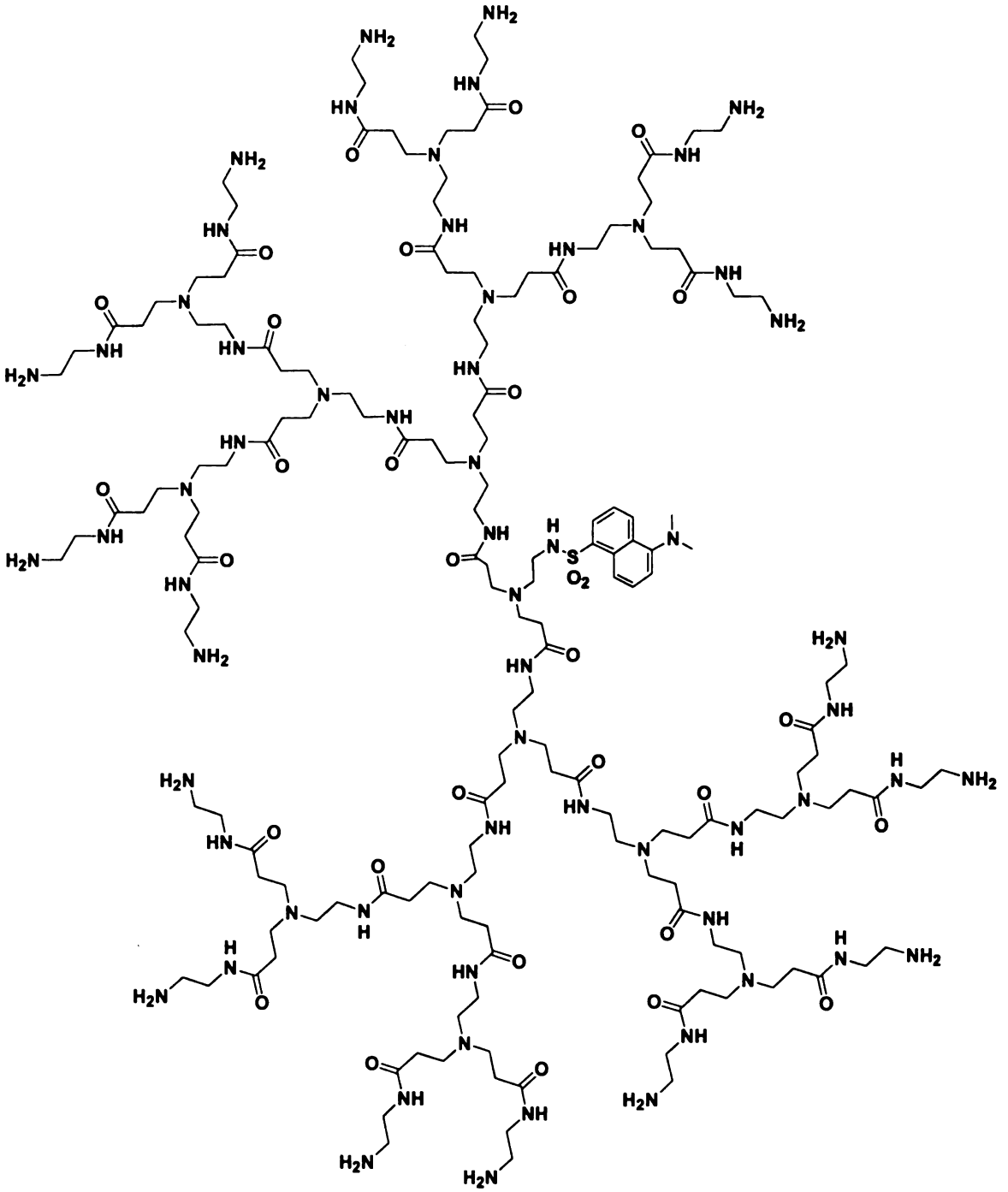

Scheme 5.2. Generation 4 dansyl-cored PAMAM dendrimer.

Experimental

Materials. All chemicals were purchased from Aldrich Chemical Co., Saint Louis, MO. Ethylenediamine was distilled under nitrogen prior to use. Methyl acrylate was distilled from KOH to remove the inhibitor. ^{1}H and ^{13}C NMR spectra were acquired on a Varian 300 or 500 MHz instrument, as indicated, with the residual proton signal from the solvent used as the reference peak. NMR spectra and assigned chemical shifts are displayed in Appendix B.

Preparation of (2-aminoethyl)-dansylamide (dansyl-EDA), 2.[19] (Scheme 4.1) A solution of dansyl chloride (2.50 g, 9.27 mmol) in dichloromethane (25 mL) was dropped into a stirred solution of ethylenediamine (62 mL, 55.7 g, 0.927 mol) cooled to 0 °C by an ice bath. When the addition was complete, the ice bath was removed and the mixture warmed to room temperature with continued stirring. The bright yellow/green reaction mixture was divided into two portions and each portion was acidified by slowly adding 6 M HCl. The pale green acidified solution was extracted with dichloromethane (2 × 200 mL). The aqueous layers were adjusted to pH 9 by slowly adding 10 M NaOH and again extracted with dichloromethane (2 × 200 mL). The combined organic layers were dried with $MgSO_4$, filtered and concentrated to give 2.62 g (96% yield) of (2-aminoethyl)-dansylamide (**2**) a yellow/green solid. ^{1}H NMR (300 MHz, $CDCl_3$) δ: 8.50 (d, 1H), 8.23 (m, 2H), 7.50 (m, 2H), 7.15 (d, 1H), 2.80 (m, 8H), and 2.64 (t, 2H).

Dansyl-PAMAM Synthesis

Dansyl-PAMAM G0.5 (3). A stirred solution of (2-aminoethyl)-dansylamide (**2**), (0.541 g, 1.84 mmol) in methanol (25 mL) was slowly dripped into 125 eq methyl acrylate (21 mL, 19.80 g, 0.23 mol) at 35 °C. The reaction was stirred for two days at 35 °C under

nitrogen and then methanol and un-reacted methyl acrylate was removed in vacuo, to provide 0.822 g (98% yield) of **3** as a pale green solid.

^{1}H NMR (300 MHz, $CDCl_3$) δ: 8.48 (d, 1H, J = 11.4 Hz), 8.36 (d, 1H, J = 9 Hz), 8.21 (d, 1H, J = 7.2 Hz), 7.54 (m, 2H), 7.13 (d, 1H, J = 8.4 Hz), 3.64 (s, 6H), 2.93 (q, 2H, J = 5.4 Hz), 2.52 (t, 4H, J = 6.6 Hz), 2.39 (t, 2H J = 5.1 Hz), and 2.47 (t, 4H J = 6.6 Hz). ^{13}C NMR ($CDCl_3$, 300MHz) δ 172.8, 151.8, 135.0, 130.1, 129.9 129.6, 129.4, 128.0, 123.1, 119.2, 115.0, 52.9, 51.7, 48.7, 45.3, 40.6, 32.1.

Dansyl G1.0 (4). A solution of dansyl-PAMAM G0.5 (**3**) (0.358 g, 0.769 mmol) was dissolved in 25 mL methanol and slowly dripped into a stirred solution of 200 eq ethylenediamine (10.30 mL, 9.24 g, 0.154 mol) 55 °C. After stirring for two days, methanol and unreacted ethylenediamine was removed in vacuo. To remove residual amounts of ethylenediamine, the residue was dissolved in octanol (100 mL) and stirred under vacuum (5 mTorr) at 40 °C for 2 days. The octanol mixture was washed with 50:50 hexane:water. The aqueous layer was collected and washed three times with hexanes (3 × 150 mL), then concentrated and dried under vacuum at 40 °C. The dried crude product was dissolved in methanol and placed in a dialysis bag (MWCO = 200 g/mol) for two days. The contents of the bag were dried under vacuum providing 0.361 g (90% yield) of **4** as a yellow/green colored oil^{1}H NMR (300 MHz, d^4-methanol) δ: 8.43 (d, 1H, J = 11.4 Hz), 8.30 (d, 1H, J = 9.0 Hz), 8.15 (d, 1H, J = 7.2 Hz), 7.50 (m, 2H), 7.20 (d, 1H, J = 8.4 Hz), 3.18 (t, 4H, J = 6.0 Hz), 2.85 (t, 2H, J = 6.0 Hz), 2.78 (s, 6H), 2.65 (t, 4H, J = 6.0 Hz), 2.54 (t, 4H, J = 6.9 Hz), 2.37 (t, 2H, J = 6.6 Hz), and 2.18 (t, 4H, J = 6.9 Hz). ^{13}C NMR (d^4-methanol, 300MHz) δ: 174.84, 152.8, 135.0, 130.8, 130.5, 130.3, 129.8, 129.1, 124.1, 120.0, 116.1, 53.6, 50.3, 49.0, 45.5, 42.6, 41.6, 34.1.

Synthesis of Dansyl-PAMAM

Formation of subsequent half and full generation PAMAM dendrimers was done by following the above methods for the formation of dansyl-G0.5 and dansyl G1.0 respectfully.

Dansyl G1.5. ^{1}H NMR (300 MHz, d^{4}-methanol) δ: 8.52 (d, 1H, , J = 11.3 Hz), 8.33 (d, 1H, J = 9.0 Hz), 8.18 (d, 1H, J = 7.2 Hz), 7.56 (m, 2H), 7.23 (d, 1H, J = 8.4 Hz), 3.58 (s, 12H), 3.20 (t, 4H, J = 6.6 Hz), 2.92 (t, 2H, J = 6.0 Hz), 2.83 (s, 6H), 2.69 (t, 8H, J = 6.0 Hz), 2.61 (t, 4H, J = 6.9 Hz), 2.49-2.39 (m, 14H), and 2.22 (t, 4H, J = 6.9 Hz). ^{13}C NMR (d^{4}-methanol, 300MHz) δ: 173.4, 173.3, 151.8, 135.7, 131.0, 129.8. 129.6, 128.7, 127.9, 123.0, 119.5, 115.9, 52.5, 52.2, 50.8, 49.3, 49.1, 44.5, 50.7, 37.1, 33.1, 32.2.

Dansyl G2.0. ^{1}H NMR (300 MHz, d^{4}-methanol) δ: 8.50 (d, 1H, J = 11.3 Hz), 8.30 (d, 1H, J = 9.0 Hz), 3.18 (d, 1H, J = 7.2 Hz), 7.54 (m, 2H), 7.22 (d, 1H, J = 8.4 Hz), 3.24-3.24 (m, 12H), 2.90 (t, 2H, J = 6.0 Hz), 2.82 (s, 6H), 2.78-2.64 (m, 16H), 2.62-2.50 (m, 8H), 2.48-2.40 (m, 2H), 2.30 (t, 8H, J = 6.6 Hz), and 2.20 (t, 4H, J = 6.6 Hz). ^{13}C NMR (d^{4}-methanol, 300MHz) δ: 174.9, 174.5, 131.2, 153.0, 138.0, 131.3, 131.2, 130.9, 130.1, 129.2, 124.4, 120.5, 116.5, 53.4, 51.2, 50.6, 45.2, 42.9, 41.9, 38.6, 34.8, 34.3.

Dansyl G2.5. ^{1}H NMR (300 MHz, d^{4} methanol) δ: 8.52 (d, 1H, J = 11.3 Hz), 8.32 (d, 1H, J = 9.0 Hz), 8.18 (d, 1H, J = 7.2 Hz), 7.56 (m, 2H), 7.24 (d, 1H, J = 8.4 Hz), 3.62 (s, 24H), 3.30-3.14 (t, 12H, J = 6.0 Hz), 2.92 (t, 2H), 2.84 (s, 6H), 2.82-2.66 (m, 24H), 2.42-2.52 (m, 8H), 2.50 (t, 10H, J = 6.3 Hz), and 2.42-2.10 (m, 24H). ^{13}C NMR (d^{4}-methanol, 300MHz) δ: 174.9, 153.5, 136.0, 131.4, 131.2, 130.9, 130.4, 120.5, 124.7, 120.9, 116.7, 54.0, 53.6, 52.4, 51.3, 50.7, 46.2, 42.3, 38.7, 38.7, 35.0, 34.6, 33.8.

Dansyl G3.0. ^{1}H NMR (300 MHz, d^4-methanol) δ: 8.60 (d, 1H, J = 11.3 Hz), 8.40 (d, 1H, J = 9.0 Hz), 8.25 (d, 1H, J = 7.2 Hz), 7.64 (m, 2H), 7.31 (d, 1H, J = 8.4 Hz), 3.40-3.15 (m, 28H), 3.00 (t, 2H), 2.91 (s, 6H), 2.90-2.70 (m, 32H), 2.69-2.48 (m, 22H), and 2.47-2.10 (m, 28H). ^{13}C NMR (d^4-methanol, 300MHz) δ: 173.8, 173.4, 151.9, 130.2, 130.0, 129.8, 129.6, 128.8, 127.9, 123.1, 119.0, 114.2, 52.1, 49.8, 49.2, 44.9, 44.5, 41.1, 40.6, 37.3, 33.4, 33.0.

Dansyl G3.5. ^{1}H NMR (300 MHz, d^4-methanol) δ: 8.50 (d, 1H, J = 11.3 Hz), 8.30 (d, 1H, J = 9.0 Hz), 8.10 (d, 1H, J = 7.2 Hz), 7.54 (m, 2H), 7.20 (d, 1H, J = 8.4 Hz), 3.59 (s, 48H), 3.18 (m, 28H), 2.88 (m, 2H), 2.84-2.44 (m, 96H), and 2.42 (2.18, 60H). ^{13}C NMR (d^4-methanol, 300MHz) δ:174.6, 174.5, 153.2, 131.5, 131.1, 131.1, 130.9, 130.2, 129.3, 124.5, 120.6, 116.5, 53.7, 53.2, 52.2, 50.9, 50.4, 45.9, 38.4, 34.5, 33.5, 30.7.

Dansyl G4.0. ^{1}H NMR (300 MHz, d^4-methanol) δ: 8.47 (d, 1H, J = 11.3 Hz), 8.26 (d, 1H, J = 9.0 Hz), 8.12 (d, 1H, J = 7.2 Hz), 7.50 (m, 2H), 7.20 (d, 1H), 3.40-3.30 (m, 60H), 2.88 (t, 2H), 2.85 (s, 6H), 2.85-2.65 (m, 88H), 2.65-2.50 (m, 34H), and 2.50-2.20 (m, 60H). ^{13}C NMR (d^4-methanol, 300MHz) δ: 176.3, 175.2, 174.7, 153.3, 136.9, 131.3, 131.2, 131.2, 130.9, 130.1, 129.3, 124.5, 120.5, 117.5, 54.6, 53.4, 51.1, 46.3, 45,8, 42.6, 41.9, 40.4, 39.9, 38.6, 37.4, 36.4, 34.7.

Dansyl G4.5. ^{1}H NMR (300 MHz, d^4-methanol) δ: 8.50 (d, 1H J = 11.3 Hz), 8.30 (d, 1H J = 9.0 Hz), 8.14 (d, 1H J = 7.2 Hz), 7.56 (m, 2H), 7.20 (d, 1H J = 8.4 Hz), 3.60 (m, 96H), 3.20 (m, 6H), 2.85 (s, 60H), 2.90 (m, 2H), 2.84 (s, 6H), 2.82-2.64 (m, 132H), 2.63 (m, 62H), and 2.40-2.20 (m, 152H). ^{13}C NMR (d^4-methanol, 300MHz) δ: 174.7, 174.5, 153.2, 131.5, 131.1, 131.1, 130.9, 130.2, 129.3, 124.5, 120.6, 116.5, 53.7, 53.2, 52.2, 50.9, 50.4, 45.9, 38.4, 34.5, 33.5, 30.7.

Dansyl G5.0. ^{1}H NMR (300 MHz, d^4-methanol) δ: 8.50 (d, 1H J = 11.3 Hz), 8.30 (d, 1H J = 9.0 Hz), 8.14 (d, 1H J = 7.2 Hz), 7.56 (m, 2H), 7.20 (d, 1H J = 8.4 Hz), 3.30-3.10 (m, 124H), 2.82-2.64 (m, 196H), 2.60-2.50 (m, 60H), and 2.40-2.20 (m, 128H). ^{13}C NMR (500 MHz, d^4-methanol) δ: 175.2, 174.9, 70.0, 153.2, 131.5, 131.1, 131.1, 130.9, 130.2, 129.3, 124.5, 120.6, 116.5, 54.4, 54.2, 53.9, 51.5, 45.9, 42.3, 41.9, 38.4, 34.5.

Fluorescence Measurements. Dansyl-PAMAM dendrimer samples were dissolved in the appropriate solvent with concentrations ranging from 5×10^{-5} to 1×10^{-3} M and we observed no change in λ_{max} as a function of concentration at these concentrations. Fluorescence measurements were performed using a Fluorolog-3 instrument from Instruments S.A., Inc. The excitation optics consisted of a 450W Xe lamp followed by a 330 nm ruled grating. The detection optics consisted of a 530 nm ruled grating and multi-alkali photo multiplier tube at 950V (Hamamatsu R928). Data processing was performed using the Datamax (version 2.2) software package supplied with the instrument. The excitation beam was centered at 360 nm with a 1 nm bandpass and the emission monochromator was scanned from 370 to 800 nm in 1nm steps.

Results and Discussion

Solvent Dependence of the Emission Spectra of (Dansyl-EDA) (2)

The dansyl group is solvatochromic with the location (wavelength) of its emission and absorption a function of solvent polarity. It undergoes a significant bathochromic (red) shift with increasing solvent polarity. We studied the emission of dansyl-EDA (**2**), which is generation 0 (dansyl G0), in methanol, ethanol, butanol, chloroform and acetonitrile and found a significant change in maximum emission wavelength (λ_{max}) with respect to solvent, Figure 5.1. The dielectric constants of the solvents are listed in Table

5.2. There is an approximately linear relationship between the dielectric constant and λ_{max} for Dansyl-EDA (**2**), Figure 5.2. The deviation from linearity occurring at the highest dielectric constant, acetonitrile, is due to the poor hydrogen bonding capabilities of this solvent. The excited state of the dansyl group (π^*) has a higher dipole moment than the ground state and is stabilized by hydrogen bonding in addition to increased solvent polarity. Although methanol is less polar than acetonitrile, it is a better hydrogen bonding solvent. In this case hydrogen bonding by methanol overcomes the polarity difference between the two solvents stabilizing the excited state of the dansyl group (shift to a lower energy, higher wavelength) more effectively than acetonitrile. This emphasizes the sensitivity of dansyl's fluorescence emission to both solvent polarity and hydrogen bonding.

Table 5.2. Solvents and their dielectric constants (ε) used in this study.

Solvent	ε
chloroform	5.5
butanol	17.8
ethanol	24.6
methanol	32.6
acetonitrile	36

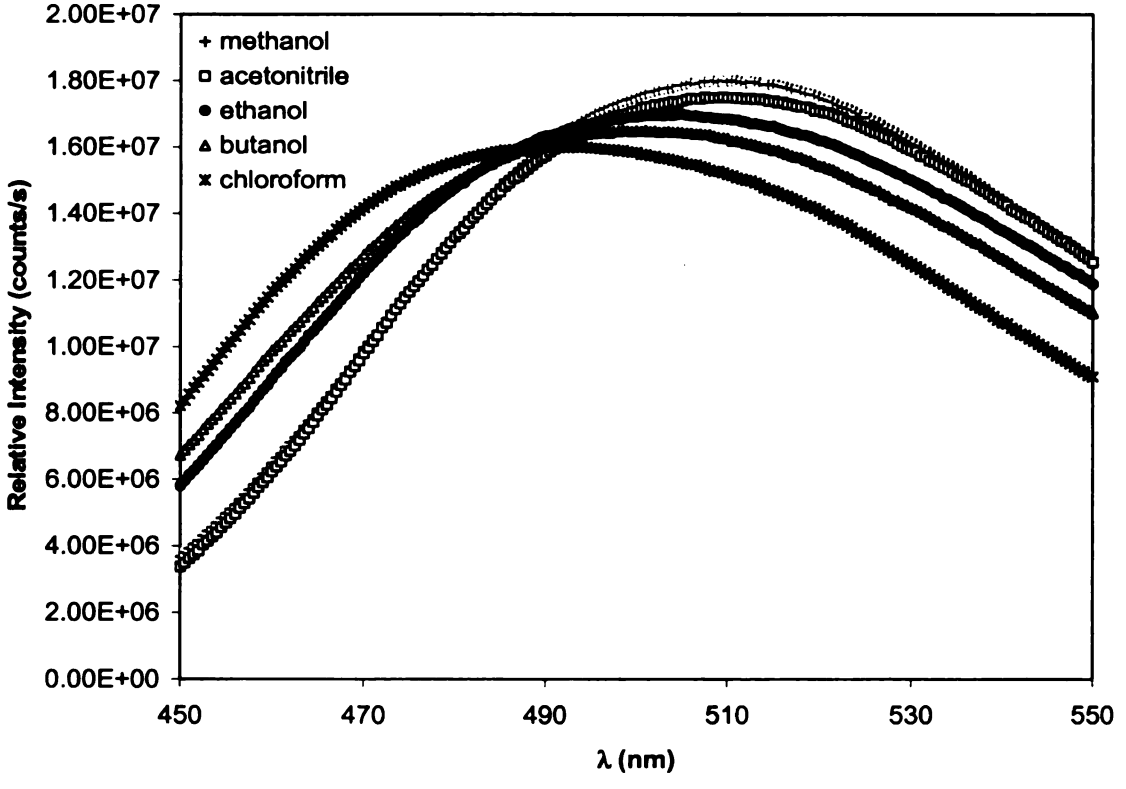

Figure 5.1. Normalized fluorescence emission spectra of (2-aminoethyl)-dansylamide.

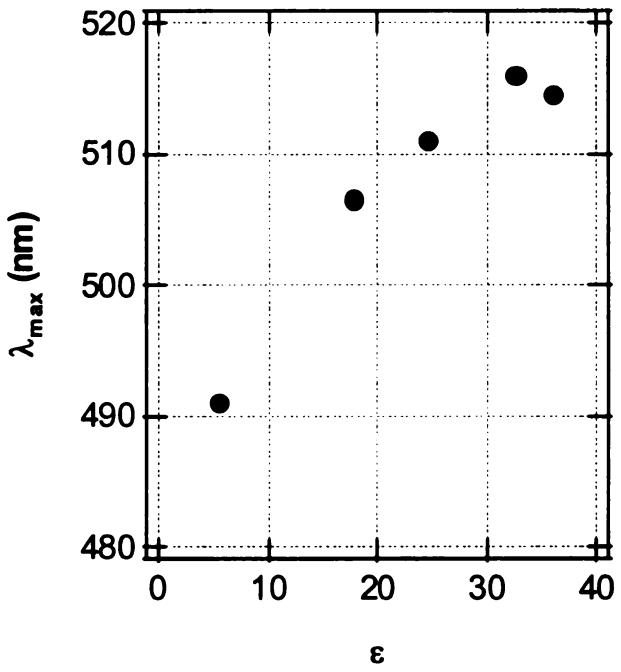

Figure 5.2. λ_{max} vs. dielectric constant for dansyl-EDA.

Fluorescence of Dansyl-PAMAM

The fluorescence emission spectra of dansyl cored PAMAM dendrimer generations 1-5 were measured in solvents of various polarities, Table 5.2. The fluorescence emission spectra of the full generations are shown in Figure 5.3 and the fluorescence emission spectra of the half generation dendrimers is displayed in Figure 5.4. A plot of λ_{max} vs. generation (Figure 5.5, Table 5.3) shows λ_{max} slowly increasing with increasing generation until dansyl G4.0 where there is a sudden red shift in λ_{max}. λ_{max} then decreases at dansyl G4.5 and increases once more at G5.0. These oscillations are consistent with a significant difference in morphology between full and half generation dendrimers. The increase in λ_{max} at generation 4 corresponds to the onset of a globular morphology, where solvent has less access to the dansyl moiety located at the focal point of the dendrimer. The amines of the dendrimers, which are good hydrogen bond participators, stabilize the dansyl group and induce the shift in λ_{max}.

The large difference between the fluorescence emission of dansyl G4.0 (primary amine end groups) and dansyl G4.5 (methyl ester end groups) demonstrates the importance of the end group functionality on the overall morphology with primary amine end groups favoring a globular dendritic state at generations higher than 4. Our neutron scattering studies of similar PAMAM di-dendrons show that the behavior of the full and half generations are quite different, with the half generations having a much smaller radius of gyration (R_g) than the full generations in methanol. The decrease in λ_{max} from dansyl G4.0 to dansyl G4.5 signals a decrease in polarity near the dansyl moiety and

could be explained by the increased number of methyl ester groups near the focal point, which are both less polar and less capable of hydrogen bonding than primary amines.

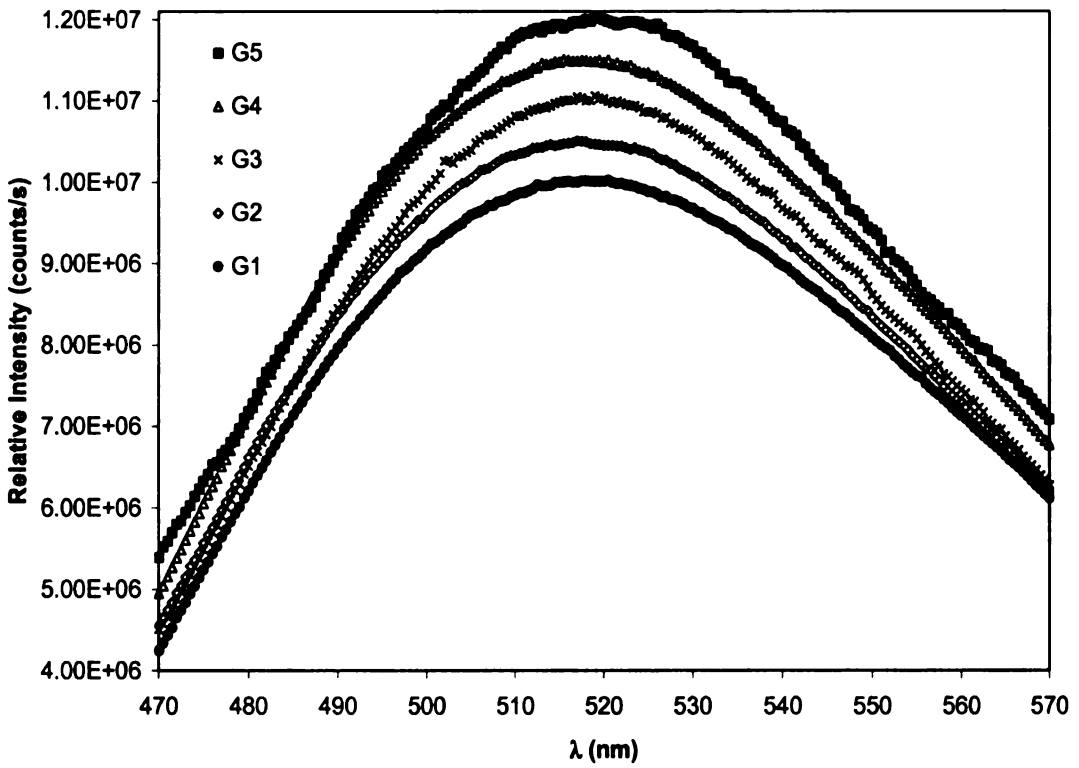

Figure 5.3. Normalized emission spectra of dansyl-PAMAM full generations (G1-G5) in methanol.

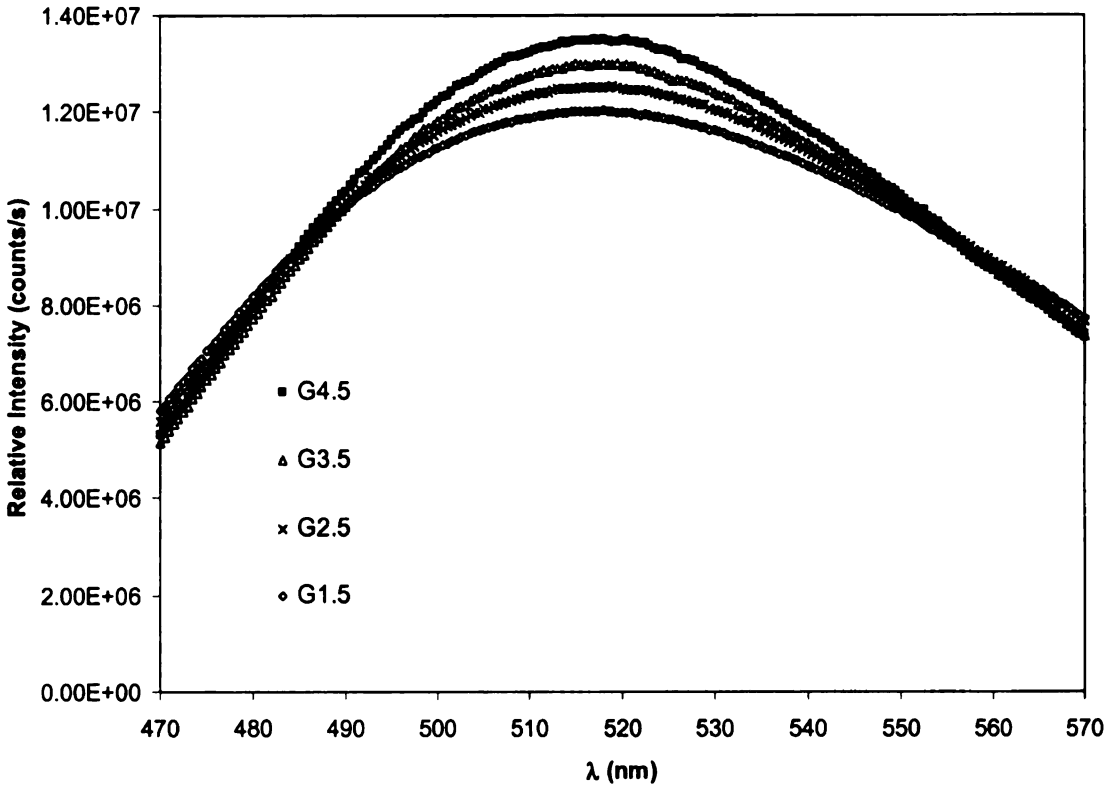

Figure 5.4. Normalized fluorescence emission spectra of dansyl-PAMAM half generations in methanol.

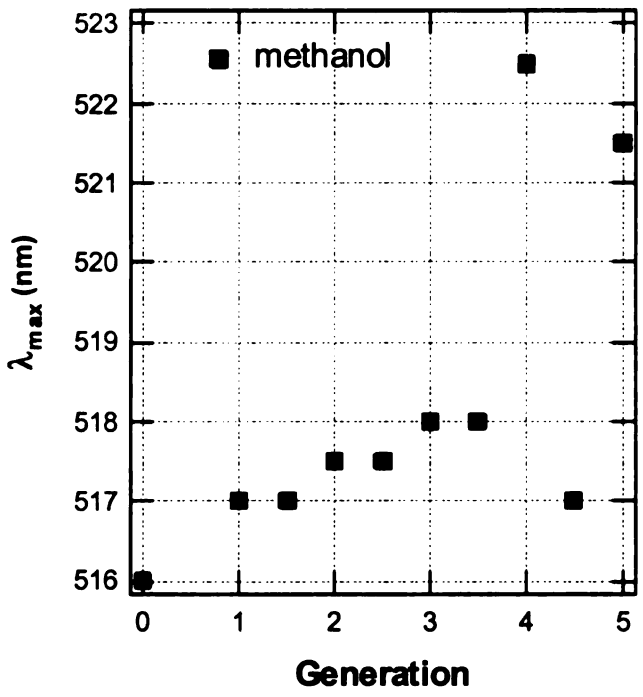

Figure 5.5. λ_{max} vs. generation for dansyl-cored PAMAM dendrimer in methanol.

Table 5.3. λ_{max} (nm) data for dansyl-PAMAM dendrimers.

	generation number									
solvent ↓	0	1.0	1.5	2.0	2.5	3.0	3.5	4.0	4.5	5.0
butanol	506.5	507	505	507	507.5	506	504	511	508	ns[a]
chloroformm	491	491.5	491.5	492	492	493	493.5	498.5	494.5	ns[a]
ethanol	511	512	511.5	513	514	514	513	516.5	514	ns[a]
methanol	5165	517.5	517	517.5	517.5	518	518	520.5	517	520
acetonitrile	514.5	516	515	516.5	516	515	514.5	510.5	514	ns[a]

[a]dendrimer insoluble in solvent.

The fluorescence of dansyl cored PAMAM dendrimers displayed the same trend in ethanol, butanol and chloroform, as methanol. We obtained λ_{max} from fluorescence emission spectra of full generation (Figure 5.6) and half generation (Figure 5.7) dansyl-PAMAM dendrimers in ethanol. A plot of λ_{max} against generation (Figure 5.8) displays a sudden increase in λ_{max} at generation 4. (Dansyl G5.0 is not adequately soluble in ethanol to obtain fluorescence data.) The increase in λ_{max} between dansyl-EDA (G0) and dansyl G4.0 is 5.5 nm in ethanol, slightly smaller than the 6.5 nm increase in λ_{max} we observed for the dendrimers in methanol.

Dansyl-PAMAM full generations were dissolved in butanol and their fluorescence emission spectra was collected. The emission spectra of full generation dendrons (Figure 5.9) show a significant shift in λ_{max} with increasing generation at dansyl G4.0 whereas the emission maximum of the dansyl-PAMAM half generation dendrimers (Figure 5.10) is relatively constant with increasing generation. A plot of λ_{max} as a function of generation of the dansyl-PAMAMs in butanol (Figure 5.11) shows a large red shift of λ_{max} at dansyl G4.0, again demonstrating the onset of a globular dendritic state. A 4.5 nm escalation in λ_{max} occurs from dansyl-G0 to dansyl-G4, which is a smaller increase than we see in methanol and ethanol. Based on our neutron scattering and dynamic light scattering experiments on similar dendrimers, we know that butanol is a poorer solvent for the dendrimers than ethanol and methanol, and the dendrimer R_g decreases as the hydrophobicity increases. Despite butanol's poor quality as a solvent, increasing from G4.0 to G4.5 results in a large blue shift in λ_{max}, as was

seen in the ethanol and methanol systems. These data demonstrate the significance of end group functionality on stabilization of dansyl's excited state.

For ethanol and butanol there appears to be an oscillating trend in λ_{max} for the half generations (Figures 5.8 and 5.11). The trend is more pronounced in the poorer solvent, butanol (Figure 5.11). For both cases there is a red shift in λ_{max} from G1.5 to G2.5. This could be due to the difference in distance between the dansyl core and the methyl ester end groups for the two generations which are less able to stabilize the dansyl excited state than butanol. For G1.5, the length of the dendritic arms is half that of G2.5, perhaps causing the methyl ester end groups to be closer to the dansyl core and a lower λ_{max}. The red shift in λ_{max} seen from G1.5 to G2.5, suggests the methyl ester end groups are further away from the dansyl core. A large blue shift in λ_{max} from G2.5 to G3.5 suggests methyl esters are near the dansyl core. This could indicate a more globular dendrimer. The observed red shift from G3.5 to G4.5 implies the dansyl core is more accessible to butanol in G4.5. This could be due to the dendrimer reaching a globular state and being able to encapsulate more solvent molecules. These hypotheses could be tested by investigating the behavior of the half generations in ethanol and butanol.

We looked at the fluorescence behavior of the dansyl-PAMAM dendrimers in chloroform, less polar than the alcohol solvents, but a moderate hydrogen bond donor. The fluorescence emission spectra of the full generations (dansyl G1.0-G4.0) show a gradual red shift with increasing generation until dansyl G4.0 where there is a significant increase in λ_{max} (Figure 5.12). The fluorescence emission spectra for the methyl ester terminated half generations also display a red shift with increasing generation, however there is no discontinuity (Figure 5.13). A plot of λ_{max} vs. generation for the chloroform

system shows a 7.5 nm red shift in λ_{max} between dansyl G0 and dansyl G4.0, which is the largest change observed. This suggests the onset of the dendritic globular state at dansyl G4.0 encapsulates the dansyl moiety in an environment that is significantly more polar and thus more capable of stabilizing dansyl's charged excited state, than chloroform. The large shift in λ_{max} is due to the greatest polarity difference between chloroform and the dendritic cage.

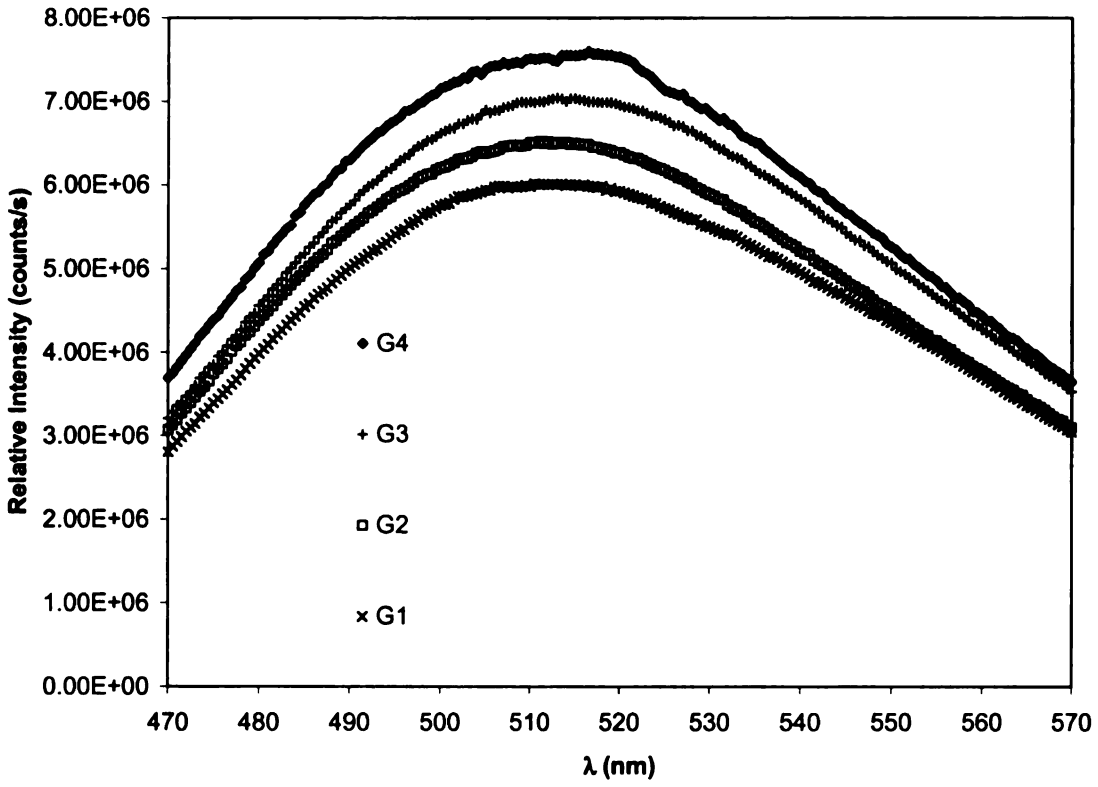

Figure 5.6. Normalized fluorescence emission spectra of full generation dansyl-PAMAM dendrimers in ethanol.

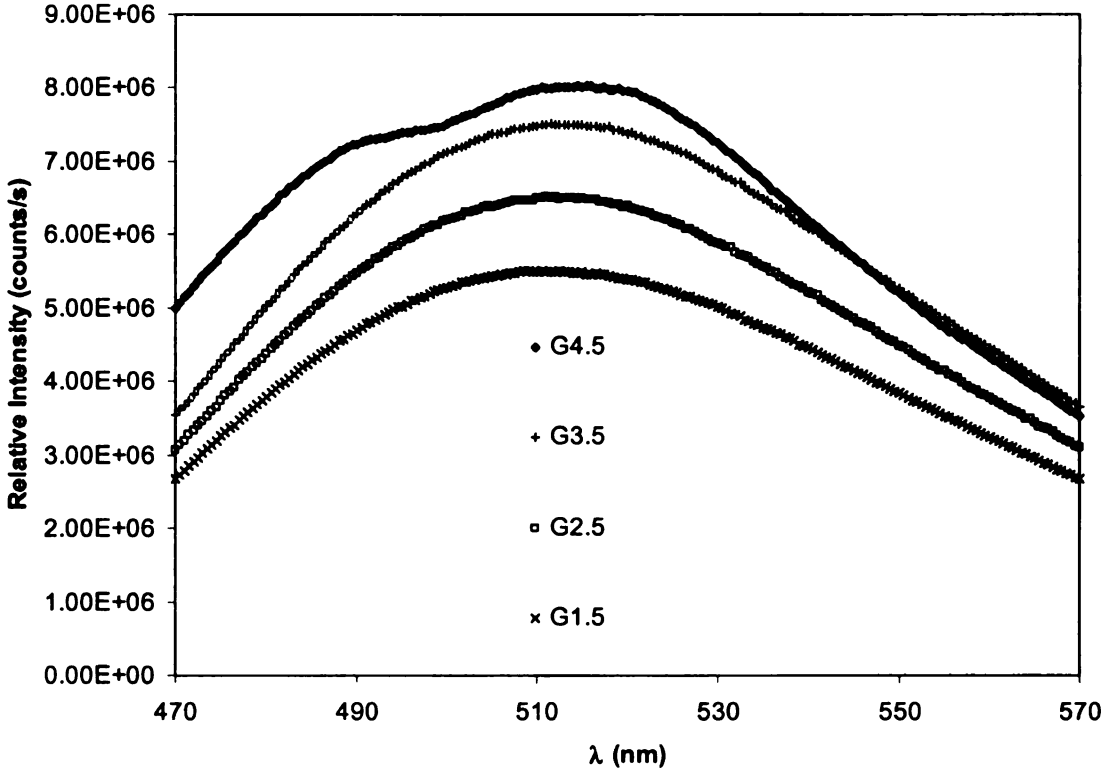

Figure 5.7. Normalized fluorescence emission spectra of dansyl-PAMAM half generation dendrimers in ethanol.

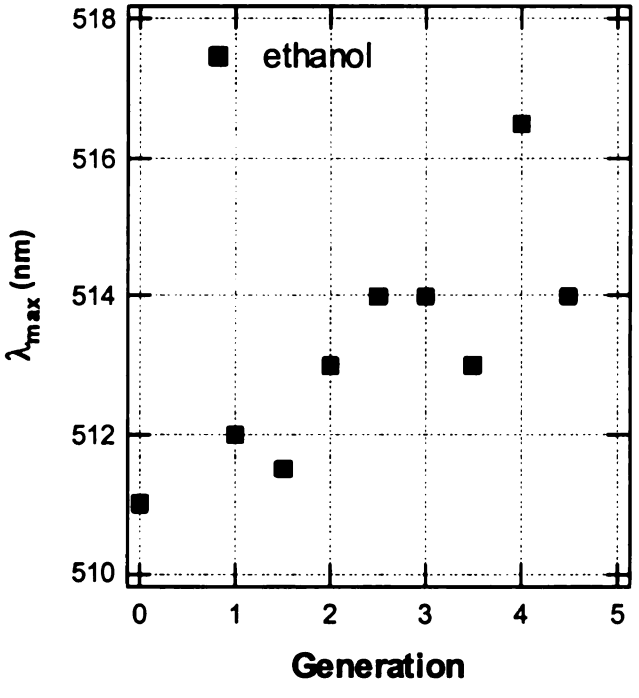

Figure 5.8. λ_{max} vs. generation for dansyl-cored PAMAM dendrimer in ethanol.

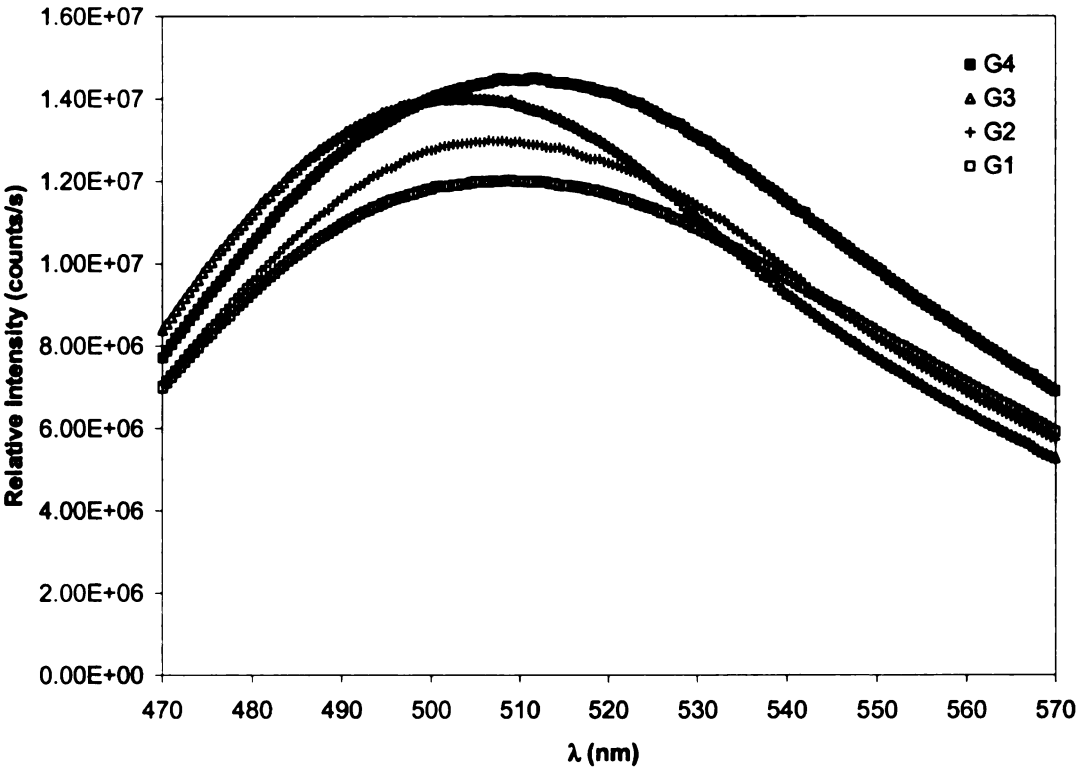

Figure 5.9. Normalized fluorescence emission spectra of dansyl-PAMAM full generations, G1-G4, in butanol.

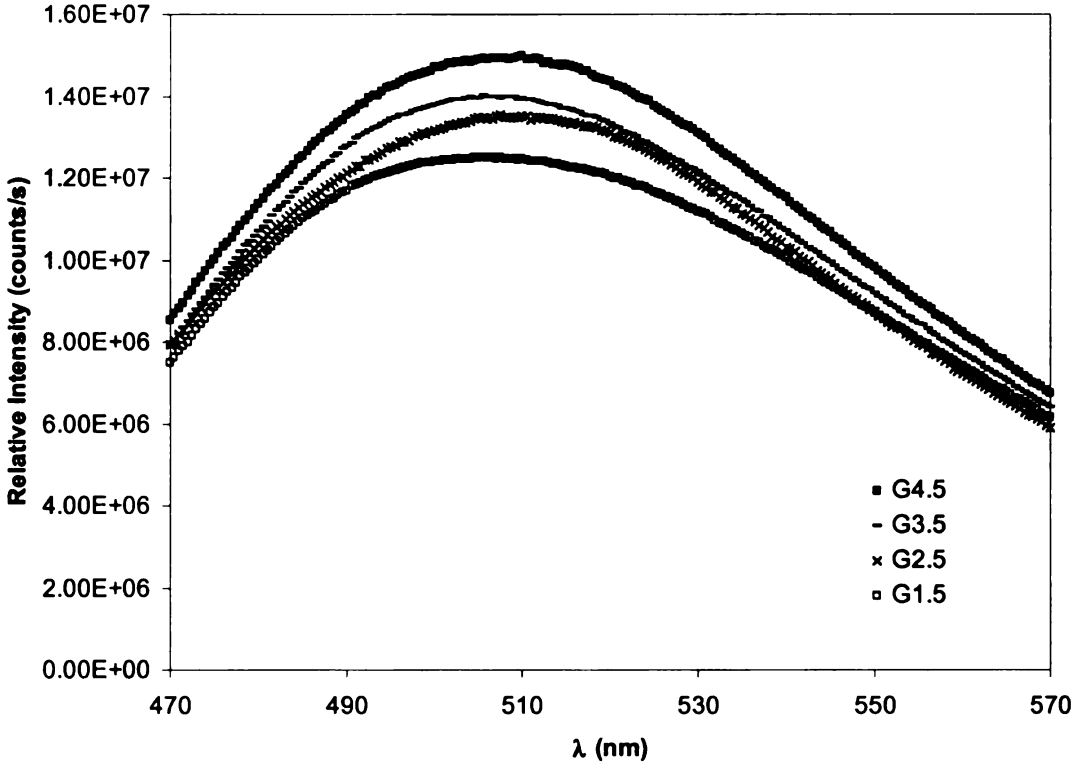

Figure 5.10. Normalized fluorescence emission spectra of dansyl-PAMAM half generation dendrimers in butanol.

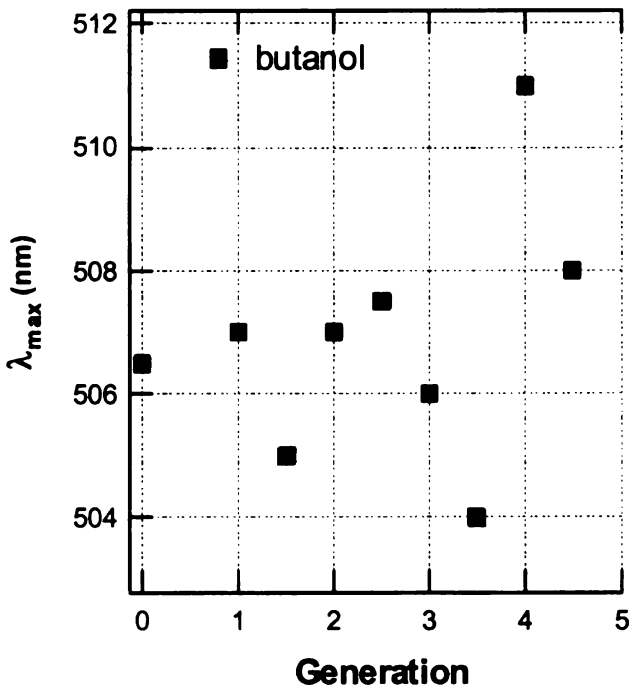

Figure 5.11. λ_{max} vs. generation for dansyl-cored PAMAM dendrimer in butanol.

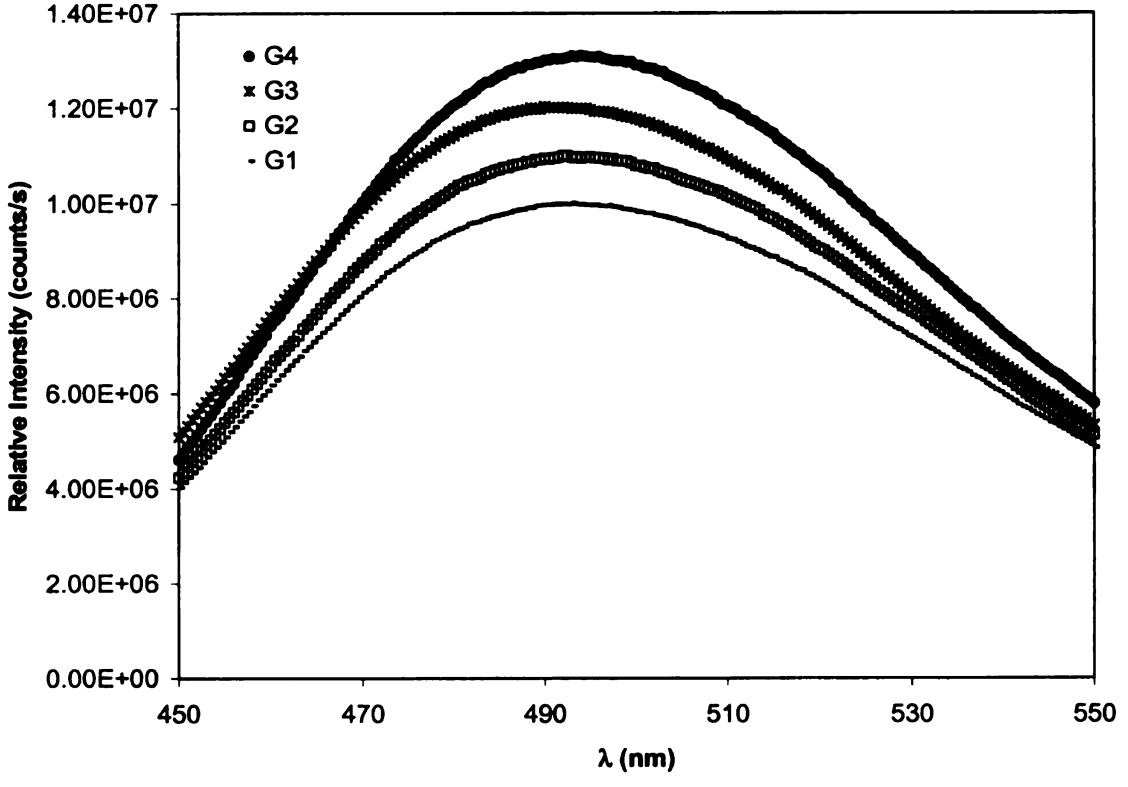

Figure 5.12. Normalized fluorescence emission spectra of dansyl-PAMAM full generation dendrimers in chloroform.

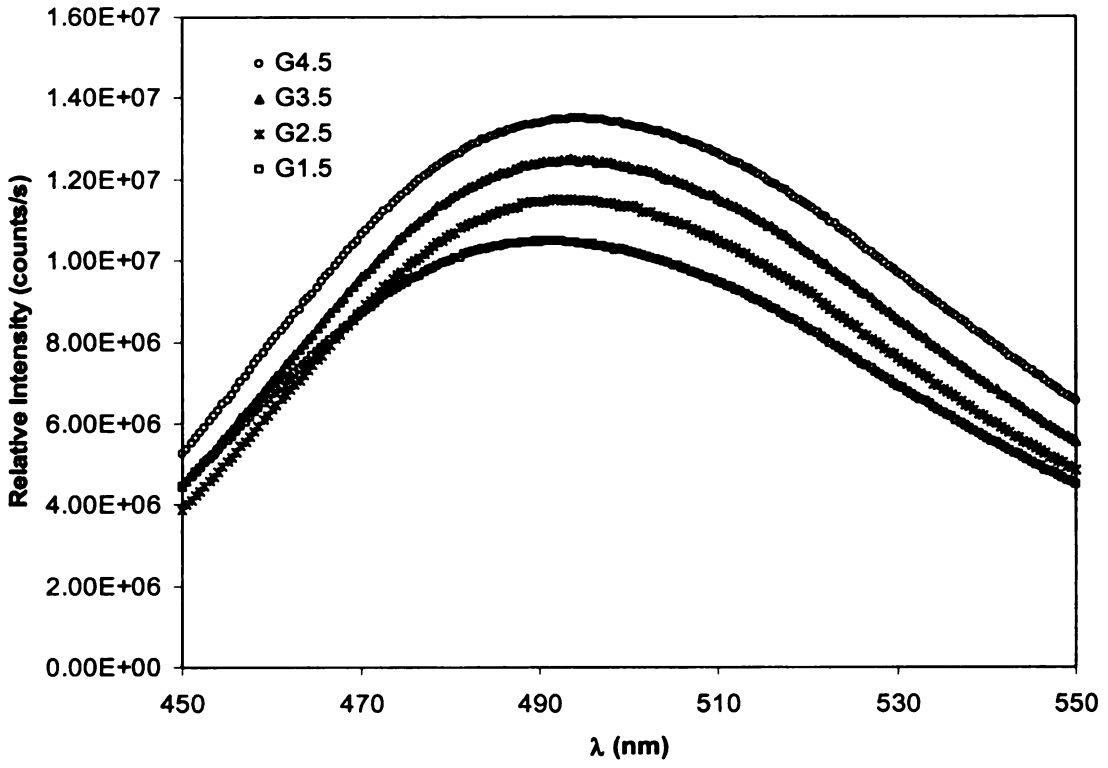

Figure 5.13. Normalized fluorescence emission spectra of dansyl-PAMAM half generation dendrimers in chloroform.

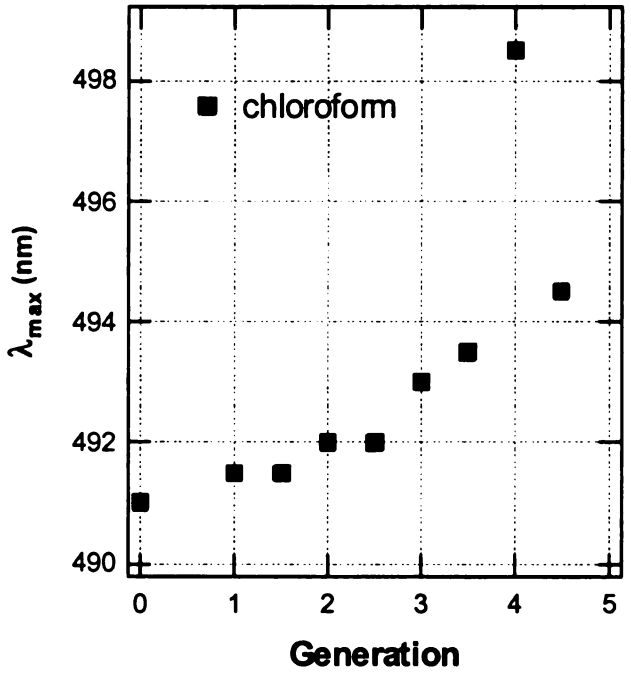

Figure 5.14. λ_{max} vs. generation for dansyl-cored PAMAM dendrimer in chloroform.

To test the interaction of the dansyl-PAMAM dendrimers with a solvent that is more polar than methanol but less capable of hydrogen bonding, we collected the emission spectra of the dansyl-cored dendrons in acetonitrile. The half generationsemission spectra showed little change with increasing generation, comparable to the results of the other solvents (Figure 5.16). The full generation fluorescence emission spectra showed a different trend than the other solvents. No change in λ_{max} was observed from dansyl G1.0 to dansyl G3.0 (Figure 5.15) and instead of the red shift of λ_{max} at dansyl G4.0 seen in methanol, ethanol, butanol and chloroform, we observed a significant blue shift (Figure 5.17). The discontinuity at dansyl G4.0 again corresponds to the transition from an extended to globular state. The decrease in λ_{max} at the globular state is consistent with a dendritic environment that is less polar than acetonitrile and thus less capable of stabilizing the excited state of the dansyl group. It has been shown for a similar chromophore that five molecules of acetonitrile are required to fully stabilize the excited state and thus shifting λ_{max} to longer wavelengths.[10] Upon the onset of a globular dendritic structure the core of the molecule is perhaps less able to accommodate the orientation of solvent molecules required to stabilize the excited state, which causes the blue shift of λ_{max}.

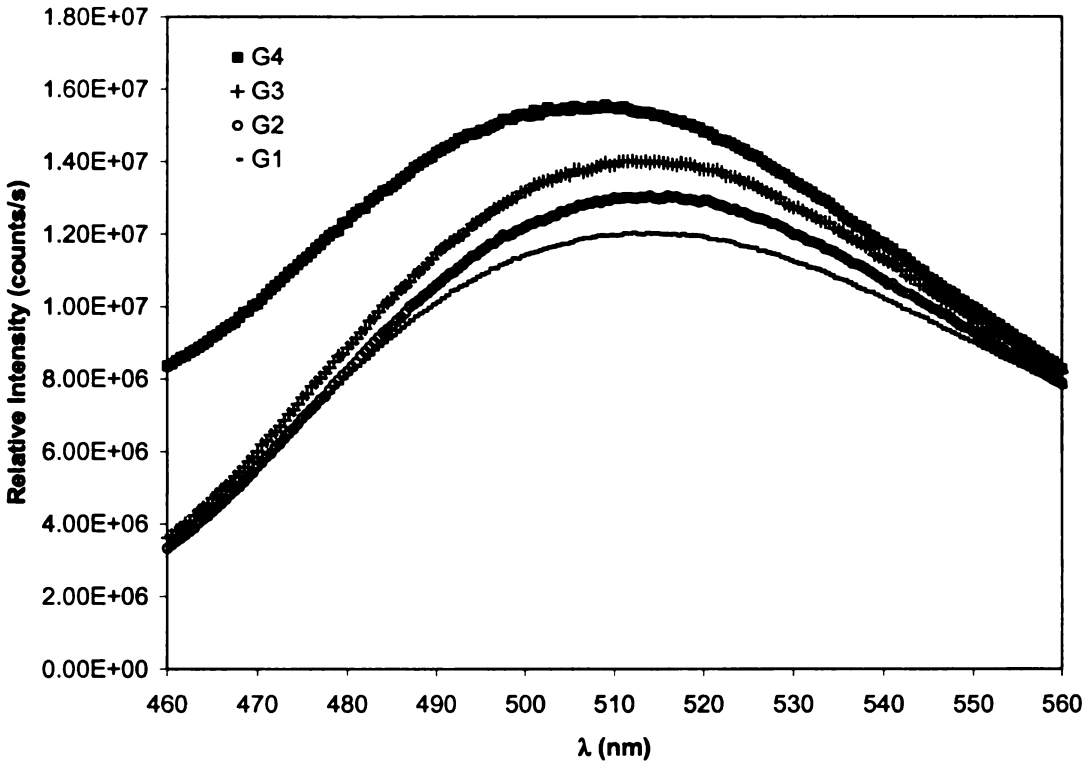

Figure 5.15. Normalized fluorescence emission spectra of dansyl-PAMAM full generations in acetonitrile.

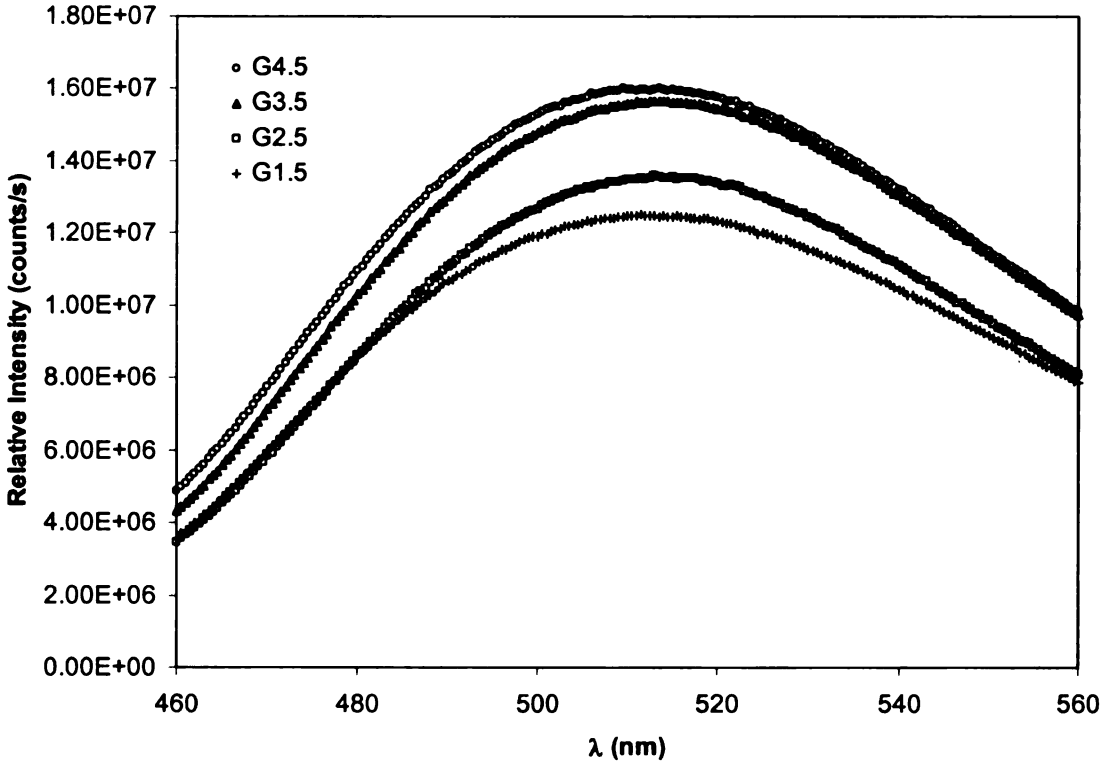

Figure 5.16. Normalized fluorescence emission spectra of dansyl-PAMAM half generations in acetonitrile.

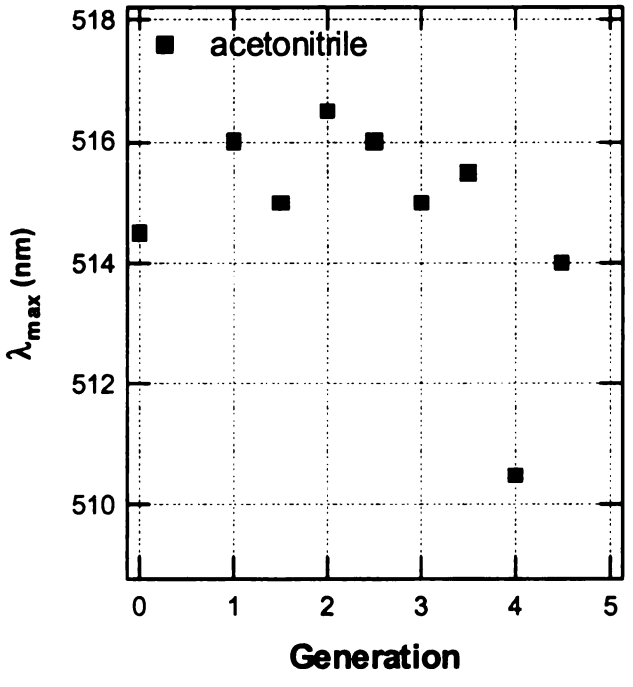

Figure 5.17. λ_{max} vs. generation for dansyl-cored PAMAM dendrimer in acetonitrile.

The transition of the PAMAM didendrons from an extended to a globular morphology depends on the generation and is independent of the solvent quality. All solvents tested show a discontinuity in the relationship between λ_{max} and generation at dansyl G3.0 to dansyl G4.0. The ability of solvent to hydrogen bond with the dendrimer does not alter the overall morphology transition of the molecule, since acetonitrile, a poor hydrogen bond acceptor, and methanol, a good hydrogen bond donor and acceptor, both demonstrate the onset of a globular dendritic state at generation 4. These results agree with the previous results of Hawker et al.[4] who saw a similar discontinuity in λ_{max} of poly(benzyl ether) dendrons with a 4-(N,N-dimethylamino)-1-nitrobenzene solvatochromic probe covalently attached at its focal point. An analogous transition has also been shown for carboxylate-terminated starburst dendrimers via photoinduced electron-transfer measurements.[20]

Conclusion

We have shown the synthesis and characterization of PAMAM di-dendrons up to generation 5 with a solvatochromic probe at their focal point. Solvatochromic probes are sensitive to the microenvironments at the core of a PAMAM dendrimer and are capable of relaying information on the overall morphology of a dendrimer when placed at the focal point. All solvents tested show a noteworthy change in λ_{max} from dansyl G3.0 to dansyl G4.0, which signifies the transition from an extended to a globular state. In all cases, the half generation dendrimers, with methyl ester end groups, show little change in λ_{max} as the generation and molecular weight increases, implying they have significantly different morphology than the primary amine terminated full generations. However due to the polarity differences of the methyl esters and primary amines, the methyl ester

groups are less able to stabilize the excited states of the dansyl group, thus explaining the low values of λ_{max} observed.

References

1. Buhleier, E. W.; Wehner, W.; Vögtle, F., *Synthesis* **1978**, 155.

2. Tomalia, D. A. B., H.; Martin, S.; J.; Hall, M.; Kallos, G.; Roeck, J.; Ryder, J.; Smith, P., *Macromolecules* **1986**, 2466.

3. Hawker, C. J.; Fréchet, J. M. J., *J. Am. Chem. Soc.* **1990,** *112*, 7638-7647.

4. Hawker, C. J.; Wooley, K. L.; Frechet, J. M. J., *J. Am. Chem. Soc.* **1993,** *115*, 4375-4376.

5. Cardona, C. M.; Alvarez, J.; Kaifer, A. E.; McCarley, T. D.; Pandey, S.; Baker, G. A.; Bonzagni, N. J.; Bright, F. V., *J. Am. Chem. Soc.* **2000,** *122*, 6139-6144.

6. Cardona, C. M.; Wilkes, T.; Ong, W.; Kaifer, A. E.; McCarley, T. D.; Pandey, S.; Baker, G. A.; Kane, M. N.; Baker, S. N.; Bright, F. V., *J. Phys. Chem. B.* **2002,** *106*, 8649-8656.

7. Pandey, S.; Redden, R. A.; Fletcher, K. A.; Sasaki, D. Y.; Kaifer, A. E.; Baker, G. A., *Chem. Commun.* **2004**, 1318-1319.

8. Cardona, C. M.; Jannach, S. H.; Huang, H.; Itojima, Y.; Leblanc, R. M.; Gawley, R. E.; Baker, G. A.; Brauns, E. E., *Helv. Chimi. Act.* **2002,** *85*, 3532-3558.

9. Wang, B. B.; Zhang, X.; Jia, X. R.; Li, Z. C.; Ji, Y.; Yang, L.; Wei, Y., *J. Am. Chem. Soc.* **2004,** *126*, 15180-15194.

10. Grabowski, Z. R.; Rotkiewicz, K.; Rettig, W., *Chem. Rev.* **2003,** *103*, 3899-4031.

11. Wang, B. B.; Zhang, X.; Jia, X. R.; Li, Z. C.; Yan, J.; Wei, Y., *J. Polym. Sci. Part A: Polym. Chem.* **2005,** *43*, 5512-5519.

12. Fuchs, S.; Otto, H.; Jehle, S.; Henklein, P.; Schluter, A. D., *Chem. Commun.* **2005**, 1830-1832.

13. Vogtle, F.; Gestermann, S.; Kauffmann, C.; Ceroni, P.; Vicinelli, V.; De Cola, L.; Balzani, V., *J. Am. Chem. Soc.* **1999,** *121*, 12161-12166.

14. Balzani, V.; Ceroni, P.; Gestermann, S.; Kauffmann, C.; Gorka, M.; Vogtle, F., *Chem. Commun.* **2000**, 853-854.

15. Vogtle, F.; Gestermann, S.; Kauffmann, C.; Ceroni, P.; Vicinelli, V.; Balzani, V., *J. Am. Chem. Soc.* **2000,** *122*, 10398-10404.

16. Vicinelli, V.; Ceroni, P.; Maestri, M.; Balzani, V.; Gorka, M.; Vogtle, F., *J. Am. Chem. Soc.* **2002,** *124*, 6461-6468.

17. Balzani, V.; Ceroni, P.; Gestermann, S.; Gorka, M.; Kauffmann, C.; Vogtle, F., *Tetrahedron* **2002,** *58*, 629-637.

18. Saudan, C.; Balzani, V.; Gorka, M.; Lee, S.; Maestri, M.; Vicinelli, V.; Vogtle, F., *J. Am. Chem. Soc.* **2003,** *125*, 4424-4425.

19. Doyle, E. L.; Hunter, C. A.; Phillips, H. C.; Webb, S. J.; Williams, N. H., *J. Am. Chem. Soc.* **2003,** *125*, 4593-4599.

20. Moreno-Bondi; M. A.; Orellana; G.; Turro, N. J.; Tomalia, D. A., *Macromolecules* **1990,** *23*, 912.

CHAPTER SIX: Synthesis and Solution Properties of PEO-PAMAM Linear-Dendrimer Diblock Copolymers

Introduction

The ability to control the morphology of macromolecules in solution has great potential for the construction of smart materials, where interest in the design and synthesis of stimuli-responsive polymers has increased dramatically due to their promising application in biomedical fields.[1-4] In previous work we performed studies on linear-dendrimer diblock copolymers, where a linear poly(styrene) (PS) chain is attached to the focal point of a generation 4 (G4) poly(benzyl ether) (PBE) dendrimer (Chapter 3).[5] Jeong et al.[6] found that the PBE-PS system undergoes a transition in intrinsic viscosity. At low molecular weights it has an intrinsic viscosity below that of PS with an equal molecular weight but an increase in intrinsic viscosity of the hybrid occurs as the molecular weight of the PS chain increases. This suggests a transition in the structure of the system due to interactions between the linear polystyrene block and the highly branched dendritic block. Through a series of small angle neutron scattering experiments and dynamic light scattering studies on a PBE G4-PS hybrid, we concluded that the relative molecular weight of the linear chain to the dendrimer block influences the conformations of the dendrimer block and linear chain, as well as the overall morphology of the hybrid.[5] At low molecular weights of PS, the linear chain is in a more contracted state than an analogous 'free' PS chain, however upon increasing the molecular weight of the linear chain, the PS chain adopts dimensions similar to a free linear chain. Concurrently, the dendrimer changes shape from a sphere-like object to a wedge or 'ice-cream' cone.

The ability of the dendrimer to change shape is critical for the occurrence of the single molecular phase transition observed for the PBE-PS system. We wish to apply this change in morphology to an advanced drug delivery scheme or a medicinal sensing application, which require the material to be water soluble. The system we chose to study is a poly(amido amine) (PAMAM) dendrimer with a linear poly(ethylene oxide) (PEO) chain attached to its focal point. We first synthesized an analogous PAMAM dendron attached to the linear PEO chain to whether it undergoes a size change in response to its environment, and if so, which generation undergoes the most drastic change in dimensions (Chapter 4). Small angle neutron scattering (SANS) and dynamic light scattering (DLS) experiments on generations 3-5 demonstrated that G4 undergoes the greatest size change and thus this generation number was used to investigate the morphology of the PEO-PAMAM linear-dendrimer diblocks.

While numerous studies have been conducted on dendrimer conjugates with PEO, there is little published work on the dilute solution behavior of these molecules. Fréchet and Gitsov[7] found that a PEO chain attached to the focal point of a PBE dendrimer can shield the hydrophobic dendrimer from a surrounding hydrophilic (methanol/water) environment when its molecular weight is large enough to allow the system to form mono-and multimolecular micelles. The formation of these micelles also depends on the dendrimer generation. When the diblocks were placed in tetrahydrofuran, THF, a good solvent for the dendrimer block, only monomolecular micelles were formed suggesting the dendrimer shields the linear chain from the solvent allowing it to occupy the dendritic cavities.

The majority of the literature on linear-dendrimer diblocks concerns forming multi-molecular self-assembled micelles. Ge and Liu[4] recently described the synthesis and self assembly of poly(benzyl ether)-b-poly(N-isopropylacrylamide) dendrimer-linear diblock copolymers where micelles form in aqueous solutions and thermoresponsive conformational changes of the poly(N-isopropylacrylamide) chains located at the micelle shell cause a sudden collapse of the system at 29-31°C. Fréchet and coworkers[8] developed a pH-responsive linear-dendrimer micelle consisting of PEO and either a poly(lysine) or polyester dendron where hydrophobic groups were attached to the dendrimer periphery via acid-sensitive acetal linkages. The diblocks were designed to form stable micelles in aqueous solutions at neutral pH that disassociate into unimers under mildly acidic conditions, where hydrolysis of the acetal releases the hydrophobic moiety, i.e. drug.

We are interested in the unimolecular behavior of linear-dendrimer diblocks in dilute solution and in particular determining the relative location of the linear chain with respect to the dendrimer block. We hope to determine what environmental factors, if any, control this morphology to allow these functionalized dendrimers to be used for the design of unique materials. There are three possible linear-dendrimer diblock conformational states in solution for a system where the linear and dendrimer blocks are compatible with each other. Each conformational state pertains to different relative locations of the two blocks.[9] The first state is a knitted coil, where the linear chain weaves in and out of the dendrimer, thus the dendrimer shields or partially shields the linear polymer from the surrounding environment. For this to occur, the dendrimer must have enough free volume to accommodate the linear block. A second hybrid

conformation consists of the linear chain wrapping itself around the dendrimer, thus shielding the dendrimer from the surroundings and forming a unimolecular micelle. This encapsulated dendrimer state would occur when the linear block is compatible with the surrounding medium and the dendrimer less compatible, resulting in a core-shell morphology. A third potential molecular arrangement consists of the linear chain completely expelled from the cavities within the dendrimer. This could occur if there is not enough free volume within the dendrimer to contain the entire linear chain and each component has similar solubility in the solvent.[6]

The ability to control the conformation of the hybrid has potential for a molecular machine which would operate as follows (Figure 6.1): A hybrid system where the linear chain has a drug or fluorescent tag attached via a cleavable linkage shields the drug/tag from the surrounding environment when the system is in a knitted coil conformation. The attachment of the dendrimer to a surface triggers a conformational change of the dendrimer from a sphere to a flattened disk, a pancake, which has been observed by atomic force microscopy.[10] Upon flattening the free volume decreases, thus expelling the linear chain from the its cavities and exposing the drug/tag to the surrounding environment.

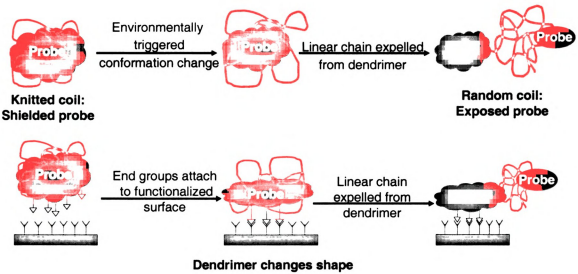

Figure 6.1. Cartoon showing the conformational changes of a linear-dendrimer diblock copolymer.

A probe, which could be a drug or fluorescent tag, is attached to the linear chain. When the linear chain is inside the cavities of the dendrimer block, the probe is shielded from the surrounding environment. A conformational change of the system from a knitted coil to a random coil exposes the probe to the surrounding environment, thus releasing the drug or producing a fluorescent signal.

A variety of strategies[11] were used to synthesize linear-dendrimer diblock copolymers with the most common being coupling a linear chain end to the focal point of a dendrimer.[7, 12-14] Alternatively, the dendrimer can be grown divergently from an appropriately functionalized chain end of the linear block,[15-17] while a third strategy is to use the focal point of the dendrimer as a macroinitiator for polymerization of the desired linear block.[18] The advantage of the first and third methods is the increased number of hybrid analogs produced from a given dendrimer, therefore minimizing the number of difficult dendrimer syntheses required to make a library of compounds. The second method has the advantage for PAMAM synthesis since the presence of the polymer simplifies the purification of each generation and we chose to use the divergent process as this is best suited for the chemical functionality of the PAMAM dendrimer.

We synthesized a series of PEO-PAMAM hybrids with five different molecular weights, 4.2 kDa, 5.4 kDa, 8.4 kDa, 12.4 kDa and 23.4 kDa, where the molecular weight includes the PAMAM G4 dendrimer (M=3422 Da) and that of the linear chain. These molecules were produced in a two step divergent process beginning with an amine terminated PEO chain.[17] We performed DLS experiments on the hybrids and linear PEO to determine the hydrodynamic radius (R_h) in dilute aqueous solutions and to compare the scaling behavior.

Experimental

Materials. Poly(ethylene oxide) monomethylether (PEO) (9 kDa and 20 kDa) was purchased from The Polymer Source, Quebec, Canada. All other chemicals were purchased from Aldrich Chemical Co., Saint Louis, MO. Ethylenediamine was distilled under nitrogen prior to use. Methyl acrylate was distilled from KOH to remove the

inhibitor. ^{1}H NMR were acquired usina Varian 300 or 500 MHz instrument, as indicated, with the residual proton signal from the solvent used as the reference peak. NMR spectra and assigned chemical shifts are displayed in Appendix C.

Synthesis of PEO-NH_2 (2 kDa)

mPEO-OMs (2) 1 (6 g, 3 mmols) was dissolved in 100 mL of dichloromethane and stirred at 0 °C under nitrogen. Triethylamine (2.10 mL, 15.0 mmol, 1.52 g) was added in one aliquot, followed by methanesulfonylchloride (1.16 mL, 15 mmol, 1.72 g) as one aliquot. The reaction mixture was stirred at 0 °C for two hours. Diethyl ether (250 mL) was added to reaction mixture causing precipitation of the polymer as a white solid. Filtration and drying gave 5.52 g of **2** as a white solid (92% yield). ^{1}H NMR ($CDCl_3$, 300 MHz) δ 4.34 (m, 2.05 H), δ 3.61 (m, 183.27 H) δ 3.35 (s, 3.02 H), δ 3.06 (s, 3.00 H).

mPEO-phthalimide (3) mPEO-OMs (2.26 g, 1.13 mmol) of was dissolved in DMF (125 mL). Potassium phthalimide (0.63g, 3.40 mmol) was added and the solution was stirred under nitrogen at 120 °C for three hours. The reaction mixture was cooled to room temperature and the resulting precipitate was removed by filtration. The DMF solution was evaporated to dryness under vacuum (100 mTorr), resulting in a light yellow solid. The solid was dissolved in dichloromethane (150 mL) and after 2 hours the solution was filtered and the solvent removed in vacuo to provide a white solid. Washing with diethyl ether (300 mL) followed by filtration gave 2.16 g of **3** (97% yield). (Scheme 6.1) ^{1}H NMR ($CDCl_3$, 300MHz) δ 7.9 (m, 2.0 H), δ 7.25 (m, 2.57 H), δ 3.40 (s, 180 H), δ 3.18 (s, 3.0 H).

mPEO-NH_2 (4) 3 (2.22 g, 1.10 mmol) was dissolved in 100 mL of ethanol and heated to reflux. Hydrazine monohydrate (0.53 mL, 11.0 mmol, 0.55 g) was added in one aliquot.

After refluxing overnight, the reaction mixture was cooled to room temperature and filtered to remove insoluble impurities. The solvent was removed in vacuo and the resulting solid was dissolved in dichloromethane (200 mL). The solids were removed by filtration and concentration of the filtrate gave a solid residue. Washing with diethylether (300 mL) gave 2.13 g of **4** as a white solid (97% yield). ^{1}H NMR ($CDCl_3$, 300 MHz) δ: 3.64 (s, 187.18 H), 3.36 (s, 3.00 H), 2.56 (t, 2.55 H).

Synthesis for PEO-NH_2 (Mw = 750 Da, 5 kDa, 9 kDa, 20 kDa)

The hydroxyl group of 5 kDa, 9 kDa and 20 kDa monomethyl ether PEO was converted to a primary amine following the procedure used for the system described above. The synthesis of PEO-NH_2 (750 Da) was similar except that precipitation required lowering temperature of ether solutions to -30 °C for 1-3 hours to obtain crystals. The ether solution was removed from the freezer and warmed for approximately 20 minutes before collecting white crystals via vacuum filtration.

mPEO 2 kDa PAMAM G0.5 (5) 4 (2.0 g, 1.0 mmol) was dissolved in 35 mL of methanol and slowly dripped into uninhibited methyl acrylate (25.8 g, 0.30 mol). The reaction was stirred at 35 °C under nitrogen for two days. Methanol and unreacted methyl acrylate was removed by rotary evaporation and the resulting white solid was washed with diethyl ether (250 mL) to give 2.15 g of **5** (99% yield). ^{1}H NMR (300 MHz, $CDCl_3$) δ: 3.60 (m, 194H), 3.27 (s, 3H), 2.68 (t, 4H), 2.56 (t, 2H), and 2.35 (t, 4H).

mPEO 2 kDa PAMAM G 1.0 (6) 5 (1.50 g, 0.70 mmol) was dissolved in 30 mL of methanol and slowly dripped into ethylenediamine (8.20 g, 0.14 mmol). The reaction was stirred at 55 °C under nitrogen for two days. Methanol and unreacted ethylenediamine were removed by rotary evaporation, and the resulting white solid was

washed with diethyl ether (300 mL) to give 1.56 g of **6** (100% yield). ^{1}H NMR (300 MHz, $CDCl_3$) δ: 3.63 (m, 185H), 3.38 (s, 3H), 3.31 (t, 4H), 2.85 (m, 8H), 2.65 (t, 2H), and 2.43 (t, 4H).

General Procedure for Growing Dendrimer. Procedures for formation of subsequent half and whole generations were analogous to the synthesis of **5** and **6** respectively. Note that care must to taken to remove all unreacted monomer, as small traces will lead to impurities. The hybrids prepared from PEO chains with molecular weights of 2 kDa and higher were purified by precipitation from ether and then soxhlet extraction with ether when necessary for complete removal of ethylenediamine. The half generation hybrids synthesized from PEO (M=750 Da) were purified by placing under vacuum (5 mTorr) at 40 °C for 2 days and then precipitating from cold (-30 °C) diethyl ether. The full generation hybrids synthesized from PEO (M=750 Da) were purified by removal of methanol and unreacted ethylenediamine under vacuum. To remove residual amounts of ethylenediamine, the waxy residue was dissolved in octanol (50 mL) and stirred under vacuum (5 mTorr) at 40 °C for 2 days. The octanol mixture was washed with 50:50 hexane:water. The water layer was collected and washed three times with hexanes, then concentrated via rotary evaporation and then dried under vacuum (5 mTorr) at 40 °C to constant mass. The resulting white wax was dissolved in methanol and placed in a dialysis bag (MWCO=200 g/mol) for 2 days after which contents remaining in the bag were concentrated.

mPEO 2 kDa OMs ^{1}H NMR (300 MHz, $CDCl_3$) δ: 4.60 (m, 2H), 3.60 (m, 1820H), 3.30 (s, 3H), and 3.00 (s, 3H).

mPEO 2 kDa phth ^{1}H NMR (300 MHz, $CDCl_3$) δ: 7.82 (m, 2H), 7.60 (m, 2H), 3.60 (m, 183H), and 3.35 (s, 3H).

mPEO 2 kDa NH_2 ^{1}H NMR (300 MHz, $CDCl_3$) δ: 3.60 (m, 190H), 3.31 (s, 3H), and 2.80 (t, 2H, J = 4.8 Hz).

mPEO 2 kDa G0.5 ^{1}H NMR (300 MHz, $CDCl_3$) δ: 3.60 (m, 194H), 3.27 (s, 3H), 2.68 (t, 4H, J = 6.9 Hz), 2.56 (t, 2H, J = 6.3 Hz), and 2.35 (t, 4H, J = 6.9 Hz).

mPEO 2 kDa G1.0 ^{1}H NMR (300 MHz, $CDCl_3$) δ: 3.63 (m, 185H), 3.38 (s, 3H), 3.31 (quartet, 4H, J = 6.3 Hz), 2.85 (m, 8H), 2.65 (t, 2H, J = 4.8 Hz), and 2.43 (t, 4H, J = 6.0 Hz).

mPEO 2 kDa G1.5 ^{1}H NMR (300 MHz, $CDCl_3$) δ: 3.62 (m, 198H), 3.34 (s, 3H), 3.22 (q, 4H, J = 6.0 Hz), 2.86 (t, 4H, J = 6.3 Hz), 2.75 (t, 8H, J = 6.6 Hz), 2.55 (t, 6H, J = 6.6 Hz), and 2.50-2.40 (m, 12H).

mPEO 2 kDa G2.0 ^{1}H NMR (300 MHz, d^4-methanol) δ: 3.60 (m, 190H), 3.32 (s, 3H), 2.28 (m, 12H), 2.85-2.62 (m, 20H), 2.60 (m, 2H), 2.48 (m, 4H), and 2.40-2.30 (m, 12H).

mPEO 2 kDa G2.5 ^{1}H NMR (300 MHz, $CDCl_3$) δ: 3.60 (m, 182H), 3.31 (s, 3H), 3.18 (m, 12H), 2.80-2.60 (m, 30H), 2.55 (m, 12H), and 2.40-2.20 (m, 28H).

mPEO 2 kDa G3.0 ^{1}H NMR (300 MHz, $CDCl_3$) δ: 3.60 (m, 186H), 3.31 (s, 3H), 3.20 (m, 28H), 2.85-2.60 (m, 46H), 2.55 (m, 12H), and 2.40-2.30 (m, 28H).

mPEO 2 kDa G3.5 ^{1}H NMR (300 MHz, d^4-methanol)δ: 3.61 (m, 181H), 3.32 (s, 3H), 3.27 (t, 28H, J = 5.7 Hz), 2.80-2.60 (m, 60H), 2.60-2.50 (m, 28H), 2.44 (t, 32H, J = 6.6 Hz), and 2.30 (t, 28H, J = 6.3 Hz).

mPEO 2 kDa G4.0: ^{1}H NMR (300 MHz, $CDCl_3$) δ: 3.60 (m, 193H), 3.31 (s, 3H), 3.23 (m, 60H), 2.80-2.60 (m, 92H), 2.55 (m, 28H), and 2.40-2.20 (m, 60H).

mPEO 750 Da-PAMAM

mPEO 750 Da OMs: ^{1}H NMR (300 MHz, $CDCl_3$) δ: 4.60 (m, 2H), 3.60 (m, 72H), 3.32 (s, 3H), and 3.01 (s, 3H).

mPEO 750 Da phth ^{1}H NMR (300 MHz, $CDCl_3$) δ: 7.82 (m, 2H), 7.60 (m, 2H), 3.60 (m, 69H), and 3.35 (s, 3H).

mPEO 750 Da NH_2 ^{1}H NMR (300 MHz, $CDCl_3$) δ: 3.60 (m, 72H), 3.31 (s, 3H), 3.0-2.9 (br s, 2H), and 3.78 (t, 3H, J = 3.6 Hz). δ: 3.60 (m, 72H), 3.31 (s, 3H), 3.0-2.9 (br s, 2H), and 3.78 (t, 3H).

mPEO 750 Da G0.5 ^{1}H NMR (500 MHz, d^4–methanol) δ: 3.60 (m, 60H), 3.31 (s, 3H), 2.65 (t, 4H, J = 10 Hz), 2.54 (t, 2H, J = 3.6 Hz), and 2.35 (t, 4H, J = 10 Hz).

mPEO 750 Da G1.0 ^{1}H NMR (500 MHz, $CDCl_3$) δ: 3.63 (m, 75H), 3.39 (s, 3H), 3.31 (quartet, 4H), 2.85 (m, 8H), 2.65 (t, 2H), and 2.43 (t, 4H).

mPEO 750 Da G1.5 ^{1}H NMR (300 MHz, D_2O) δ: 3.54 (m, 82H), 3.21 (s, 3H), 3.15 (t, 4H, J = 3.6 Hz), 2.80-2.50 (m, 14H), 2.40 (m, 12H), and 2.30 (t, 4H, J = 7.2 Hz).

mPEO 750 Da G2.0 ^{1}H NMR (300 MHz, D_2O) δ: 3.59 (m, 83H), 3.21 (s, 3H), 3.15 (m, 12H), 2.80-2.50 (m, 22H), 2.45 (t, 4H, J = 6.9 Hz), and 2.30 (m, 12H).

mPEO 750 Da G2.5 ^{1}H NMR (300 MHz, d^4–methanol) δ: 3.59 (m, 98H), 3.31 (s, 3H), 3.20 (t, 12H, J = 6 Hz), 2.80-2.60 (m, 30H), 2.50 (m, 12H), 2.40 (t, 16H, J = 6.6 Hz), and 2.30 (t, 12H, J = 6.3 Hz).

mPEO 750 Da G3.0 ^{1}H NMR (300 MHz, D_2O) δ: 3.60 (m, 78H), 3.20 (s, 3H), 3.15 (m, 28H), 2.80-2.50 (m, 46H), 2.44 (t, 12H, J = 6.6 Hz), and 2.22 (m, 28H).

mPEO 750 Da G3.5 ^{1}H NMR (300 MHz, d^4–methanol) δ: 3.59 (m, 100H), 3.33 (s, 3H), 3.28 (t, 28H, J = 6.3 Hz), 2.80-2.60 (m, 60H), 2.60-2.50 (m, 28H), 2.40 (t, 32H, J = 7.2 Hz), and 2.35 (t, 28H, J = 6.0 Hz).

mPEO 750 Da G4.0 ^{1}H NMR (300 MHz, D_2O) δ: 3.60 (m, 74H), 3.31 (s, 3H), 3.23 (m, 60H), 2.80-2.60 (m, 92H), 2.55 (t, 28H, J = 6.7 Hz), and 2.40-2.20 (t, 60H, J = 6 Hz).

mPEO 5 kDa-PAMAM

mPEO 5 kDa OMs ^{1}H NMR (300 MHz, $CDCl_3$) δ: 4.60 (m, 2H), 3.60 (m, 456H), 3.32 (s, 3H), and 3.01 (s, 3.1H).

mPEO 5 kDa phth ^{1}H NMR (300 MHz, $CDCl_3$) δ: 7.80 (m, 1.9H), 7.60 (m, 2.1H), 3.60 (m, 454.3H), and 3.30 (s, 3H).

mPEO 5 kDa NH_2 ^{1}H NMR (300 MHz, $CDCl_3$) δ: 3.60 (m, 457.2H), 3.27 (s, 3H), and 2.79 (t, 2H, J = 4.8 Hz).

mPEO 5 kDa-PAMAM G0.5 ^{1}H NMR (300 MHz, $CDCl_3$) δ: 3.60 (m, 464.1H), 3.27 (s, 3.1H), 2.67 (t, 4.1H, J = 7.2 Hz), 2.54 (t, 2H, J = 7.2 Hz), and 2.33 (t, 4.2H, J = 7.2 Hz).

mPEO 5 kDa-PAMAM G1.0 ^{1}H NMR (300 MHz, $CDCl_3$) δ: 3.63 (m, 451.3H), 3.37 (s, 3H), 3.31 (m, 4.2H), 2.85 (m, 8.1H), 2.64 (t, 2H, J = 4.8 Hz), and 2.41 (t, 4.1H, J = 6.6 Hz).

mPEO 5 kDa-PAMAM G1.5 ^{1}H NMR (300 MHz, d^4–methanol) δ: 3.62 (m, 458.7H), 3.38 (s, 3H), 3.28 (t, 4H, J = 6 Hz), 2.85 (t, 4H, J = 7.2 Hz), 2.74 (t, 8H, J = 6.9 Hz), 2.56 (t, 6H, J = 6.9 Hz), 2.50 (t, 8H, J = 6.9 Hz), and 2.40 (t, 4H, , J = 7.2 Hz).

mPEO 5 kDa-PAMAM G2.0 ^{1}H NMR (300 MHz, D_2O) δ: 3.60 (m, 449.9H), 3.41 (s, 3H), 3.25 (m, 12H), 2.83-2.60 (m, 20H), 2.57 (m, 2H), 2.52 (m, 4H), and 2.36 (m, 12H).

mPEO 5 kDa-PAMAM G2.5 ^{1}H NMR (300 MHz, $CDCl_3$) δ: 3.63 (m, 454.4H), 3.39 (s, 3H), 3.25 (m, 12H), 2.85-2.70 (m, 30H), 2.54 (m, 12H), and 2.40-2.30 (m, 28H).

mPEO 5 kDa-PAMAM G3.0 ^{1}H NMR (300 MHz, $CDCl_3$) δ: 3.60 (m, 459H), 3.31 (s, 3H), 3.20 (m, 28H), 2.85-2.60 (m, 46H), 2.56 (m, 12H), and 2.40-2.30 (m, 28H).

mPEO 5 kDa-PAMAM G3.5 ^{1}H NMR (300 MHz, d^4–methanol) δ: 3.59 (m, 460H), 3.33 (s, 3H), 3.28 (t, 28H, J = 6.0 Hz), 2.80-2.60 (m, 62H), 2.60-2.50 (m, 28H), 2.43 (t, 32H, J = 6.9 Hz), and 2.35 (t, 28H, J = 6.6 Hz).

mPEO 5 kDa-PAMAM G4.0 ^{1}H NMR (300 MHz, $CDCl_3$) δ: 3.60 (m, 457H), 3.31 (s, 3H), 3.23 (m, 60H), 2.80-2.60 (m, 92H), 2.55 (m, 28H), and 2.40-2.20 (m, 60H).

PEO 9 kDa-PAMAM

mPEO 9 kDa OMs ^{1}H NMR (300 MHz, $CDCl_3$) δ: 4.60 (m, 2H), 3.60 (m, 850H), 3.32 (s, 3H), and 3.81 (m, 28H).

mPEO 9 kDa phth ^{1}H NMR (500 MHz, $CDCl_3$) δ: 7.82 (m, 2H), 7.60 (m, 2H), 3.87 (t, 2H), 3.60 (m, 854H), and 3.35 (s, 3H).

mPEO 9 kDa NH_2 ^{1}H NMR (500 MHz, $CDCl_3$) 1H NMR (300 MHz, CDCl3) δ: 3.60 (m, 845H), 3.25 (s, 3H), and 2.80 (t, 2H, J = 5.7 Hz).

mPEO 9 kDa-PAMAM G0.5 ^{1}H NMR (300 MHz, d^4-methanol) δ: 3.60 (m, 814H), 3.18 (s, 3H), 2.68 (t, 4H, J = 4.2 Hz), 2.52 (t, 2H, J = 2.1 Hz), and 2.32 (t, 4H, J = 4.2 Hz).

mPEO 9 kDa-PAMAM G1.0 ^{1}H NMR (300 MHz, D_2O) δ: 3.61 (m, 810H), 3.30 (s, 3H), 3.21 (t, 4H, J = 5.4 Hz), 2.80 (t, 4 H, J = 5.4 Hz), 2.60 (m, 4H), 2.51 (m, 2H), and 2.41 (m, 4H).

mPEO 9 kDa-PAMAM G1.5 ^{1}H NMR (300 MHz, D_2O) δ: 3.60 (m, 828H), 3.20 (s, 3H), 3.18 (m, 4H), 2.80-2.50 (m, 18H), and 2.40 (m, 12H).

mPEO 9 kDa-PAMAM G2.0 ^{1}H NMR (300 MHz, $CDCl_3$) δ: 3.60 (m, 1821H), 3.20 (s, 3H), 3.18 (t, 12H, J = 6.3 Hz), 2.80-2.60 (m, 20.3H), 2.56 (t, 2H, J = 6.3 Hz), 2.45 (t, 4H, J = 7.8 Hz), and 2.31 (m, 12H).

mPEO 9 kDa-PAMAM G2.5 ^{1}H NMR (300 MHz, d^4–methanol) δ: 3.60 (m, 820H), 3.31 (s, 3H), 3.18 (t, 12H, J = 6.0 Hz), 2.80-2.60 (m, 28H), 2.52 (t, 12H, J = 6.3 Hz), 2.38 (t, 16H, J = 6.6 Hz), and 2.30 (m, 12H).

mPEO 9 kDa-PAMAM G3.0 ^{1}H NMR (300 MHz, d^4–methanol) δ: 3.61 (m, 808H), 3.40 (s, 3H), 3.21 (m, 28H), 2.80-2.60 (m, 46 H), 2.54-2.42 (m, 12H), and 2.40-2.22 (m, 28H).

mPEO 9 kDa-PAMAM G3.5 ^{1}H NMR (300 MHz, D_2O) δ: 3.60 (m, 824H), 3.31 (s, 3H), 3.18 (m, 28H), 2.8-2.6 (m, 60H), 2.40 (m, 28H), 2.39 (t, 32H, J = 6.6 Hz), and 2.29 (m, 28H).

mPEO 9 kDa-PAMAM G4.0 ^{1}H NMR (500 MHz, d^4–methanol) δ: 3.60 (m, 813H), 3.31 (s, 3H), 3.23 (m, 60H), 2.80-2.60 (m, 92H), 2.55 (m, 28H), and 2.40-2.20 (m, 60H).

PEO 20 kDa-PAMAM

mPEO 20 kDa-OMs ^{1}H NMR (300 MHz, $CDCl_3$) δ: 4.60 (m, 2H), 3.60 (m, 1820H), 3.32 (s, 3H), and 3.81 (m, 28H).

mPEO 20 kDa phth ^{1}H NMR (300 MHz, $CDCl_3$) δ: 7.82 (m, 2H), 7.60 (m, 2H), 3.87 (t, 2H), 3.60 (m, 1820H), and 3.35 (s, 3H).

mPEO 20 kDa-NH_2 ^{1}H NMR (300 MHz, $CDCl_3$) δ: 3.60 (m, 1820H), 3.25 (s, 3H), and 2.80 (t, 2H, J = 5.4 Hz).

mPEO 20 kDa-PAMAM G0.5 ^{1}H NMR (300 MHz, $CDCl_3$) δ: 3.60 (m, 1824H), 3.21 (s, 3H), 2.70 (t, 4H, J = 6.5 Hz), 2.58 (t, 2H, J = 6.0 Hz), and 2.39 (t, 4H, J = 6.5 Hz).

mPEO 20 kDa-PAMAM G1.0 ^{1}H NMR (300 MHz, D_2O) δ: 3.65 (m, 1820H), 3.41 (s, 3H), 3.30 (m, 4H), 2.85 (m, 8H), 2.65 (m, 2H), and 2.40 (m, 4H).

mPEO 20 kDa-PAMAM G1.5 ^{1}H NMR (300 MHz, $CDCl_3$) δ: 3.61 (m, 1819H), 3.41 (s, 3H), 3.30 (m, 4H), 2.80-2.60 (m, 14H), 2.50 (t, 4H J = 5.4 Hz), and 2.40-2.20 (m, 12H).

mPEO 20 kDa-PAMAM G2.0 ^{1}H NMR (300 MHz, d^4–methanol) δ: 3.56 (m, 1808.7H), 3.35 (s, 3H), 3.18 (m, 12H), 2.80-2.58 (m, 22H), 2.51 (m, 4H), and 2.30 (m, 12H).

mPEO 20 kDa-PAMAM G2.5 ^{1}H NMR (300 MHz, $CDCl_3$) δ: 3.60 (m, 1821H), 3.40 (s, 3H), 3.25 (m, 12H), 2.82-2.60 (m, 28H), 2.60-2.44 (m, 12H), and 2.44-2.30 (m, 28H).

mPEO 20 kDa-PAMAM G3.0 ^{1}H NMR (300 MHz, d^4–methanol) δ: 3.60 (m, 1802H), 3.40 (s, 3H), 3.21 (m, 28H), 2.80-2.60 (m, 46H), 2.54-2.40 (m, 12H), and 2.40-2.20 (m, 24H).

mPEO 20 kDa-PAMAM G3.5 ^{1}H NMR (300 MHz, d^4–methanol) δ: 3.60 (m, 1853H), 3.20 (m, 32H), 2.80-2.60 (m, 62H), 2.50-2.40 (m, 28H), 2.38 (t, 32H J = 6.6 Hz), and 2.30 (m, 28H J = 6.0 Hz).

mPEO 20 kDa-PAMAM G4.0 ^{1}H NMR (300 MHz, $CDCl_3$) δ: 3.60 (m, 1803H), 3.38 (s, 3H), 3.20 (m, 60H), 2.80-2.60 (m, 92H), 2.50 (m, 28H), and 2.40-2.20 (m, 60H).

Dynamic Light Scattering (DLS). Measurements were performed with a Protein Solutions Dyna Pro-MS/X system with temperature control. All samples were filtered through a 0.1μm Whatman Anodisc 13 filter as and allowed to equilibrate in the instrument for 15 minutes at 25 °C before measurements were taken resulting in calculation of the R_h. The sample is illuminated by a semi-conductor laser with ~ 830 nm wavelength. The light scattered at an angle of 90° is collected and guided via a fiber

optic cable to an actively quenched, solid state Single Photon Counting Module (SPCM), where the photons are converted to electrical pulses and correlated. Autocorrelation is used to analyze the time scale of the scattered light intensity fluctuations. The translational diffusion coefficient (D) of the molecules in the sample cell is determined from the decay of the intensity autocorrelation data. The R_h of the sample is then derived from D, using the Stokes-Einstein equation.

$$D = \frac{k_B T}{6\pi\eta R_h} \tag{6.1}$$

Here, D is the translational diffusion coefficient, k is Boltzmann's constant, T is the absolute temperature, η is the viscosity of the solvent and R_h is the effective Stokes radius or the hydrodynamic radius. The uniformity of the sample sizes is determined by a monomodal curve fit, cumulants, which assumes a single particle size with a Gaussian distribution. The regularization algorithm makes no assumptions regarding the number of size populations and can fit a multimodal system. All systems in this study are monomodal.

Results and Discussion

Synthesis of PEO-PAMAM

PAMAM dendrons were grown divergently from a primary amine terminated PEO chain to result in linear-dendrimer diblock copolymers that are water soluble (Scheme 6.1 and 6.2). Each full generation was obtained by exhaustive Michael addition of the primary amine functionality with methyl acrylate to result in methyl-ester terminated generation 0.5 (G0.5) (**5**). The methyl ester end groups were amidated with excess ethylenediamine to yield primary amine terminated full generation 1.0 (G1.0) (**6**).

Most PEO-PAMAM diblocks are white solids. The higher generation PEO 750 Da series are waxy solids at room temperature. We used ^{1}H NMR to confirm end group functionalization of the PEO chain as well as growth of the dendrimer. For the molecular weight of PEO used, ^{1}H NMR is a reliable end group characterization method.[19]

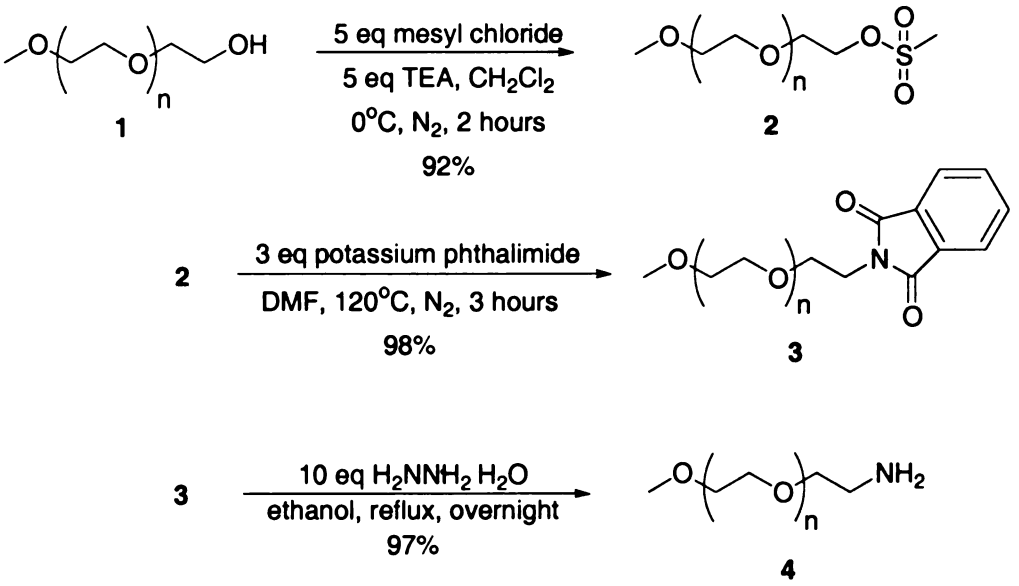

Scheme 6.1. Synthesis of methoxy-amine terminated poly(ethylene oxide).

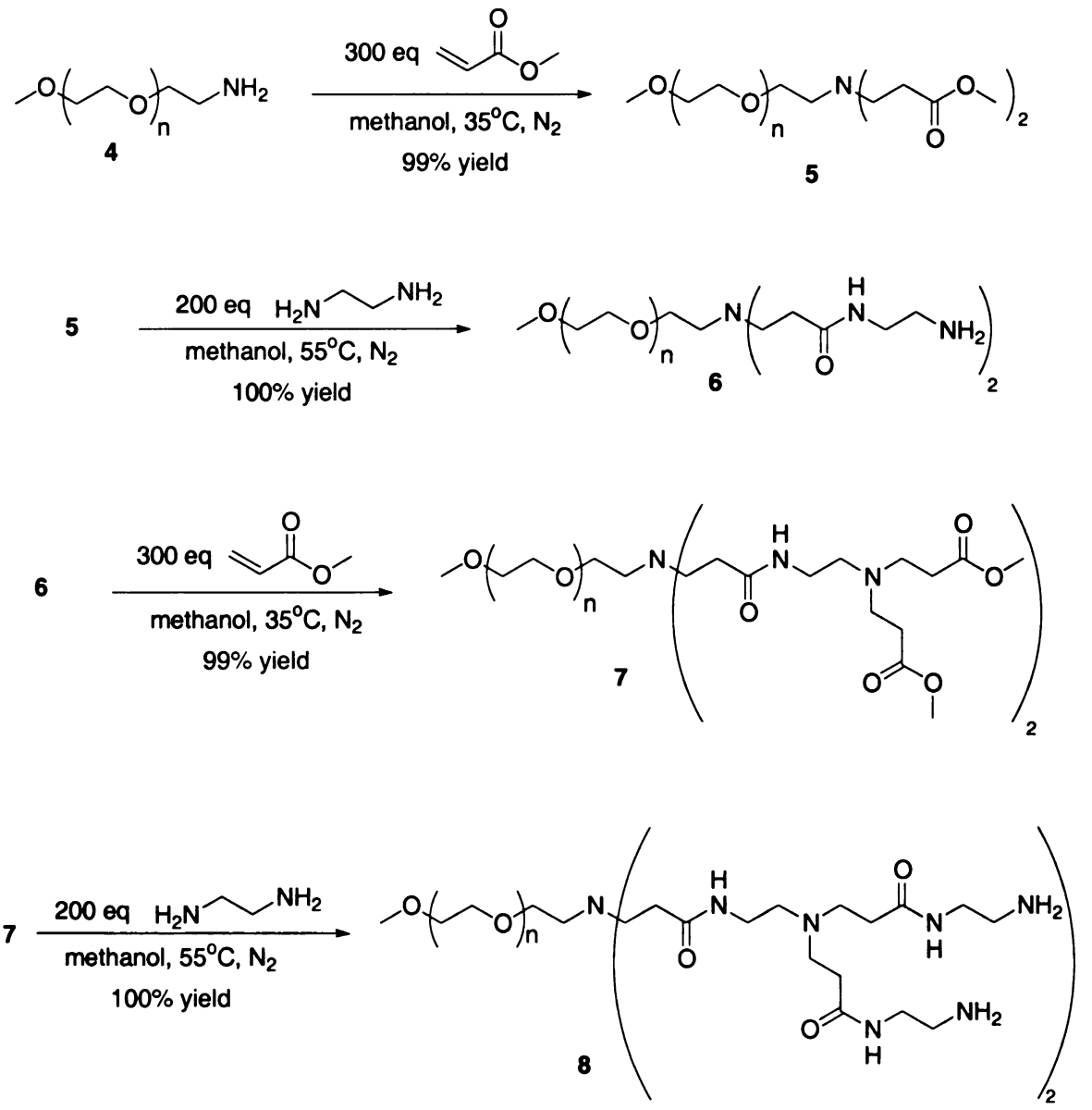

Scheme 6.2. Synthesis of PEO-PAMAM diblock copolymers.

Dynamic Light Scattering

We performed DLS experiments on the diblocks and PEO in Milli Q water at 25 °C to obtain the hydrodynamic radius (R_h) from eq 6.1 above. All measurements were conducted at a concentration of 10 mg/mL as this is the lowest concentration that allowed a reasonable intensity of scattering. At this concentration we observed a negligible change in radii with decreasing concentration.

PEO-PAMAM diblock copolymers were dissolved in Milli Q water and filtered before performing DLS experiments. The theoretical molecular weights of all samples tested are listed in Table 6.1. The percent mass vs. hydrodynamic radius for PEO 750 Da-G4 has a maximum at an R_h of 1.20 ± 0.09 nm (Figure 6.2a), obtained from both the cummulant and regularization fit (Figure 6.1b). Figures 6.2-6.6 display both the percent mass vs. R_h and the cummulant and regularization fits to the intensity autocorrelation function of the hybrids. In all samples both the cummulant and regularization fit resulted in the same value of R_h indicating a monomodal system. The hydrodynamic radius increased as the molecular weight of the PEO chain attached to dendrimers' focal point increased, R_h values of 1.50 ± 0.10 nm, 1.90 ± 0.05 nm, 2.60 ± 0.10 nm and 4.00 ± 0.12 nm were found for PEO 2 kDa-G4, PEO 5 kDa-G4, PEO 9 kDa-G4 and PEO 20 kDa-G4 respectively (Table 6.2).

Table 6.1. Sample codes and number average molecular mass (M) of compounds used in this study[a]

Sample code	M-dendrimer(Da) /M-poly(ethylene oxide) (kDa)/M (kDa)	Sample code	M-dendrimer(Da) /M-poly(ethylene oxide) (kDa)/M (kDa)
PEO 750 Da-G4	3422/750/4.2	PEO 2 kDa	0/2.0./2.0
PEO 2 kDa-G4	3422/2.0/5.4	PEO 5 kDa	0/5.0/5..0
PEO 5 kDa-G4	3422/5.0/8.4	PEO 8 kDa	0/8.0/8.0
PEO 9 kDa-G4	3422/9.0/12.4	PEO 20 kDa	0/20.0/20.0
PEO 20 kDa-G4	3422/20.0/23.4	PEO 36 kDa	0/36.0/36.0
		G4	3422/0/0

[a] M-dendrimer represents the mass of the dendrimer; M-poly(ethylene oxide) , mass of the poly(ethylene oxide) and M, total mass.

Table 6.2. Hydrodyamic radii (nm) of PEO and PEO-PAMAM samples.

Sample code	R_h(nm)	Sample code	R_h (nm)
PEO 750 Da-G4	1.20 ± 0.10	PEO 2 kDa	1.20 ± 0.09
PEO 2 kDa-G4	1.50 ± 0.10	PEO 5 kDa	1.80 ± 0.10
PEO 5 kDa-G4	1.20 ± 0.09	PEO 8 kDa	2.30 ± 0.11
PEO 9 kDa-G4	1.90 ± 0.05	PEO 20 kDa	4.20 ± 0.10
PEO 20 kDa-G4	2.60 ± 0.08	PEO 36 kDa	5.90 ± 0.12
		G4	1.90 ± 0.05

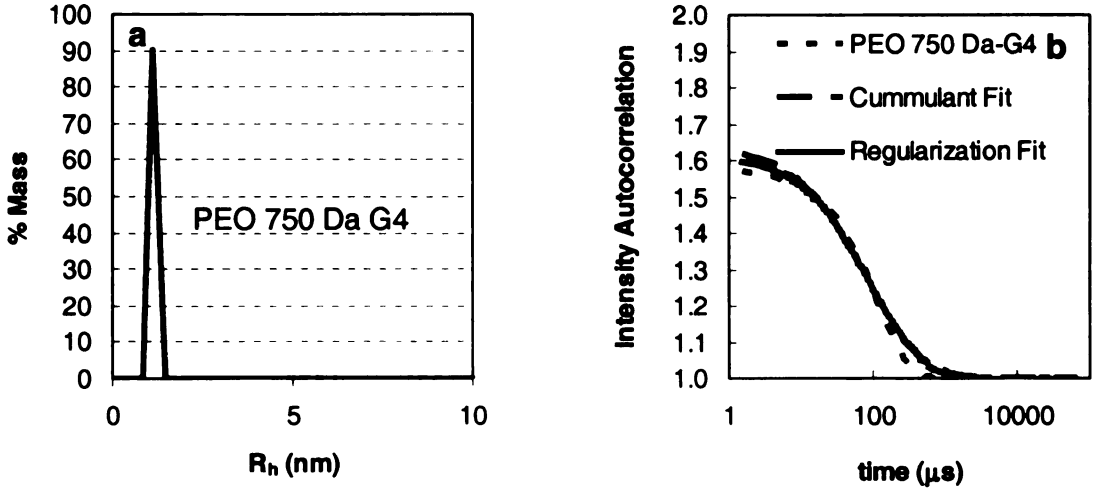

Figure 6.2. Dynamic light scattering results for PEO 750 Da-G4 in Milli Q water.

a. Percent mass vs. R_h (nm), shows a maximum at 1.20 ± 0.10 nm. b. Intensity autocorrelation for the sample, cummulant and regularization fits vs. time.

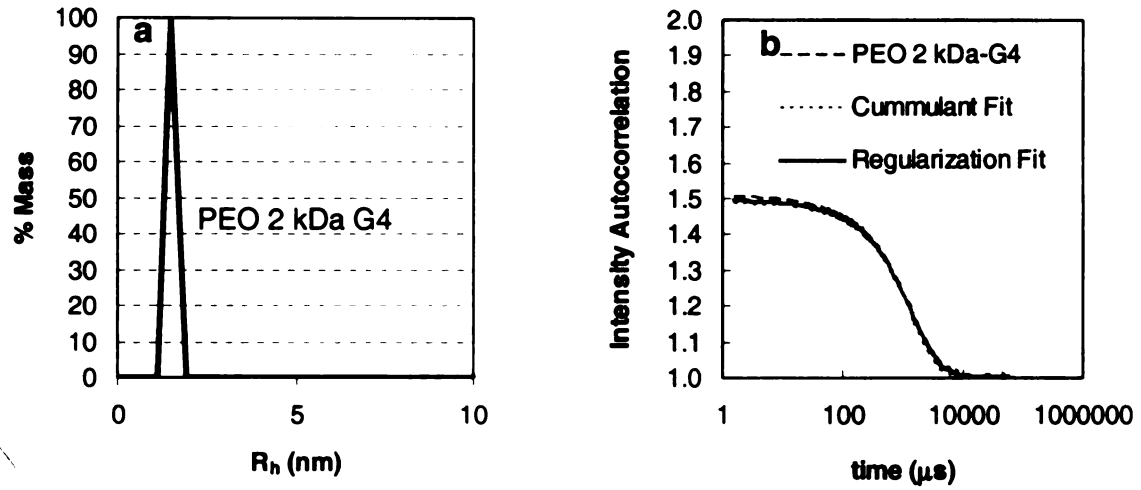

Figure 6.3. Dynamic light scattering results for PEO 2 kDa-G4 in Milli Q water.

a. Percent mass vs. R_h (nm), shows a maximum at 1.50 ± 0.10 nm. b. Intensity autocorrelation for the sample, cummulant and regularization fits vs. time.

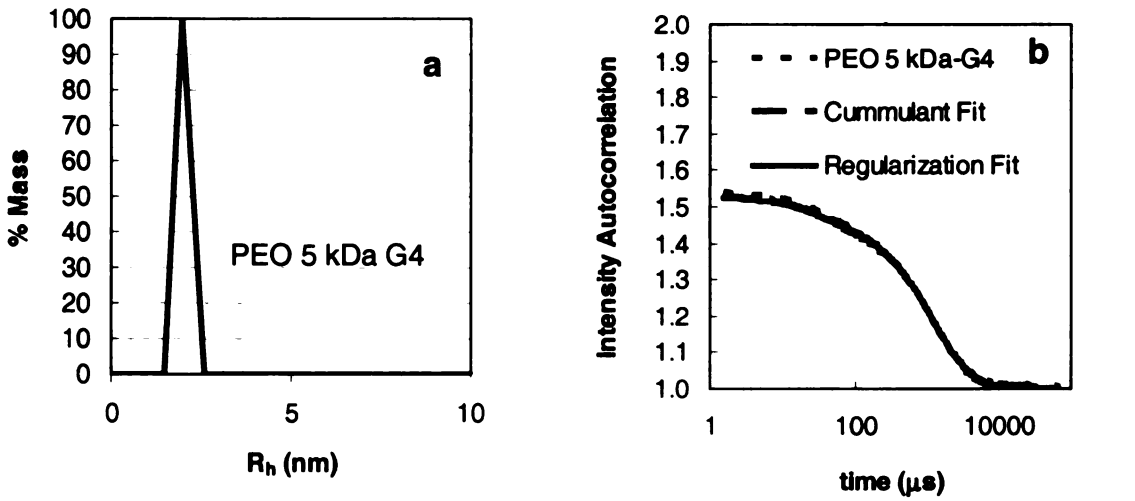

Figure 6.4. Dynamic light scattering results for PEO 5 kDa-G4 in Milli Q water.

a. Percent mass vs. R_h (nm), shows a maximum at 1.90 ± 0.05 nm. b. Intensity autocorrelation for the sample, cummulant and regularization fits vs. time.

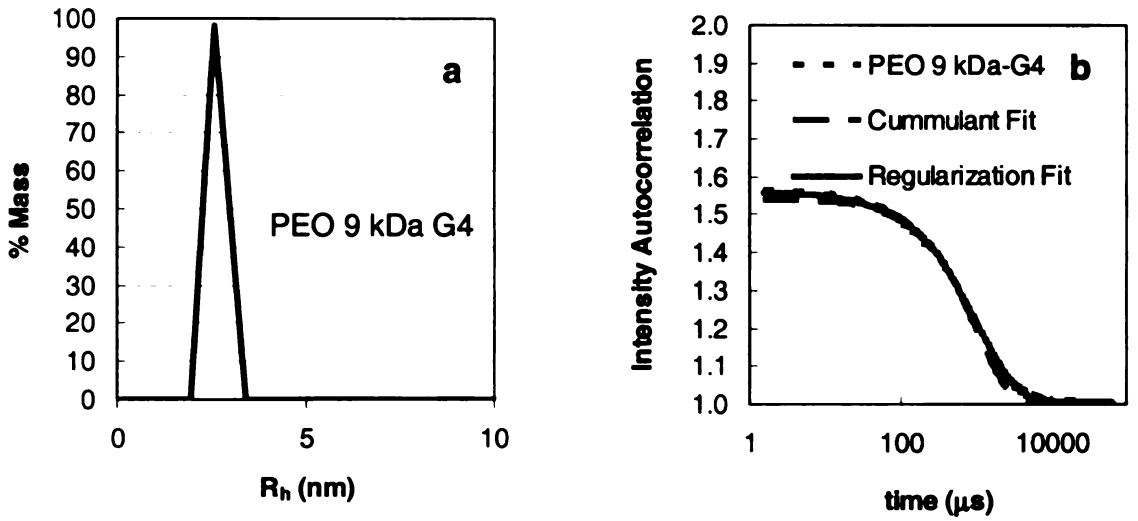

Figure 6.5. Dynamic light scattering results for PEO 9 kDa-G4 in Milli Q water.

a. Percent mass vs. R_h (nm), shows a maximum at 2.60 ± 0.08 nm. b. Intensity autocorrelation for the sample, cummulant and regularization fits vs. time.

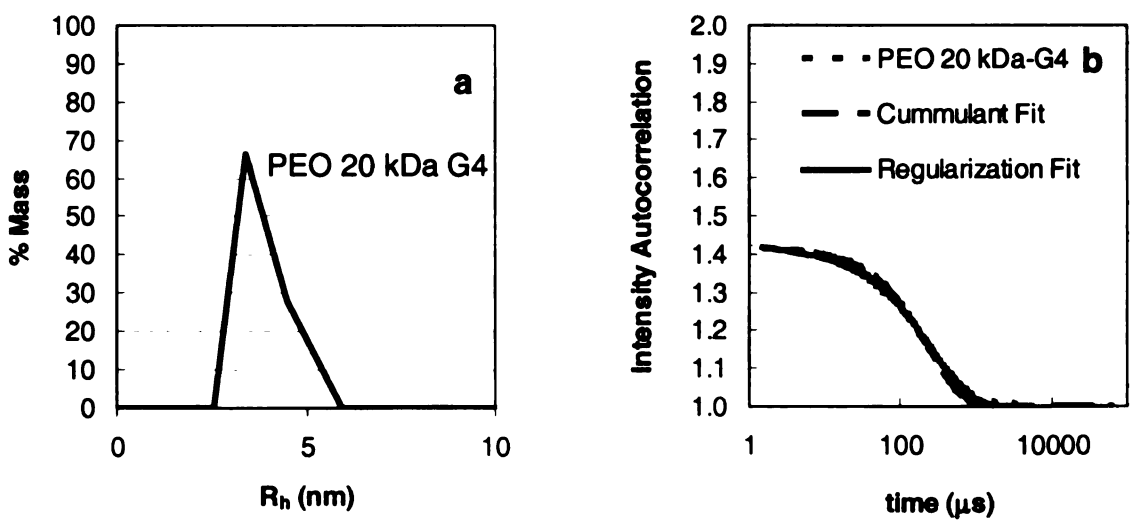

Figure 6.6. Dynamic light scattering results for PEO 20 kDa-G4 in Milli Q water.

a. Percent mass vs. R_h (nm), shows a maximum at 4.00 ± 0.09 nm. b. Intensity autocorrelation for the sample, cummulant and regularization fits vs. time.

The R_h values of PEO with molecular weight ranging from 2 kDa to 36 kDa were determined via DLS experiments (Table 6.2). We observed no agglomeration during the time scale of the experiment. Figure 6.7a displays the percent mass vs. R_h for PEO 2 kDa with a peak at an R_h value of 1.20 ± 0.09 nm, which was obtained from both the cummulant and regualization fit of the autocorrelation function. PEO chains with molecular weights of 5 kDa, 8 kDa, 20 kDa and 36 kDa have R_h values of 1.80 ± 0.10 nm, 2.30 ± 0.11 nm, 4.20 ± 0.10 nm and 5.90 ± 0.12 nm respectively (Figures 6.8-6.11).

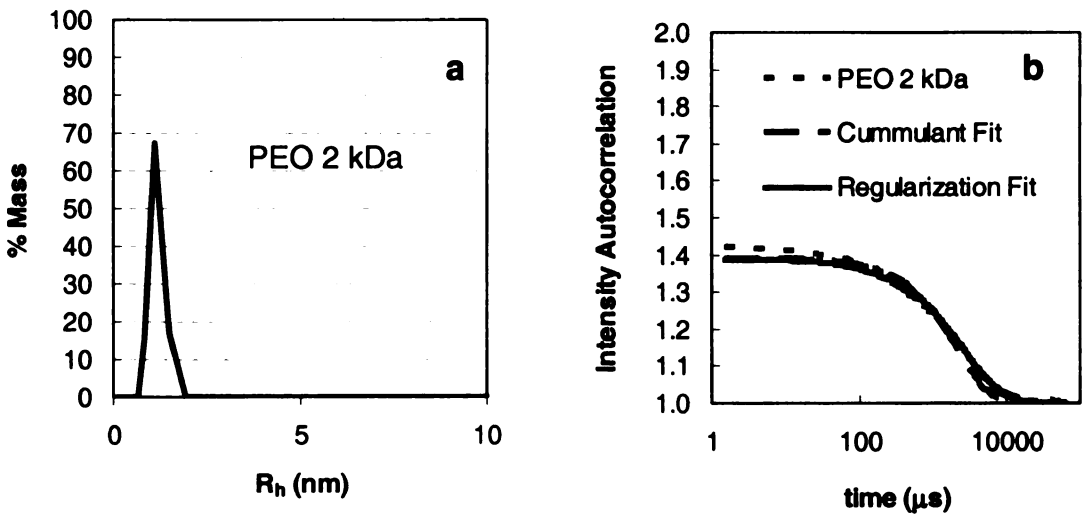

Figure 6.7. Dynamic light scattering results for PEO 2 kDa in Milli Q water.

a. Percent mass vs. R_h (nm), shows a maximum at 1.20 ± 0.09 nm. b. Intensity autocorrelation for the sample, cummulant and regularization fits vs. time.

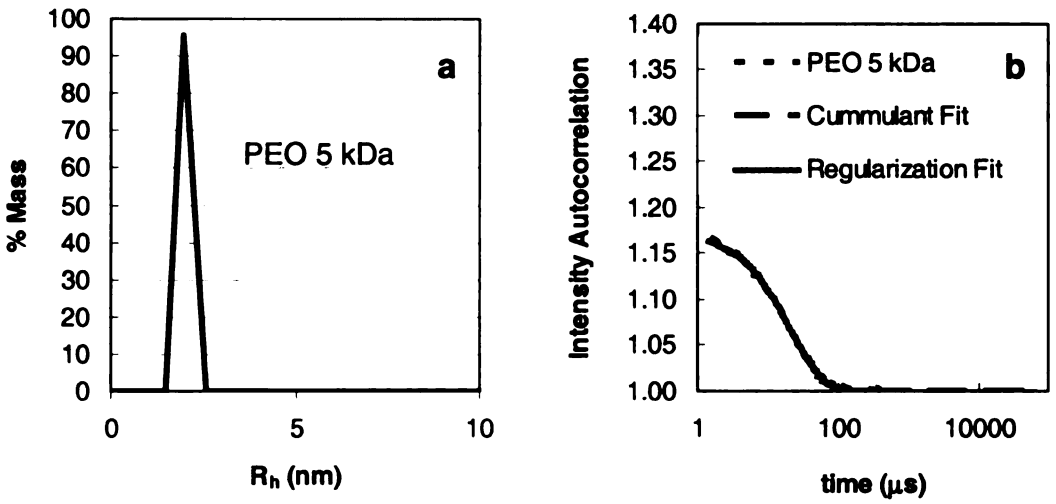

Figure 6.8. Dynamic light scattering results for PEO 5 kDa in Milli Q water.

a. Percent mass vs. R_h (nm), shows a maximum at 1.80 ± 0.10 nm. b. Intensity autocorrelation for the sample, cummulant and regularization fits vs. time.

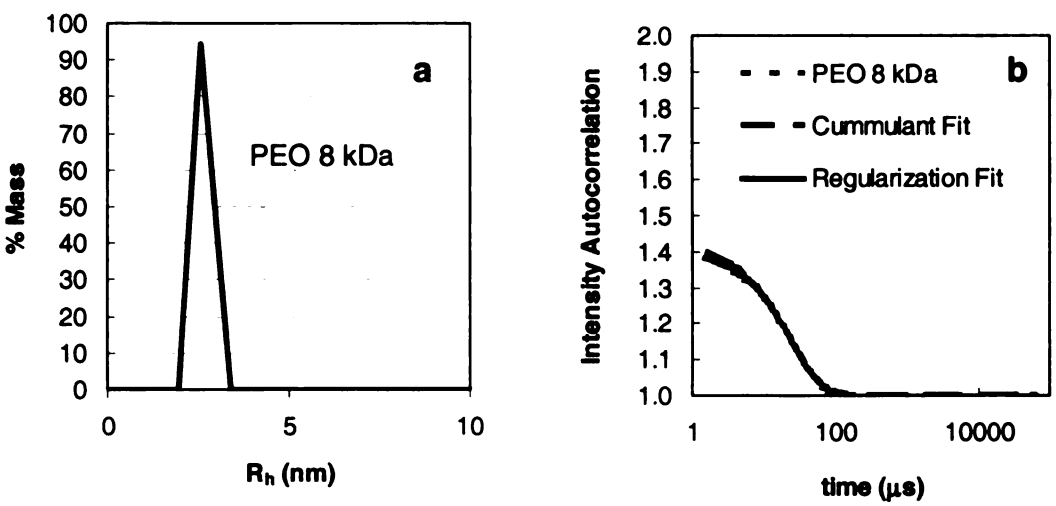

Figure 6.9. Dynamic light scattering results for PEO 8 kDa in Milli Q water.

a. Percent mass vs. R_h (nm), shows a maximum at 2.30 ± 0.11 nm. b. Intensity autocorrelation for the sample, cummulant and regularization fits vs. time.

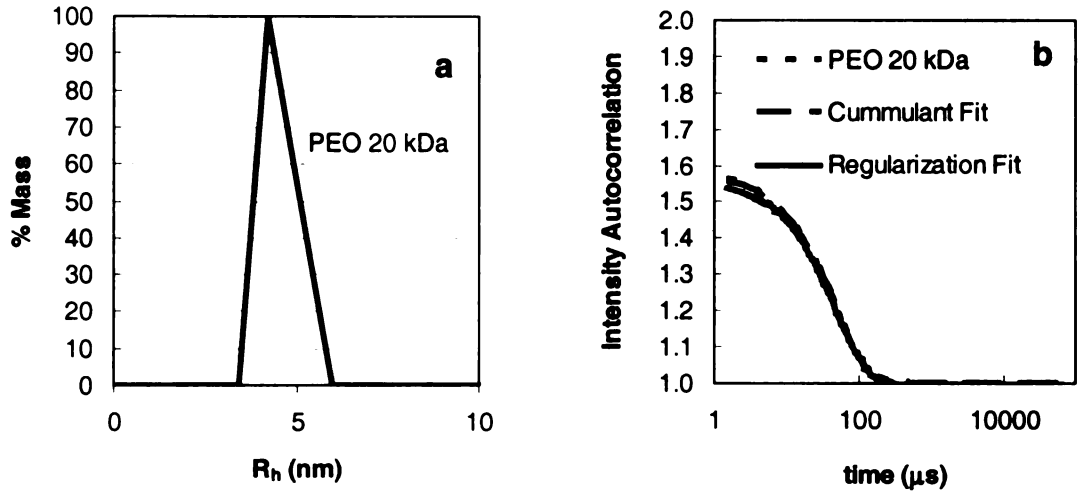

Figure 6.10. Dynamic light scattering results for PEO 20 kDa in Milli Q water.

a. Percent mass vs. R_h (nm), shows a maximum at 4.20 ± 0.10 nm. b. Intensity autocorrelation for the sample, cummulant and regularization fits vs. time.

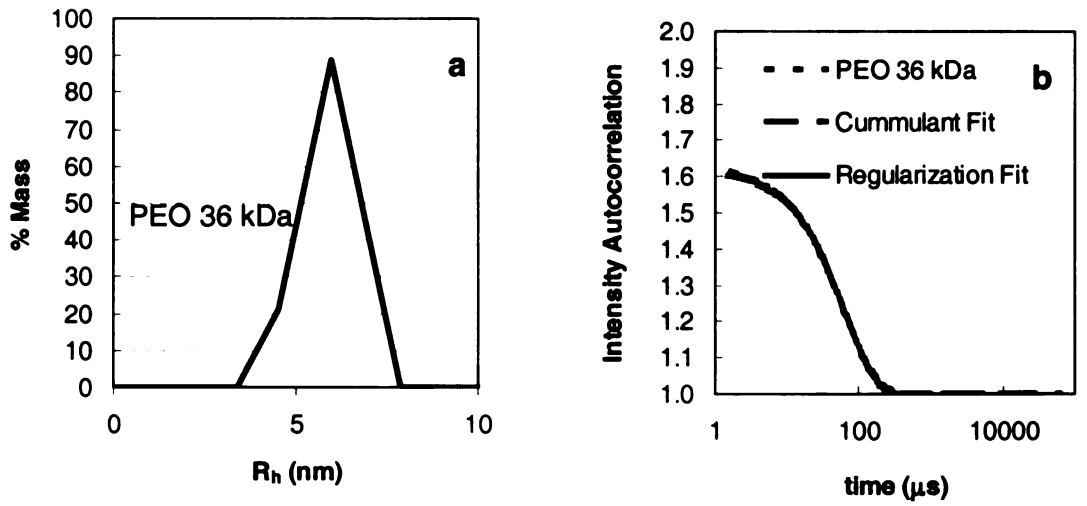

Figure 6.11. Dynamic light scattering results for PEO 36 kDa in Milli Q water.

a. Percent mass vs. R_h (nm), shows a maximum at 5.90 ± 0.12 nm. b. Intensity autocorrelation for the sample, cummulant and regularization fits vs. time.

The scaling behavior of the PEO and PEO-PAMAM diblock copolymers were compared by plotting R_h vs molecular weight (M) (Figure 6.12). It is clear that the lower molecular weight hybrids have an R_h value that is smaller than a PEO chain of an analogous molecular weight. The dimension of 750 kDa-G4, 2 kDa-G4 and 5 kDa-G4 are smaller in solution than a free PEO chain indicating the dendrimer is causing the molecule to be in a more compact state. Both the 9 kDa-G4 and 20 kDa-G4 hybrids have molecular dimensions in solution that are similar to a PEO chain with no dendrimer attached, indicating that increasing of the molecular weight of the linear chain cause the hybrid to transition from a state that is more compact than PEO to an expanded state similar to a free PEO chain in solution.

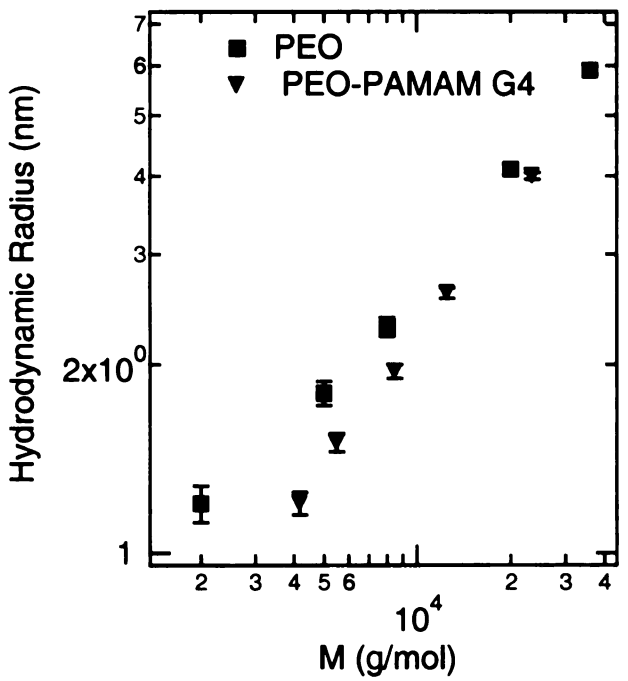

Figure 6.12. Hydrodynamic radius vs. molecular weight of PEO and PEO-PAMAM hybrids in Milli Q water at concentrations of 10 mg/mL.

These results parallel those found by Jeong et al.[6] for the poly(benzyl ether) (PBE)-poly(styrene) (PS) hybrid where smaller molecular weight hybrids were found to have a lower intrinsic viscosity than a PS chain of equal molecular weight. However, a sudden increase in intrinsic viscosity was observed for the hybrids between molecular weights of 60 kDa and for hybrids greater than 80 kDa, the intrinsic viscosity was equal to that of linear PS. This suggests that changes in the overall molecular conformation of the hybrid depend on the relative molecular weight of the two blocks. We performed neutron scattering experiments on PBE dendrons with a deuterated PS chain attached to the focal point and via a series of contrast matching experiments and concluded that increasing the molecular weight of the linear PS chain causes the dendrimer to change shape with the linear chain changing from a compact to more expanded state.[5]

These data suggest that the linear chain occupies the free volume of the dendrimer when the hybrids are in a compact state. To see if there is sufficient room within the dendrimer for the linear chain, we calculated the free volume of a PAMAM dendron (G4), analogous in structure to that attached to the PEO chain. DLS experiments of di-functional PAMAM G4 in Milli Q water (Figure 6.13) displays good cummulant and regularization fits of the autocorrelation intensity function resulting in an R_h of 1.90 ± 0.05 nm.

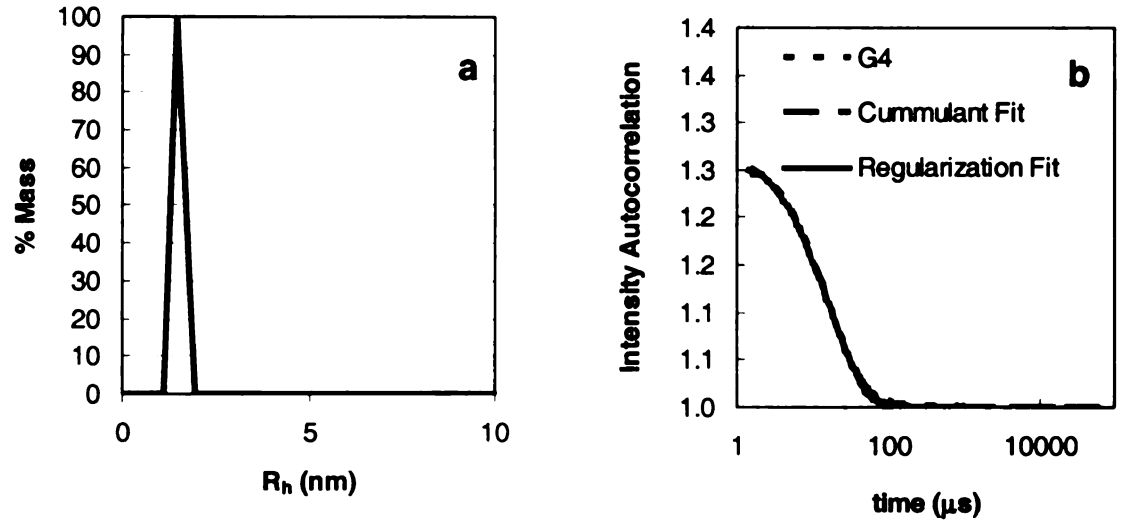

Figure 6.13. Dynamic light scattering results for G4 in Milli Q water.

a. Percent mass vs. R_h (nm), shows a maximum at 1.90 ± 0.05 nm. b. Intensity autocorrelation for the sample, cummulant and regularization fits vs. time.

Several techniques can be used to calculate the free volume within the G4 dendrimer. The free volume, V_f, is defined through the partition function for a molecule in the liquid state as[20-22]

$$V_f = c^3\left\{V_{mol}^{1/3} - V_{hc}^{1/3}\right\}^3 \tag{6.2}$$

where c is a numerical factor representing molecular packing and intermolecular interaction effects, V_{mol} is molecular volume and V_{hc} is a characteristic or hard-core volume. Here we use a value of 2 for c as suggested previously,[20] and V_{mol} as V_h, which was calculated from the hydrodynamic radius, Table 6.2, assuming the dendron is shaped as a sphere. V_{hc} is taken as the van der Waals volume, V_{vdw}. The molecular increments of Edward[23] were used to determine the volume contributions of the dendrimers core

V_{vdw} (C) = 63.50 Å^3, branching unit, V_{vdw} (BU) = 219.90 Å^3, and end group, V_{vdw} (E) = 17.60 Å^3. The total van der Waal's volume for any generation dendrimer, g, is given by

$$V_{vdw} = V_{vdw}(C) + \left[2^g - 1\right]V_{vdw}(BU) + 2^g V_{vdw}(E) \tag{6.3}$$

The free volume for a gas is defined as

$$V_f = V_{mol} - V_{hc} \tag{6.4}$$

Both eq 6.2 and 6.3 were used and the smaller of the two resulting values was taken as the free volume, which came from the gas state equation.

Due to the experimental error of the R_h measurement, the free volume of the G4 dendron ranges from 23 to 28 nm^3. The number of repeat units of PEO that can 'fit' within in this free volume range was found by dividing the free volume of the dendrimer by the V_{vdw} of a PEO repeat unit, 0.041 nm,^{3} resulting in a maximum of 668 repeat units (a PEO of 29 kDa) that can be accommodated in the cavities of the dendrimer. These calculations suggest that the dendrimer can contain the largest PEO chains of the hybrids that are in a collapsed state in addition to the PEO chains of the expanded hybrids (Figure 6.12). However, using V_{vdw} as the volume of the repeat units underestimates the space required by the PEO chain and is one explanation of the transition in structure occurring at a molecular weight below that predicted by free volume calculations. Intramolecular hydrogen bonding as well as hydrogen bonding with the solvent also could be impacting the amount of free volume within the dendrimer.

The change in hydrodynamic radii seen in the PEO-PAMAM hybrids suggests that this hydrophilic system is undergoing a similar single molecular phase transition that was observed for the hydrophobic PBE-PS system.[6] Neutron scattering contrast

matching experiments that allow visualization of each block could confirm this transition. In addition, it would be interesting to investigate the behavior of the of these hybrids as a function of solvent quality as our scattering experiments on a PAMAM analogous dendron show that dendron size is very sensitive to the surrounding environment and this could alter the morphology of the hybrid.

Conclusion

We have synthesized a series of PEO-PAMAM linear-dendrimer diblock copolymers and investigated their morphology in dilute aqueous solution via a series of DLS experiments. We measured the R_h values of both hybrids and linear PEO chains and compared the change in size of the two systems with respect to molecular weight. The hybrid system is smaller in dimensions than an analogous PEO chain when the molecular weight of the PEO of the hybrids is 750 Da, 2 kDa or 5k Da. Hybrids with a PEO chain of mass greater than 5 kDa have an R_h value within experimental error of a PEO chain of analogous molecular weight, indicating they are in a more expanded state, suggesting a random coil conformation. The overall morphology of the PEO-PAMAM system is sensitive to the molecular weight of the PEO chain, which was also observed for PBE-PS systems.[6] Further SANS studies on deuterated analogs could confirm the relative location of the two blocks to determine if one or both blocks change conformation. It appears that the water soluble hybrid system is converting from a knitted coil to a random coil upon increasing molecular weight of the linear block.

References

1. Gohy, J. F.; Lohmeijer, B. G. B.; Varshney, S. K., *Macromolecules* **2002,** *35*, 9748.

2. Rodriguez-Hernandez, J.; Lecommandoux, S., *J. Am. Chem. Soc.* **2005,** *127*, 2026-2027.

3. Arotcarena, M.; Heise, B.; Ishaya, S.; Laschewsky, A., *J. Am. Chem. Soc.* **2002,** *124*, 3787.

4. Ge, Z.; Luo, S.; Liu, S., *J. Polym. Sci.Part A: Polym. Chem.* **2006,** *44*, 1357-1371.

5. Passeno, L. M.; Mackay, M. E.; Baker, G. L.; Vestberg, R.; Hawker, C. J., *Macromolecules* **2006,** *39*, 740-746.

6. Jeong, M.; Mackay, M. E.; Hawker, C. J.; Vestberg, R., *Macromolecules* **2001,** *34*, 4927-4936.

7. Gitsov, I.; Fréchet, J. M. J., *Macromolecules* **1993,** *26*, 6536-6537.

8. Gillies, E. R.; Jonsson, T. B.; Frechet, J. M. J., *J. Am. Chem. Soc.* **2004,** *126*, 11936-11943.

9. Tande, B. M.; Wagner, N. J.; Mackay, M. E., *Compt. Ren. Chim.* **2003,** *6*, 853-864.

10. Mecke, A.; Lee, I.; Baker, J. R.; Holl, M. M. B.; Orr, B. G., *Eur. Phys. J. E* **2004,** *14*, 7-16.

11. Gitsov, I.; Newkome, G. R., *Advances in Dendritic Macromolecules*. Elsevier Science: Amsterdam, 2002; Vol. 5, p 45-87.

12. Gitsov, I.; Wooley, K. L.; Hawker, C. J.; Ivanova, P. T.; Fréchet, J. M. J., *Macromolecules* **1993,** *26*, 5621-5627.

13. Namazi, H.; Adeli, M., *J. Polym. Sci. Part A: Poly Chem* **2005,** *43*, 28.

14. Gitsov, I.; Wooley, K. L.; Frechet, J. M. J., *Angew. Chem. Int. Ed. Engl.* **1992,** *31*, 1200-1202.

15. Hest, J. C. M. v.; Baars, M. W. P. L.; Elissen-Román, C.; Genderen, M. H. P. v.; Meijer, E. W., *Macromolecules* **1995,** *28*, 6689.

16. Chapman, T. M.; Hillyer, G. L.; Mahan, E. J.; Schaffer, K. A., *J. Am. Chem. Soc.* **1994,** *116*, 11195-11196.

17. Iyer, J.; Fleming, K.; Hammond, P. T., *Macromolecules* **1998,** *31*, 8758-8765.

18. Sill, K.; Emerick, T., *J. Polym. Sci. Part A: Polym. Chem.* **2005,** *43*, 5429.

19. Dust, J. M.; Fang, Z.; Harris, J. M., *Macromolecules* **1990,** *23*, 3742-3746.

20. Glasstone, S.; Laidler, K. J.; Eyring, H., *The Theory of Rate Processes*. McGraw-Hill Book Co.: New York, 1941.

21. Flory, P. J.; Orwoll, R. A.; Vrij, A., *J. Am. Chem. Soc.* **1964,** *86*, 3507-3514.

22. Prausnitz, J. M.; Lichtenthaler, R. N.; Gomes-de-Azevedo, E., *Molecular Thermodynamics of Fluid-Phase Equilibria*. Prentice Hall: Upper Saddle River, 1999.

23. Edward, J. T., *J. Chem. Educ.* **1970,** *47*, 261-270.

APPENDICIES

APPENDIX A

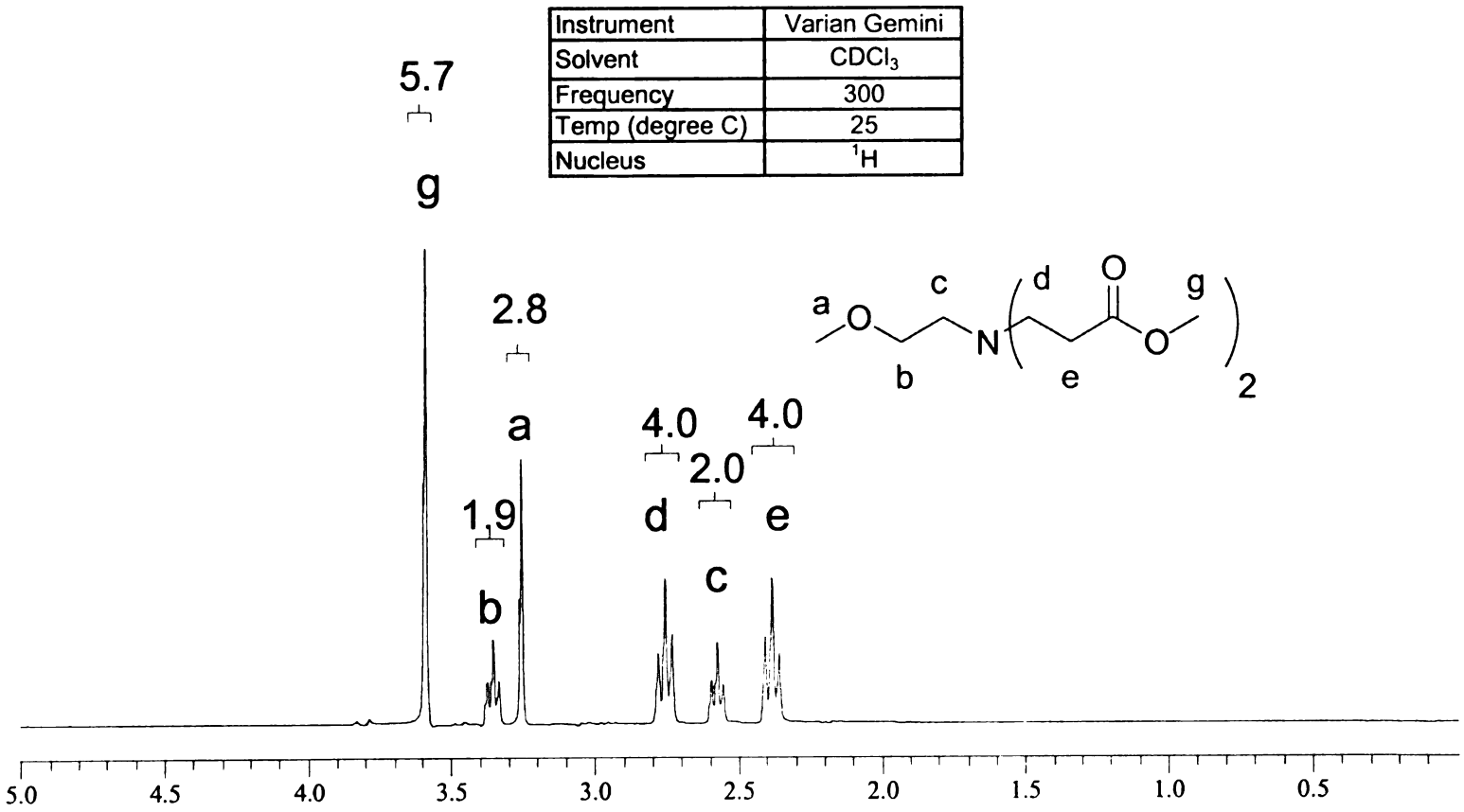

Figure A.1. ^{1}H NMR MEA G0.5

Instrument	Varian Gemini
Solvent	$CDCl_3$
Frequency	300
Temp (degree C)	25
Nucleus	^{13}C

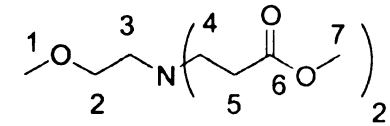

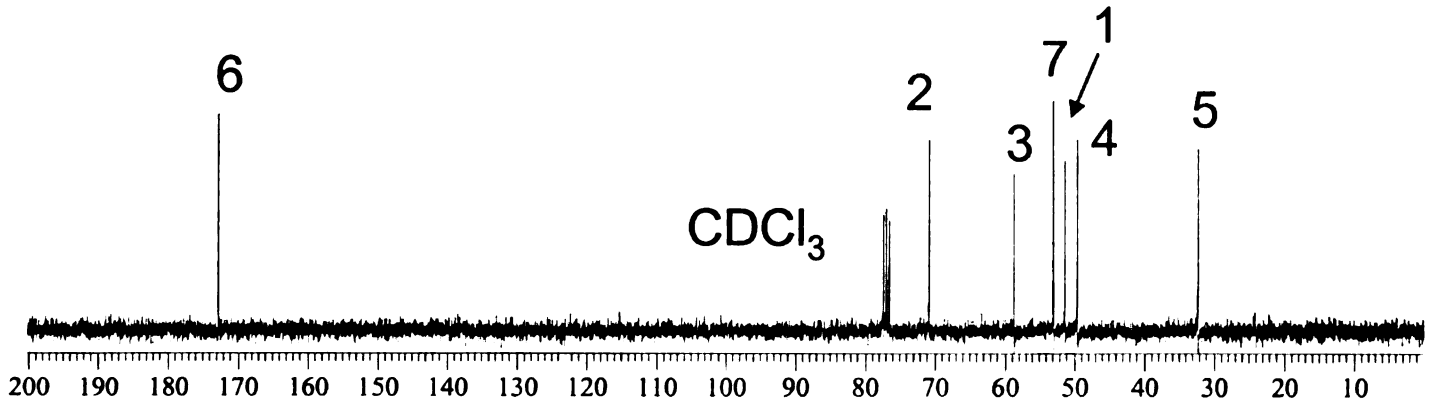

Figure A.2. ^{13}C NMR MEA G0.5

Instrument	Varian Gemini
Solvent	$CDCl_3$
Frequency	300
Temp (degree C)	25
Nucleus	^1H

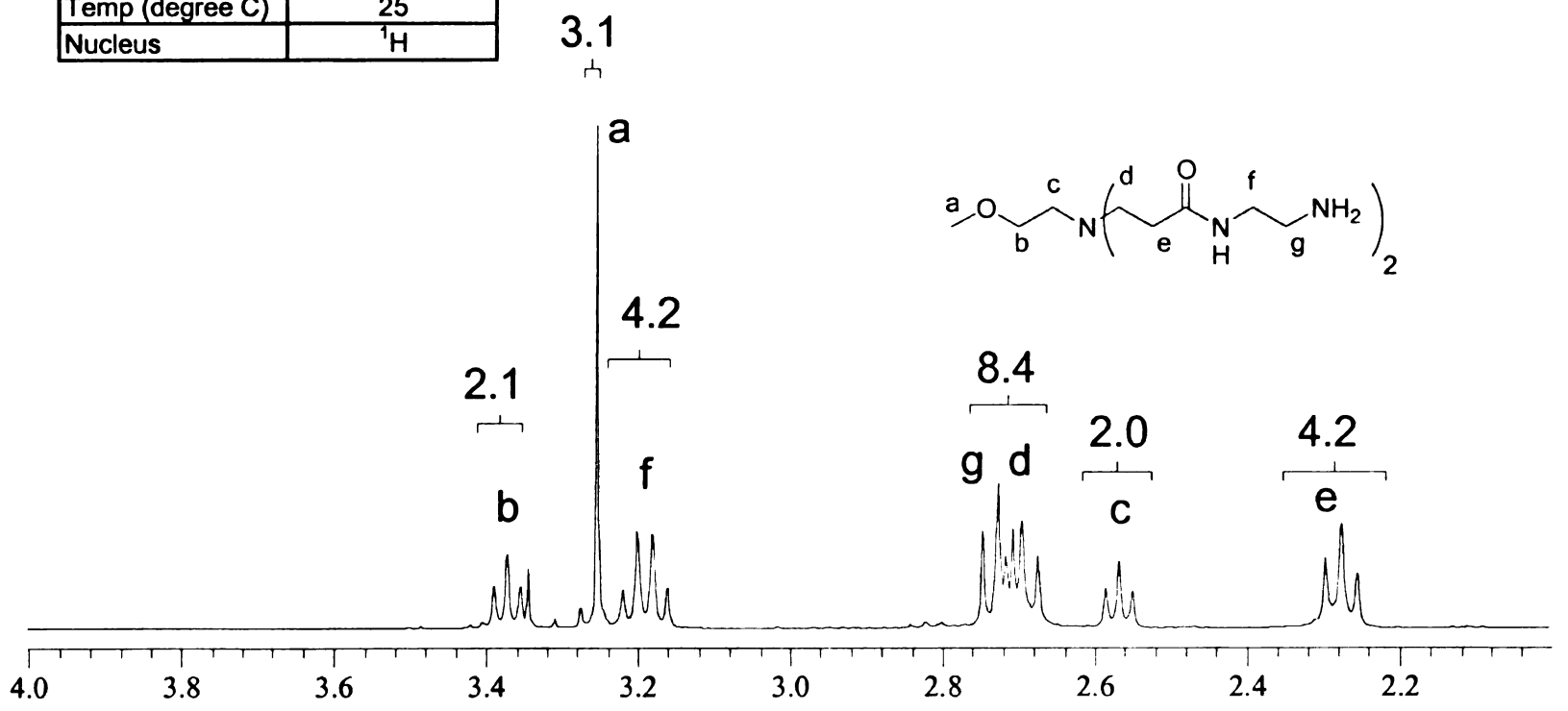

Figure A.3. ^1H NMR MEA G1.0

Instrument	Varian Gemini
Solvent	$CDCl_3$
Frequency	300
Temp (degree C)	25
Nucleus	^{13}C

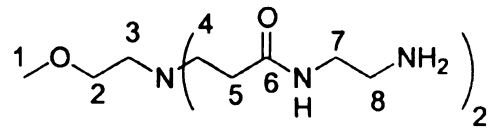

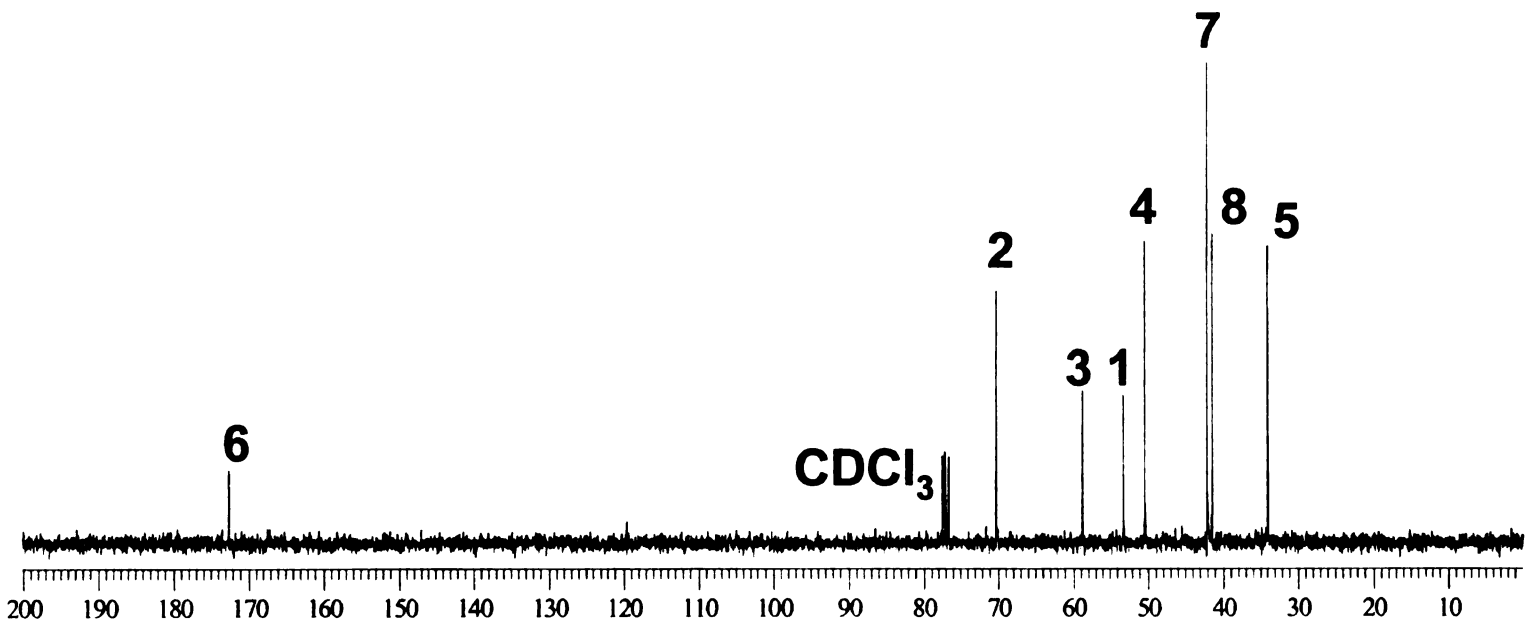

Figure A.4. ^{13}C NMR MEA G1.0

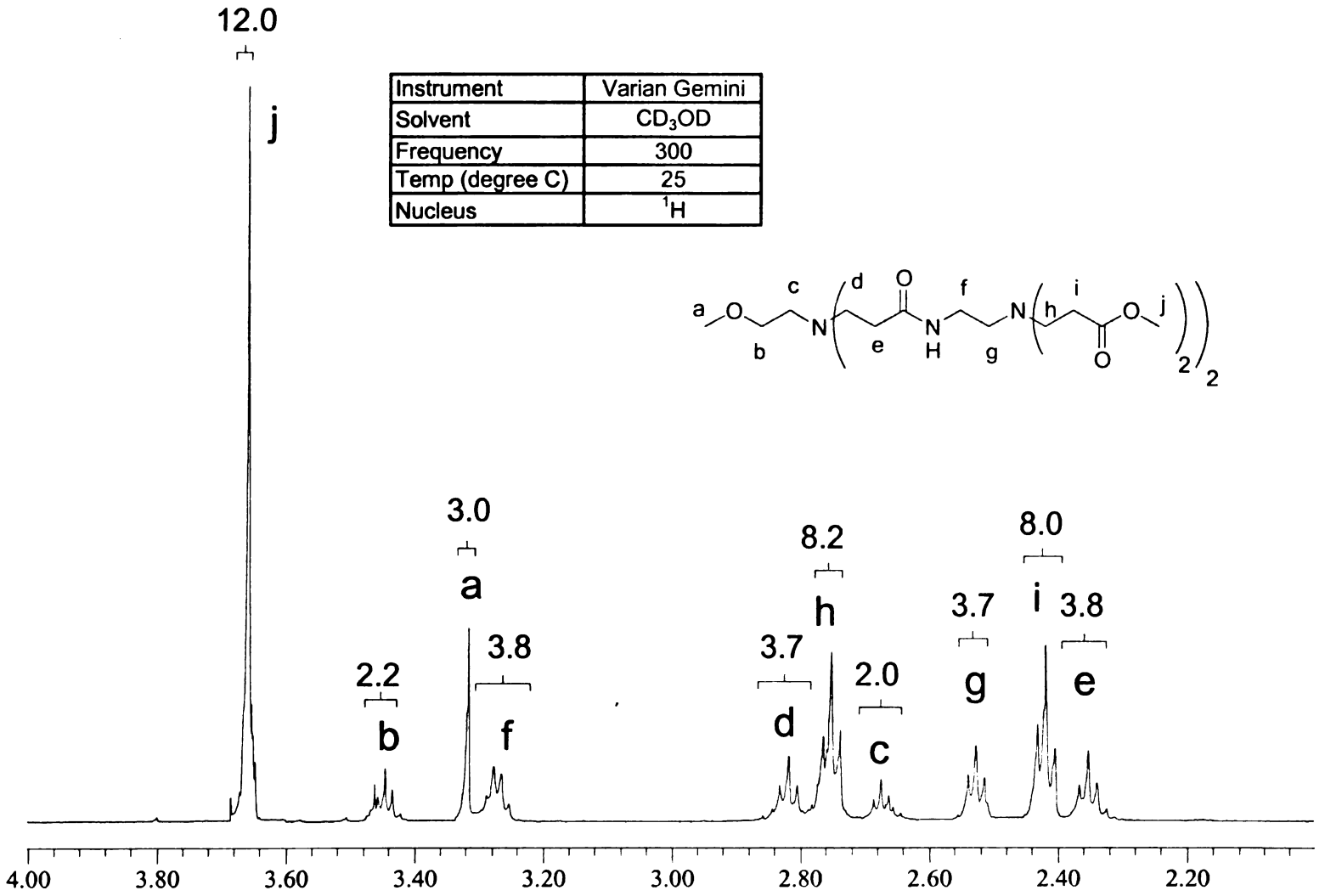

Figure A.5. ^{1}H NMR MEA G1.5

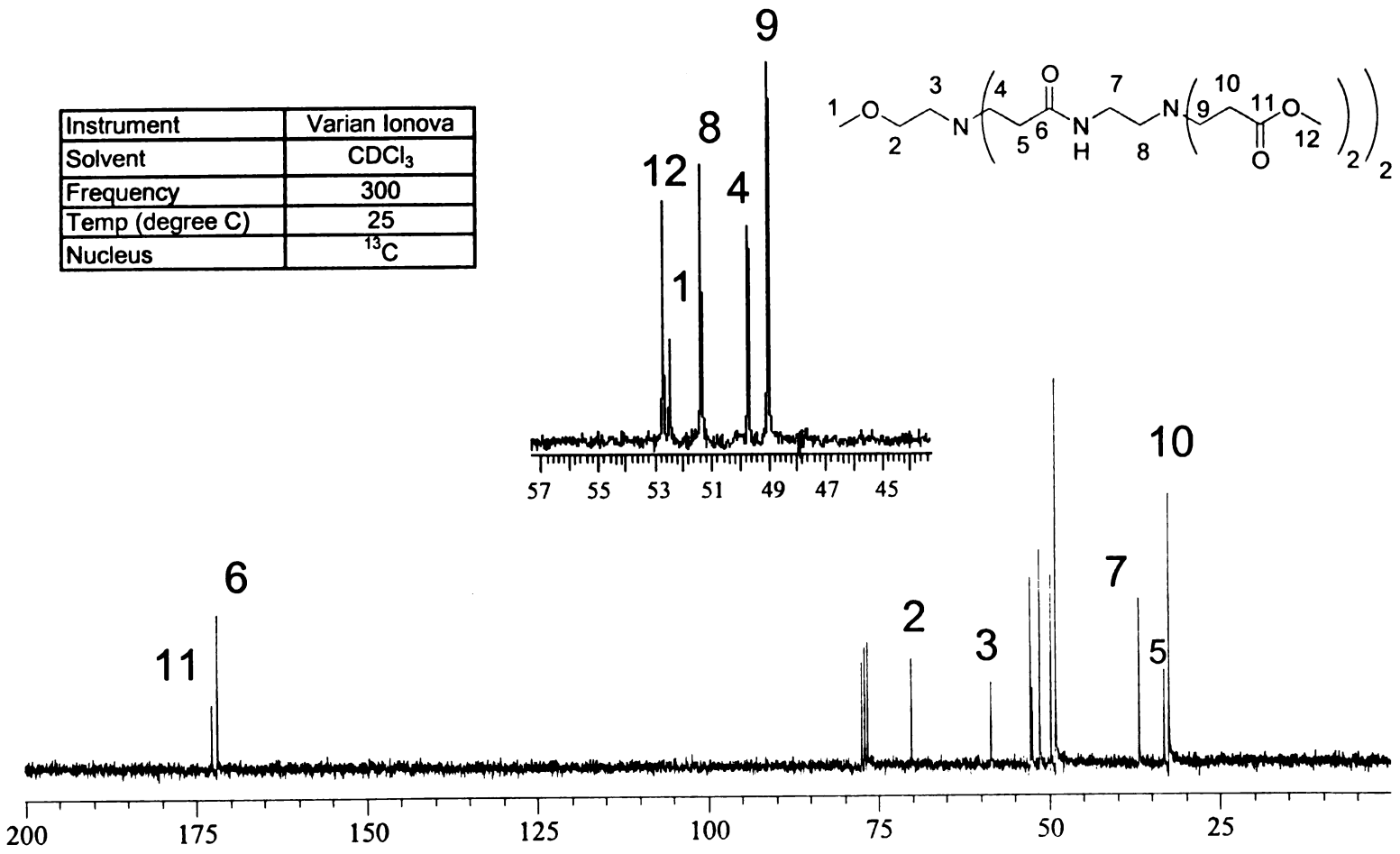

Figure A.6. ^{13}C NMR MEA G1.5

Instrument	Varian Gemini
Solvent	CD_3OD
Frequency	300
Temp (degree C)	25
Nucleus	^1H

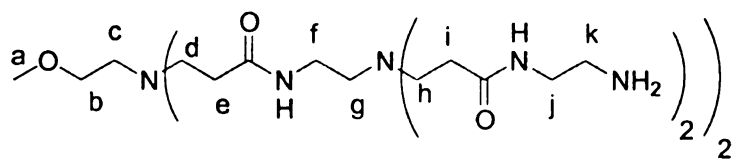

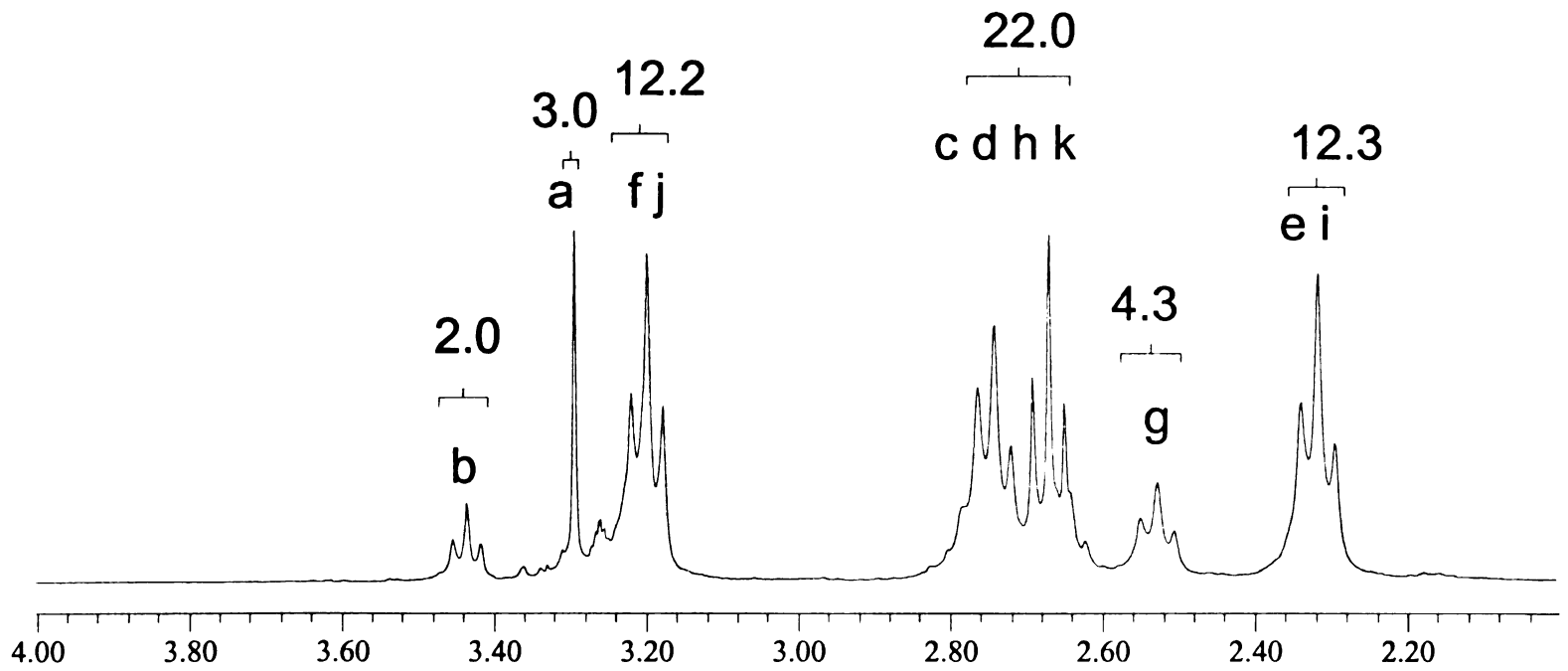

Figure A.7. ^1H NMR MEA G2.0

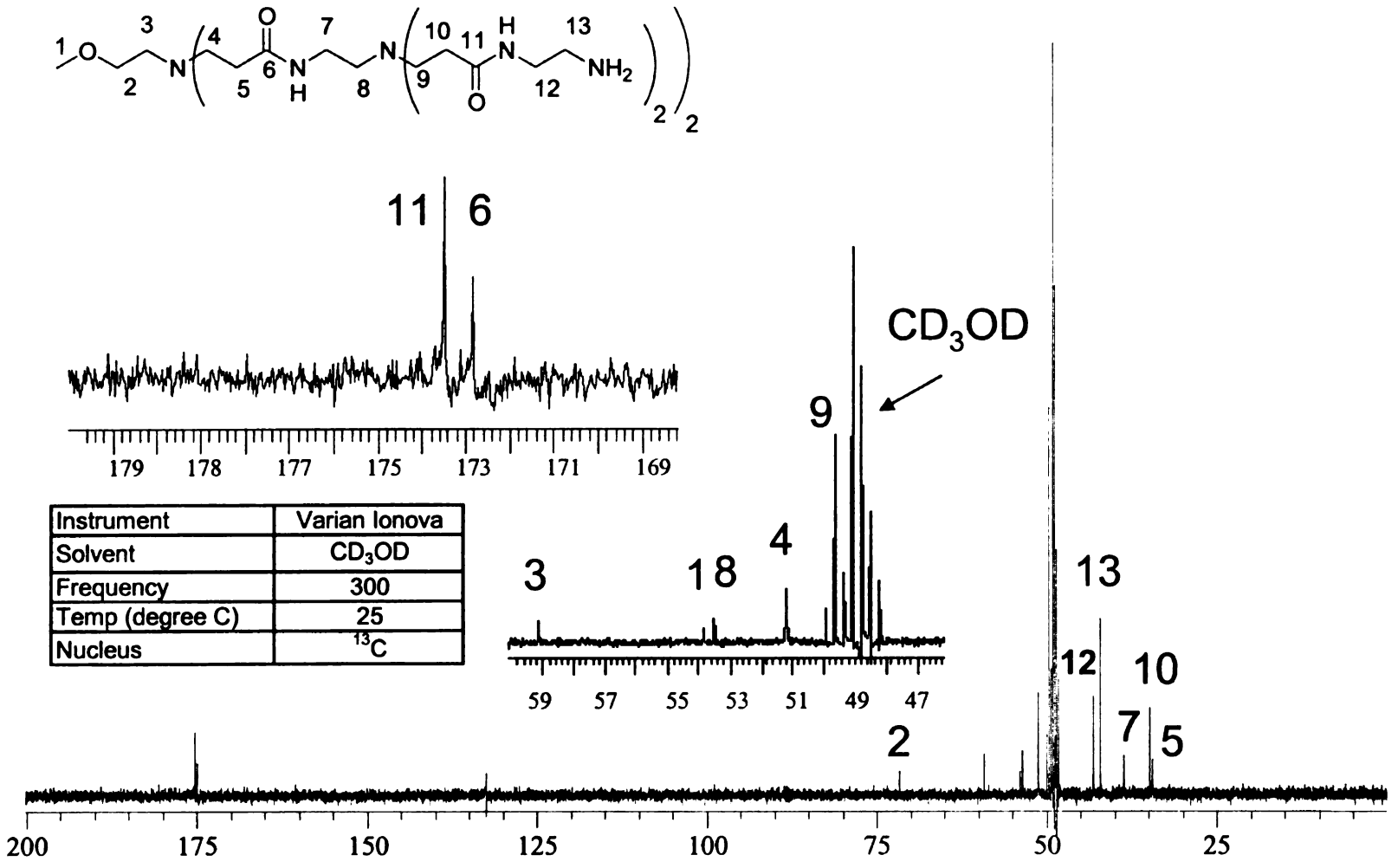

Figure A.8. ^{13}C NMR MEA G2.0

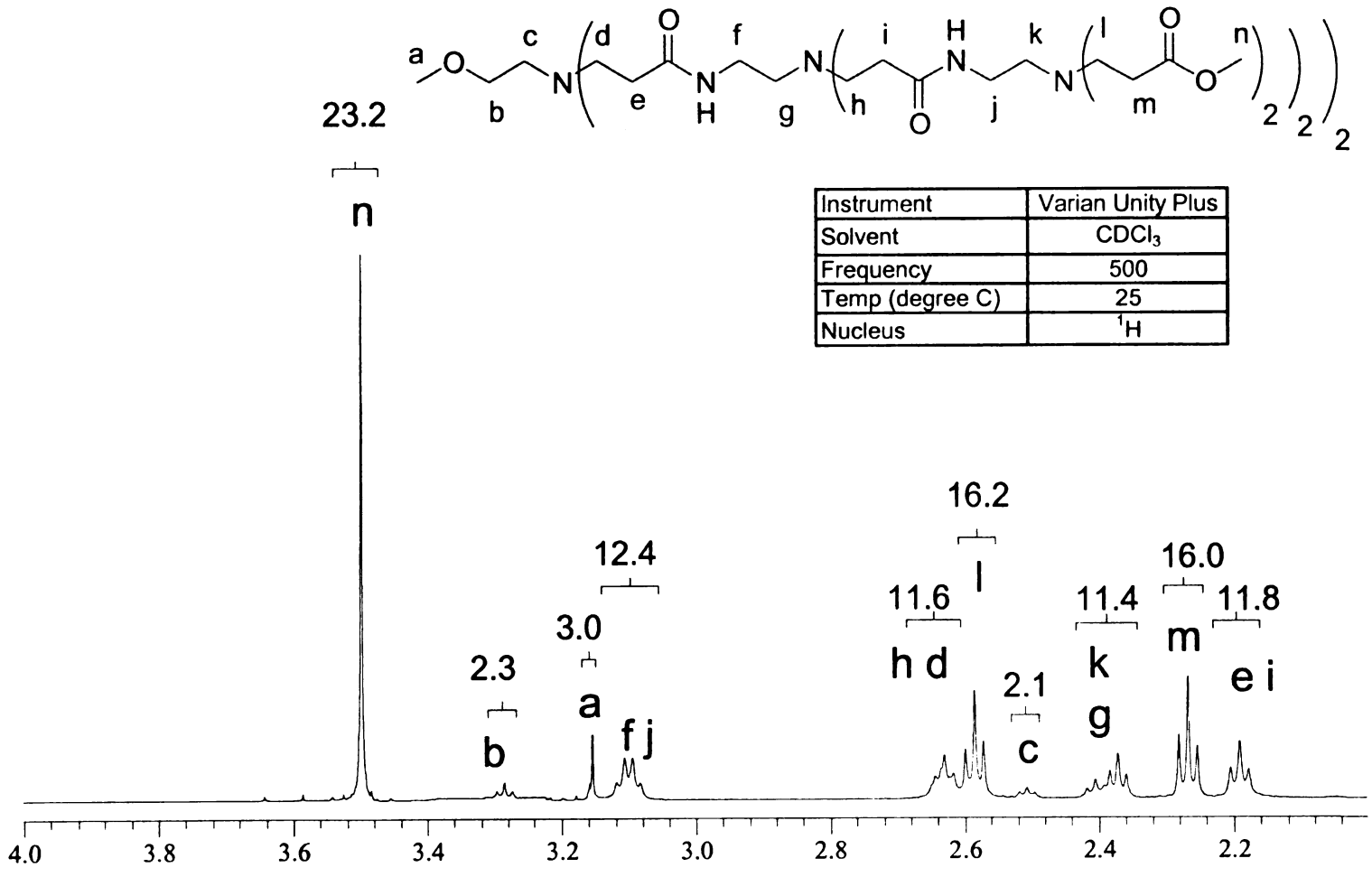

Figure A.9. ^{1}H NMR MEA G2.5

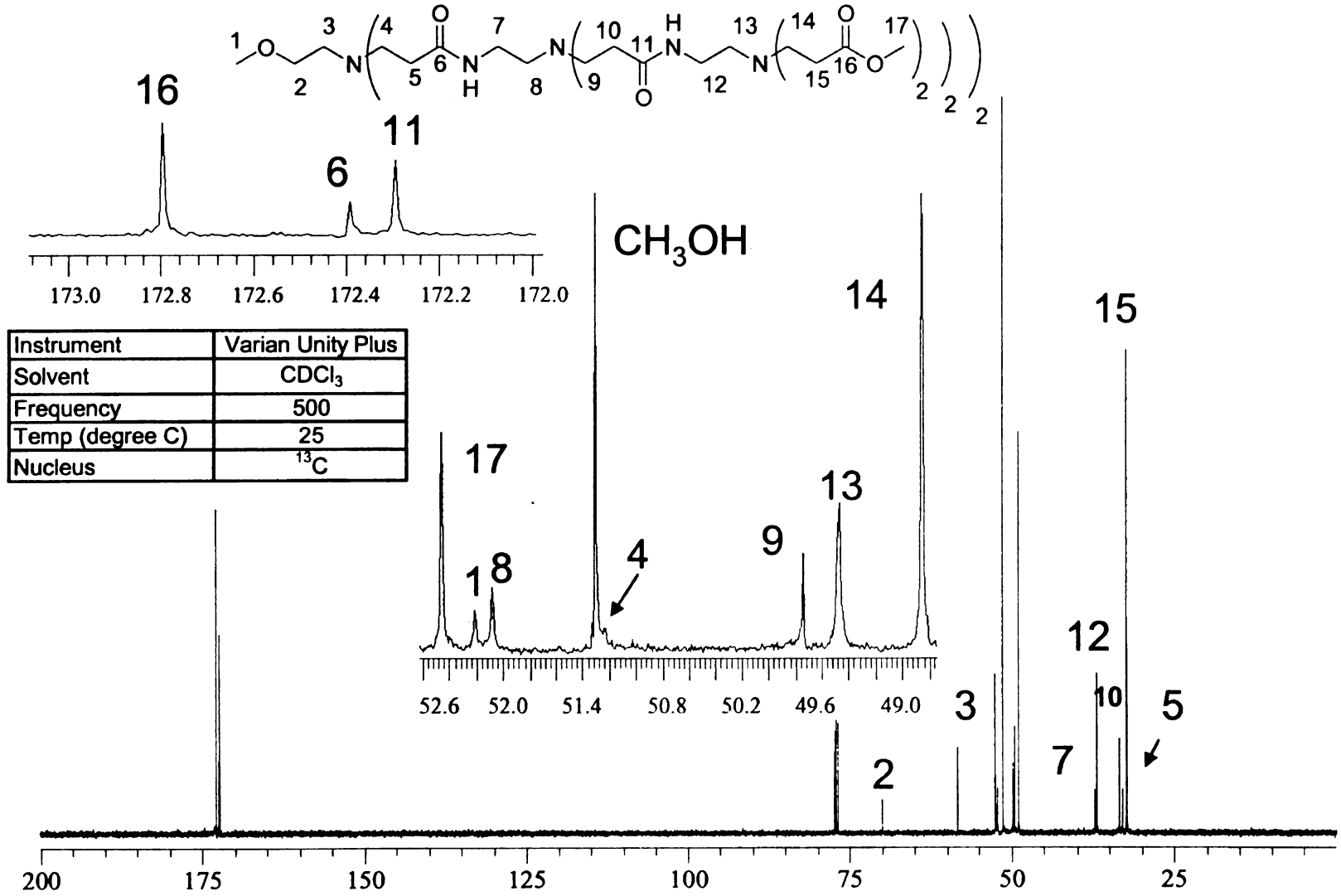

Figure A.10. ^{13}C NMR MEA G2.5

Instrument	Varian Unity Plus
Solvent	$CDCl_3$
Frequency	500
Temp (degree C)	25
Nucleus	^1H

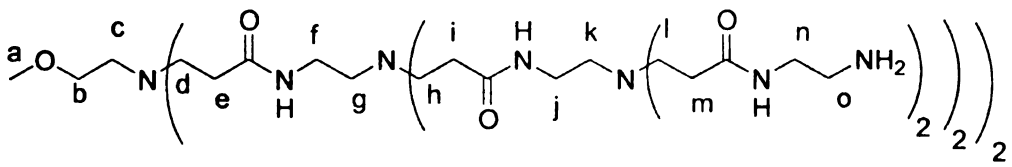

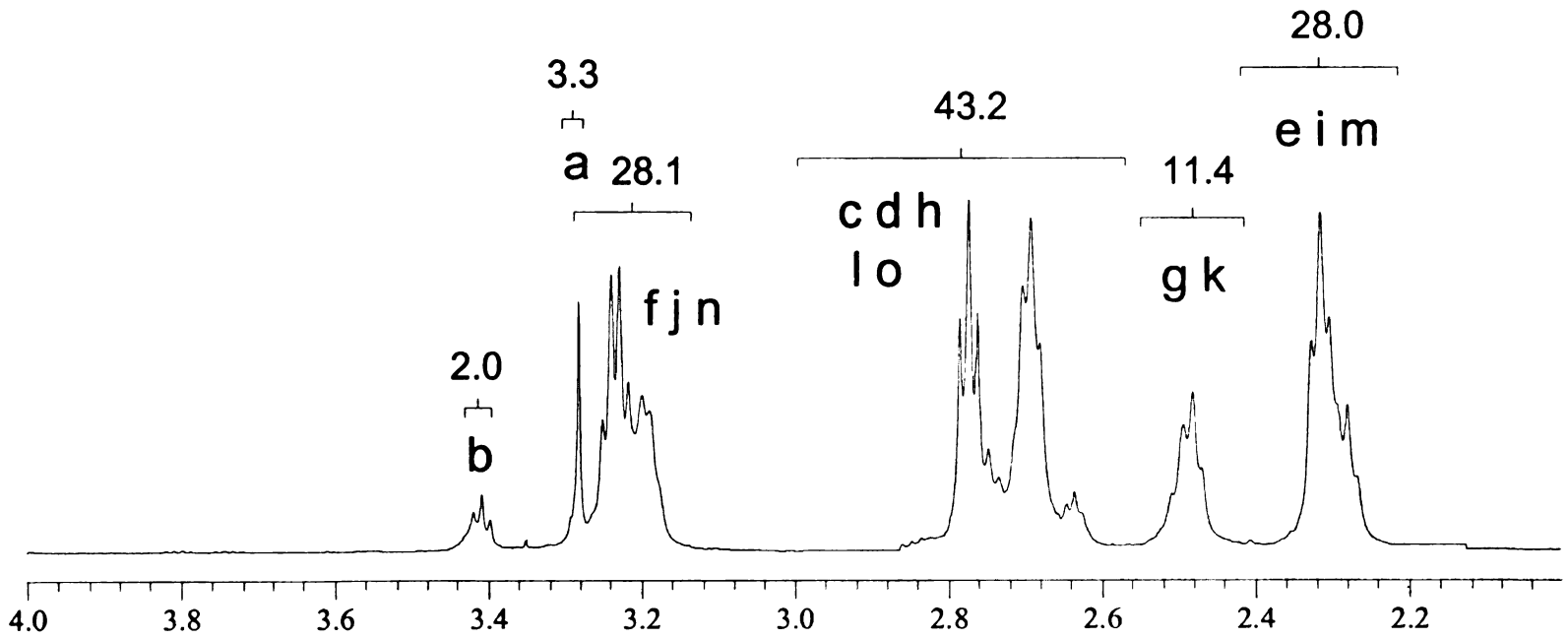

Figure A.11. ^1H NMR MEA G3.0

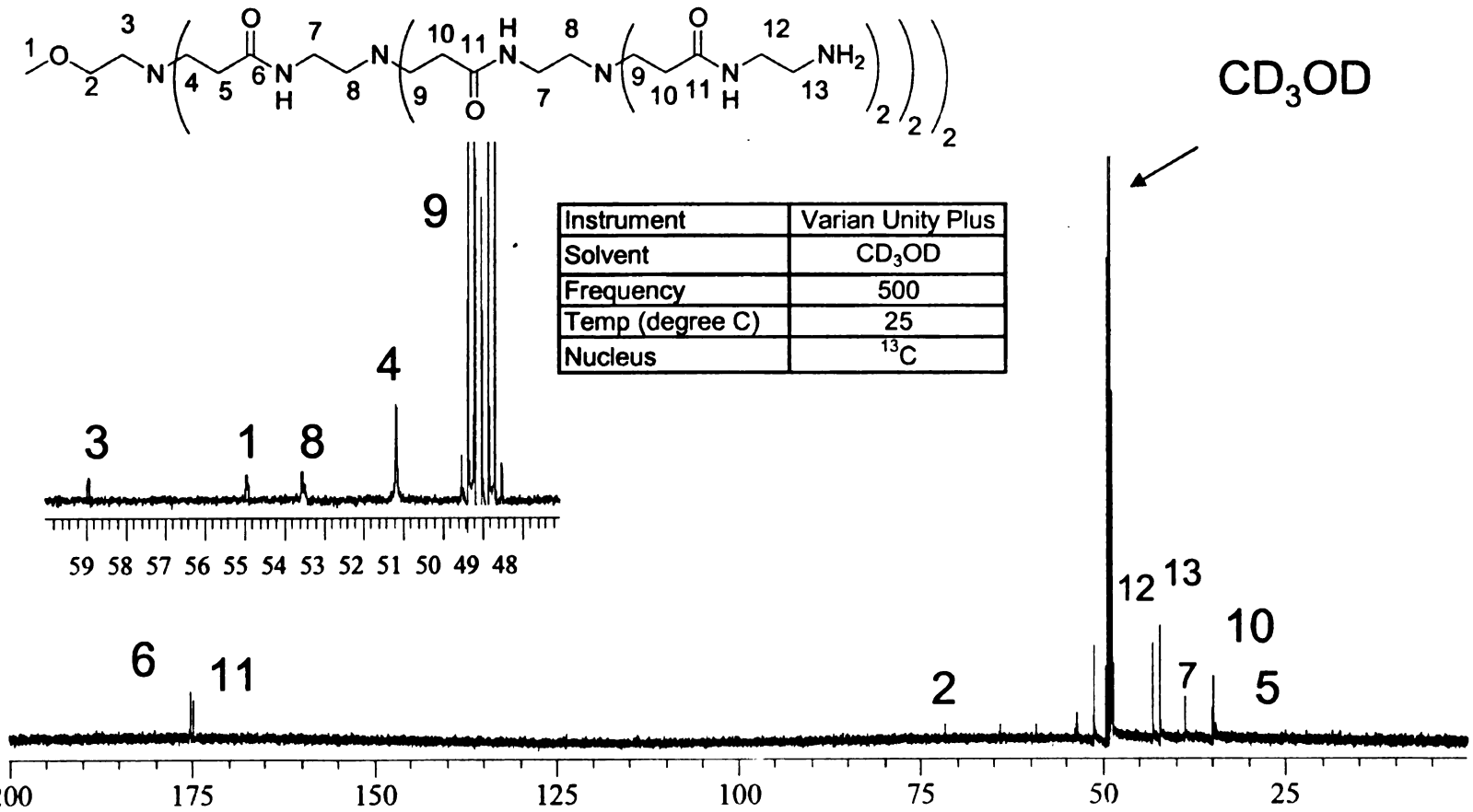

Figure A.12. ^{13}C NMR MEA G3.0

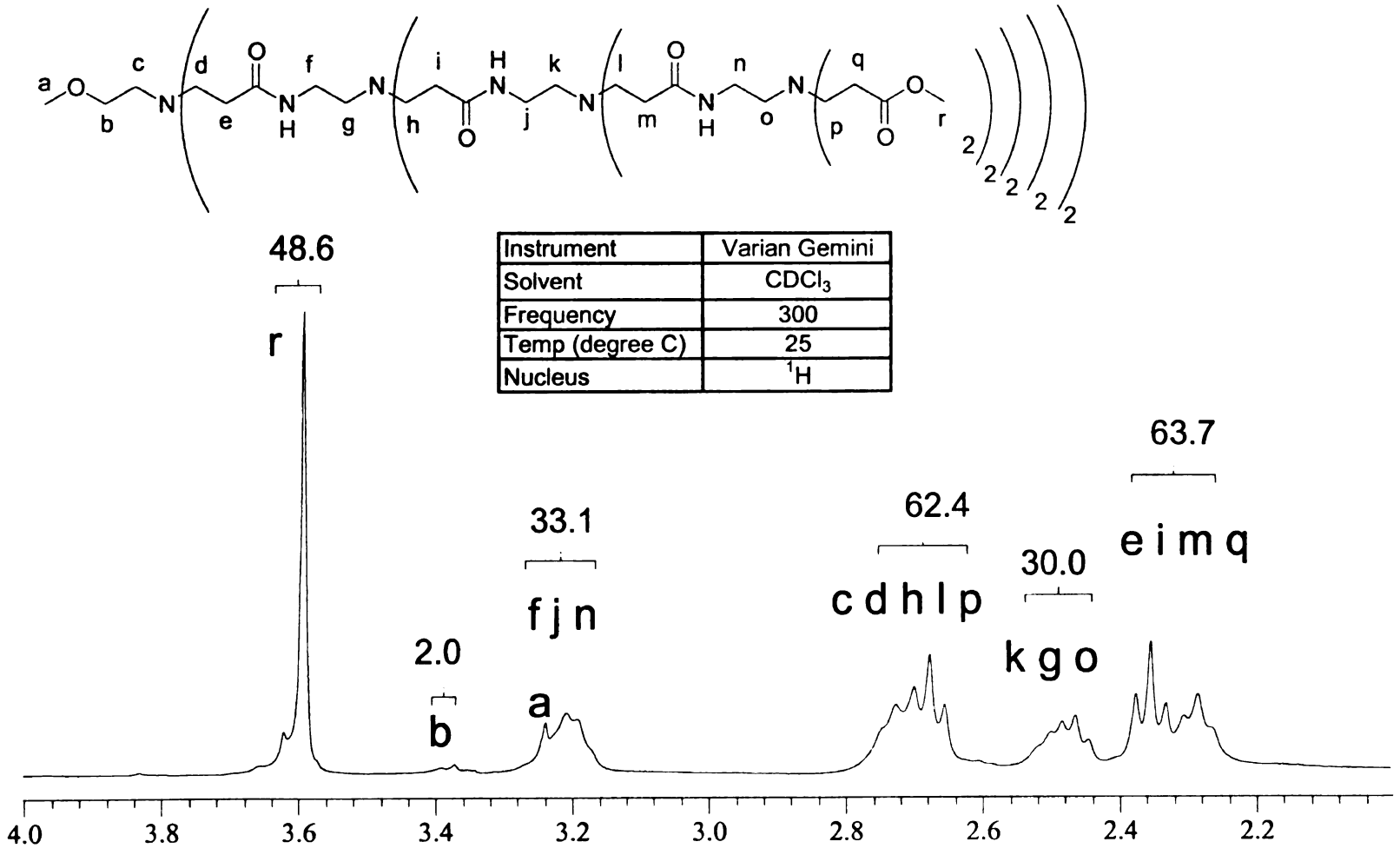

Instrument	Varian Gemini
Solvent	$CDCl_3$
Frequency	300
Temp (degree C)	25
Nucleus	^1H

Figure A.13. ^1H NMR MEA G3.5

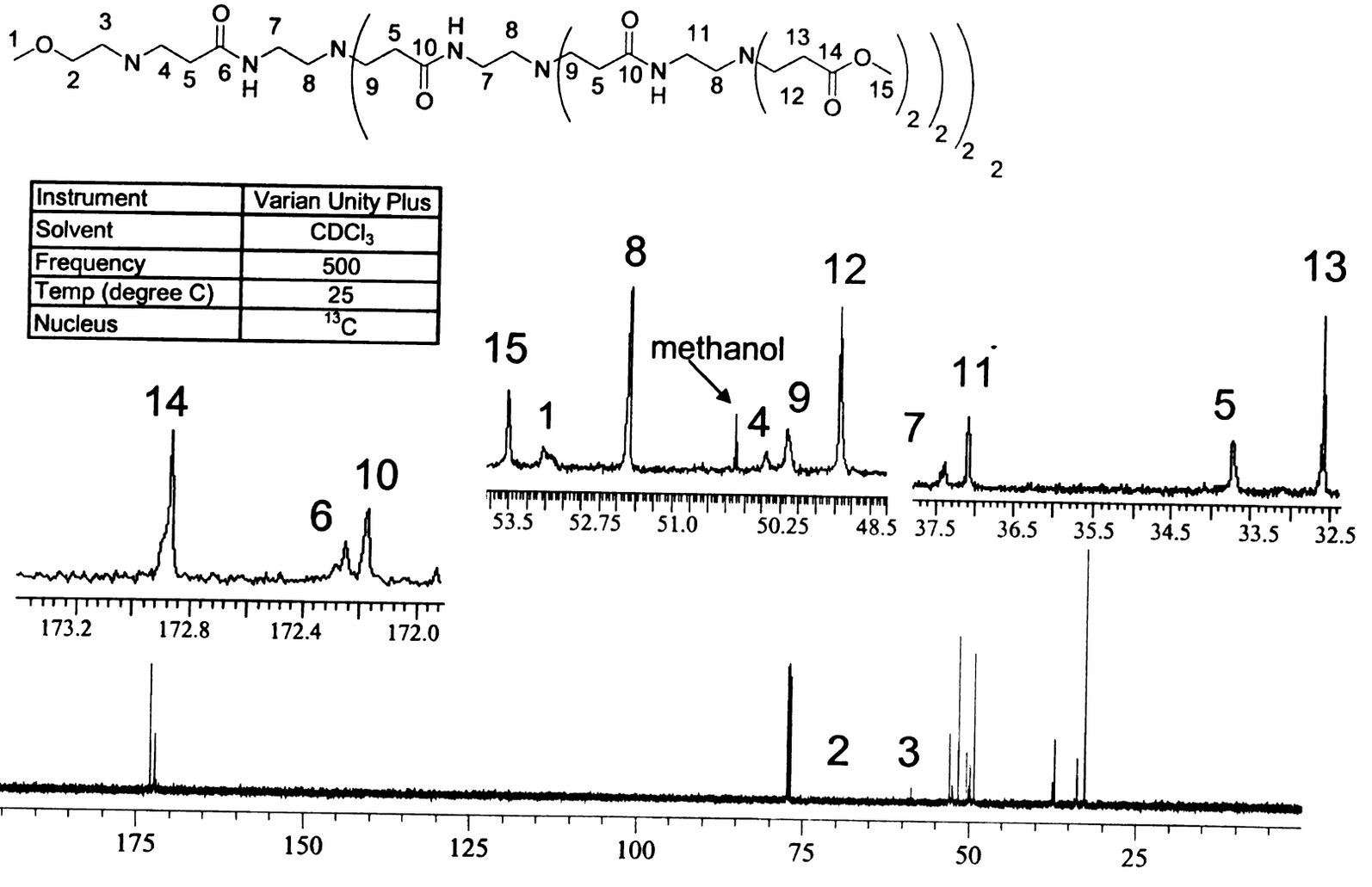

Figure A.14. ^{13}C NMR MEA G3.5

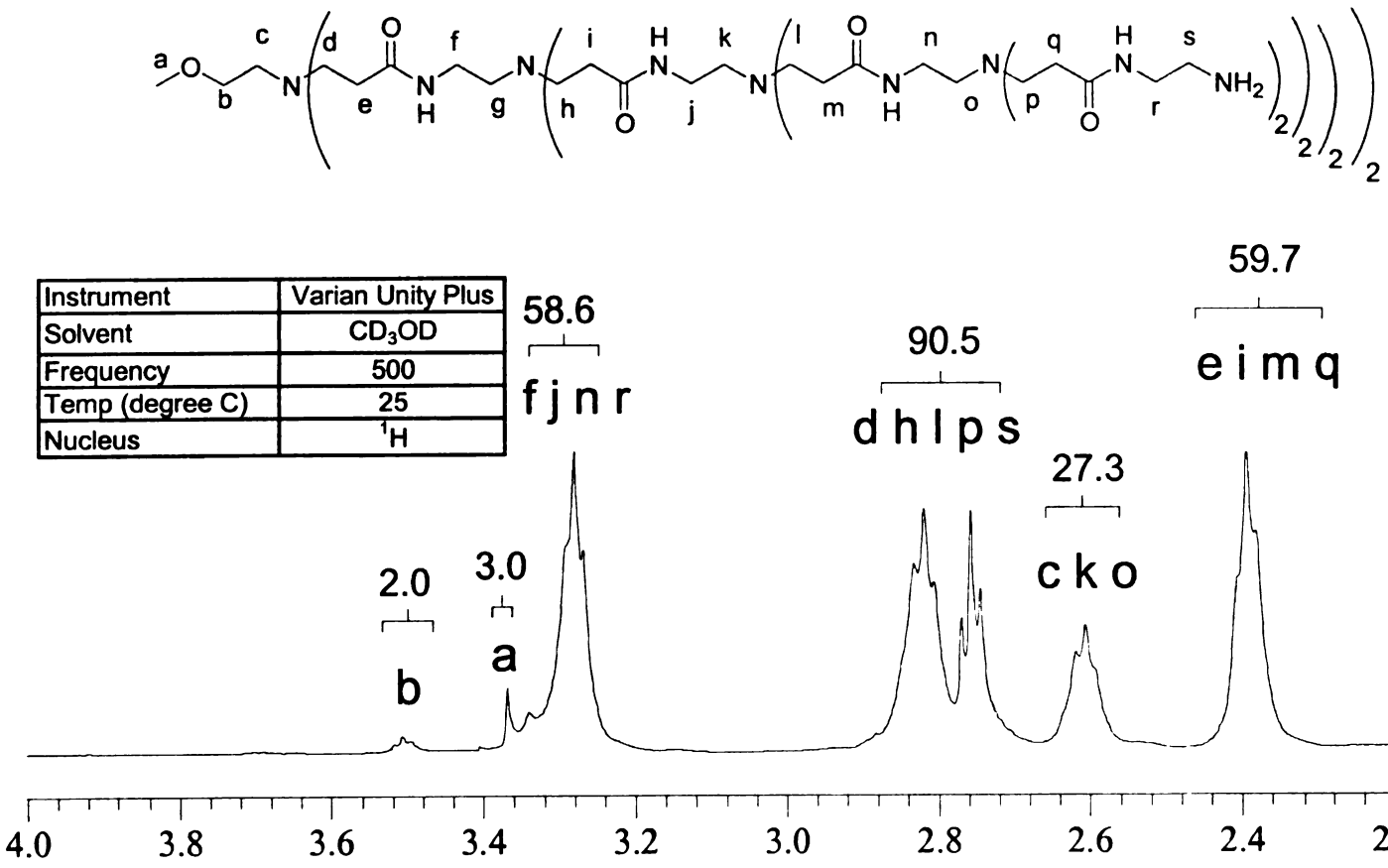

Figure A.15. ^{1}H NMR MEA G4.0

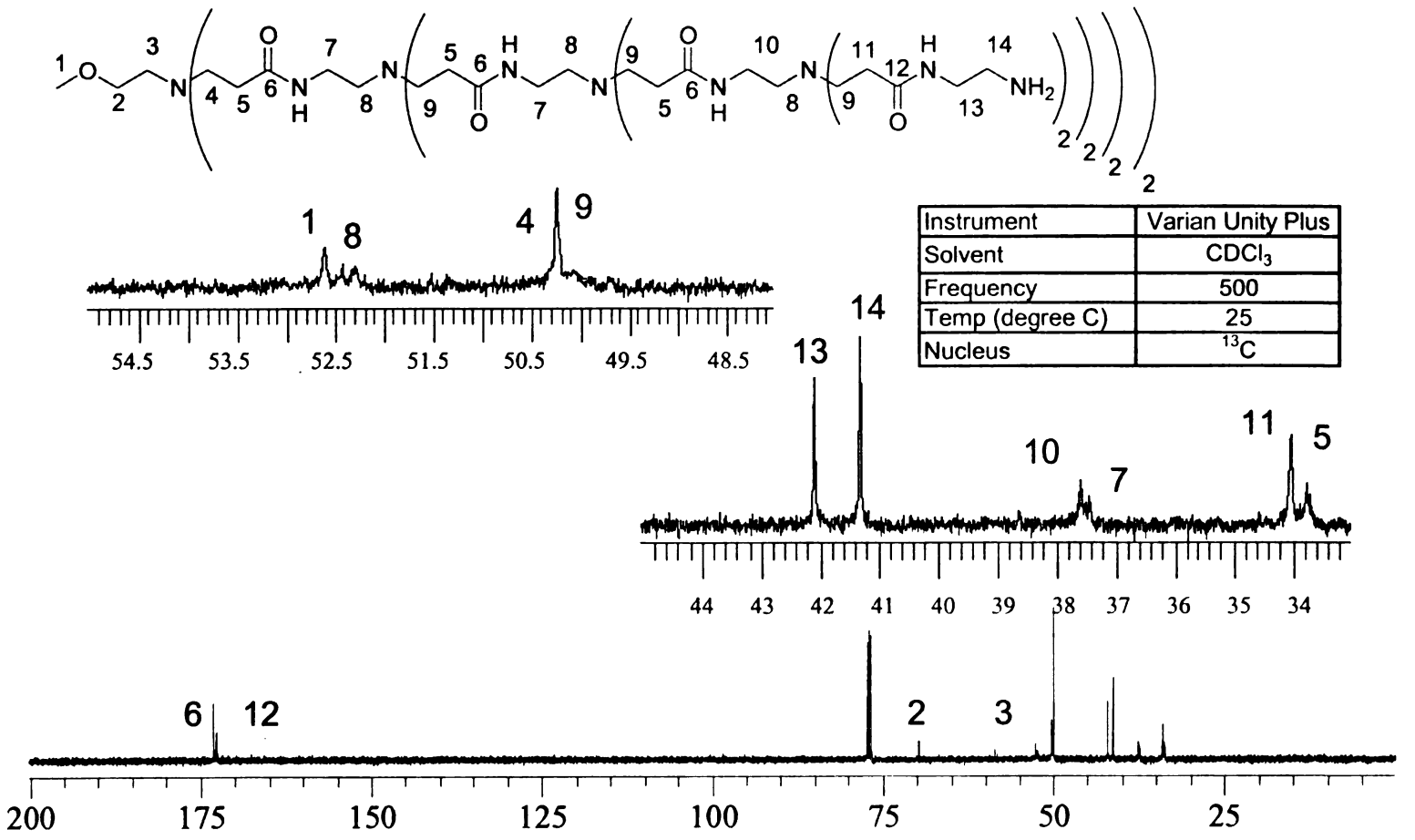

Figure A.16. ^{13}C NMR MEA G4.0

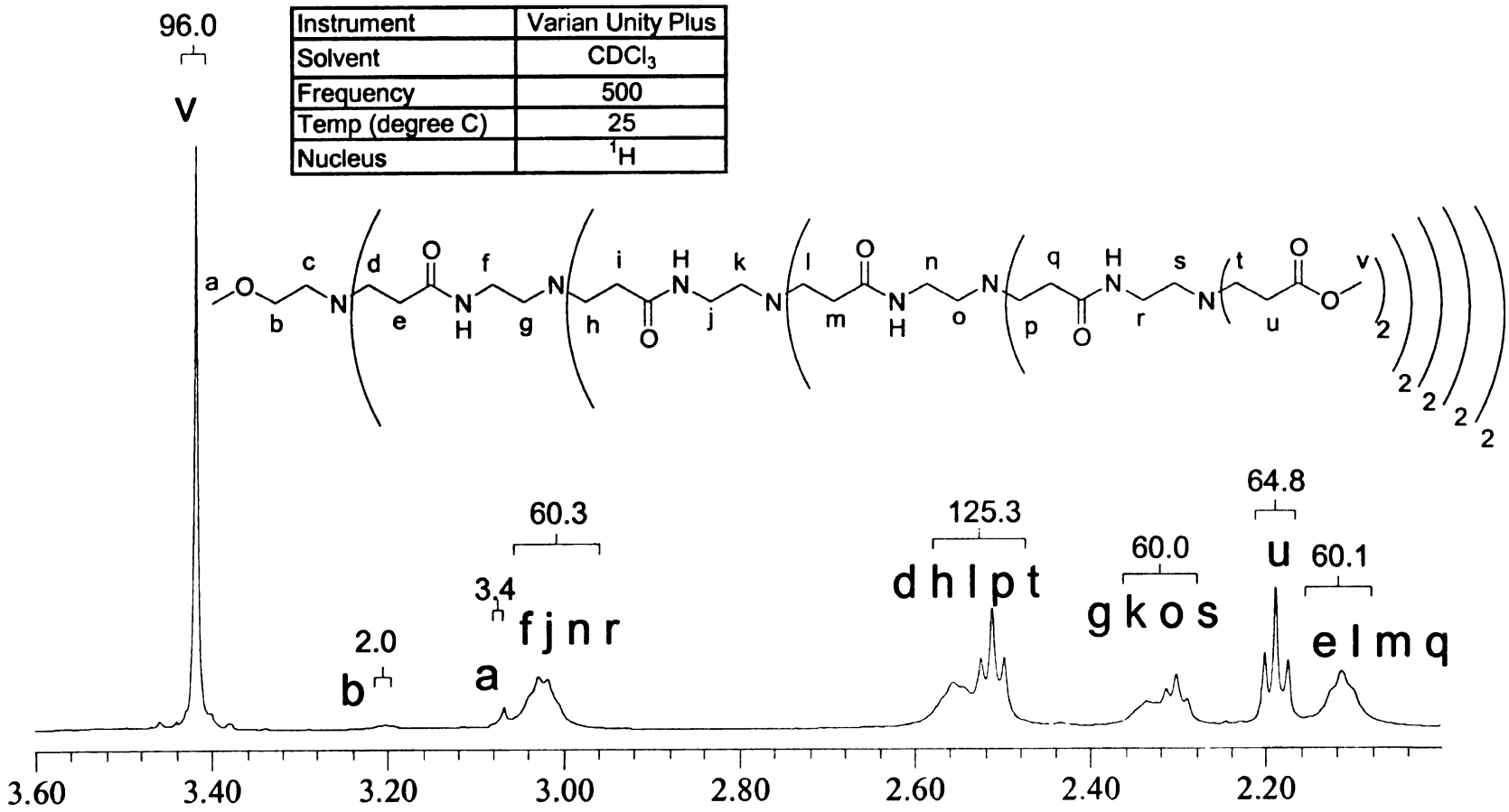

Figure A.17. ^{1}H NMR MEA G4.5

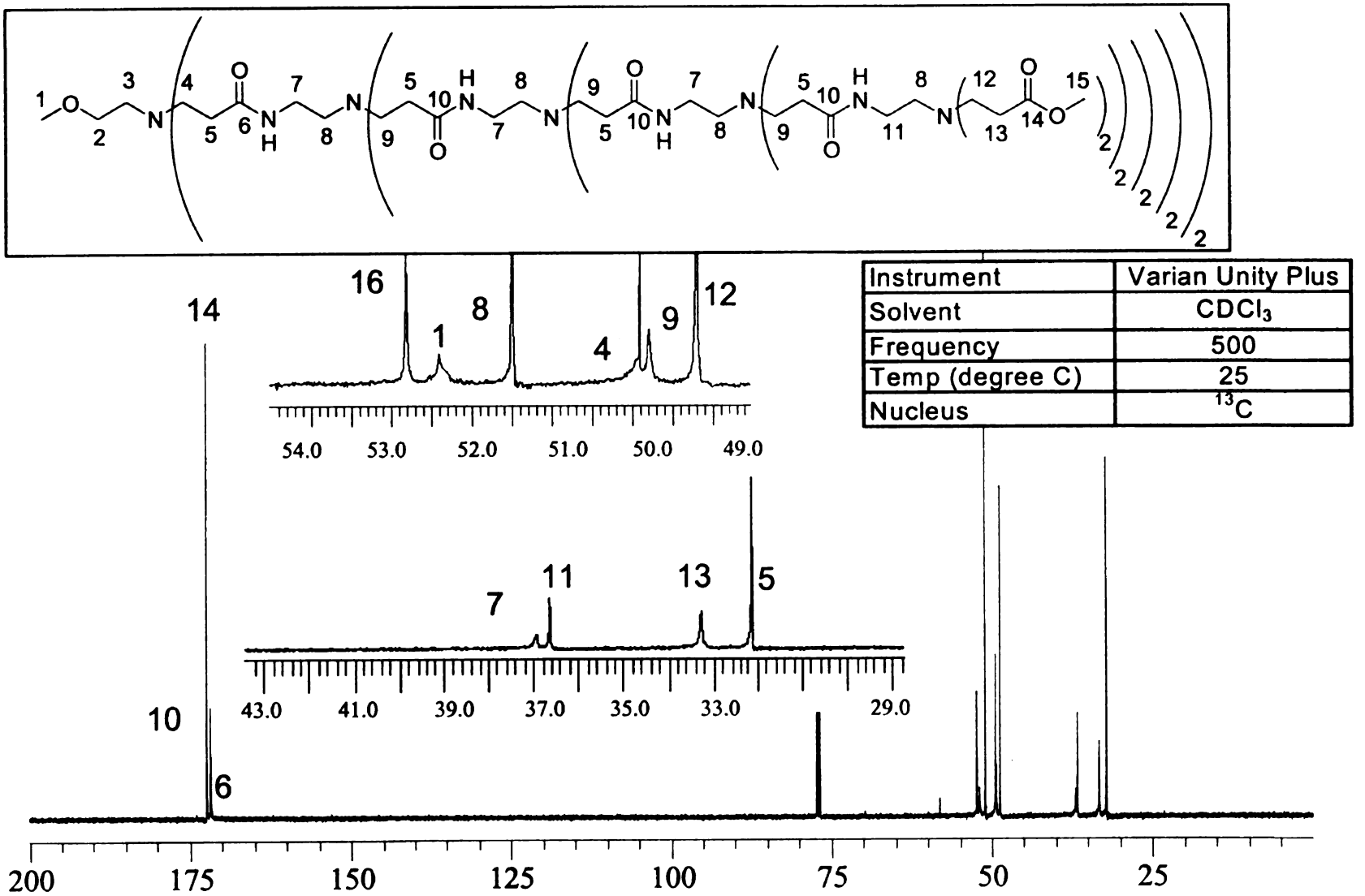

Figure A.18. ^{13}C NMR MEA G4.5

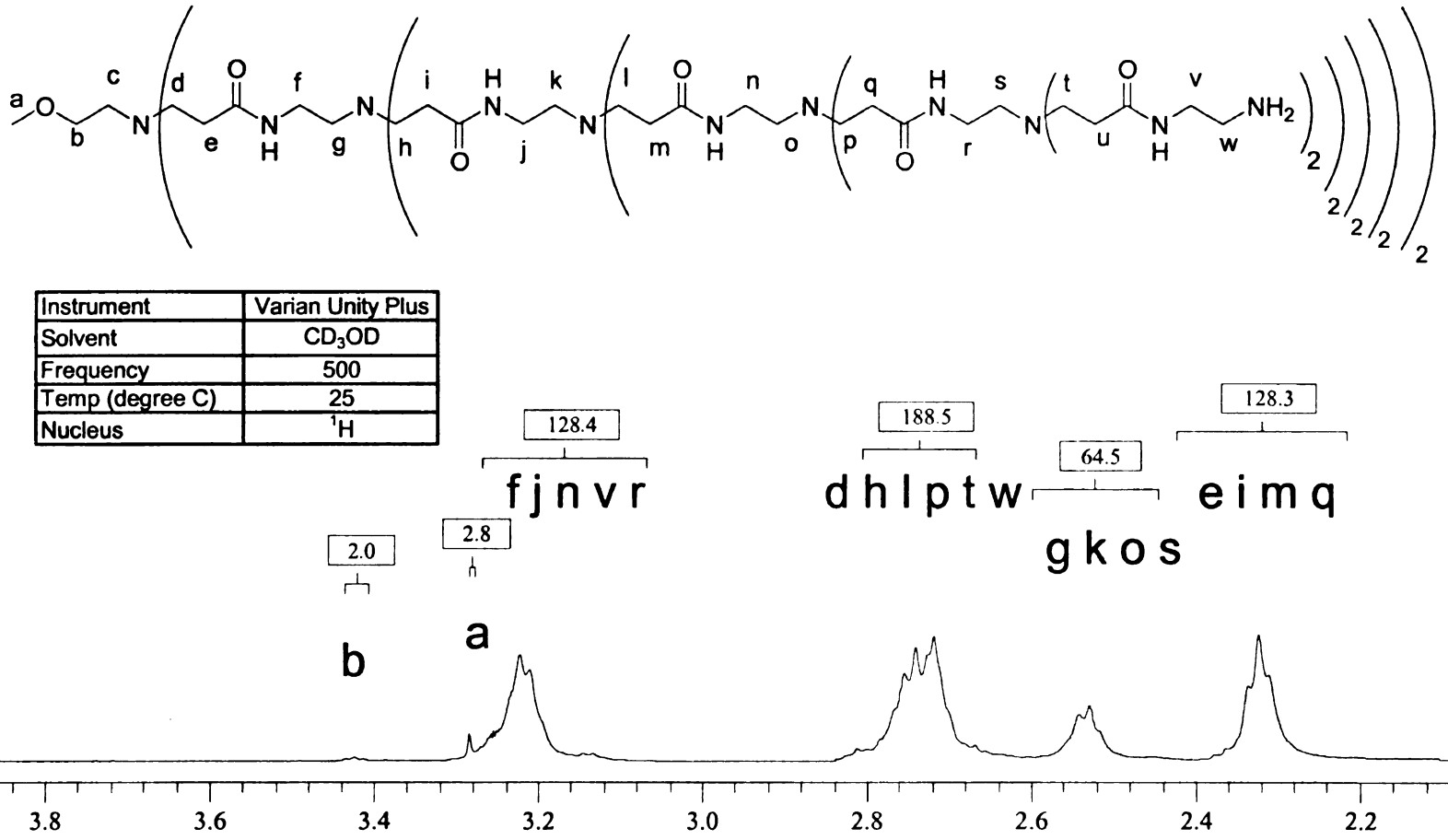

Figure A.19. ^{1}H NMR MEA G5.0

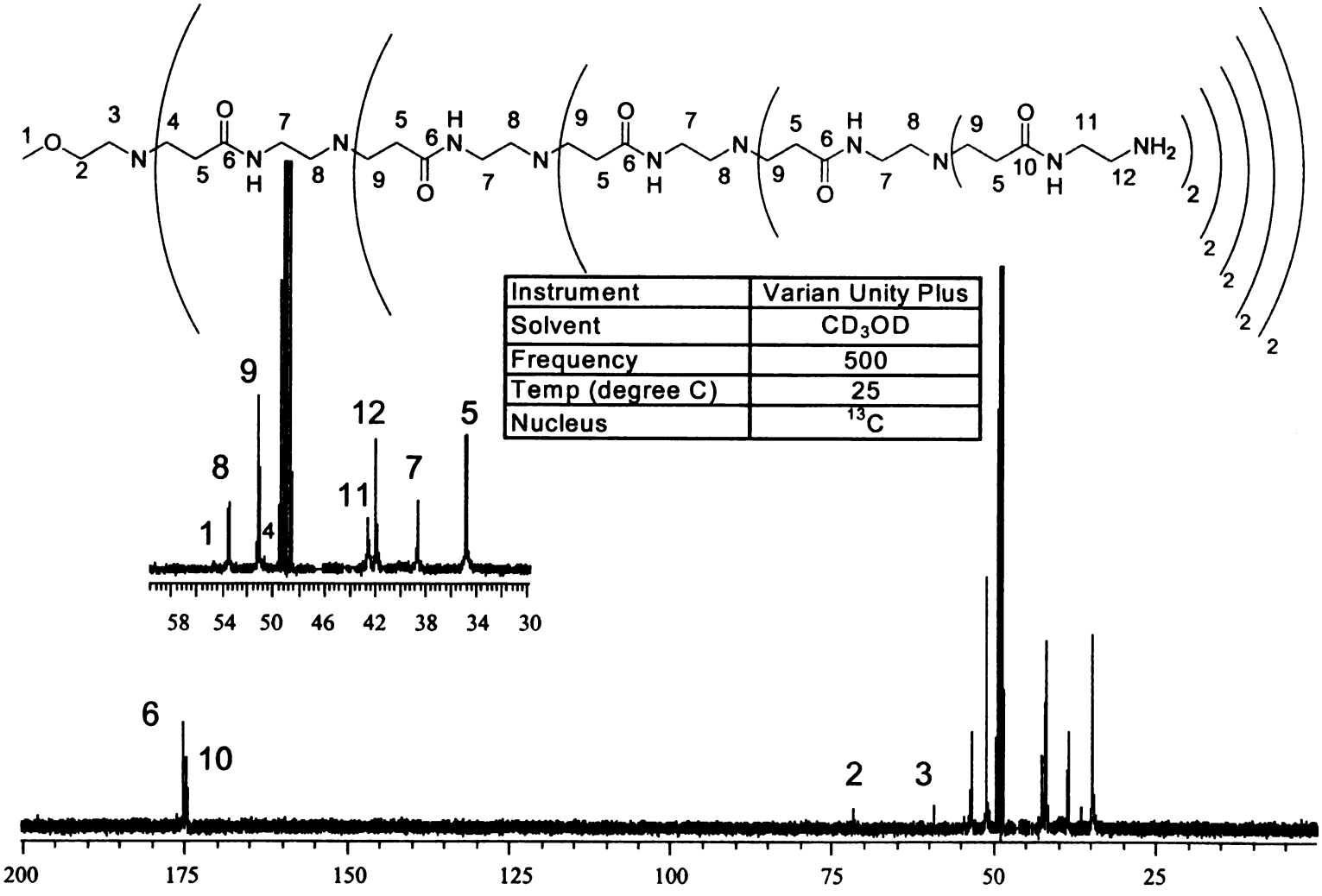

Figure A.20. ^{13}C NMR MEA G5.0

APPENDIX B

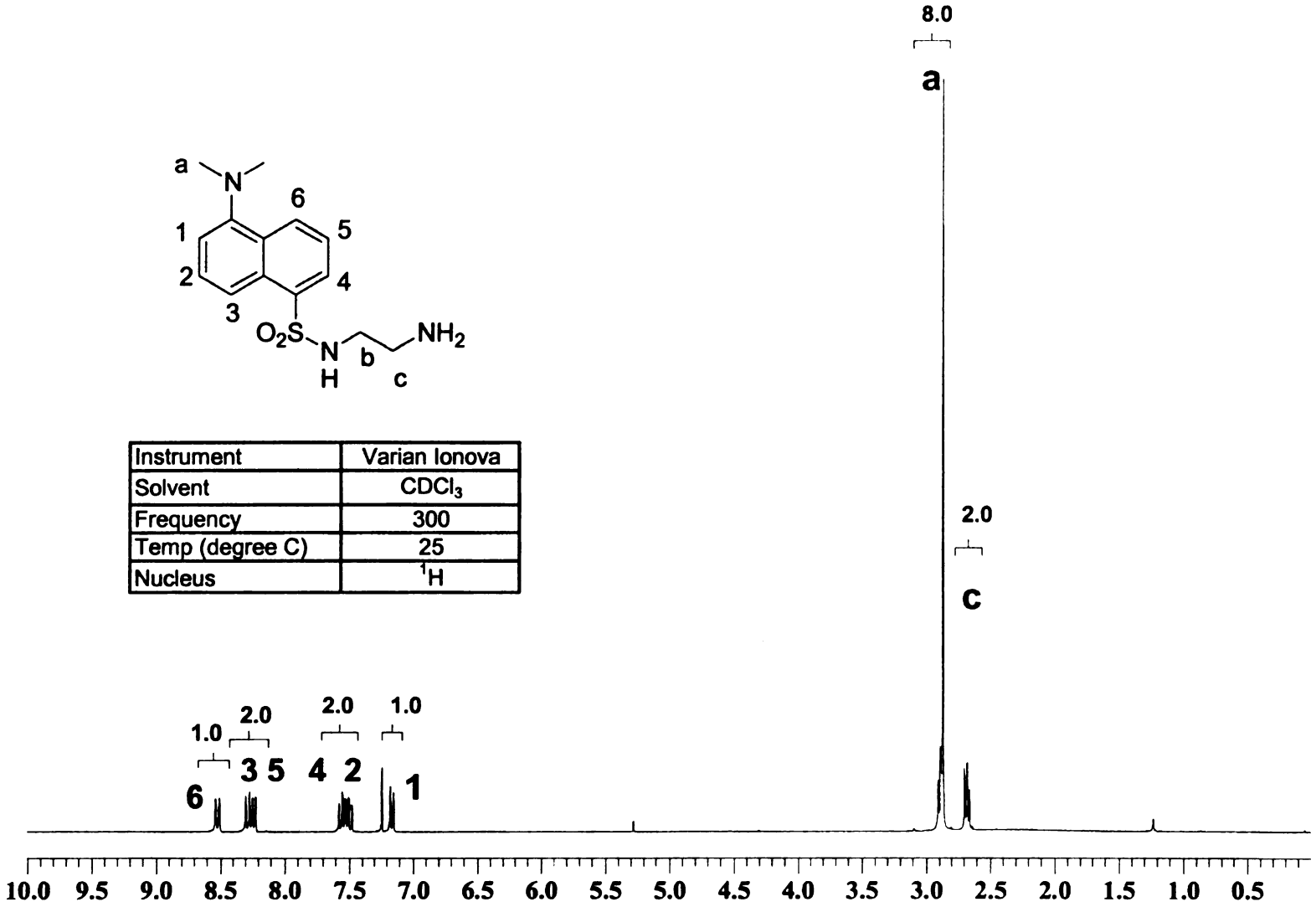

Instrument	Varian Ionova
Solvent	$CDCl_3$
Frequency	300
Temp (degree C)	25
Nucleus	^1H

Figure B.1. ^1H NMR Dansyl EDA

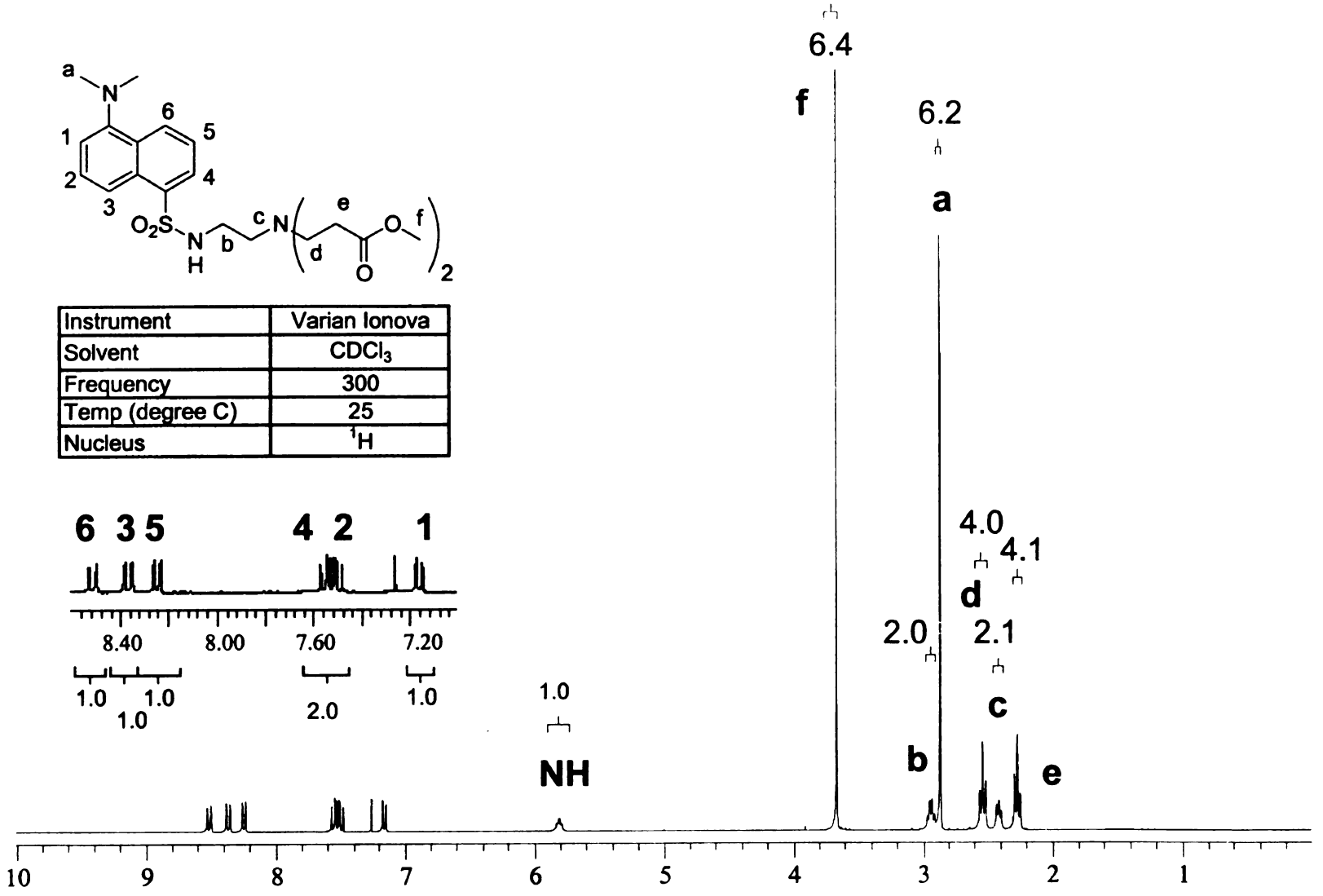

Figure B.2. ^1H NMR Dansyl G0.5

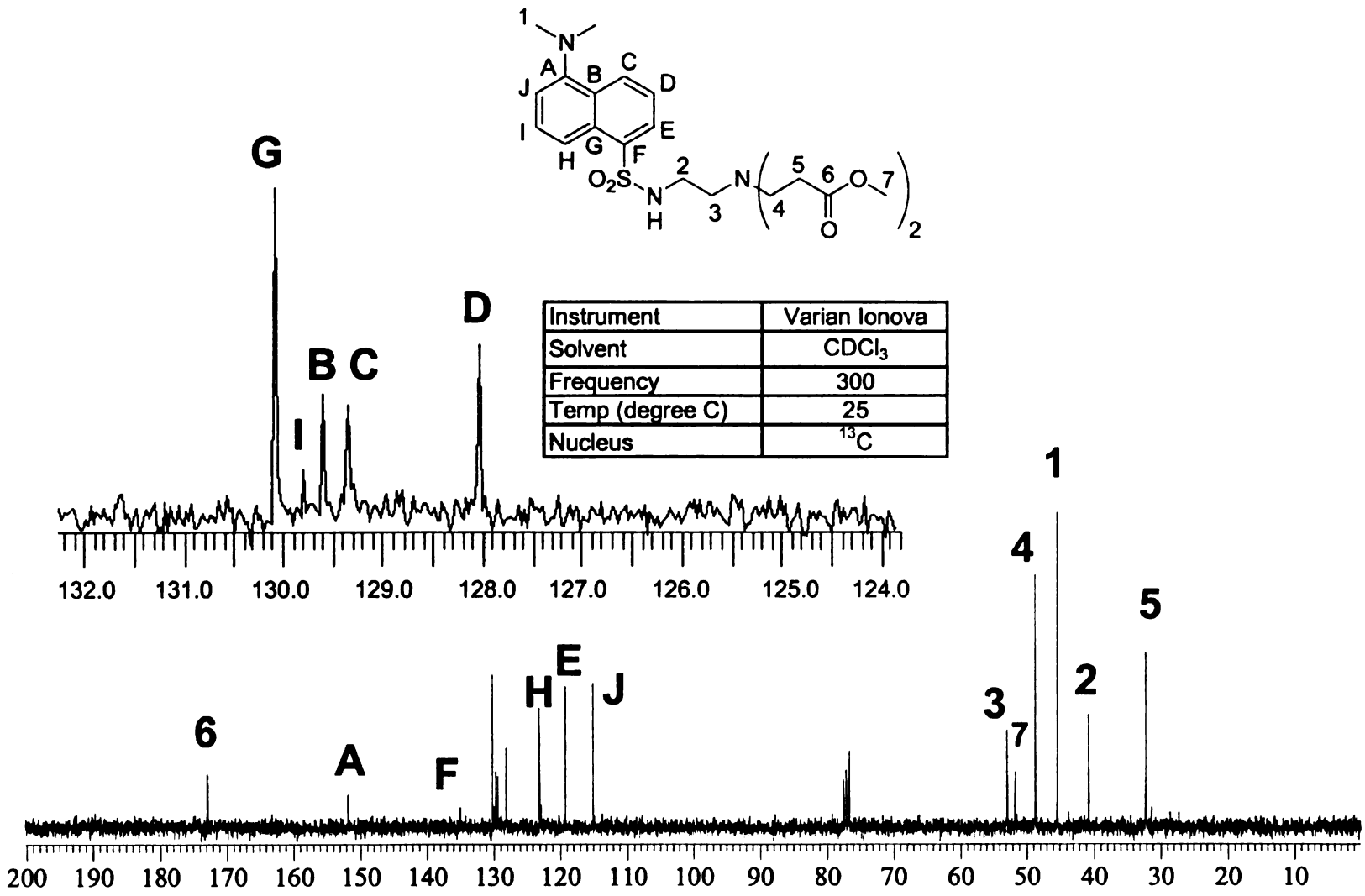

Figure B.3. ^{13}C NMR Dansyl G0.5

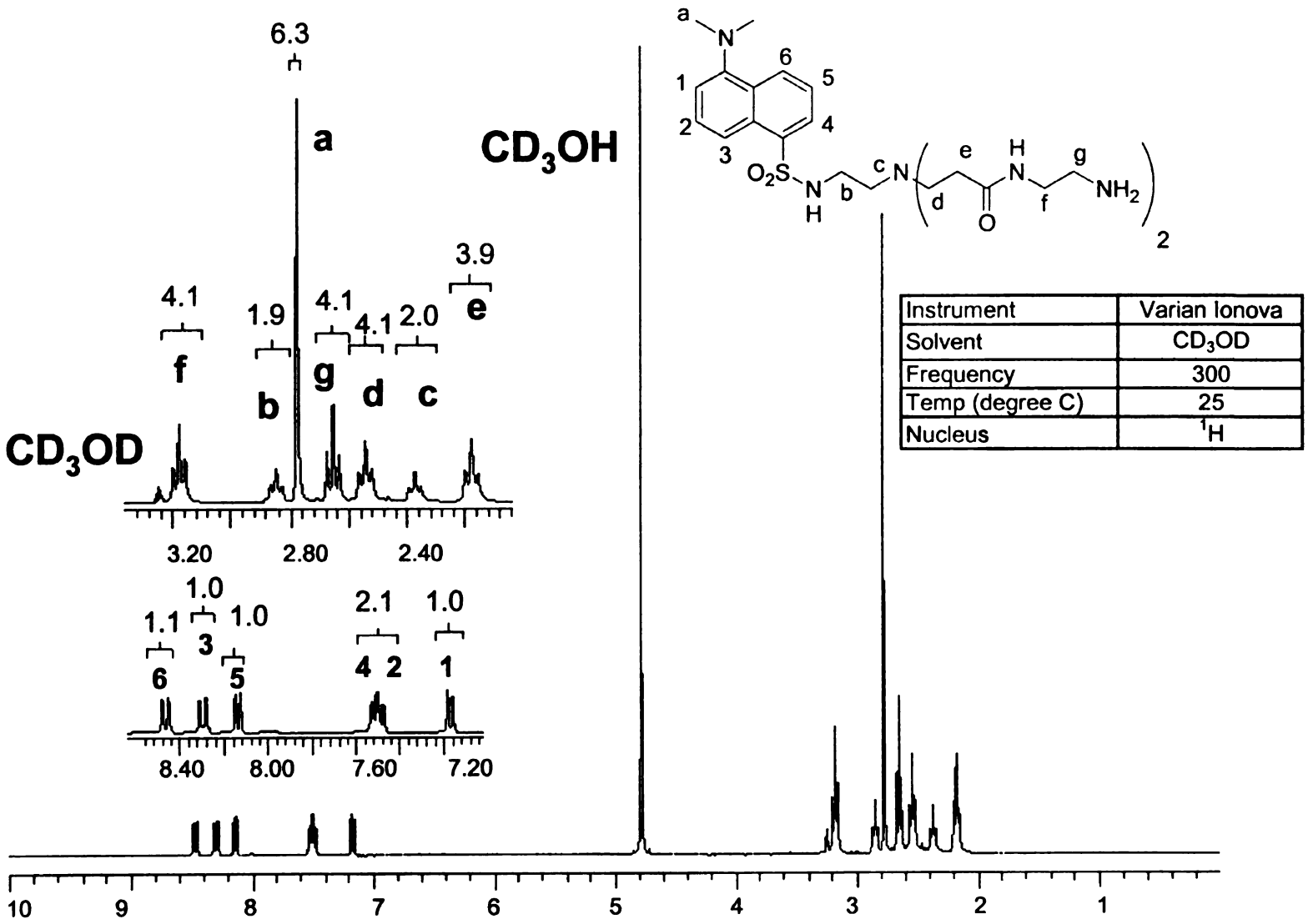

Figure B.4. ^{1}H NMR Dansyl 1.0

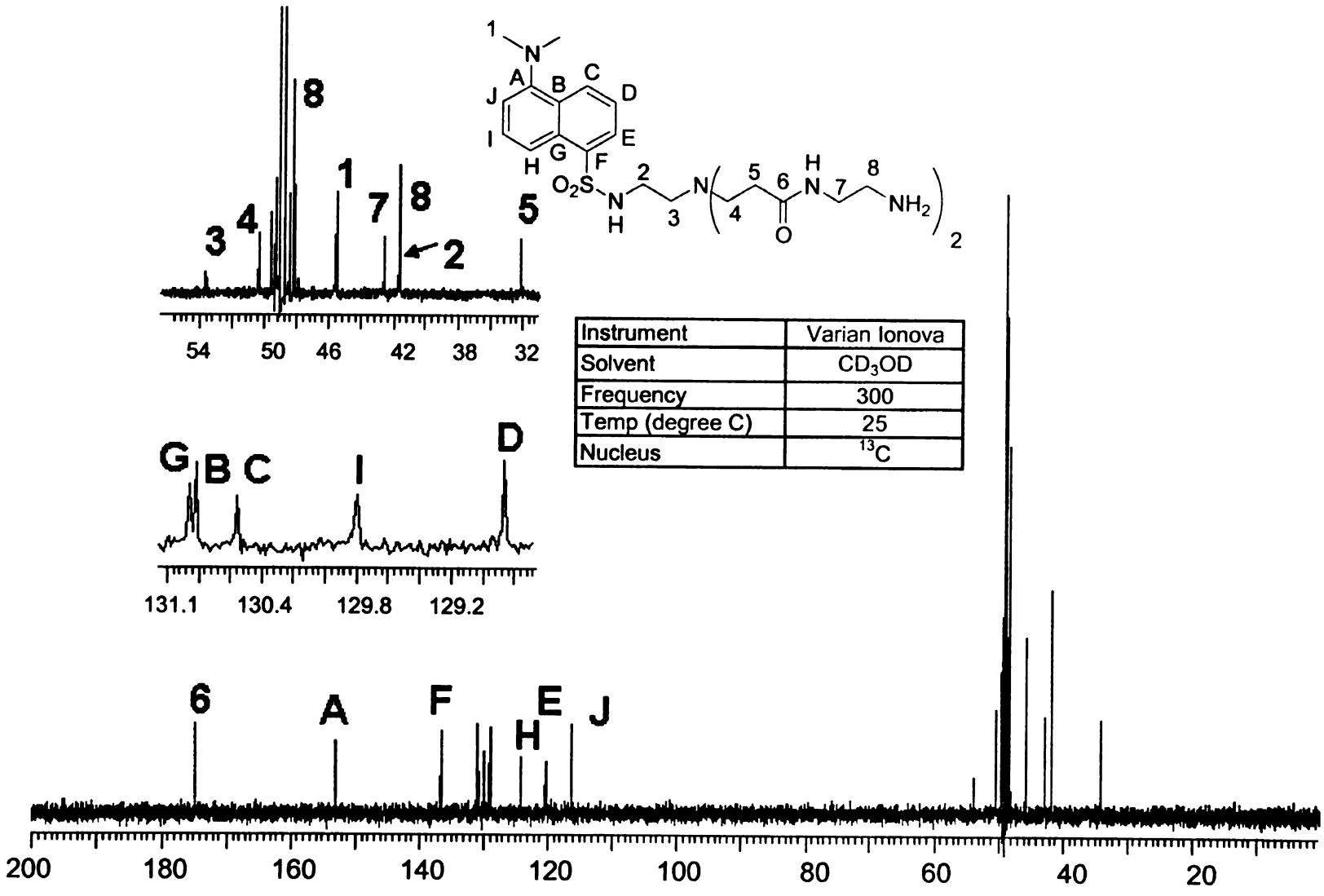

Figure B.5. ^{13}C NMR Dansyl G1.0

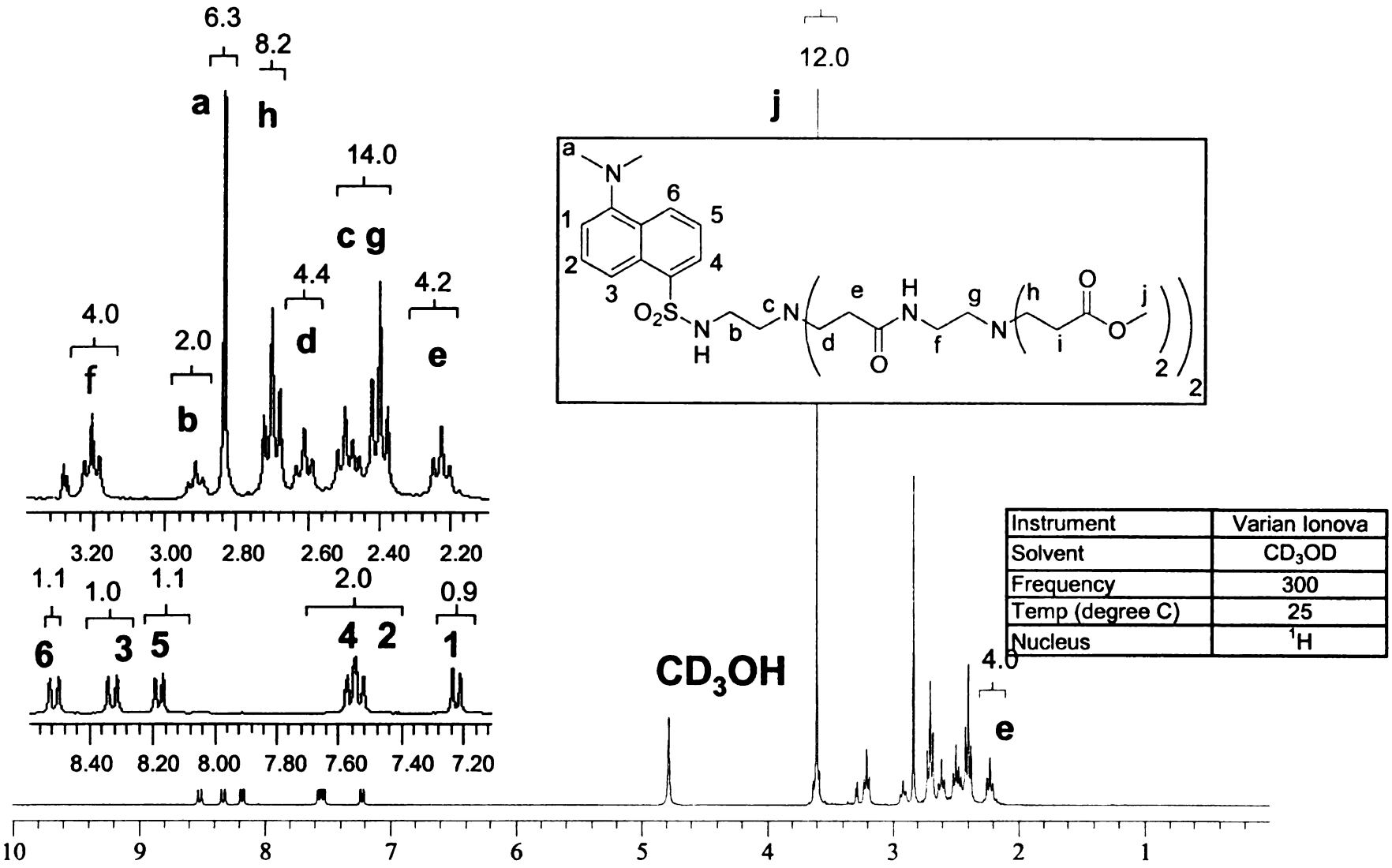

Figure B.6. ^{1}H NMR Dansyl G1.5

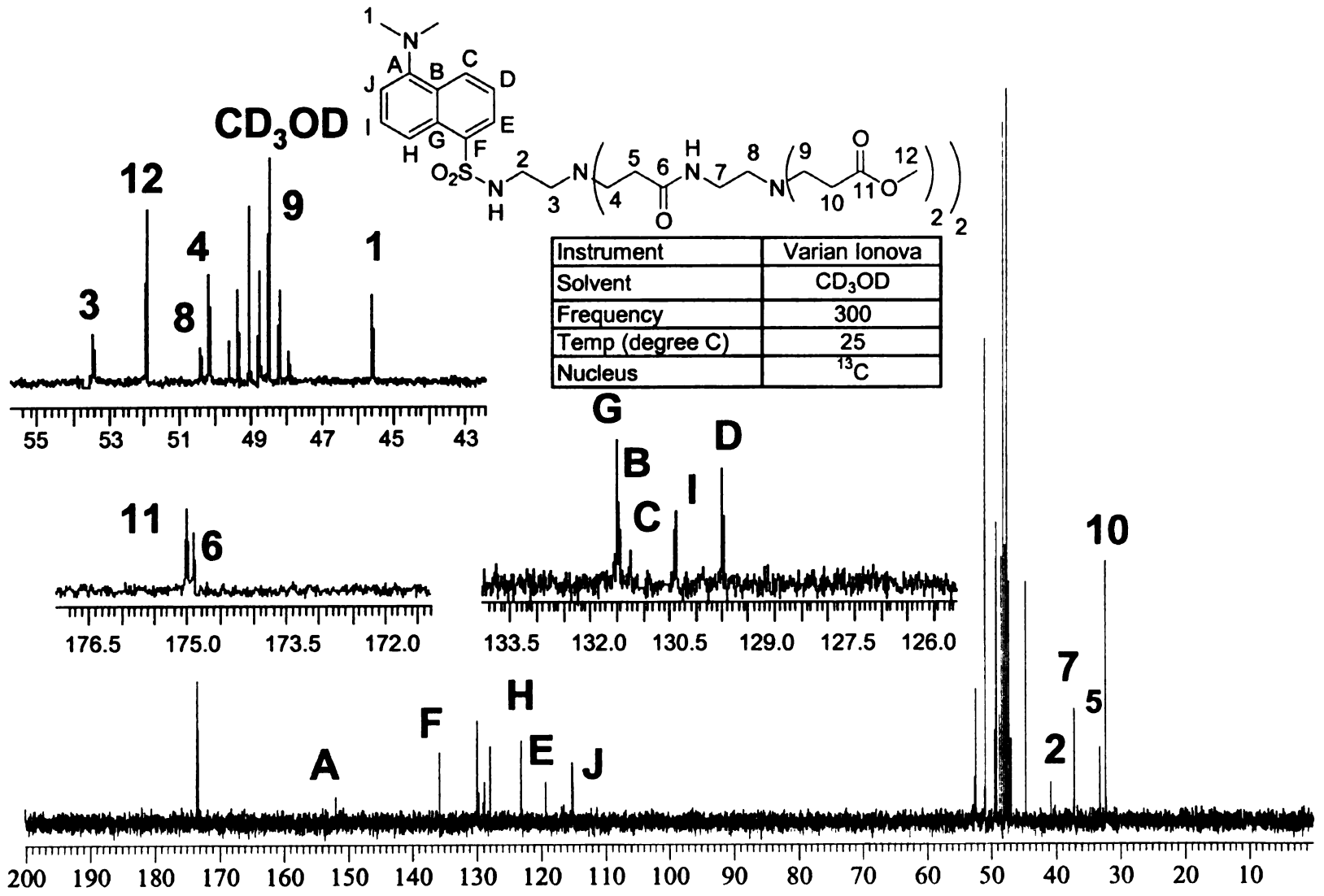

Figure B.7. ^{13}C NMR Dansyl G1.5

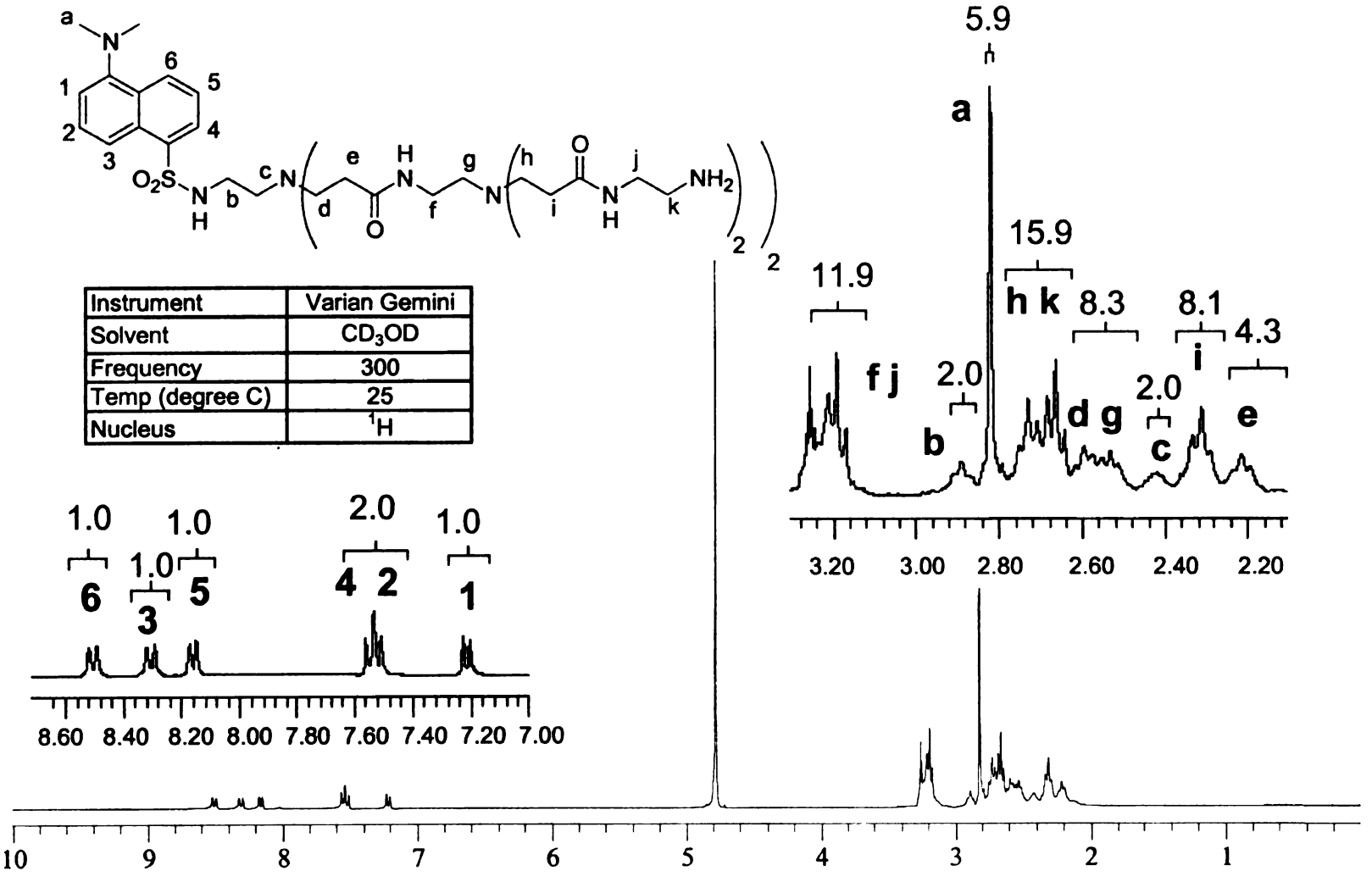

Figure B.8. ^{1}H NMR Dansyl G2.0

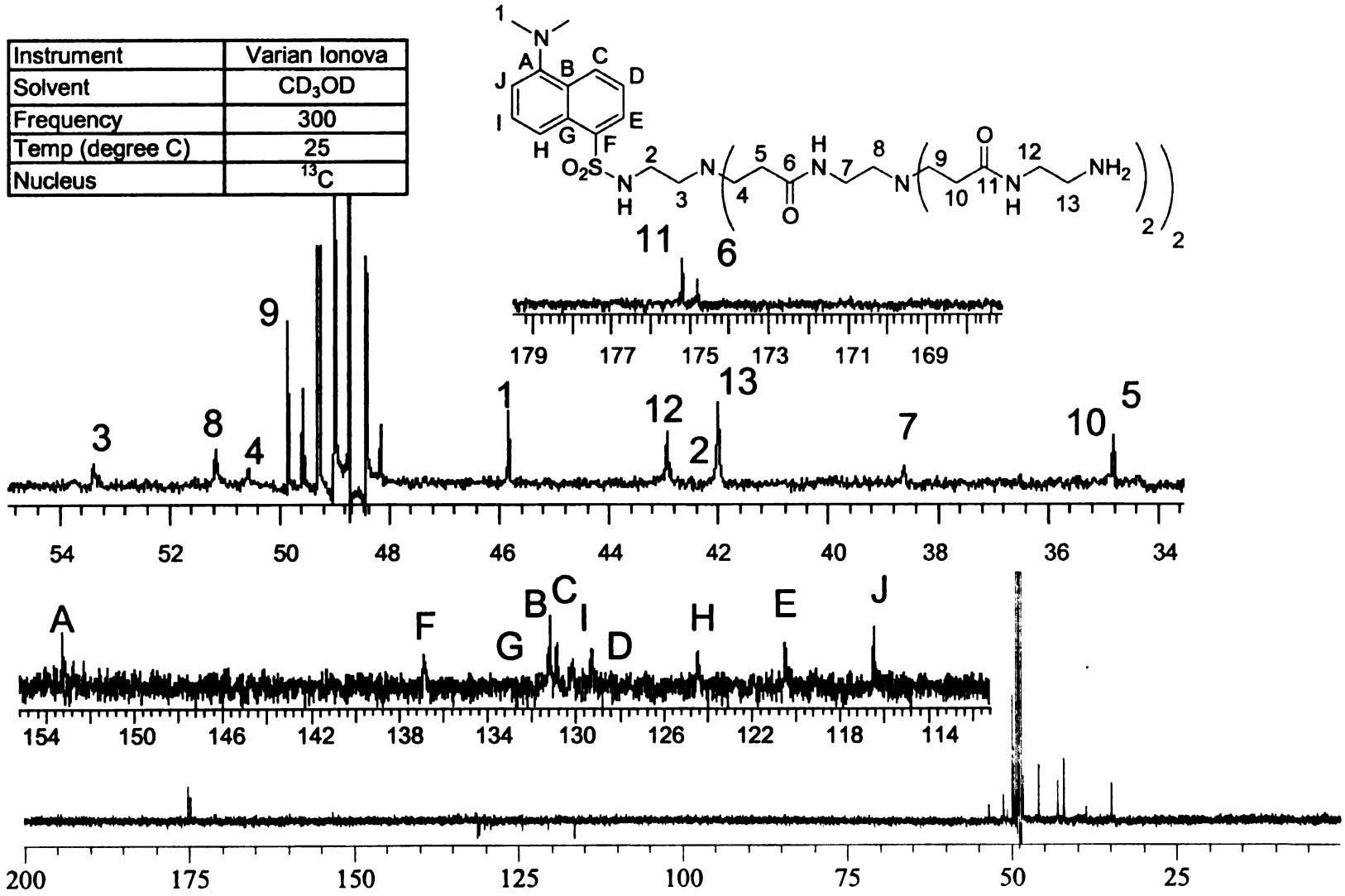

Figure B.9. ^{13}C NMR Dansyl G2.0

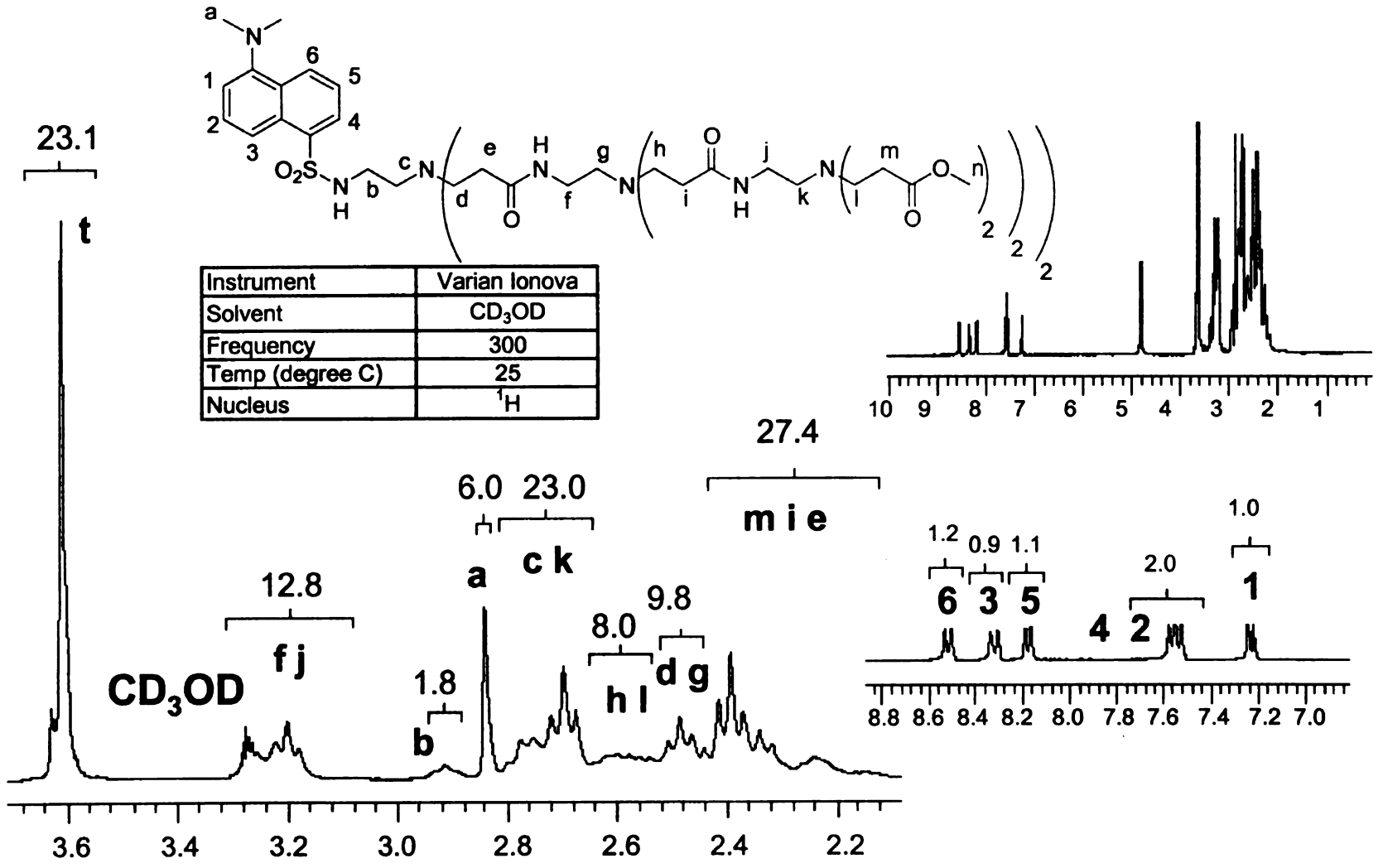

Figure B.10. ^{1}H NMR Dansyl G2.5

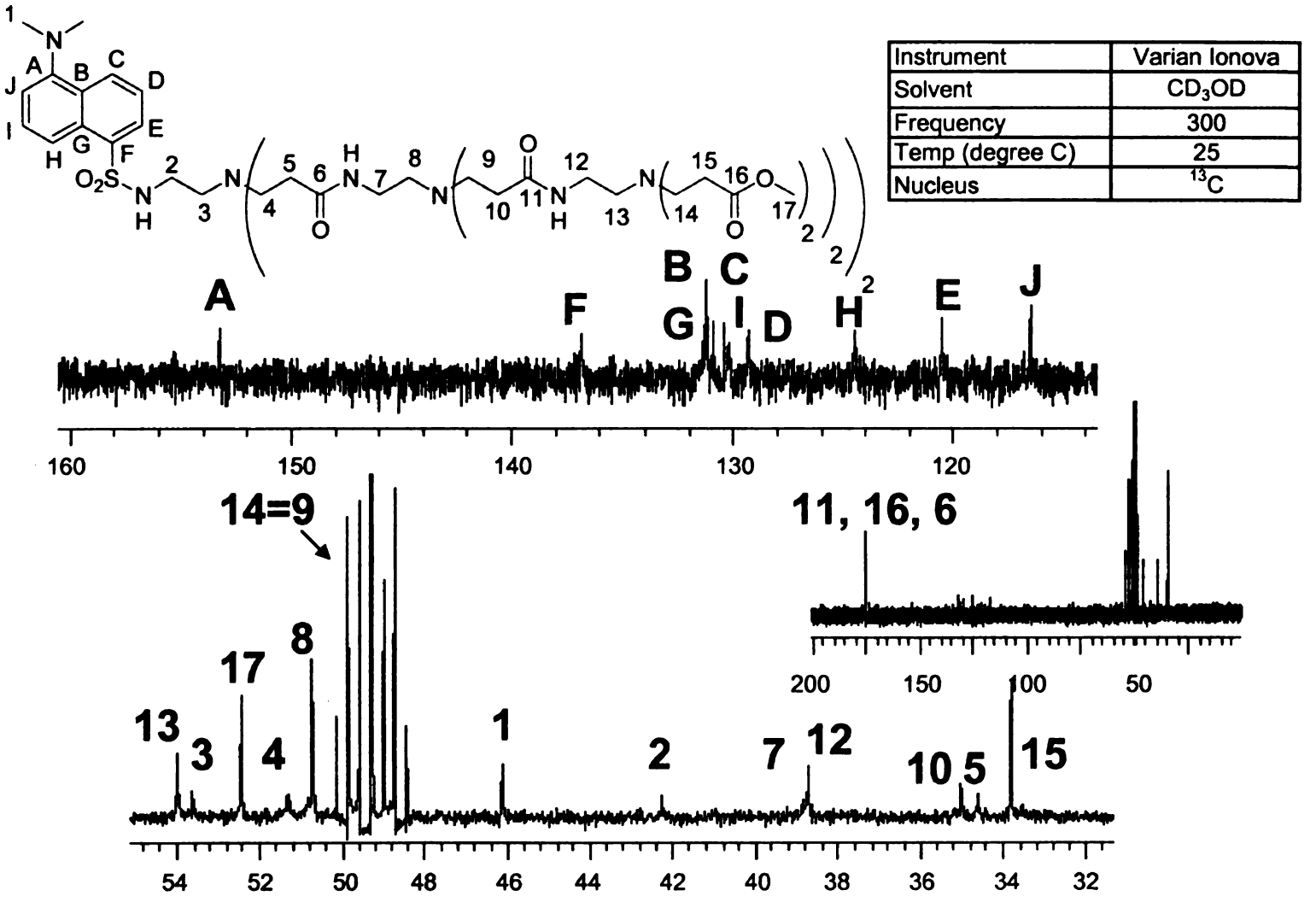

Figure B.11. ^{13}C NMR Dansyl G2.5

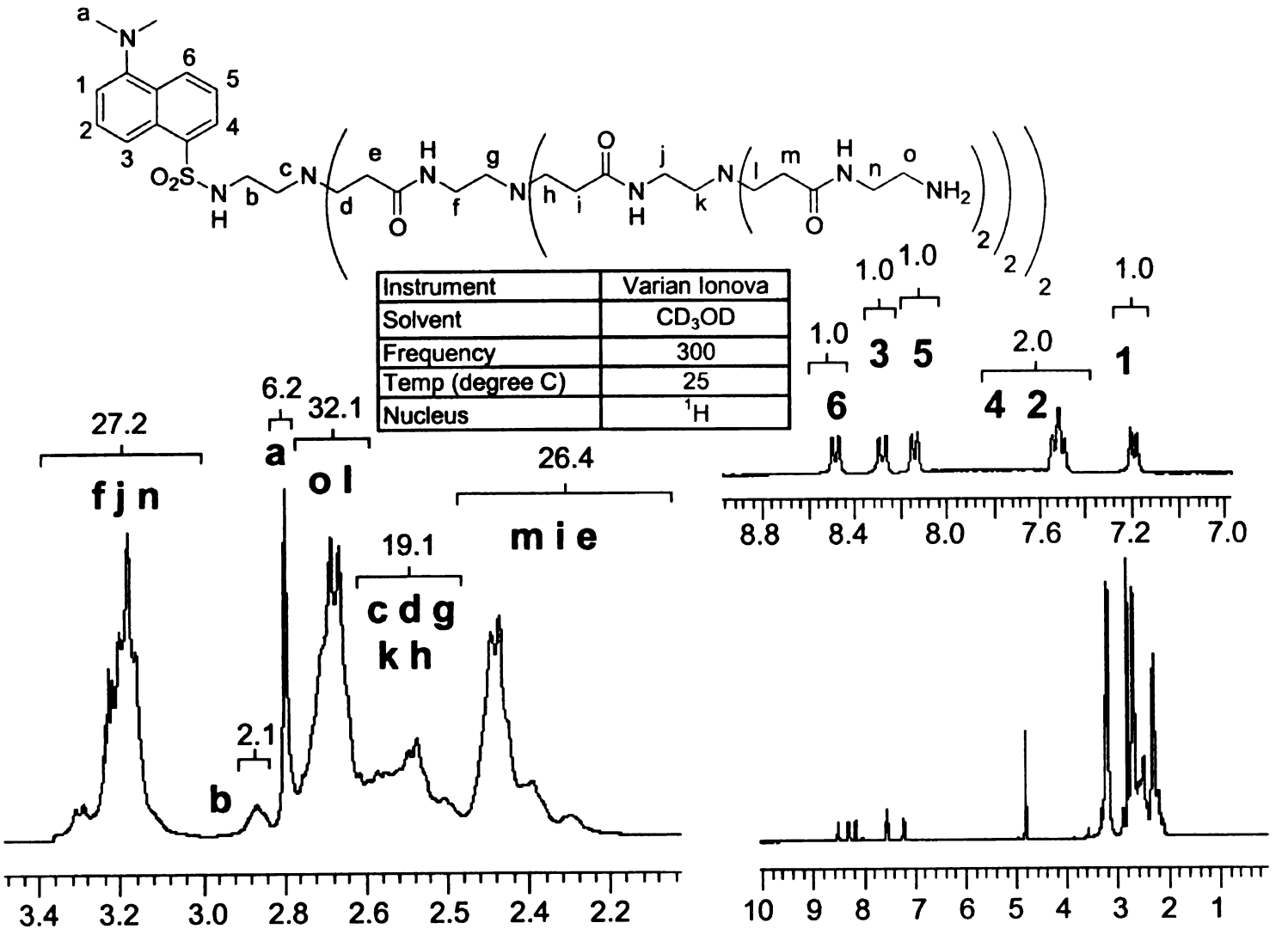

Figure B.12. ^{1}H NMR Dansyl G3.0

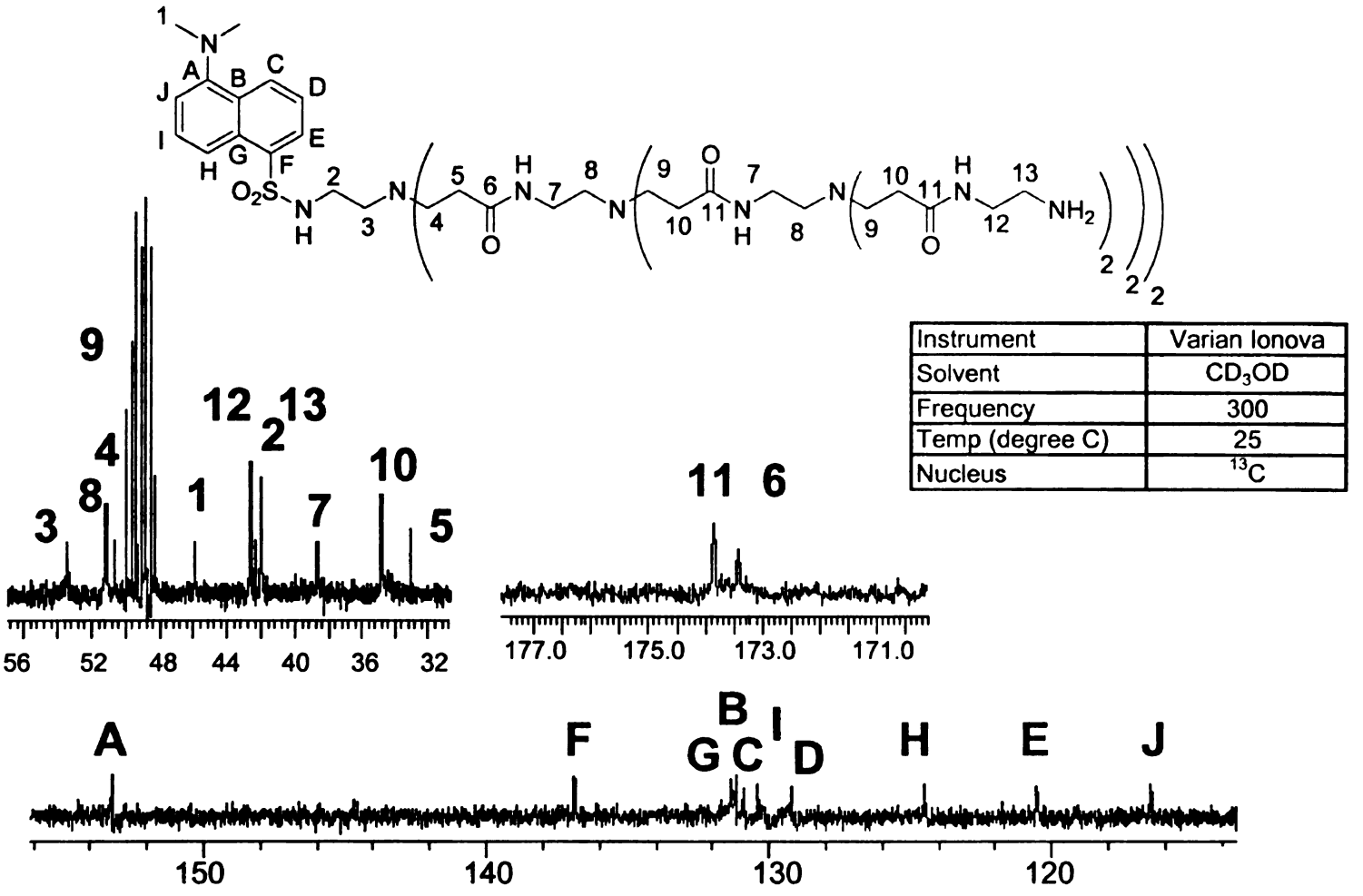

Figure B.13. ^{13}C NMR Dansyl G3.0

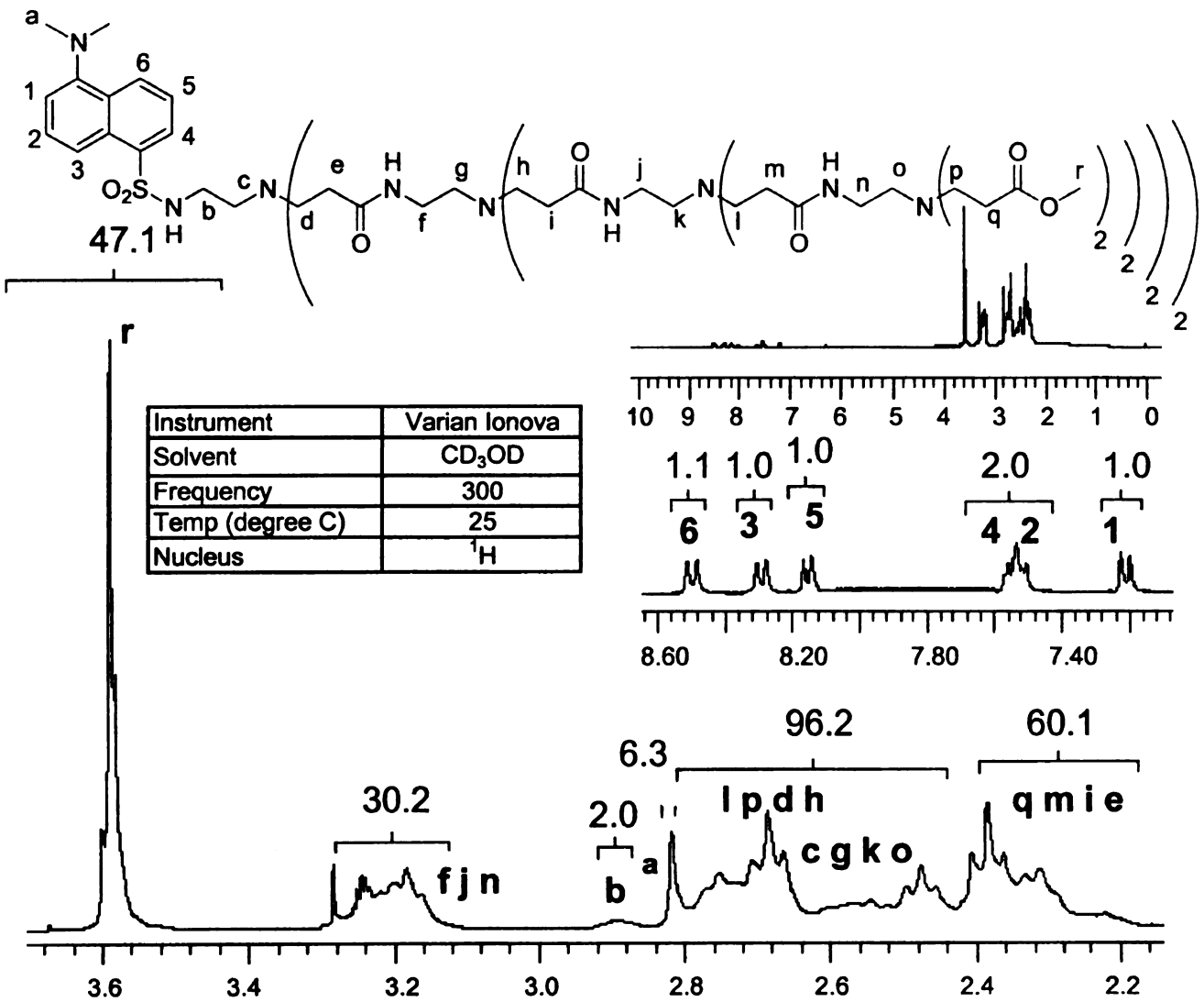

Figure B.14. ^{1}H NMR Dansyl G3.5

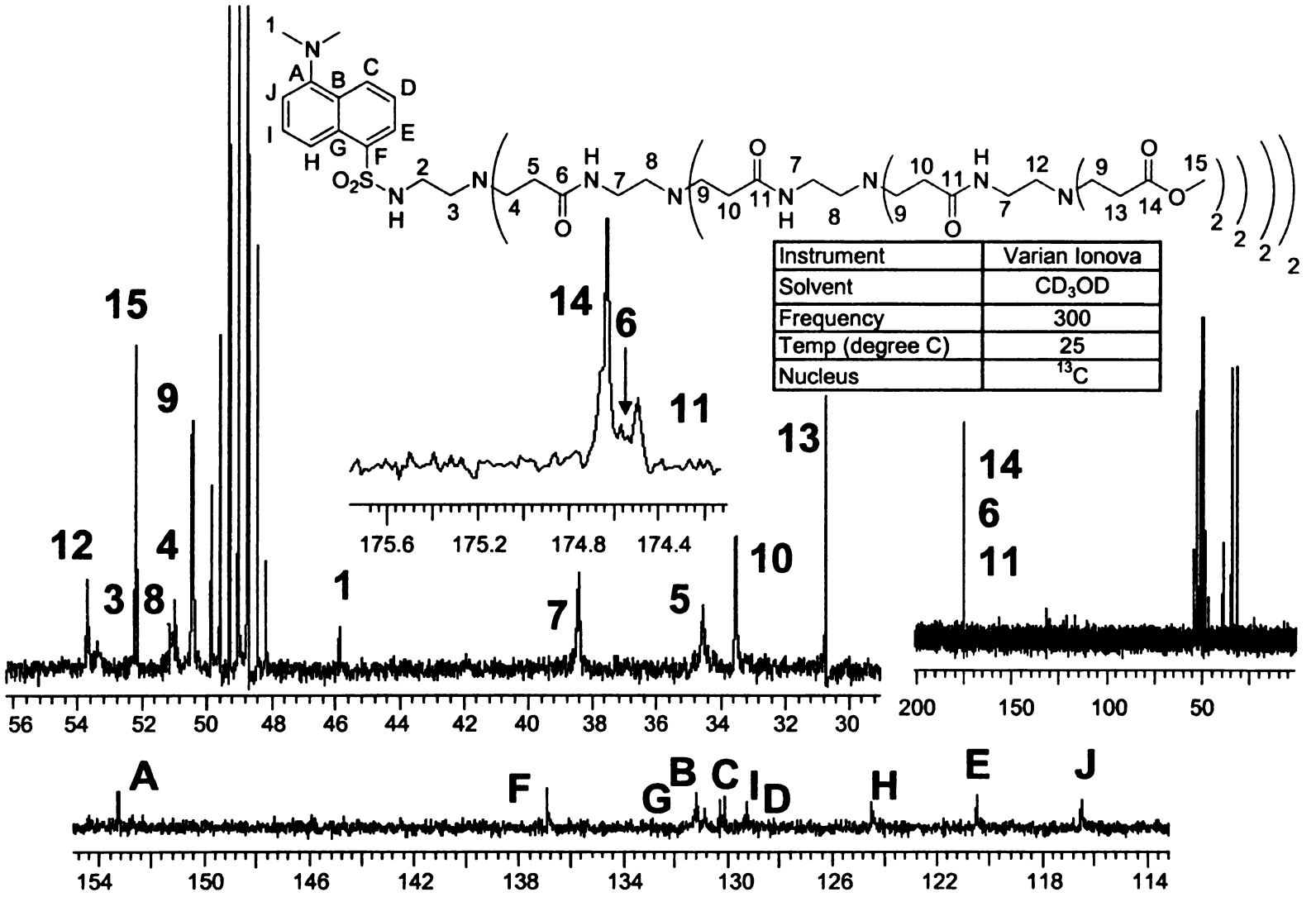

Figure B.15. ^{13}C NMR Dansyl G3.5

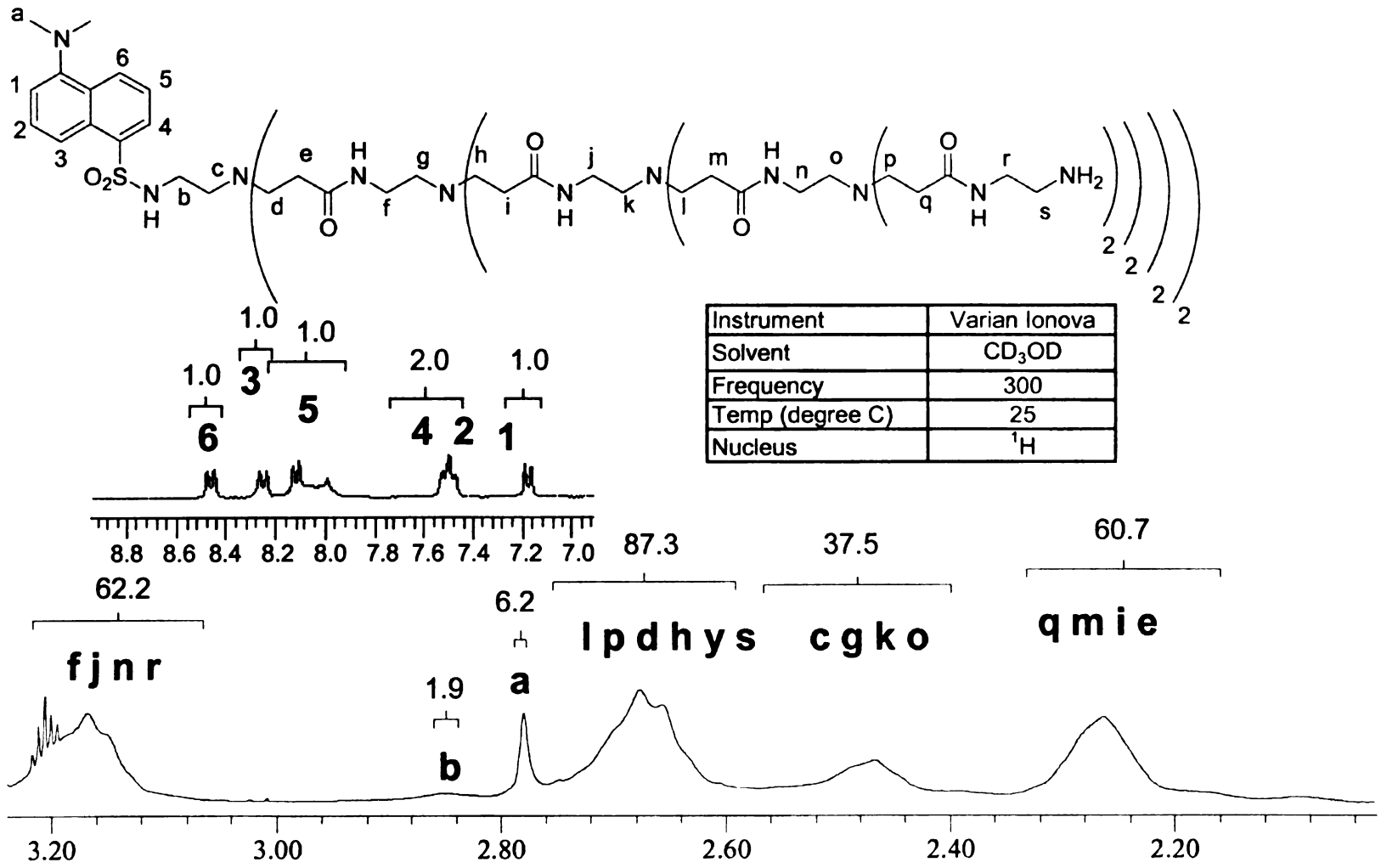

Figure B.16. ^{1}H NMR Dansyl G4.0

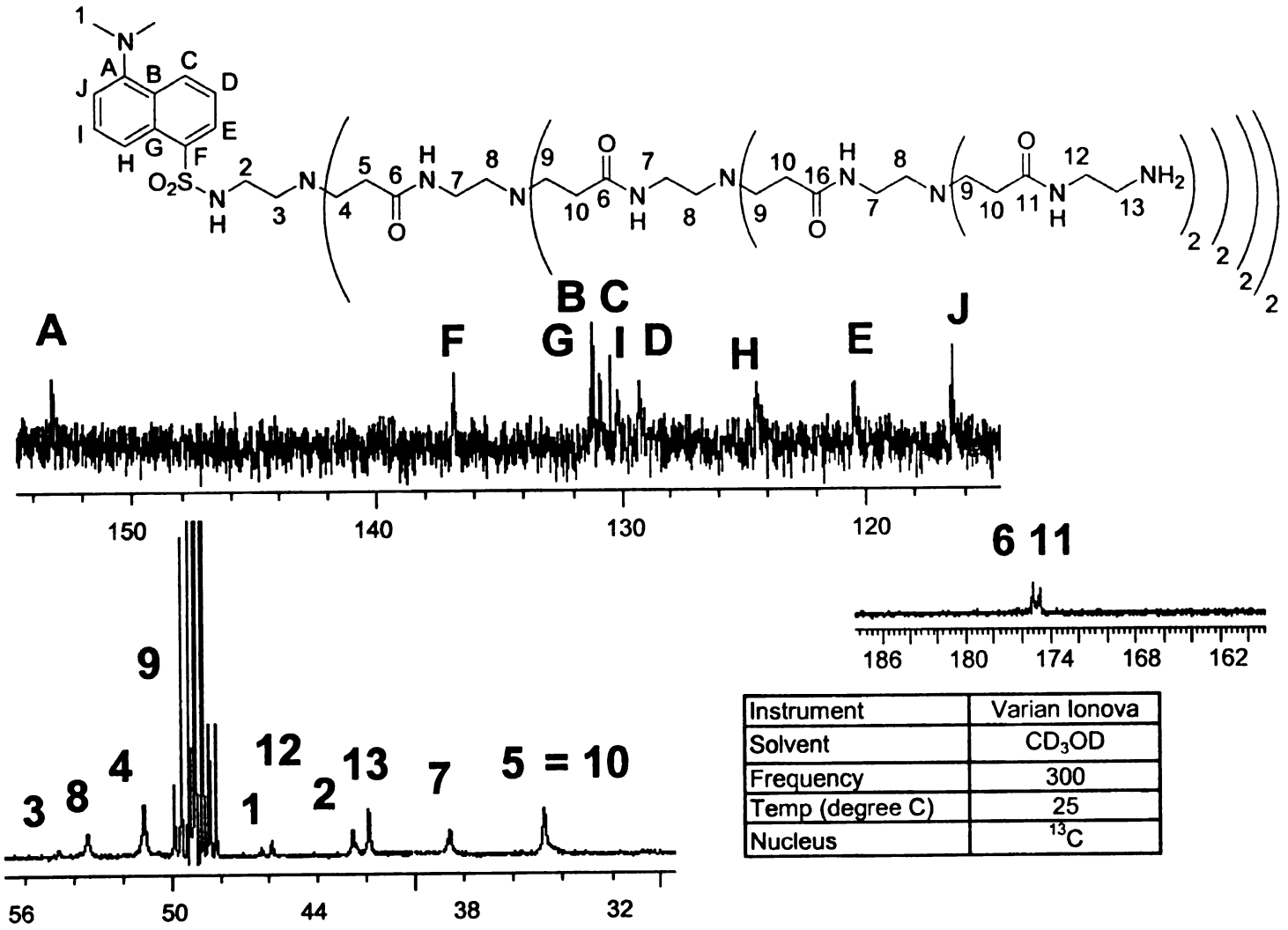

Figure B.17. ^{13}C NMR Dansyl G4.0

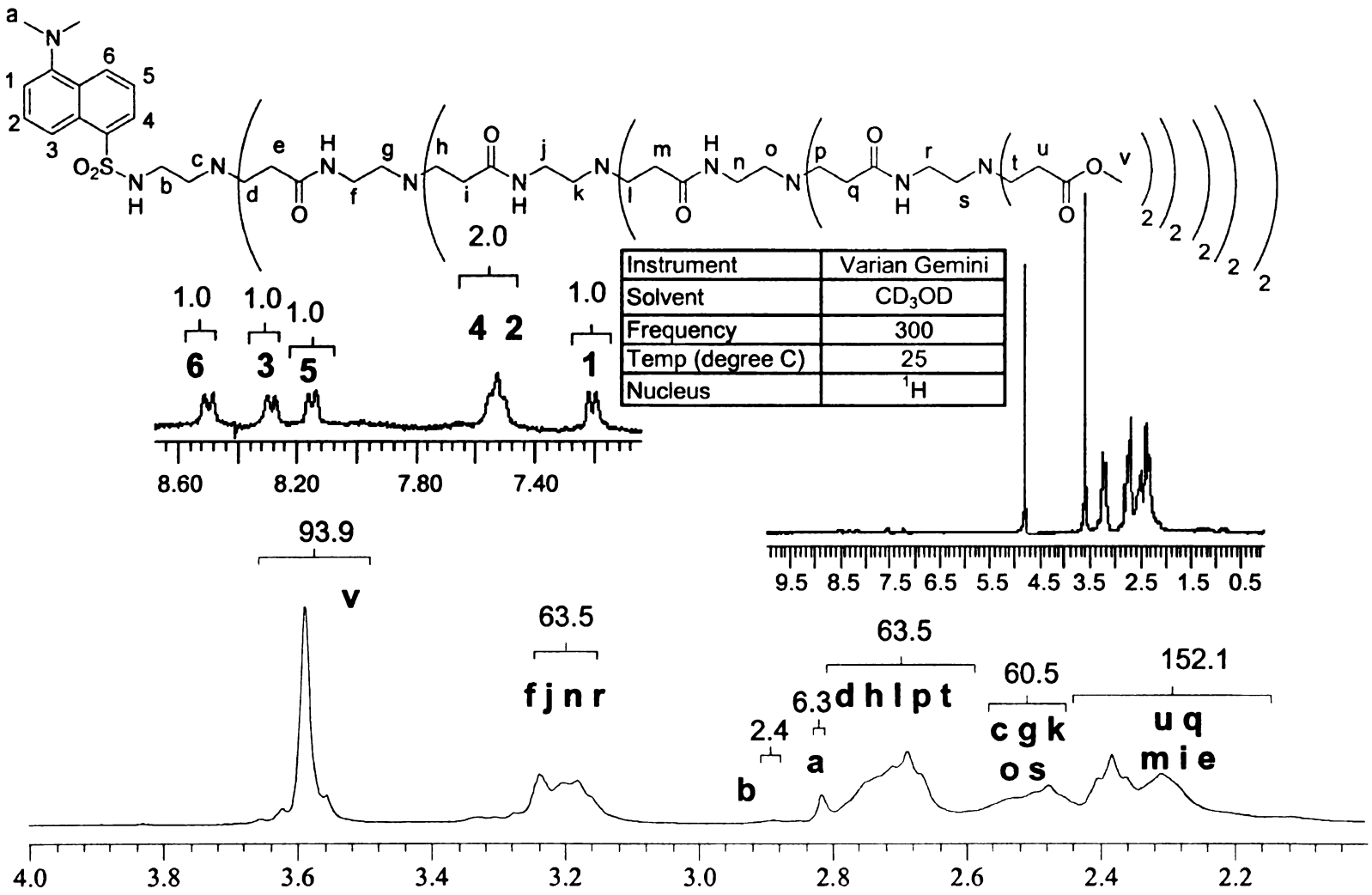

Figure B.18. ^{1}H NMR Dansyl G4.5

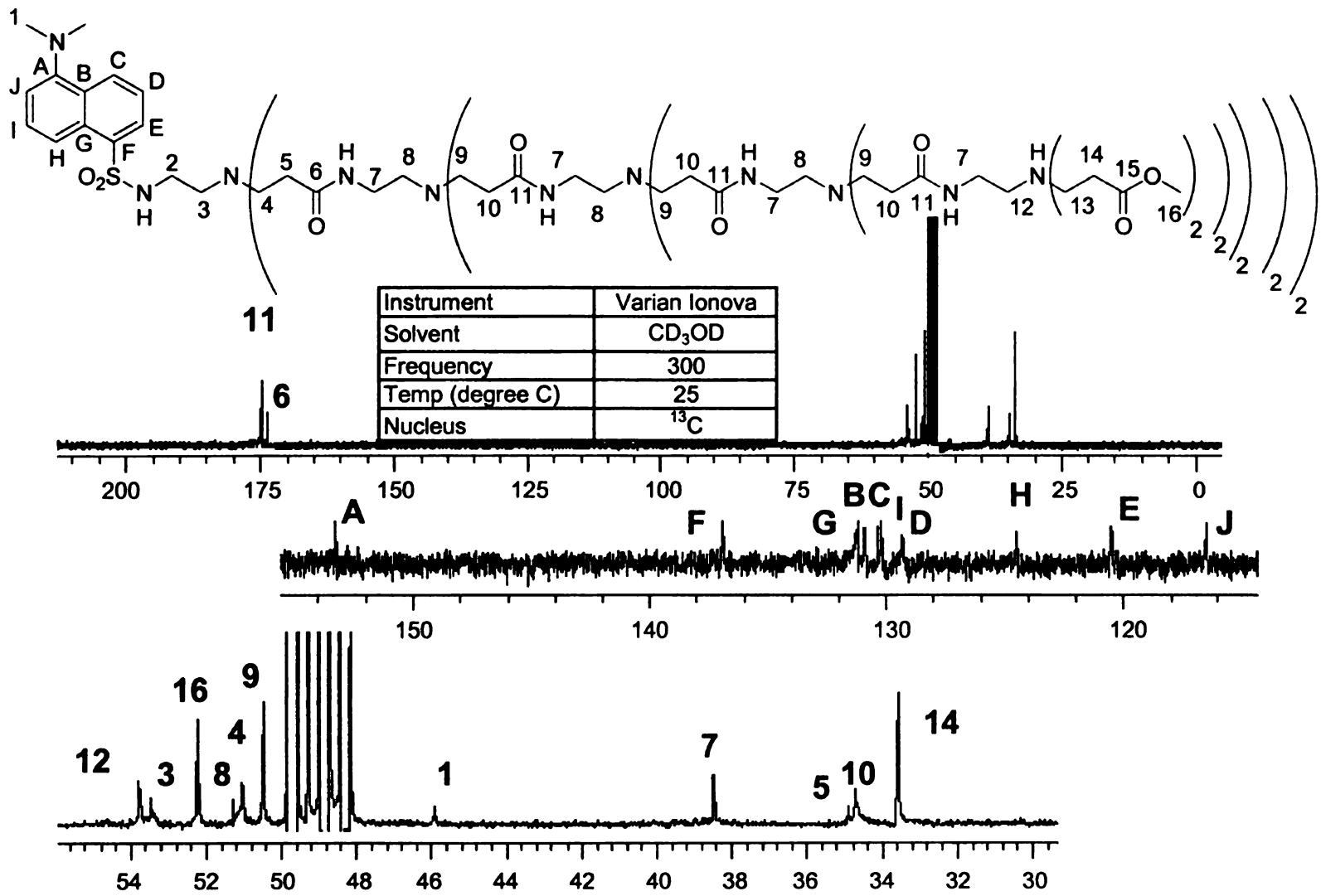

Figure B.19. ^{13}C NMR Dansyl G4.5

APPENDIX C

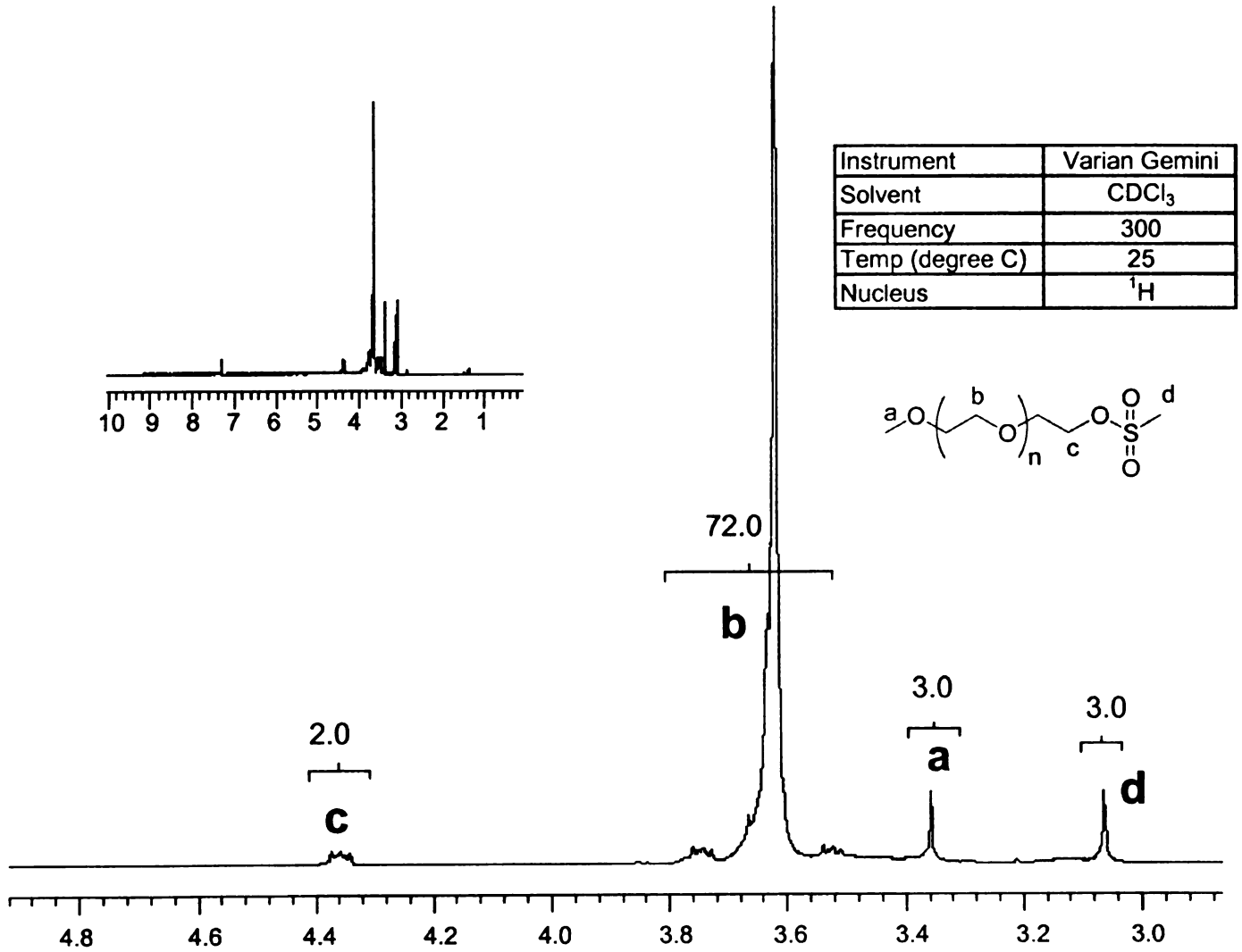

Figure C.1. ^{1}H NMR PEO 750 Da OMs

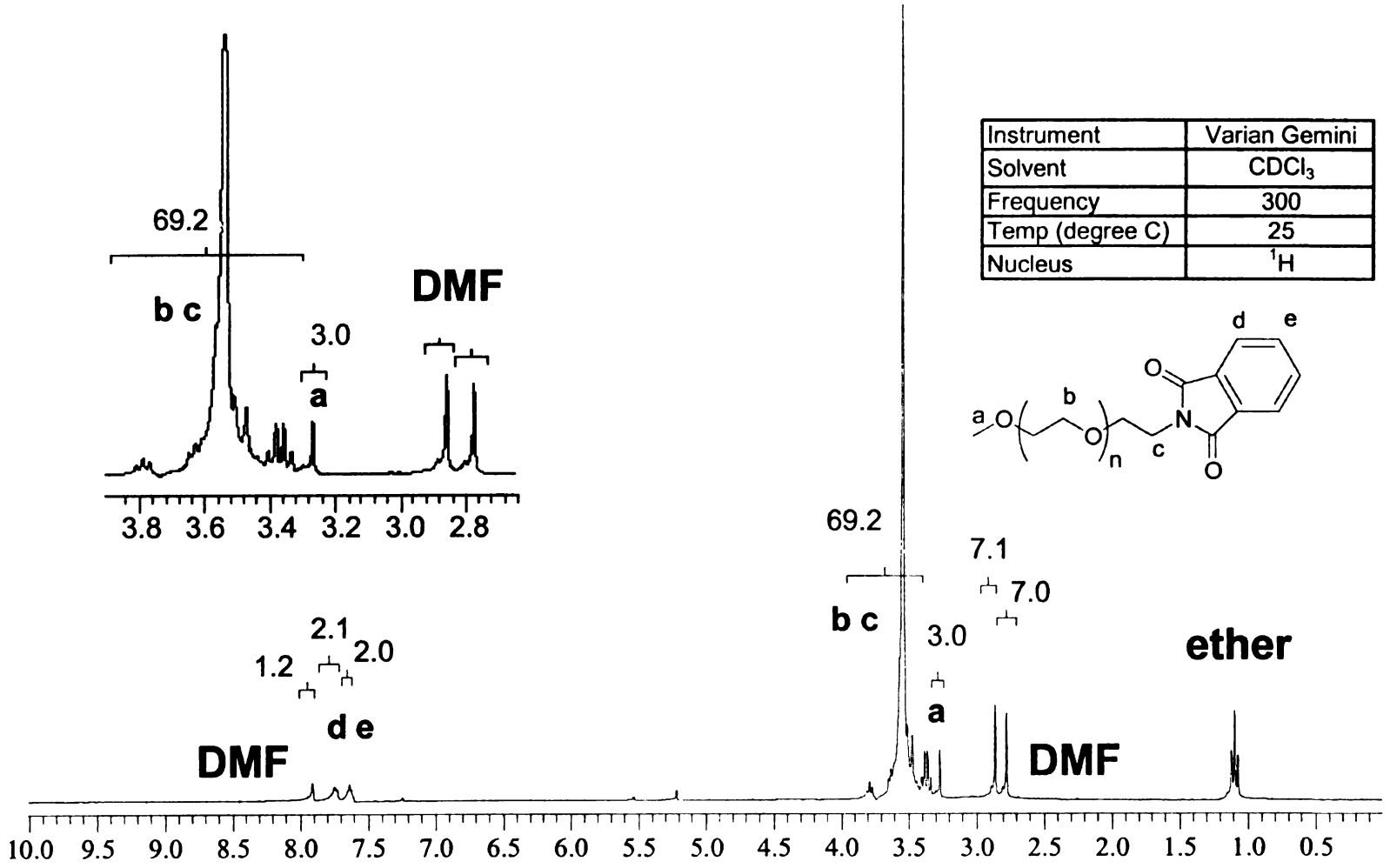

Figure C.2. ^{1}H NMR PEO 750 Da phth

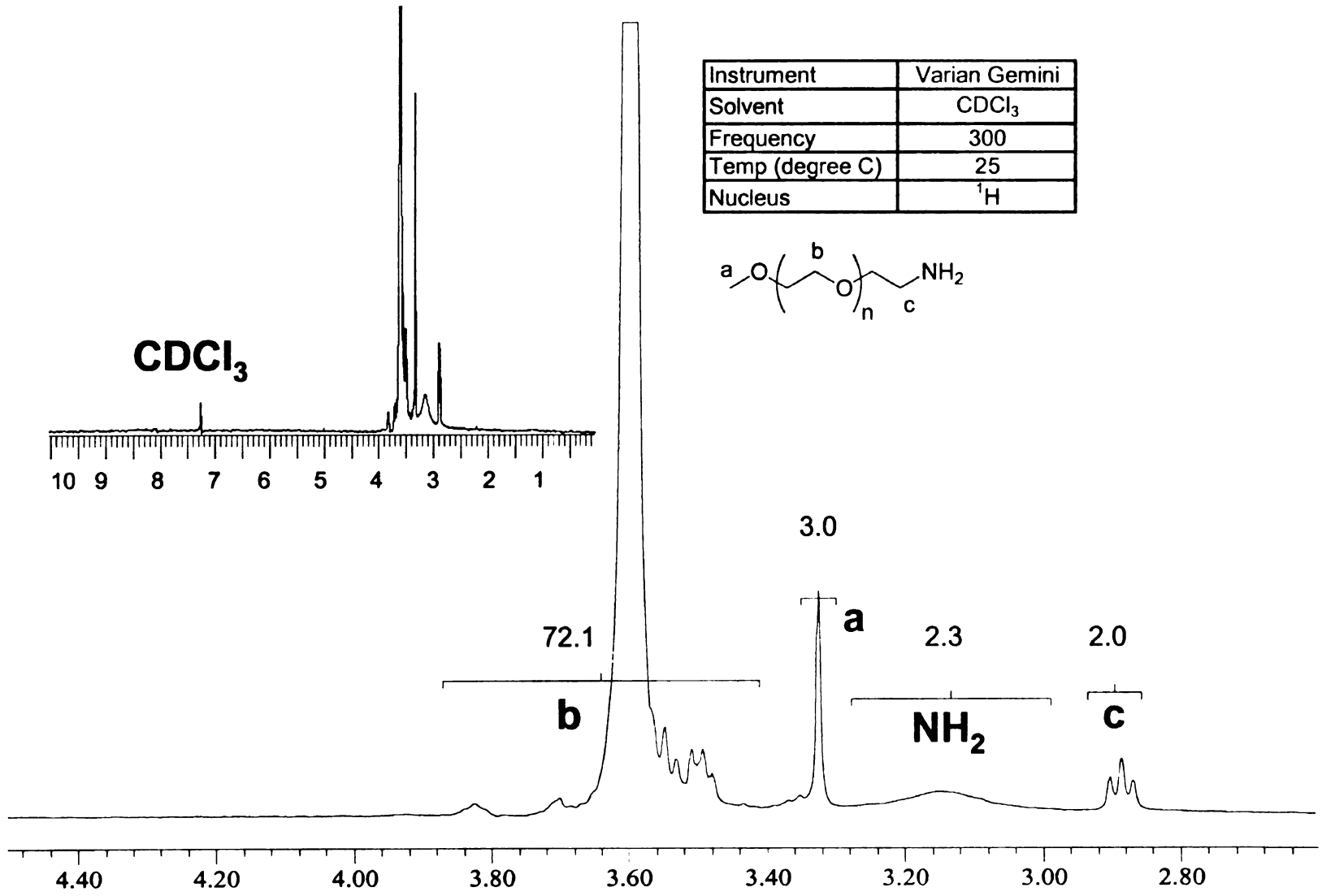

Figure C.3. ^{1}H NMR PEO 750 Da NH_2

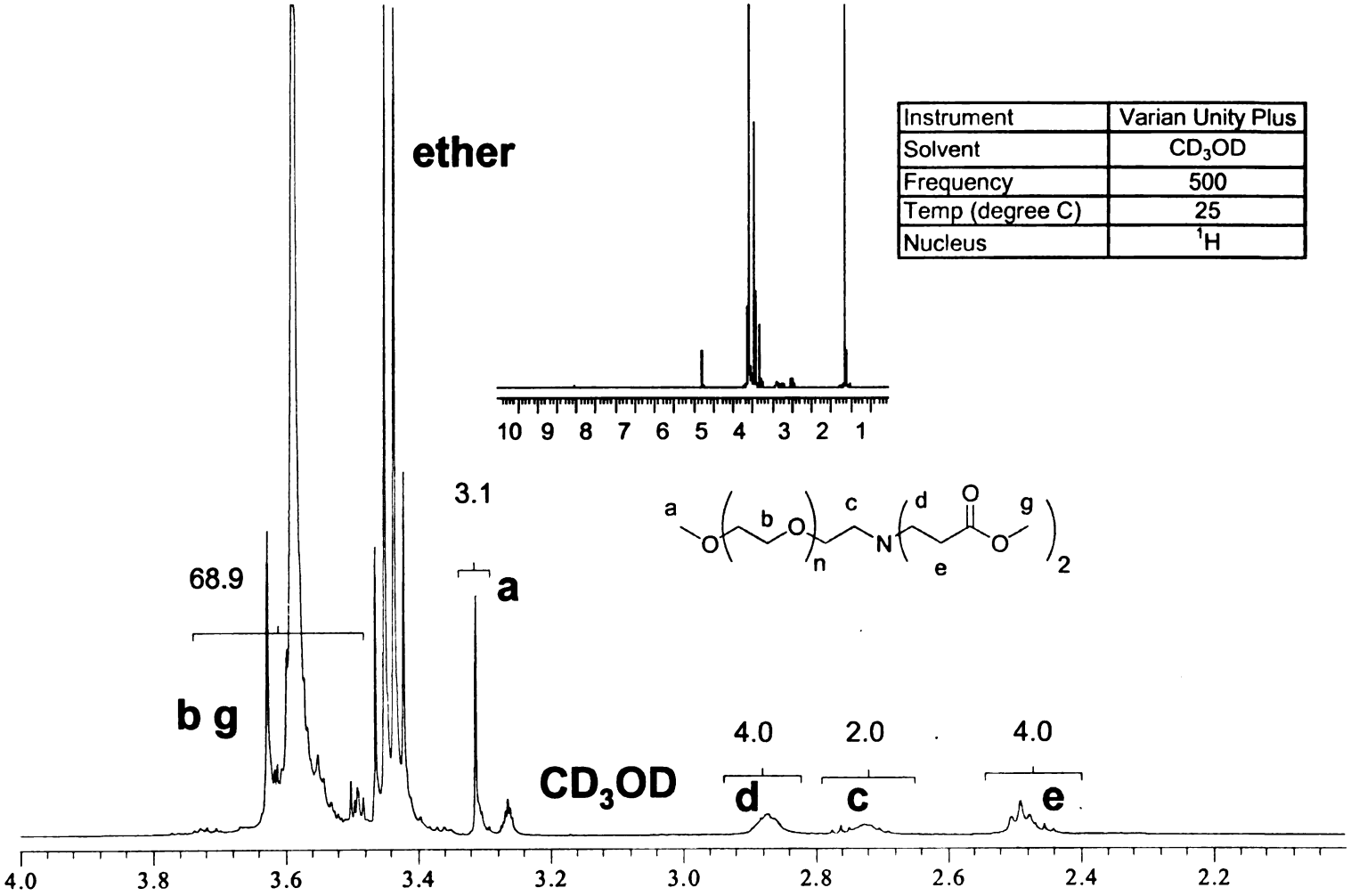

Figure C.4. ^{1}H NMR PEO 750 G0.5

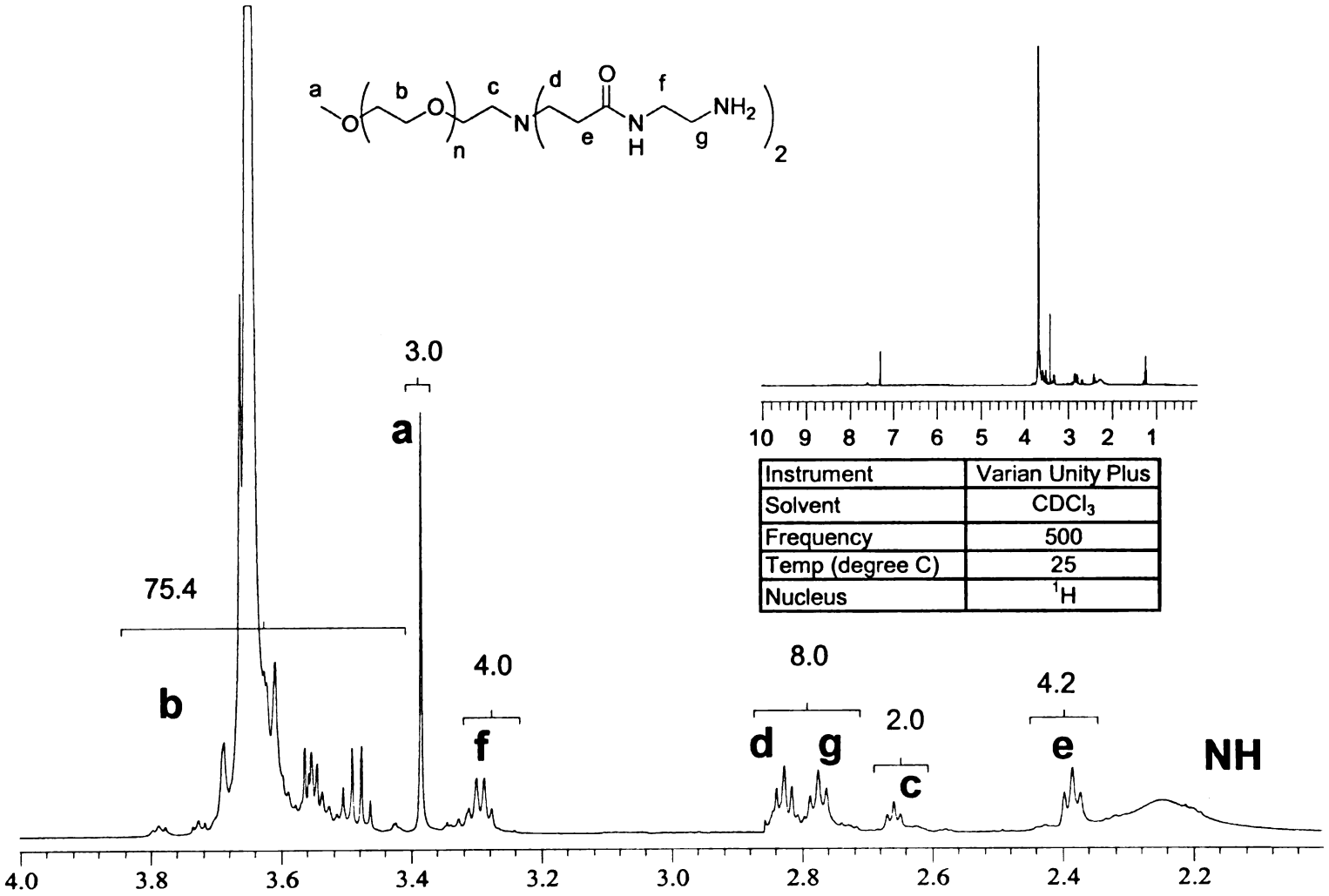

Figure C.5. ^{1}H NMR PEO 750 Da G1.0

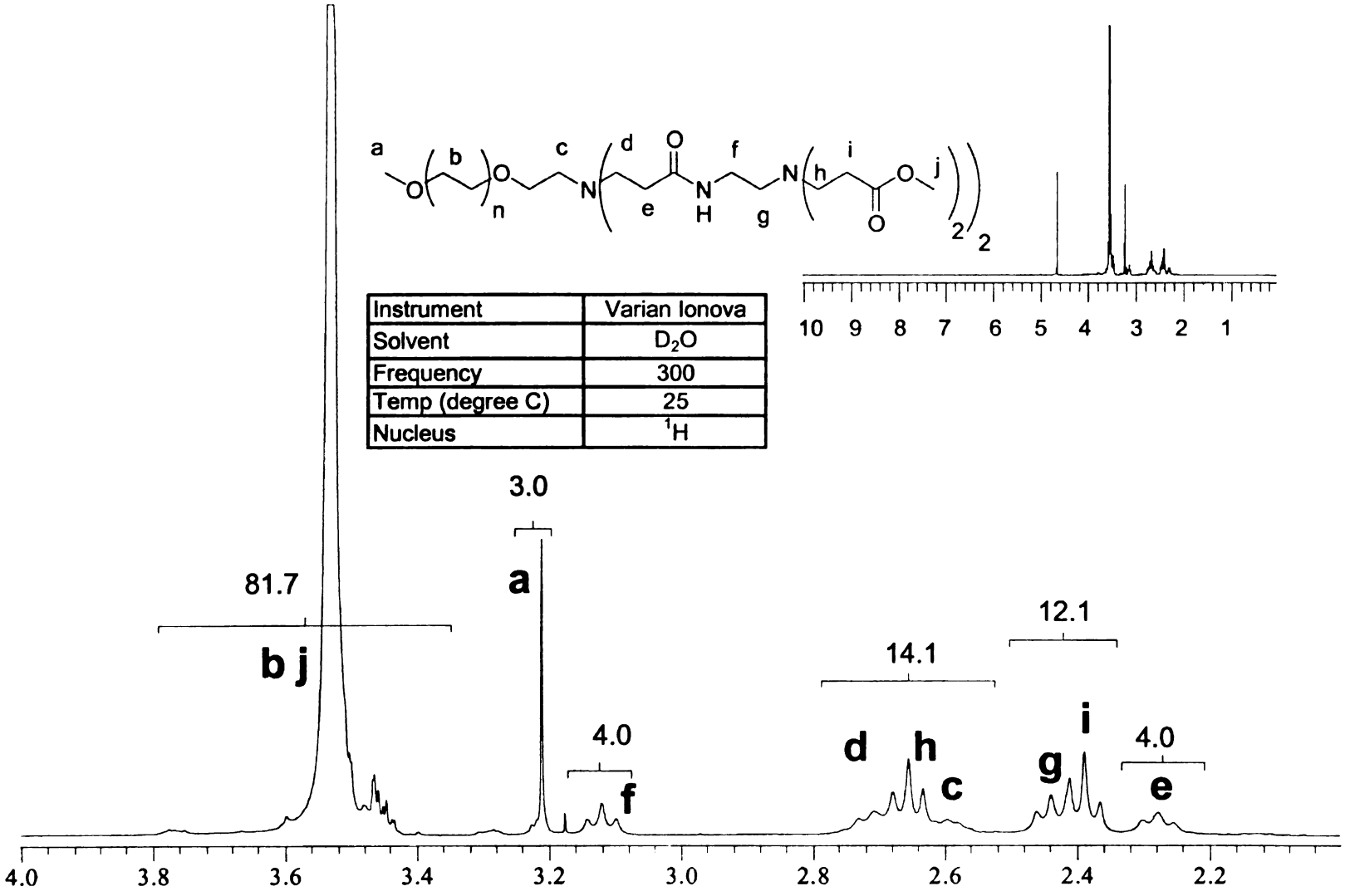

Figure C.6. ^{1}H NMR PEO 750 Da G1.5

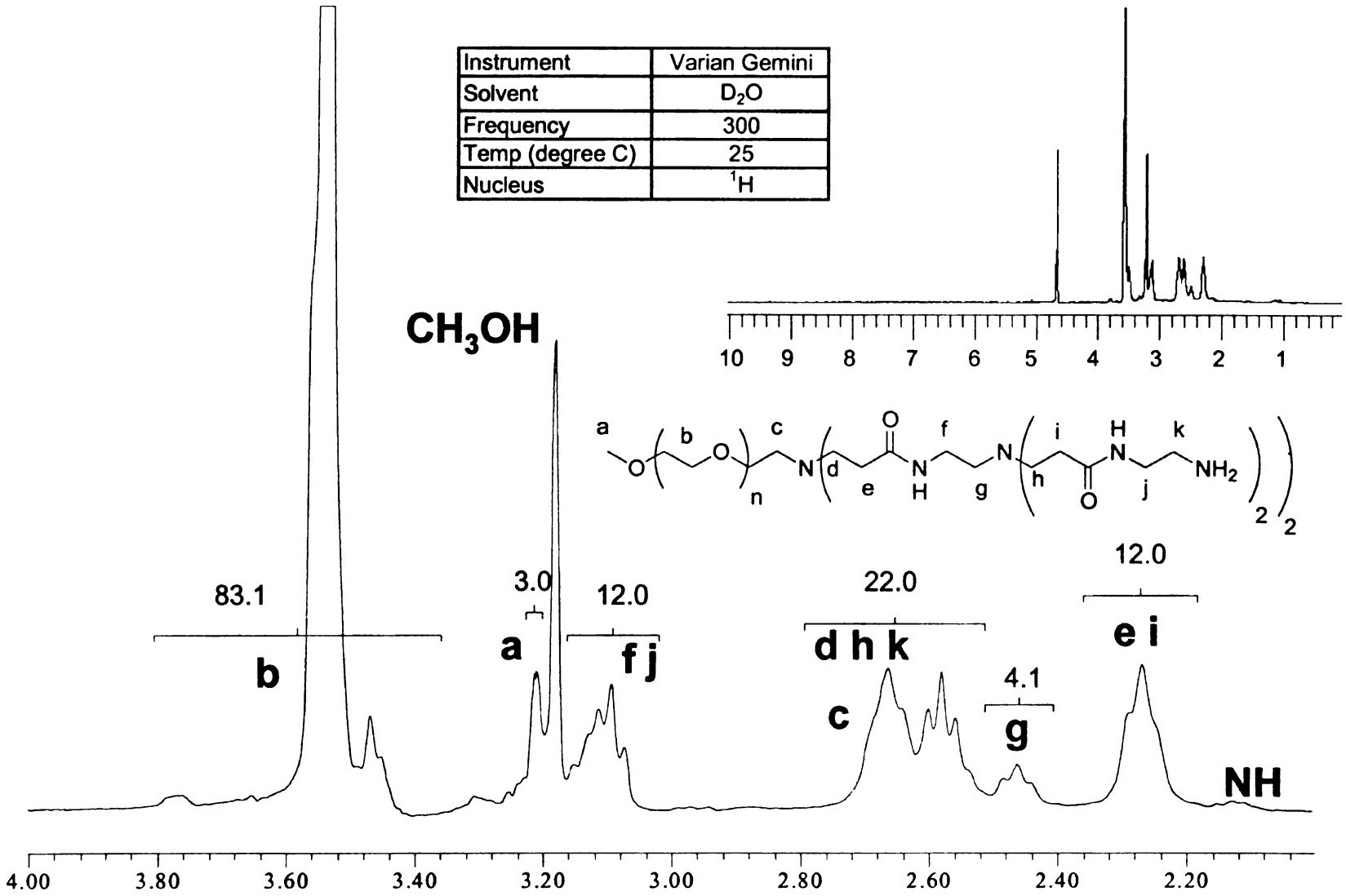

Figure C.7. ^1H NMR PEO 750 Da G2.0

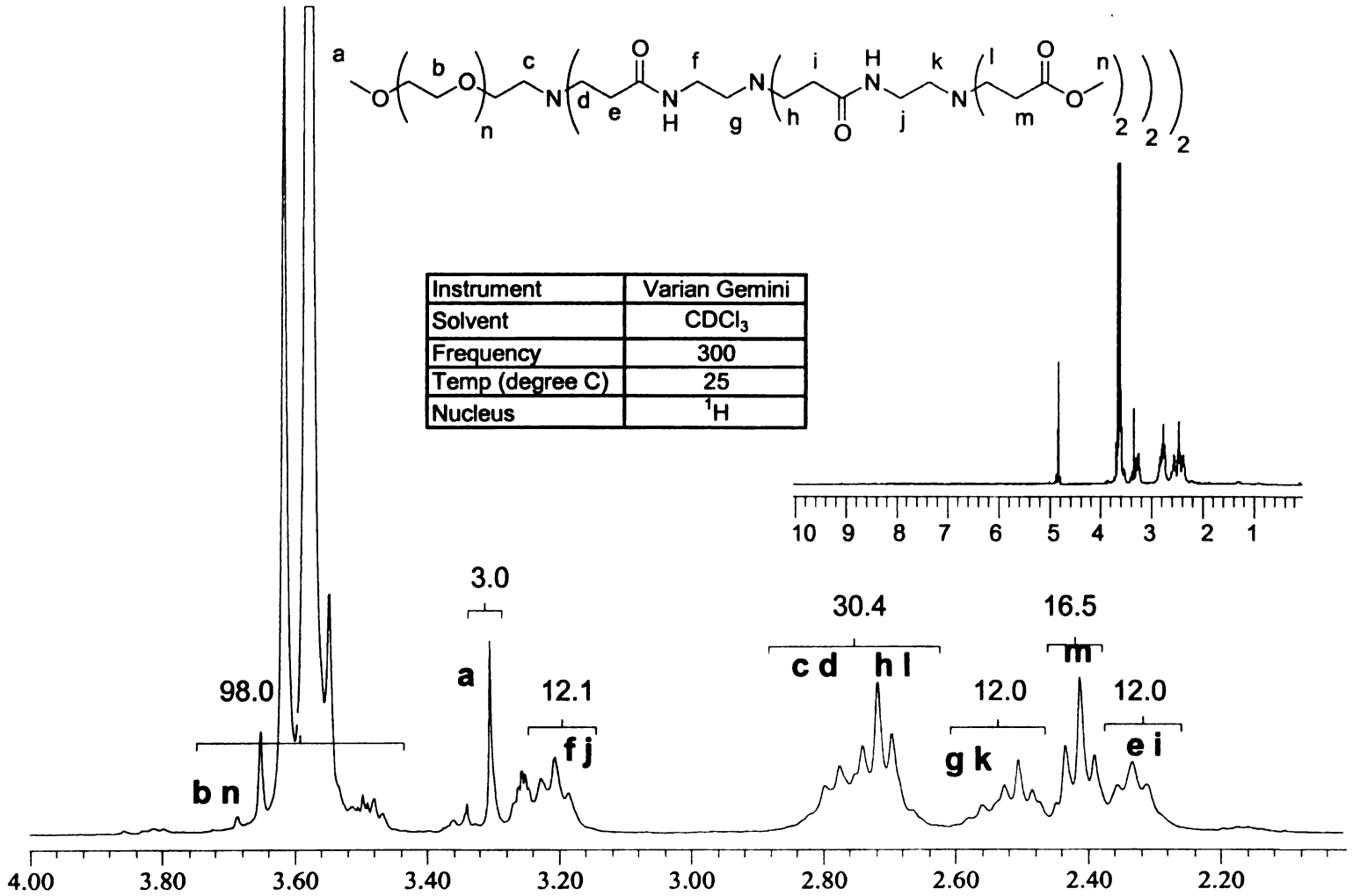

Figure C.8. ^{1}H NMR PEO 750 Da G2.5

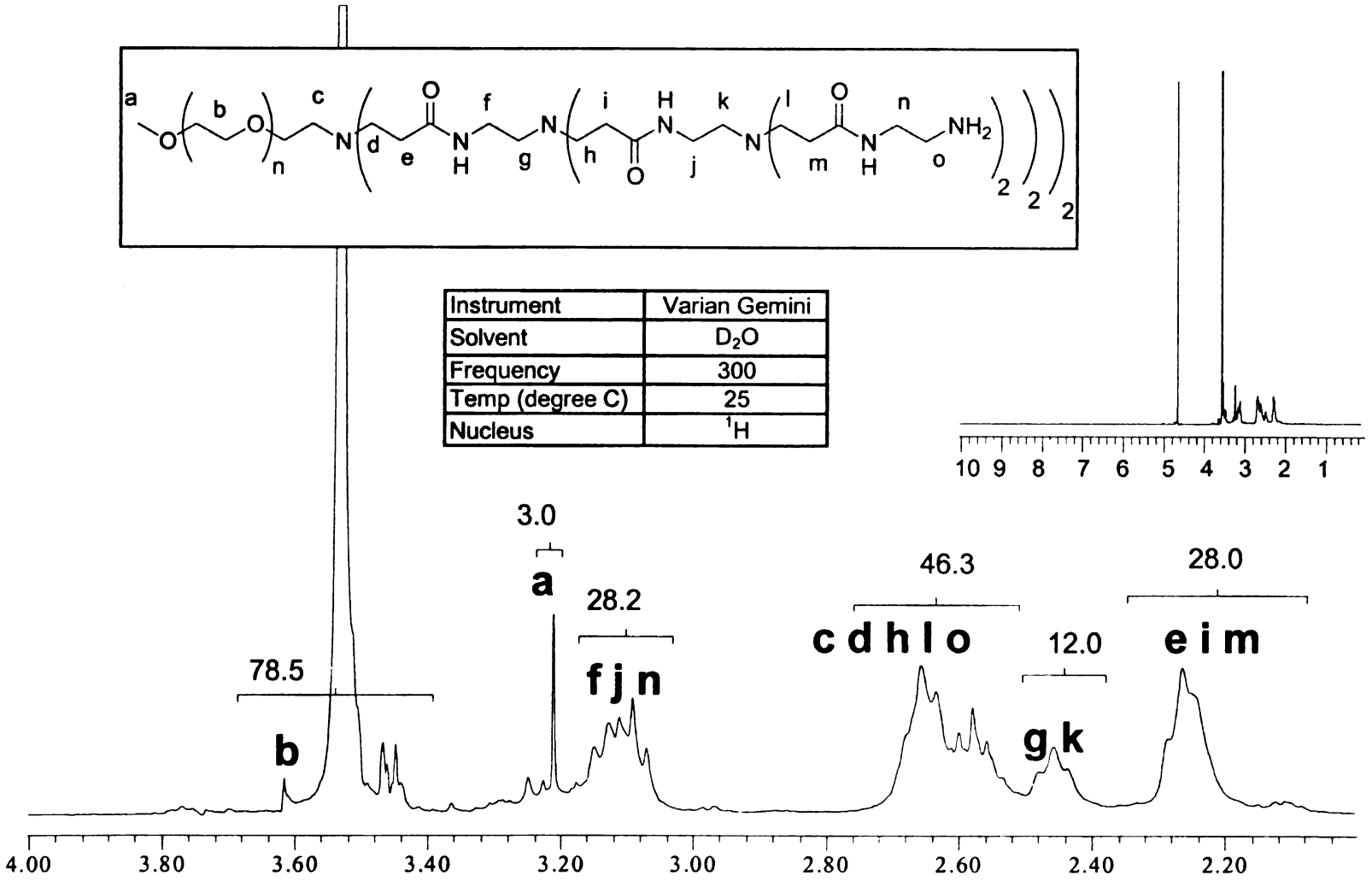

Figure C.9. ^{1}H NMR PEO 750 Da G3.0

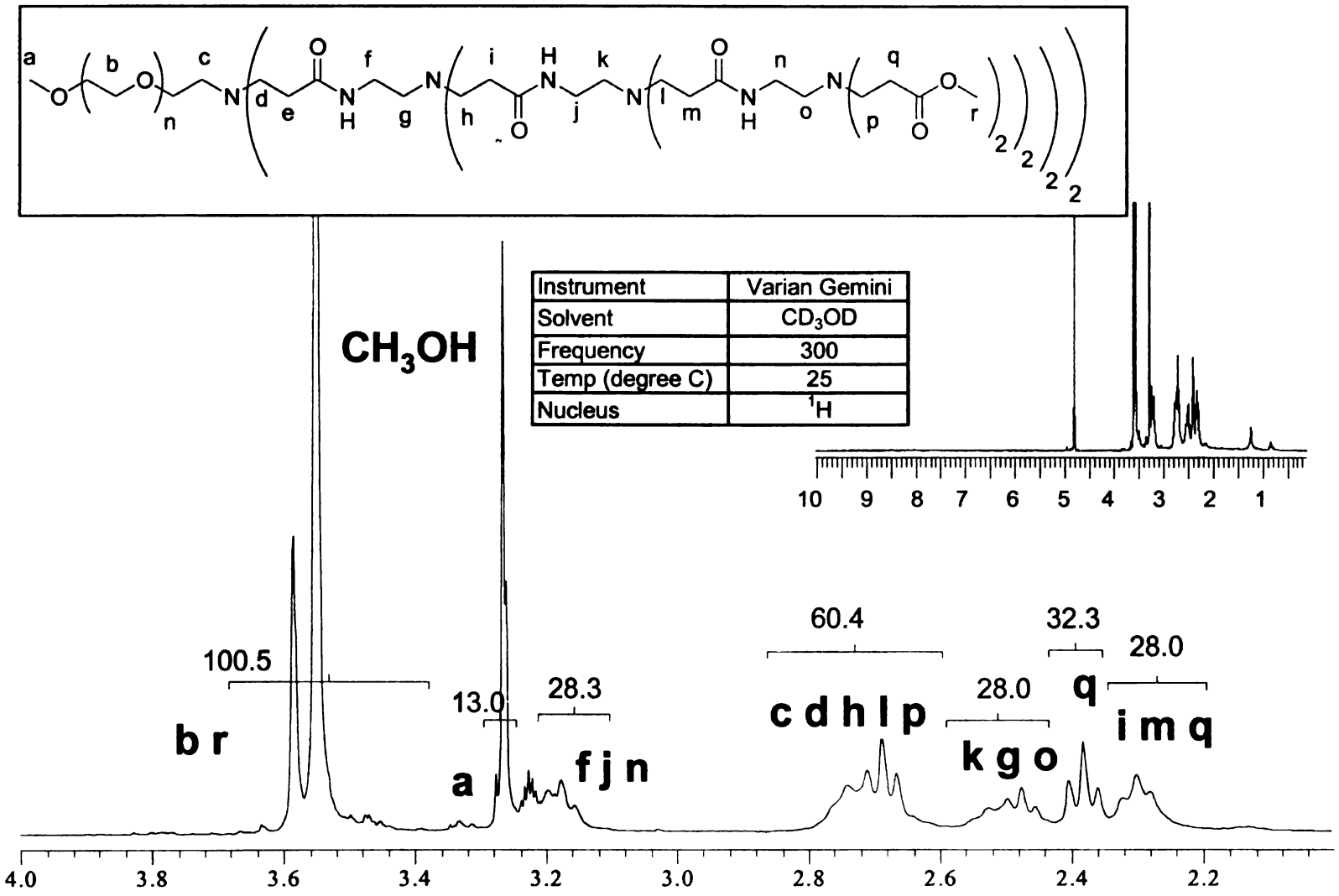

Figure C.10. ^{1}H NMR PEO 750 Da G3.5

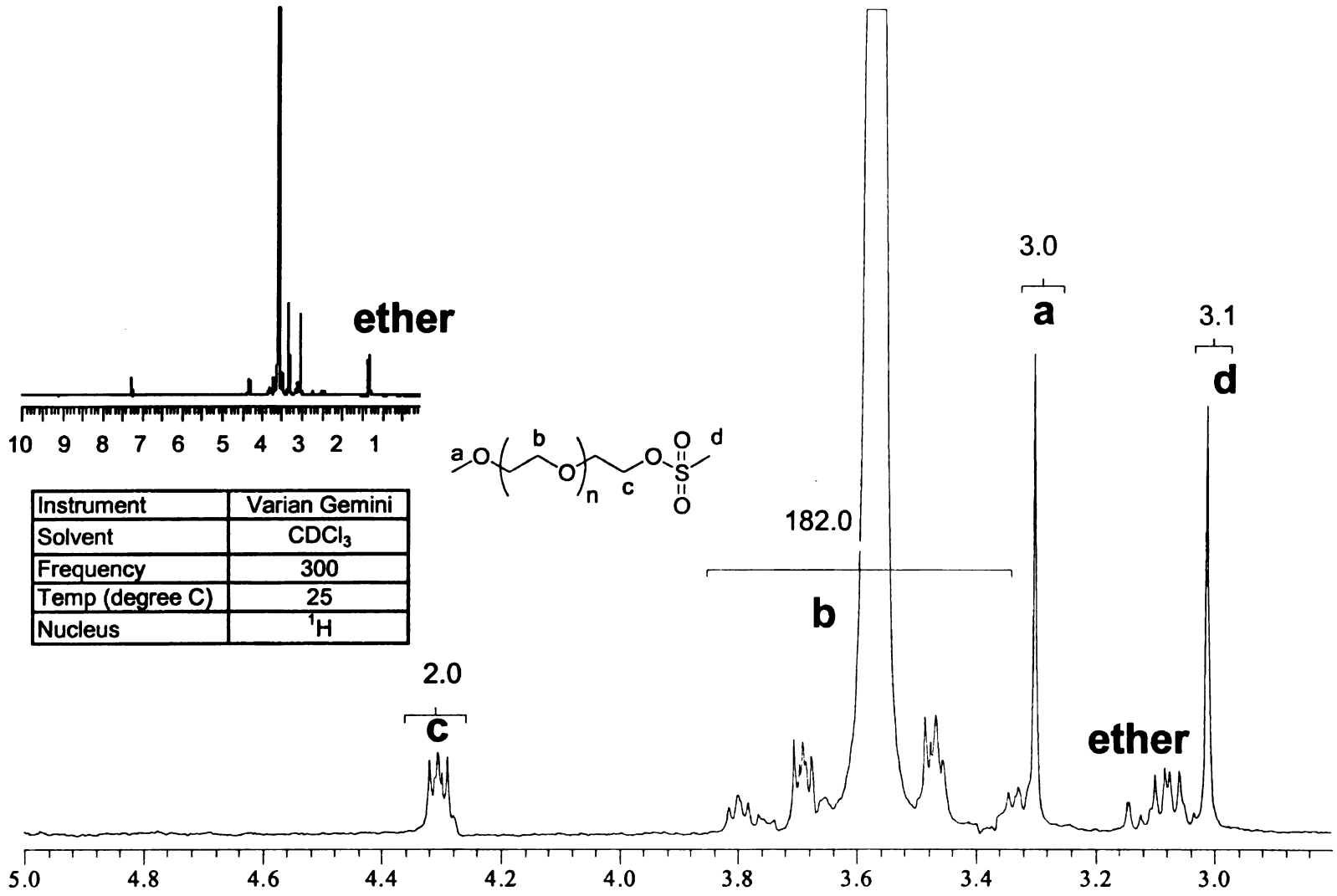

Figure C.11. ^{1}H NMR PEO 2 kDa OMs

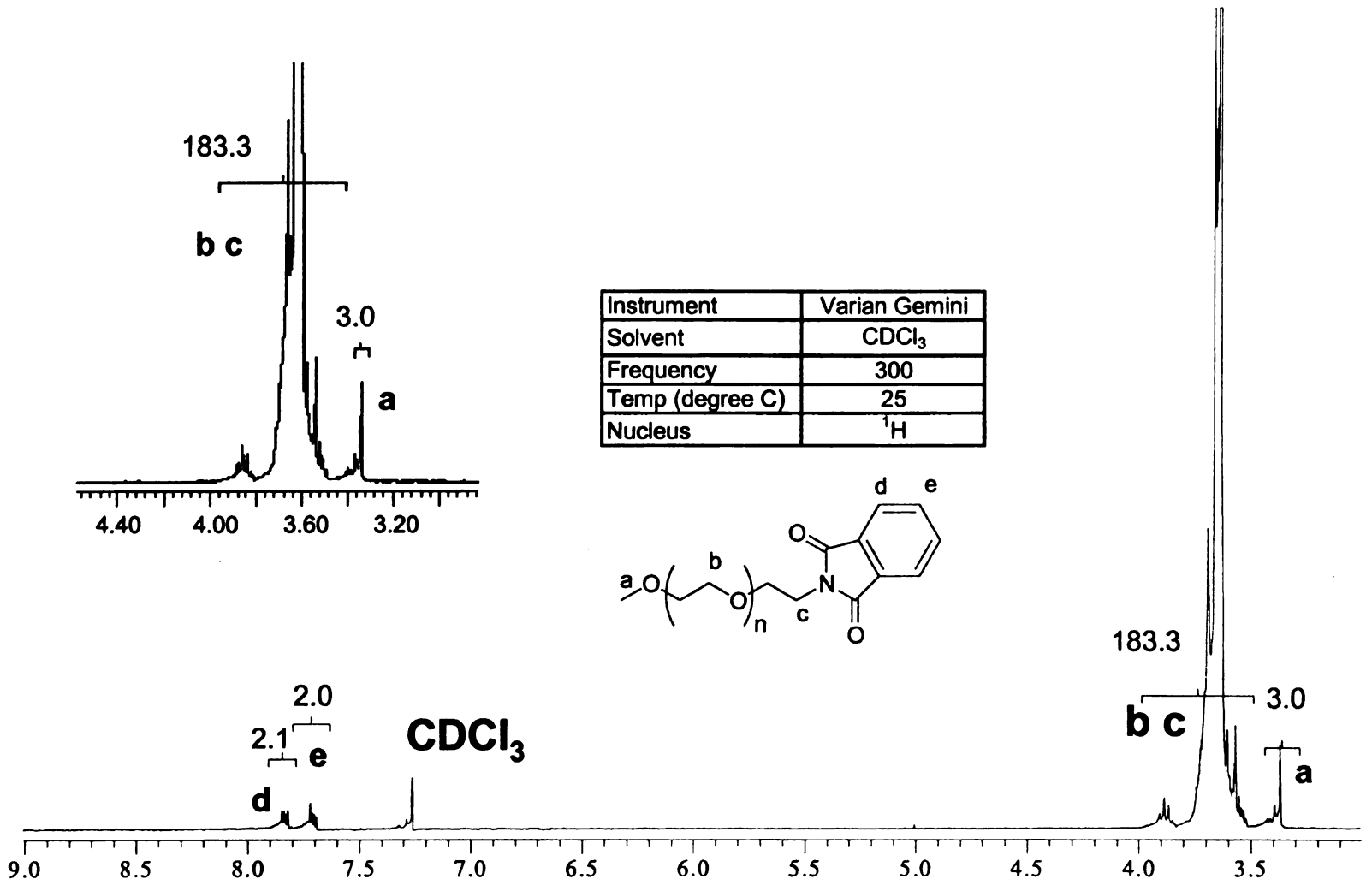

Figure C.12. ^{1}H NMR PEO 2 kDa phth

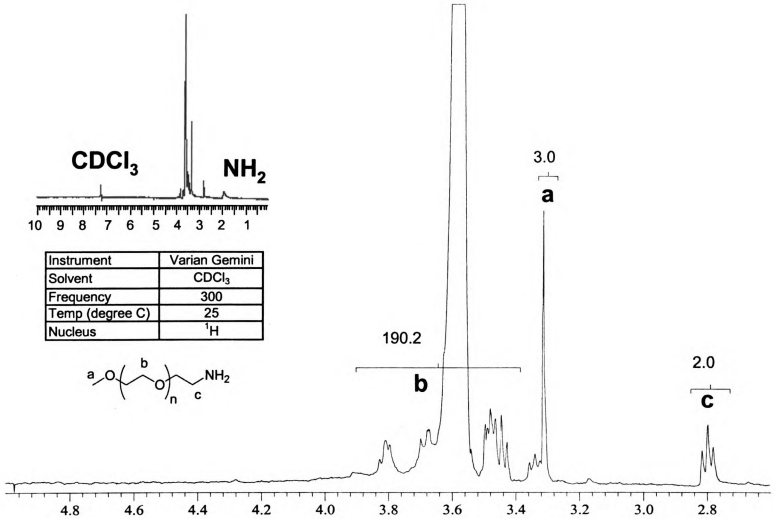

Figure C.13. ^{1}H NMR PEO 2 kDa NH_2

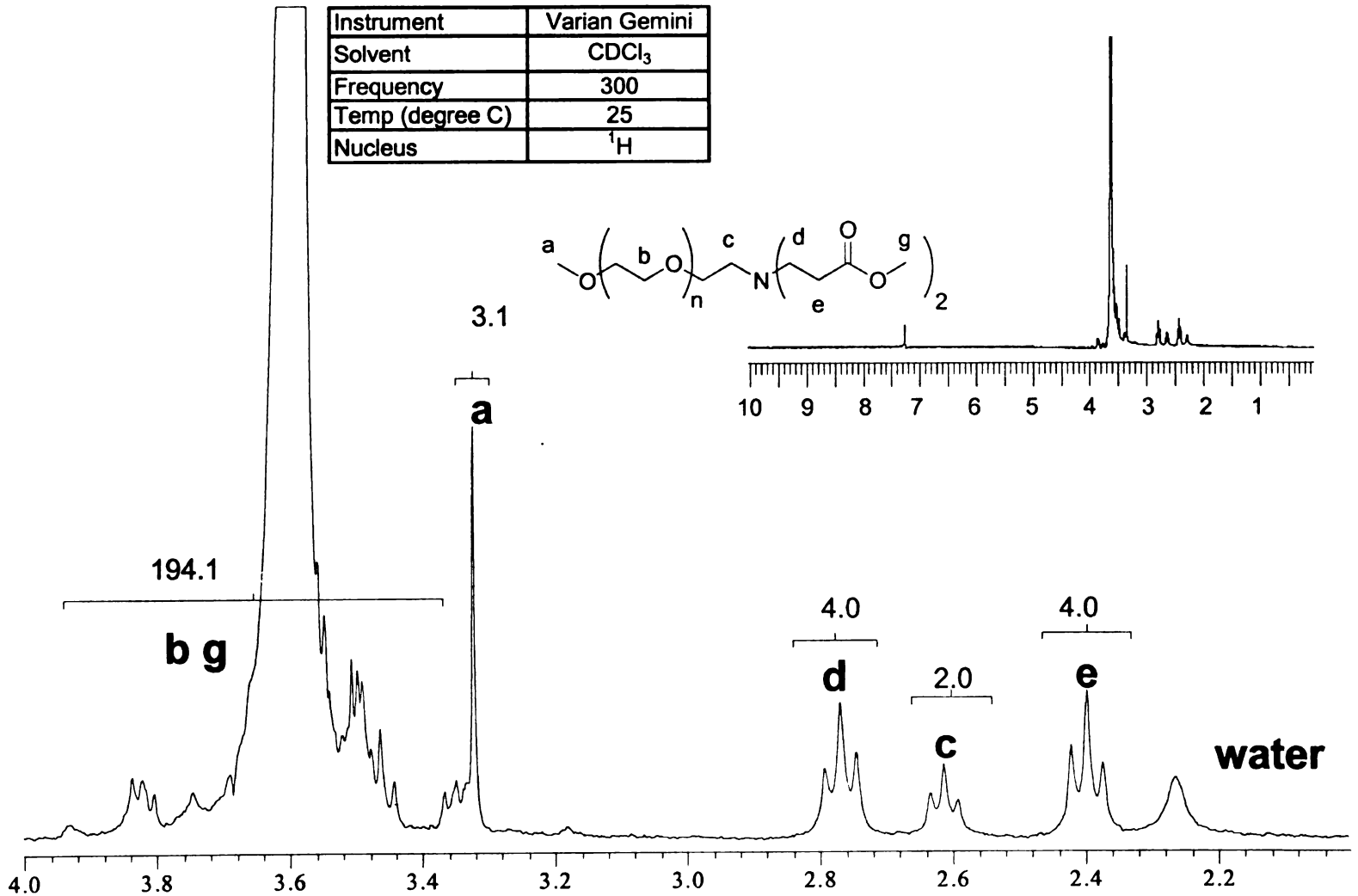

Figure C.14. ^{1}H NMR PEO 2 kDa G0.5

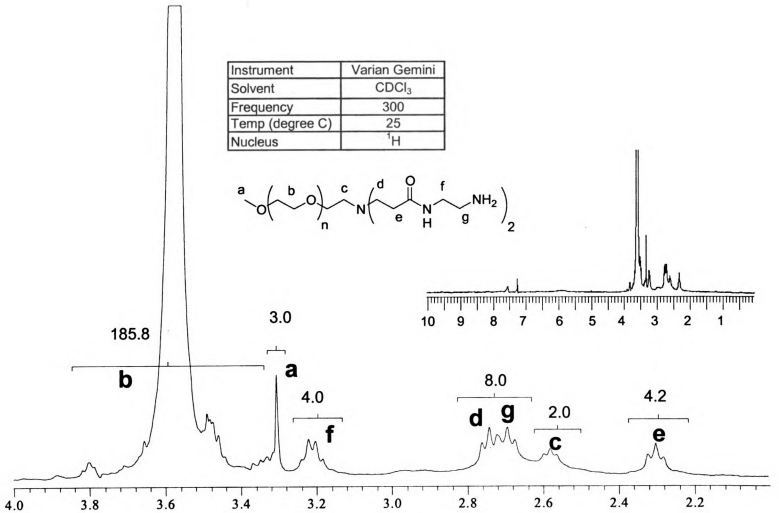

Figure C.15. ^{1}H NMR PEO 2 kDa G1.0

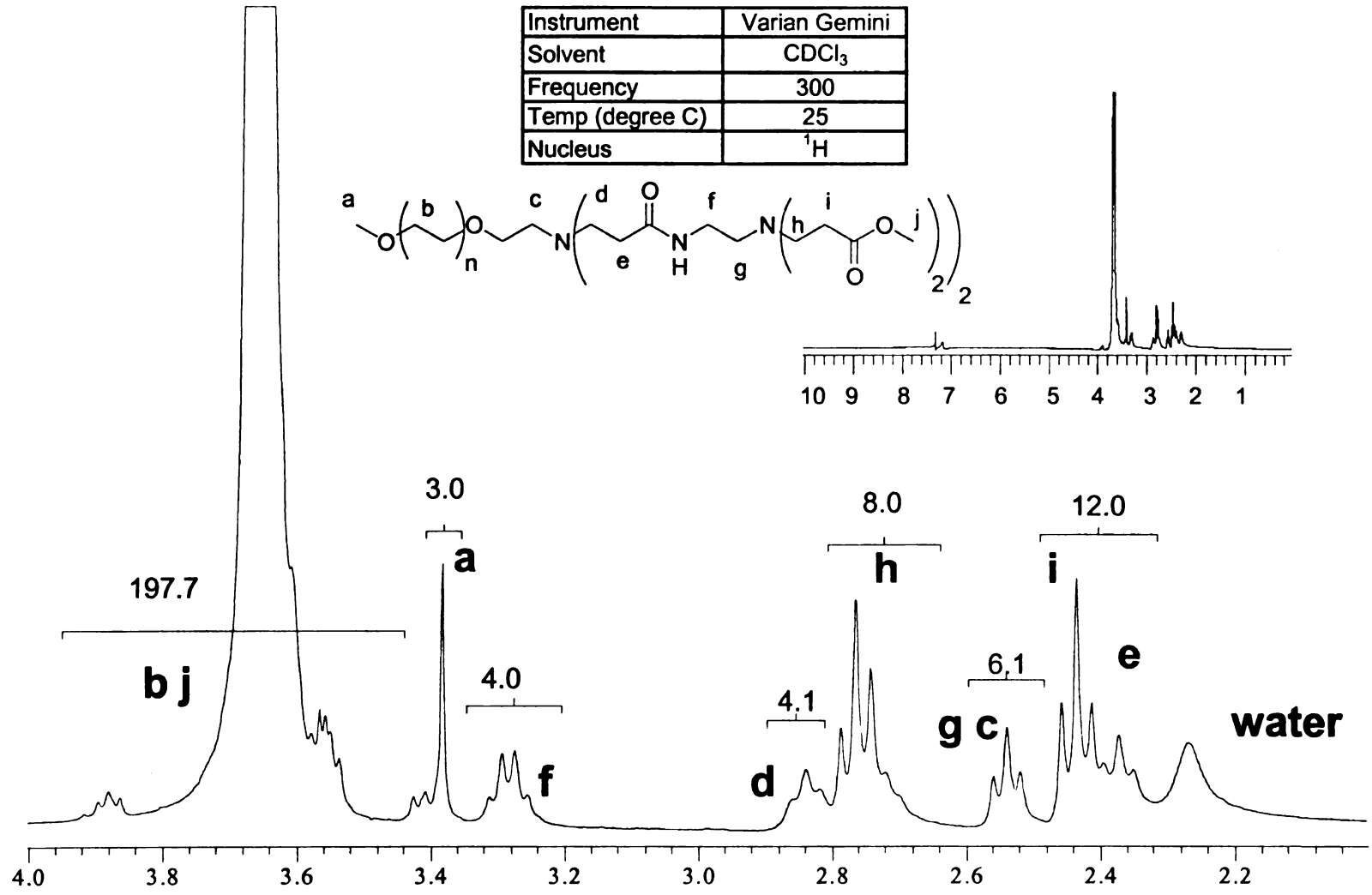

Figure C.16. ^{1}H NMR PEO 2 kDa G1.5

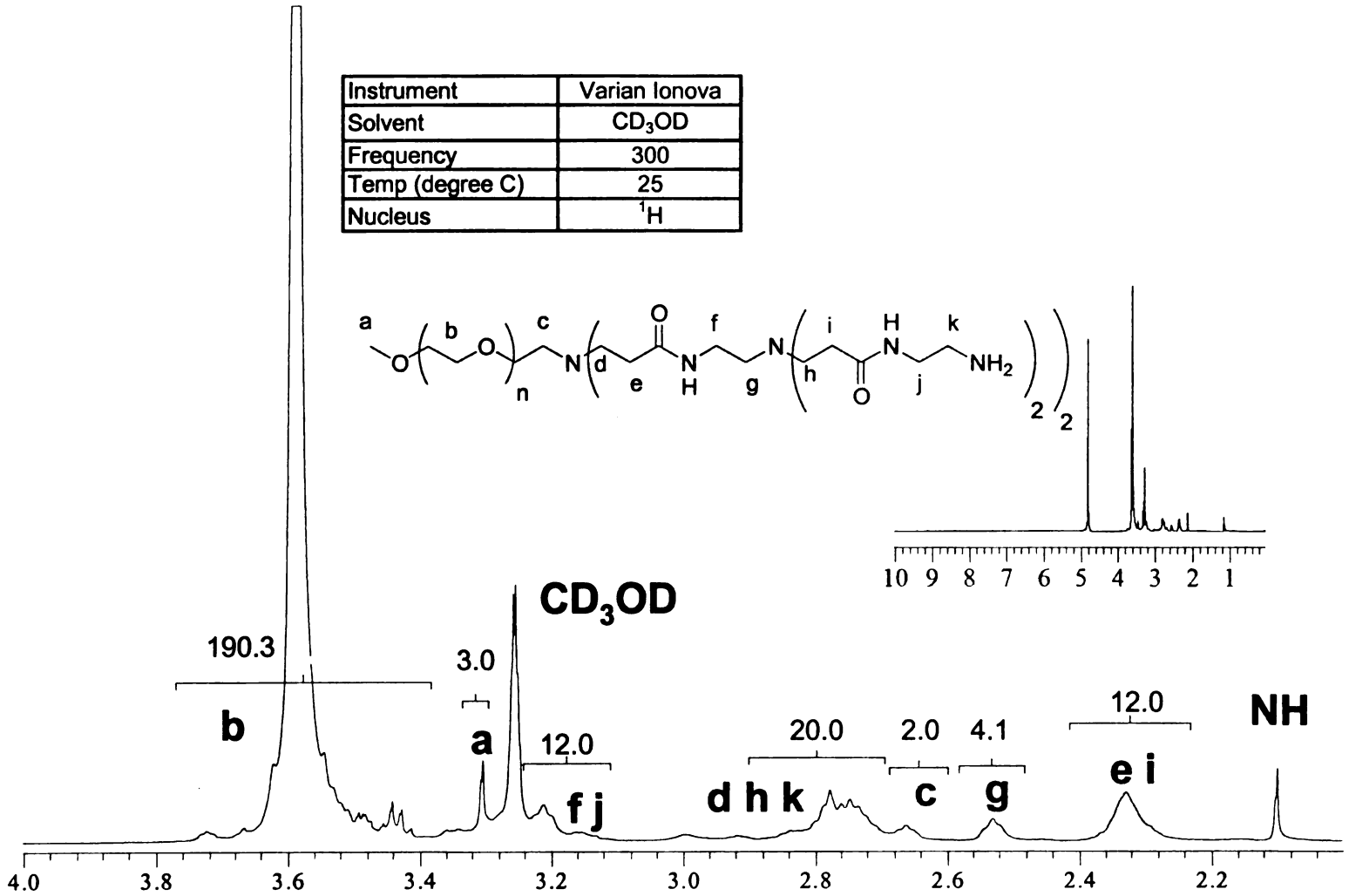

Figure C.17. ^{1}H NMR PEO 2 kDa G2.0

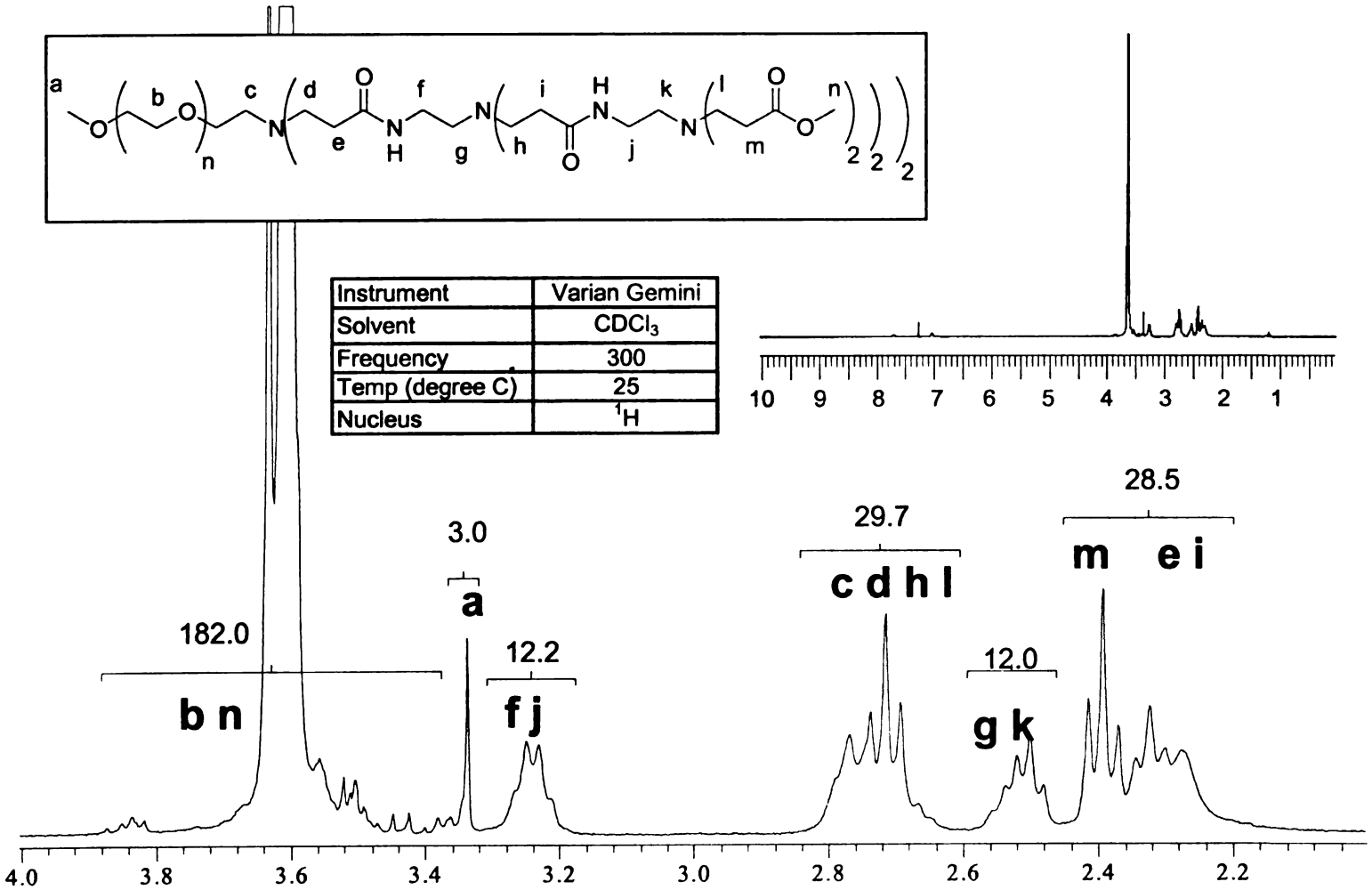

Figure C.18. ^{1}H NMR PEO 2 kDa G2.5

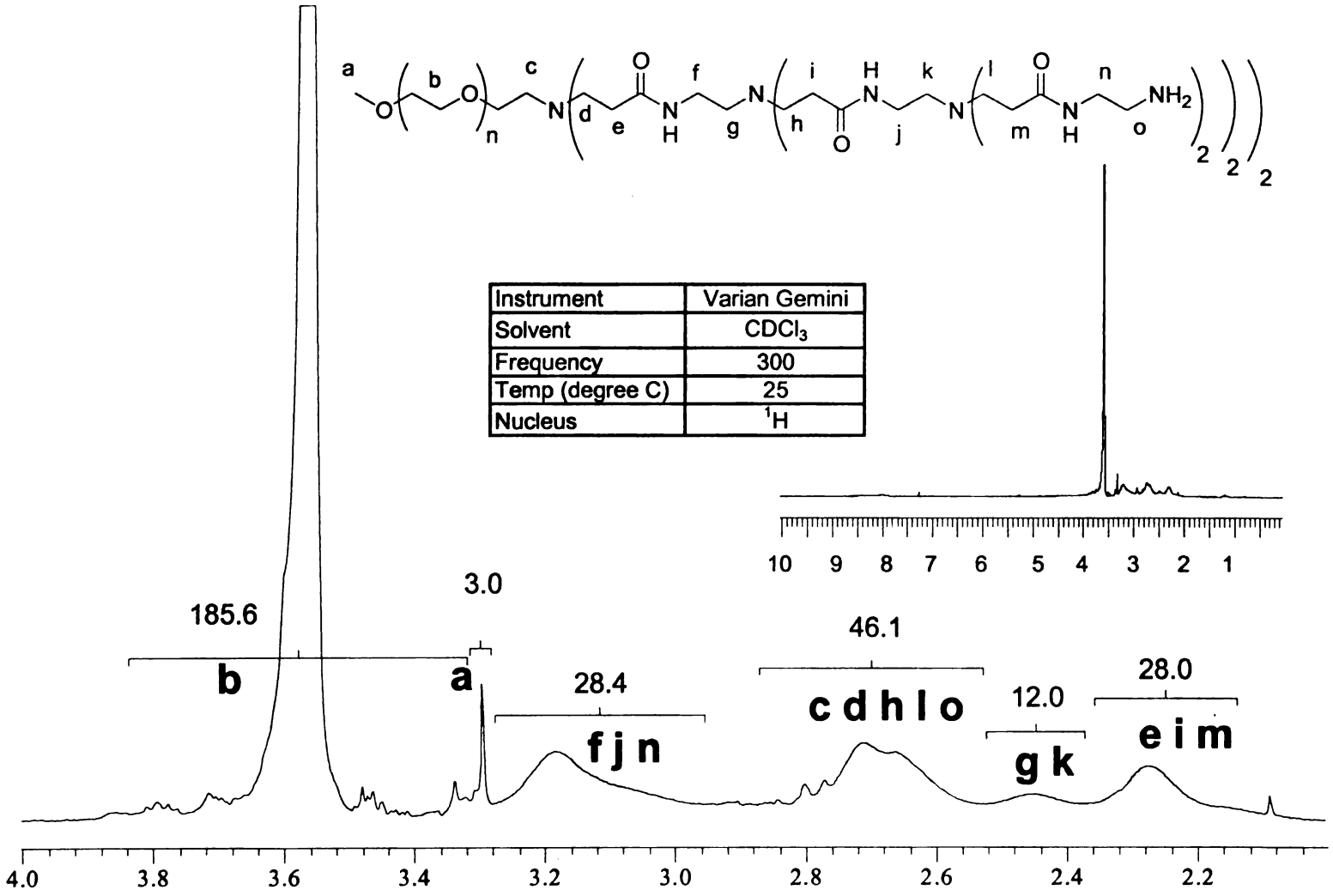

Figure C.19. ^{1}H NMR PEO 2 kDa G3.0

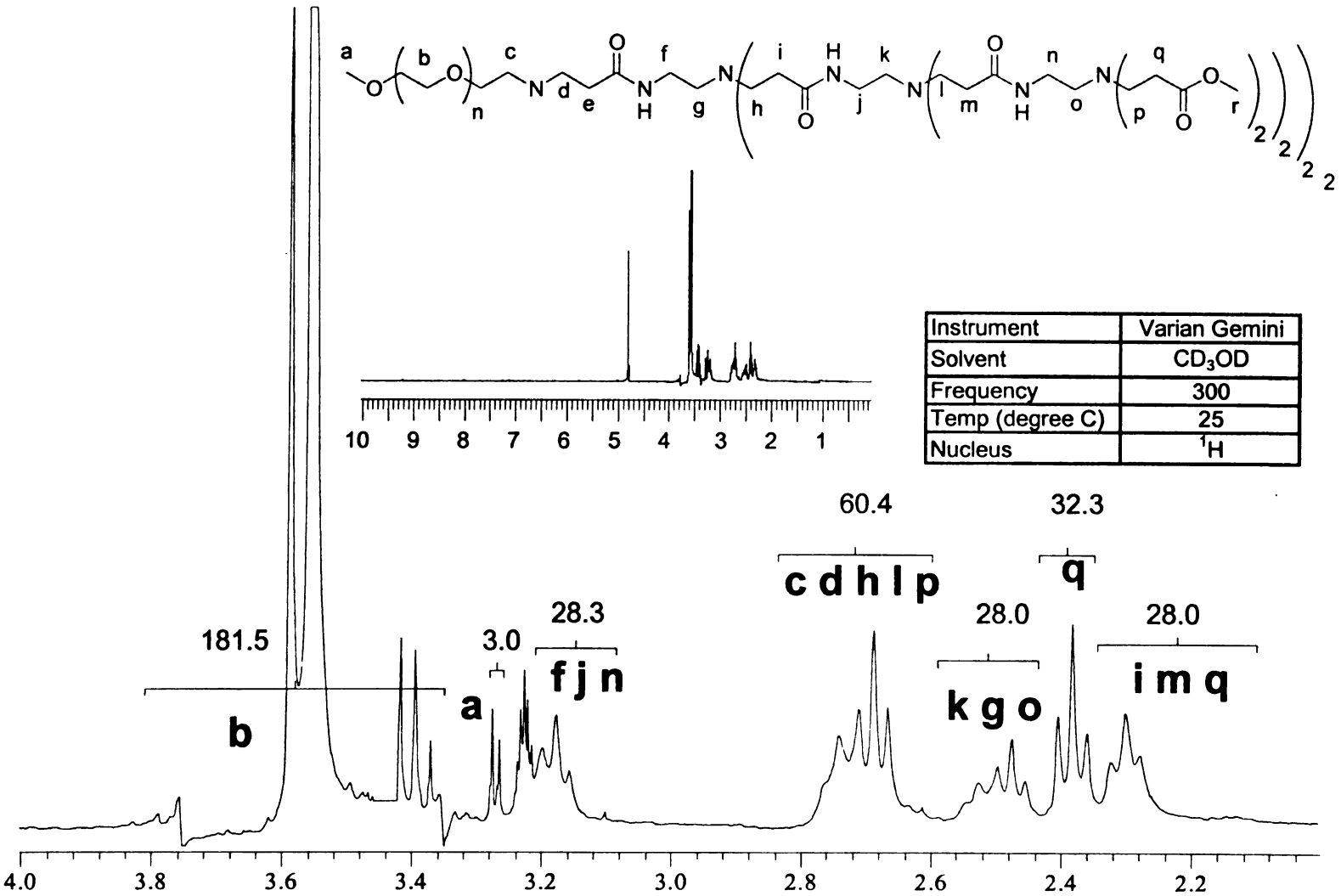

Figure C.20. ^{1}H NMR PEO 2 kDa G3.5

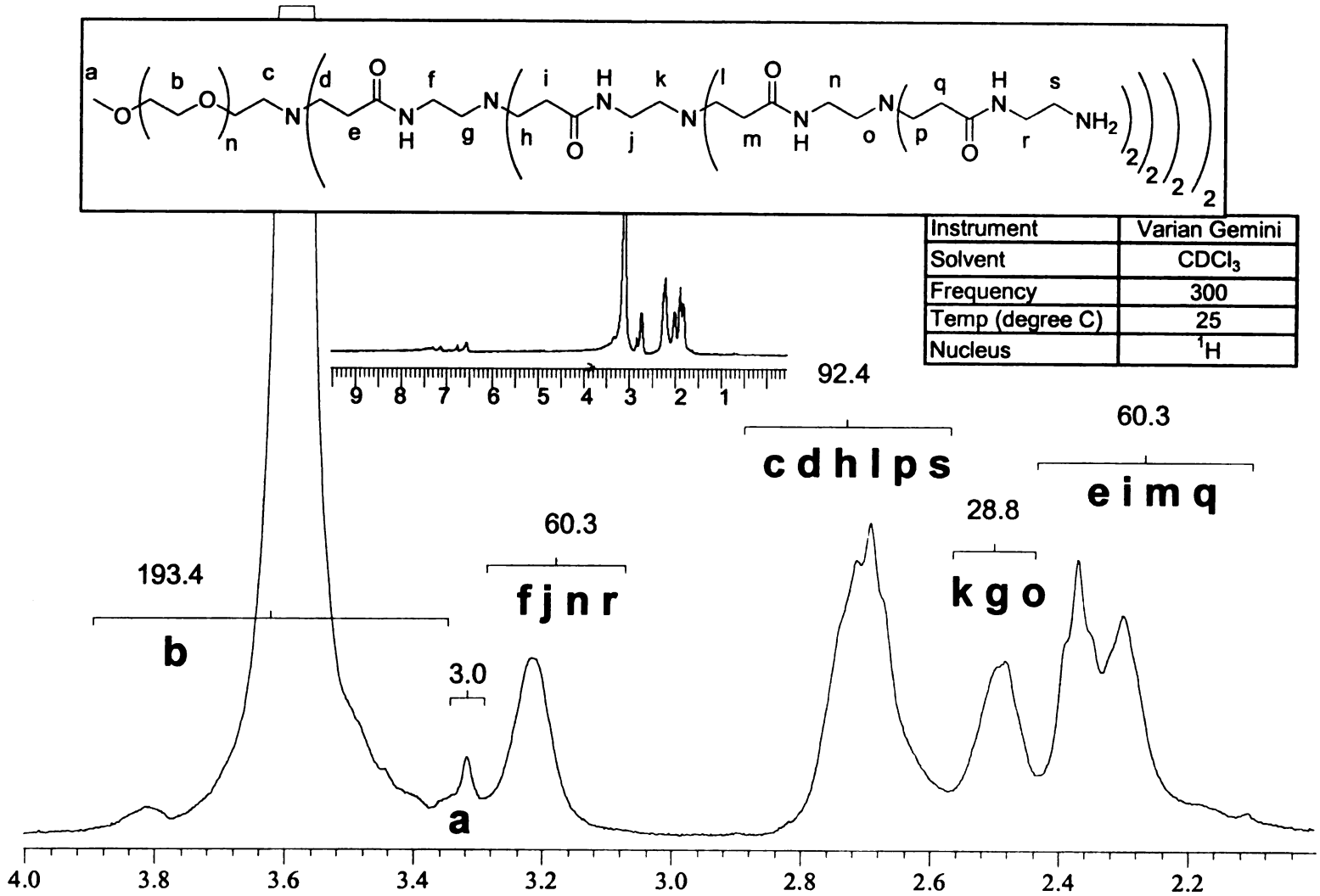

Figure C.21. ^{1}H NMR PEO 2 kDa G4.0

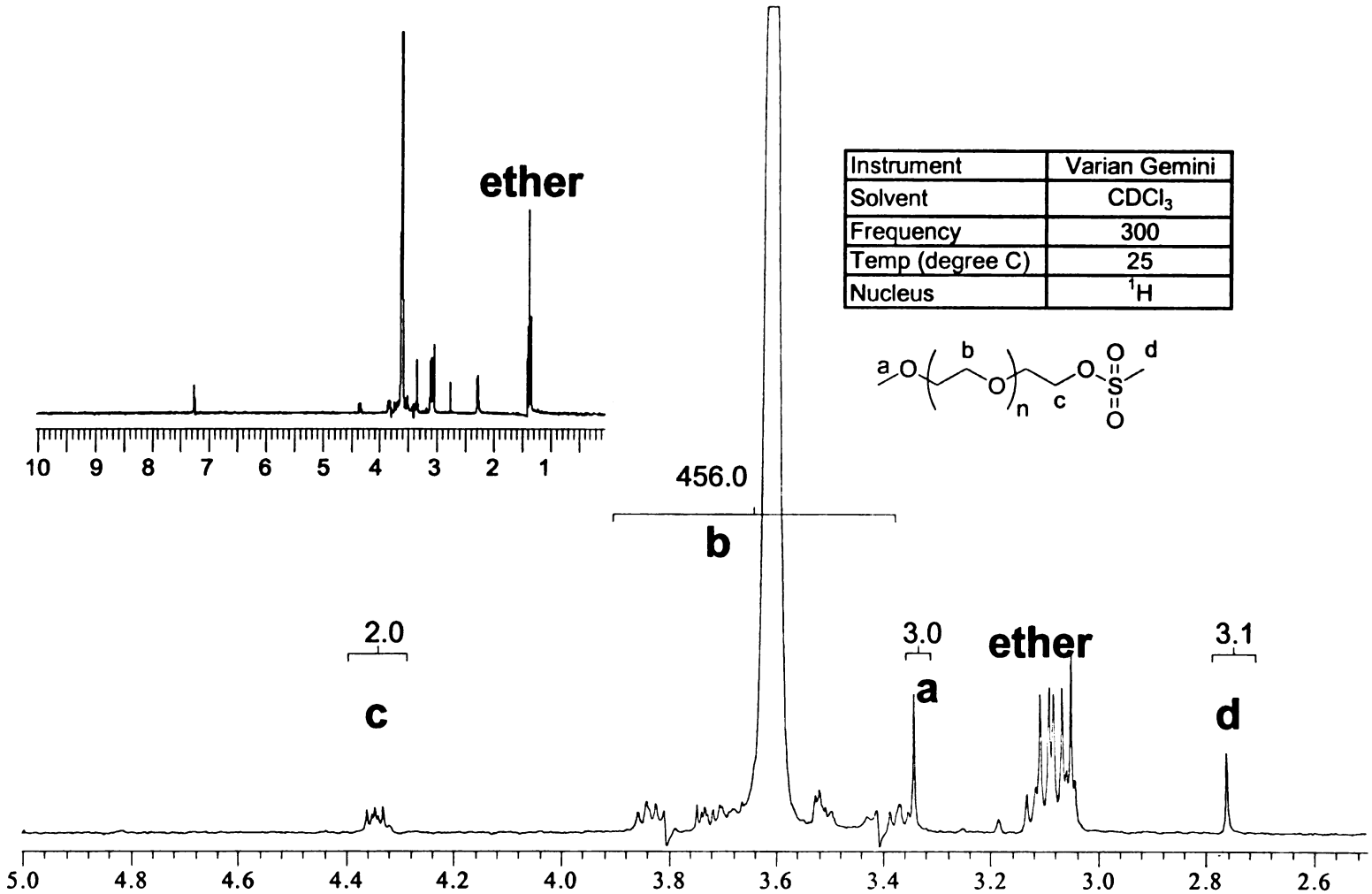

Figure C.22. ^{1}H NMR PEO 5 kDa OMs

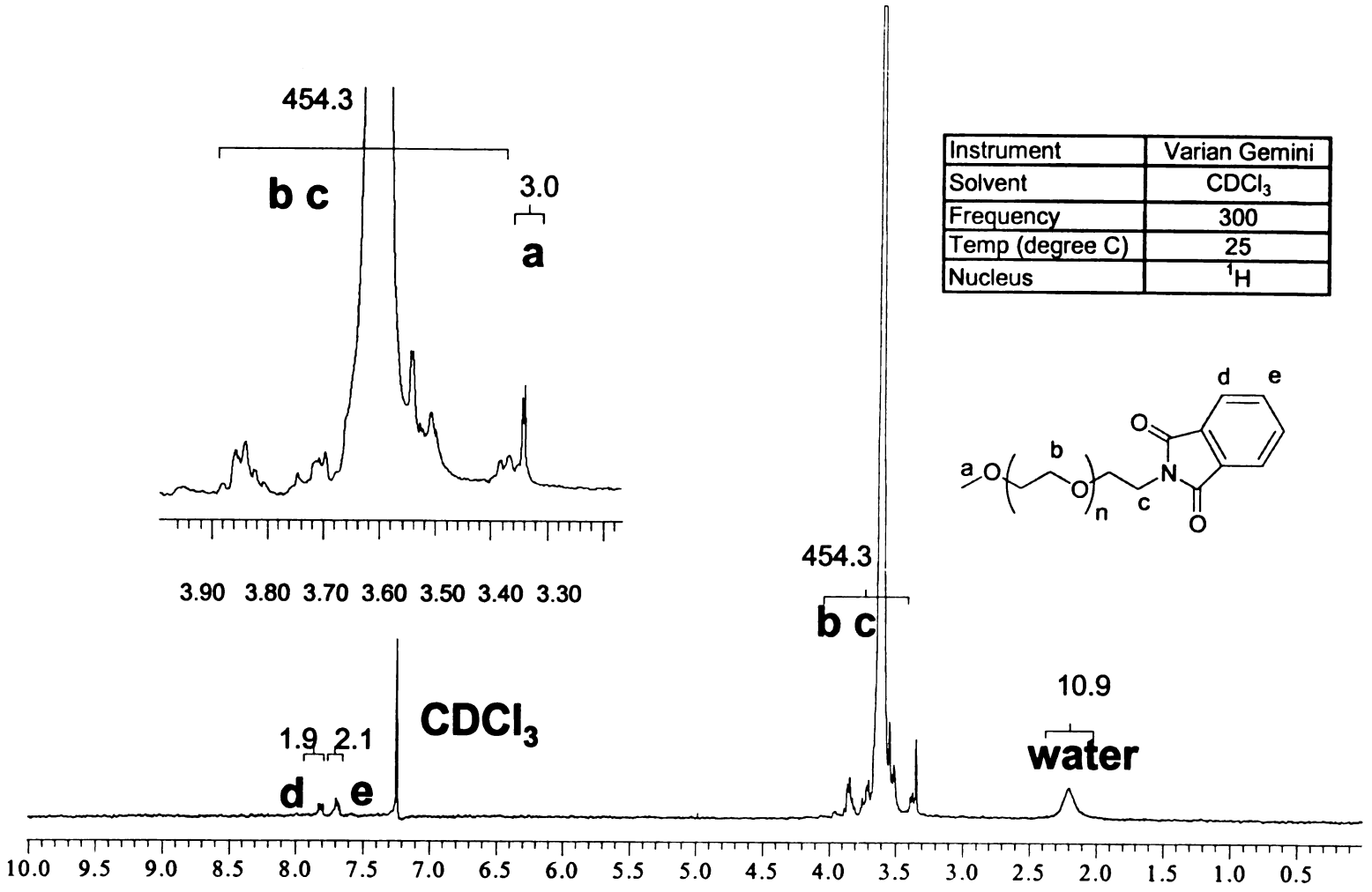

Figure C.23. ^{1}H NMR PEO 5 kDa phth

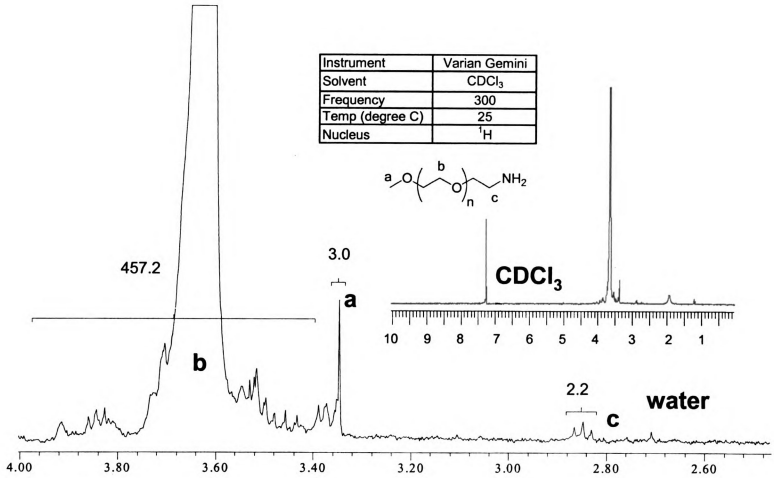

Figure C.24. ^{1}H NMR PEO 5 kDa NH_2

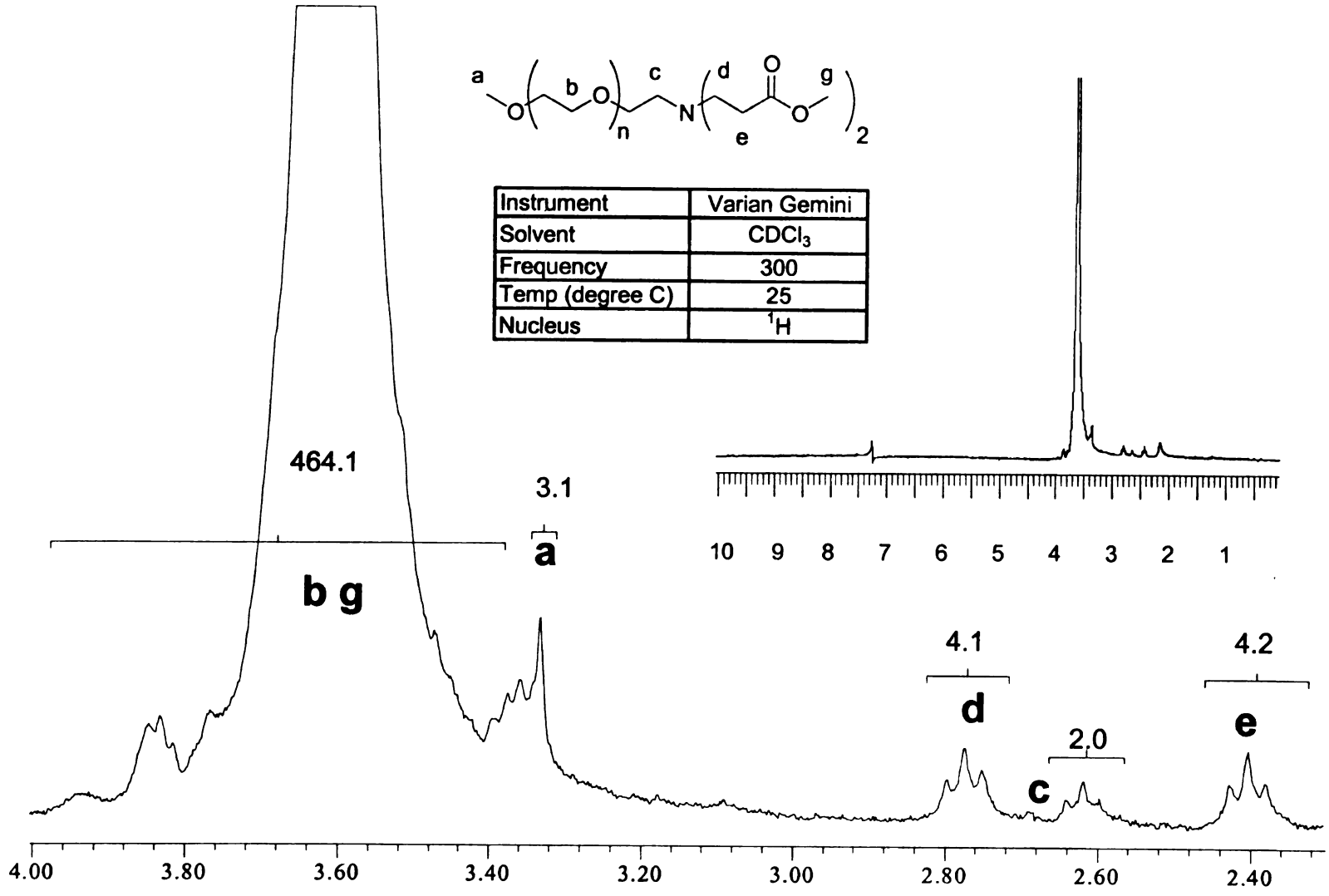

Figure C.25. ^{1}H NMR PEO 5 kDa G0.5

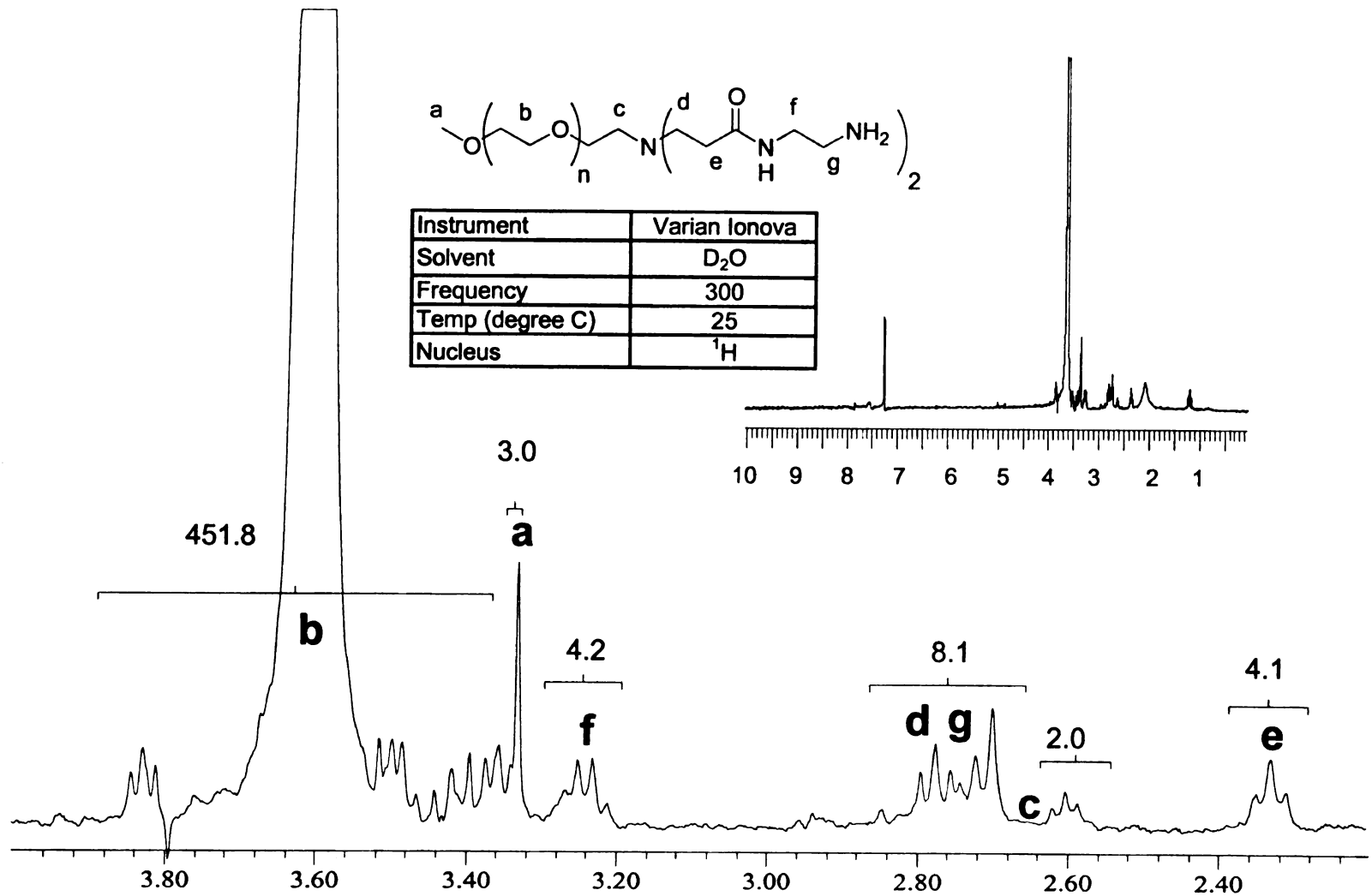

Figure C.26. ^{1}H NMR PEO 5 kDa G1.0

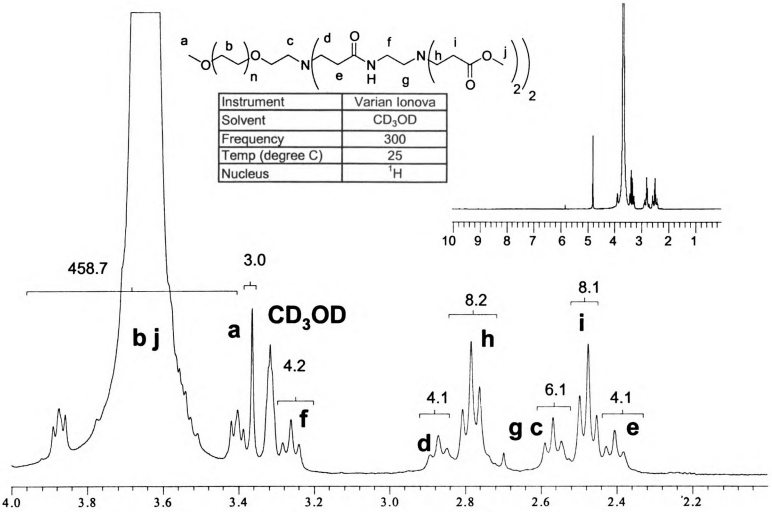

Figure C.27. ^{1}H NMR PEO 5 kDa G1.5

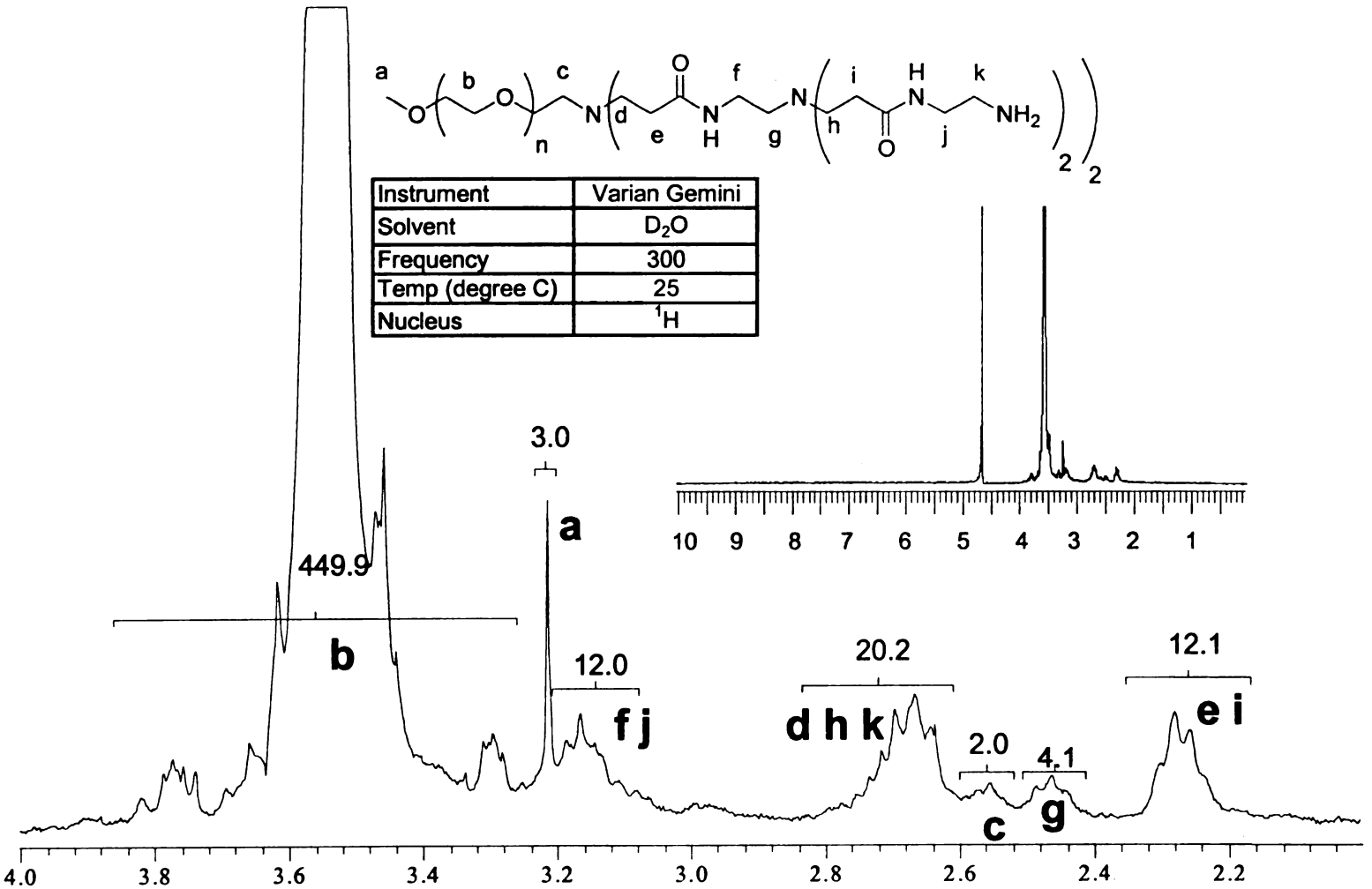

Figure C.28. ^{1}H NMR PEO 5 kDa G2.0

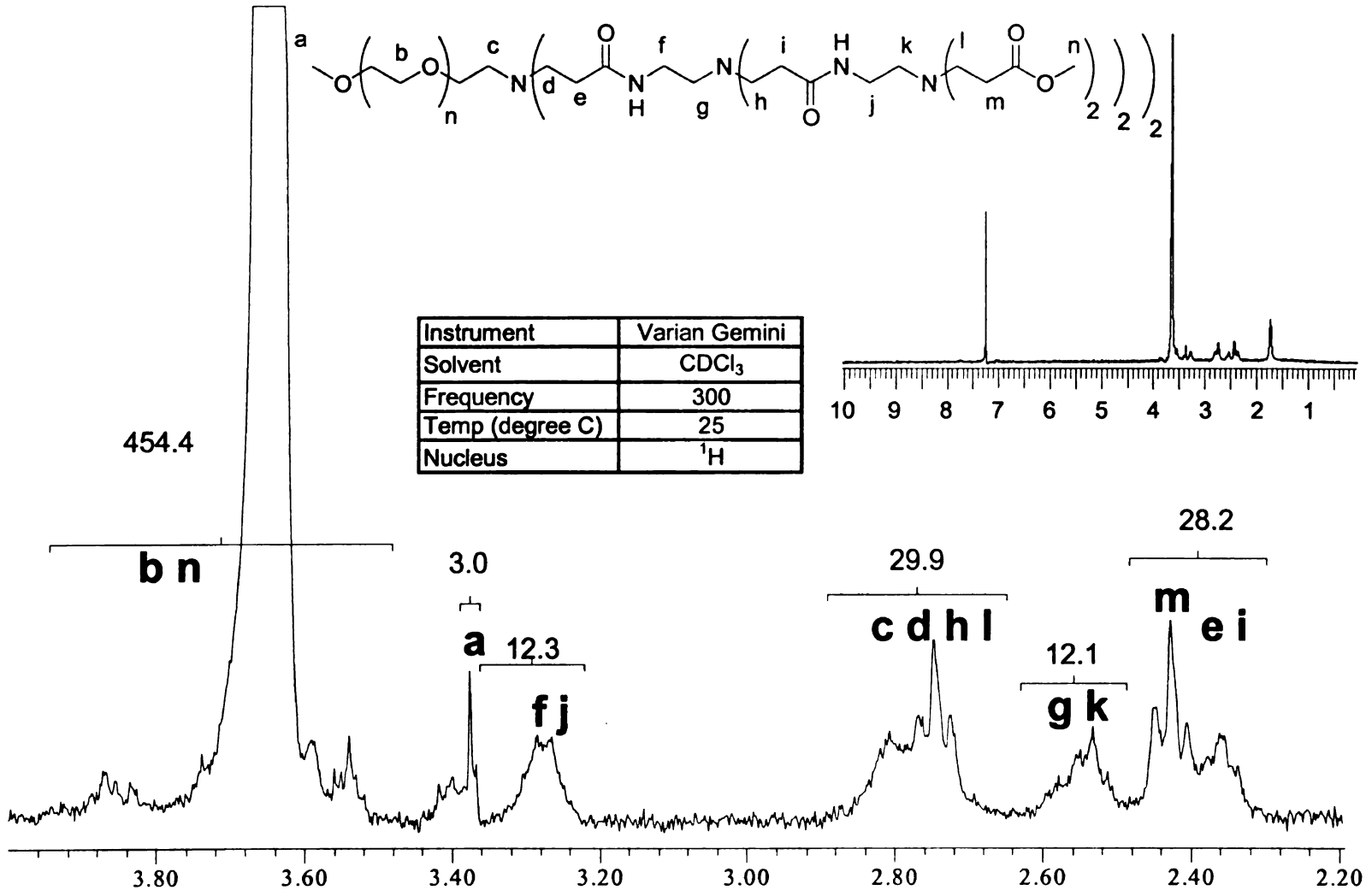

Figure C.29. ^{1}H NMR PEO 5 kDa G2.5

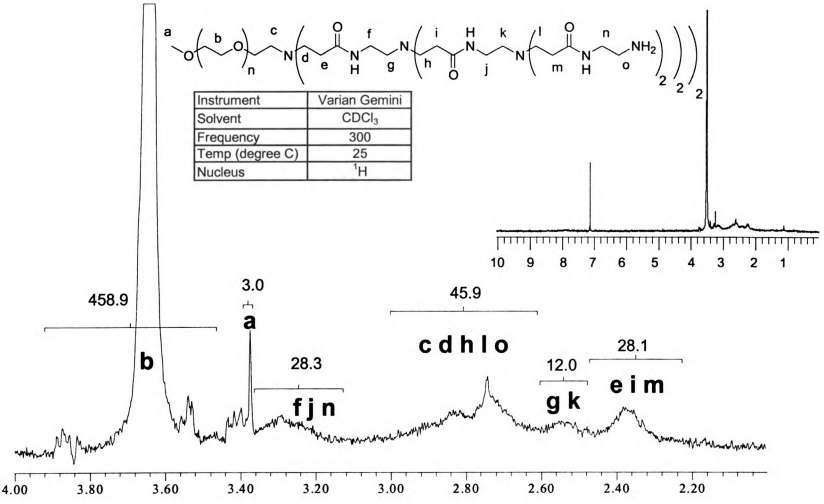

Figure C.30. ^{1}H NMR PEO 5 kDa G 3.0

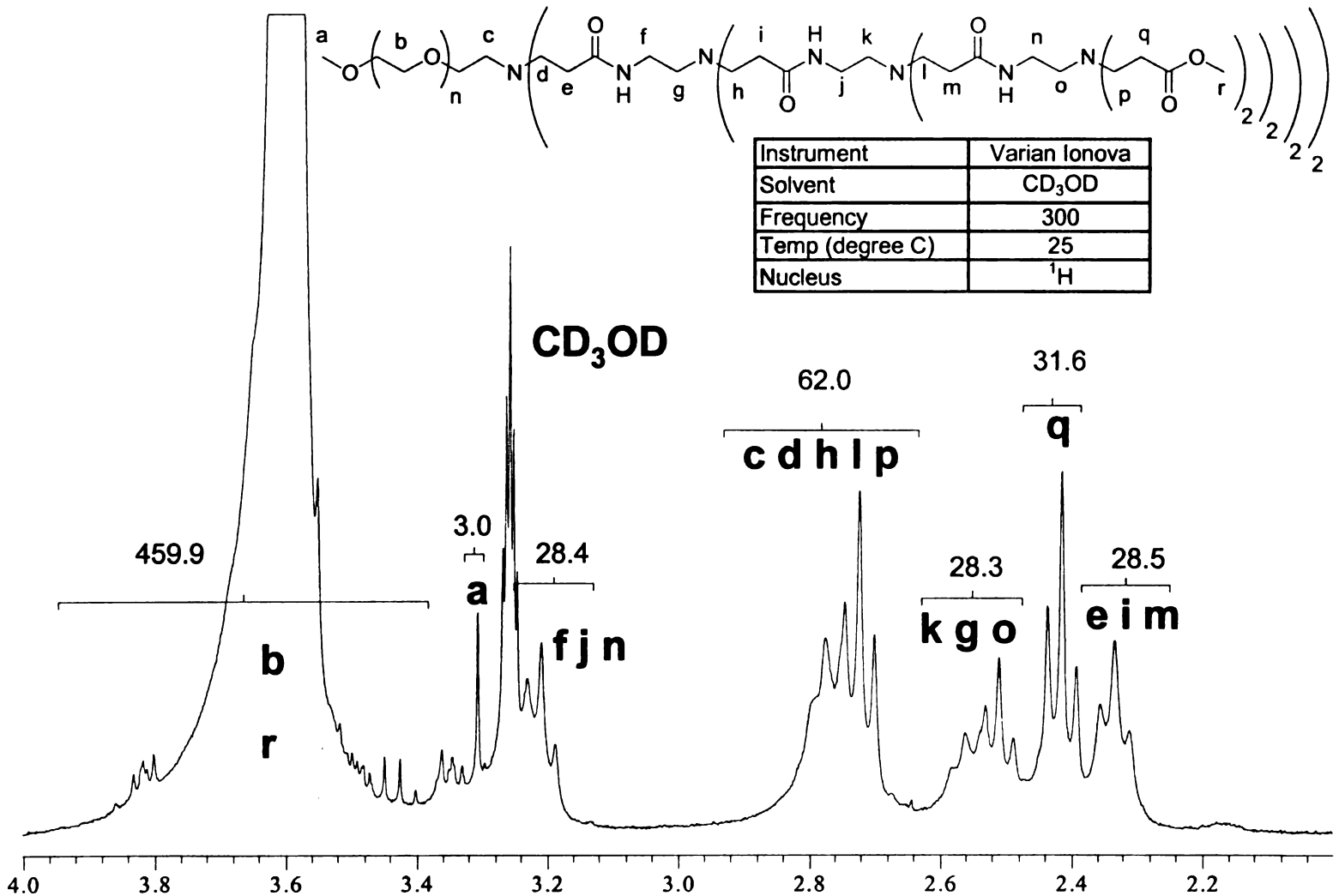

Figure C. 31. ^{1}H NMR PEO 5 kDa G3.5

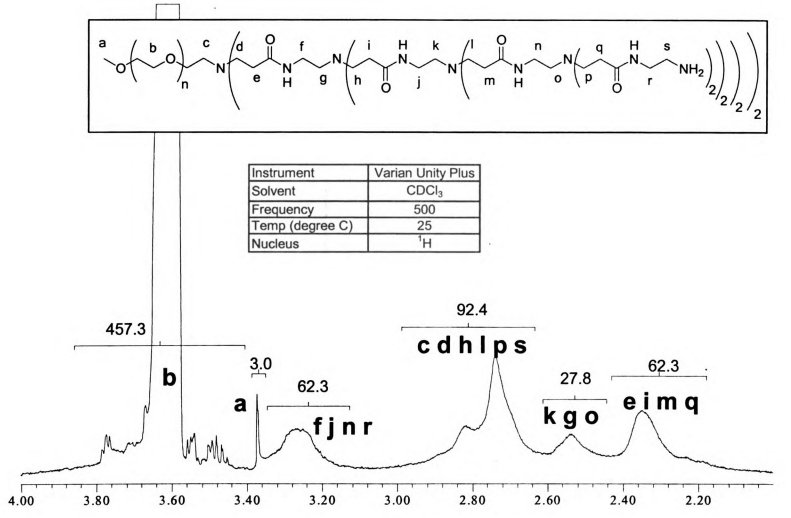

Figure C.32. ^{1}H NMR PEO 5 kDa G4.0

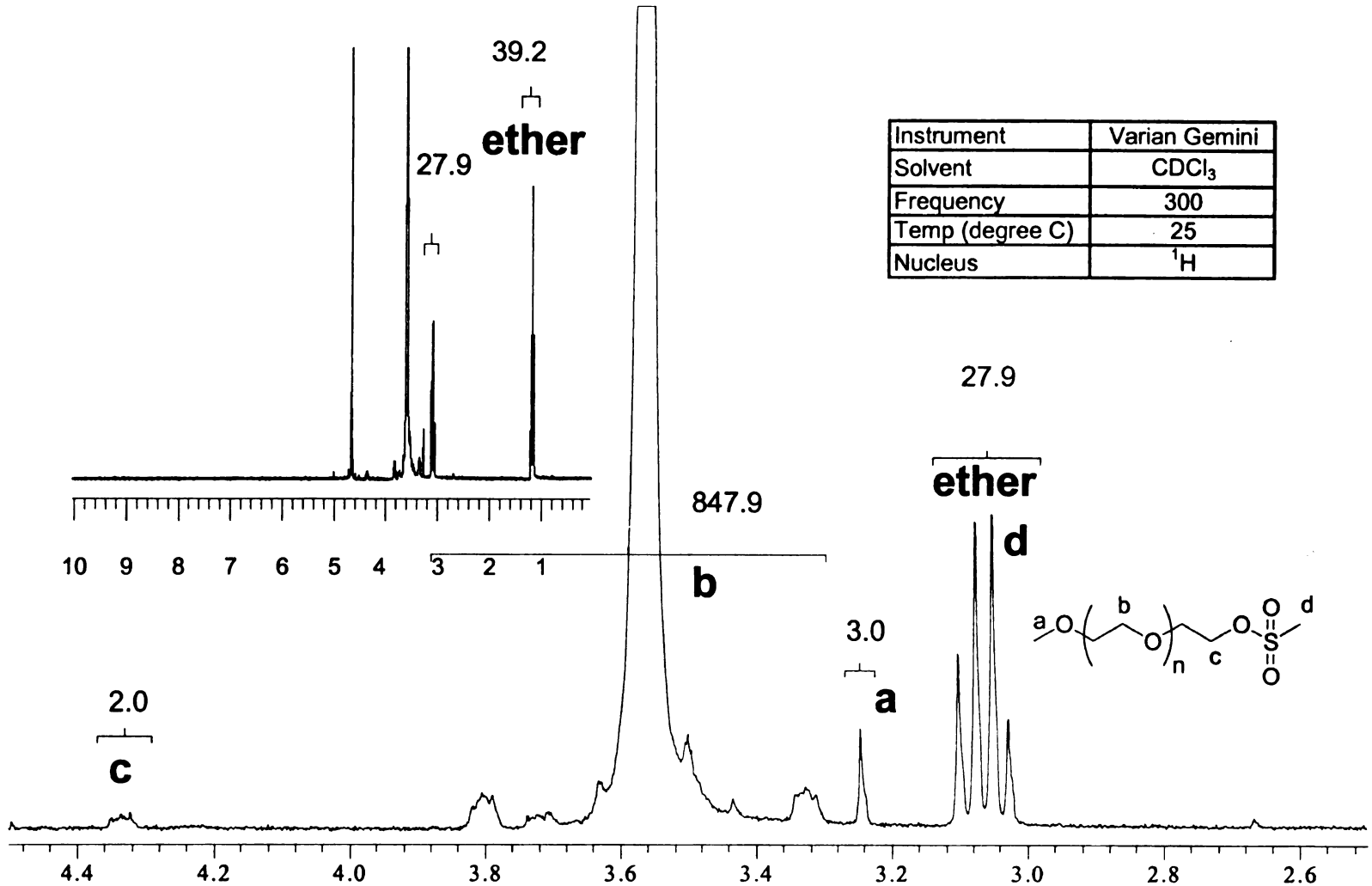

Figure C.33. ^{1}H NMR PEO 9 kDa OMs

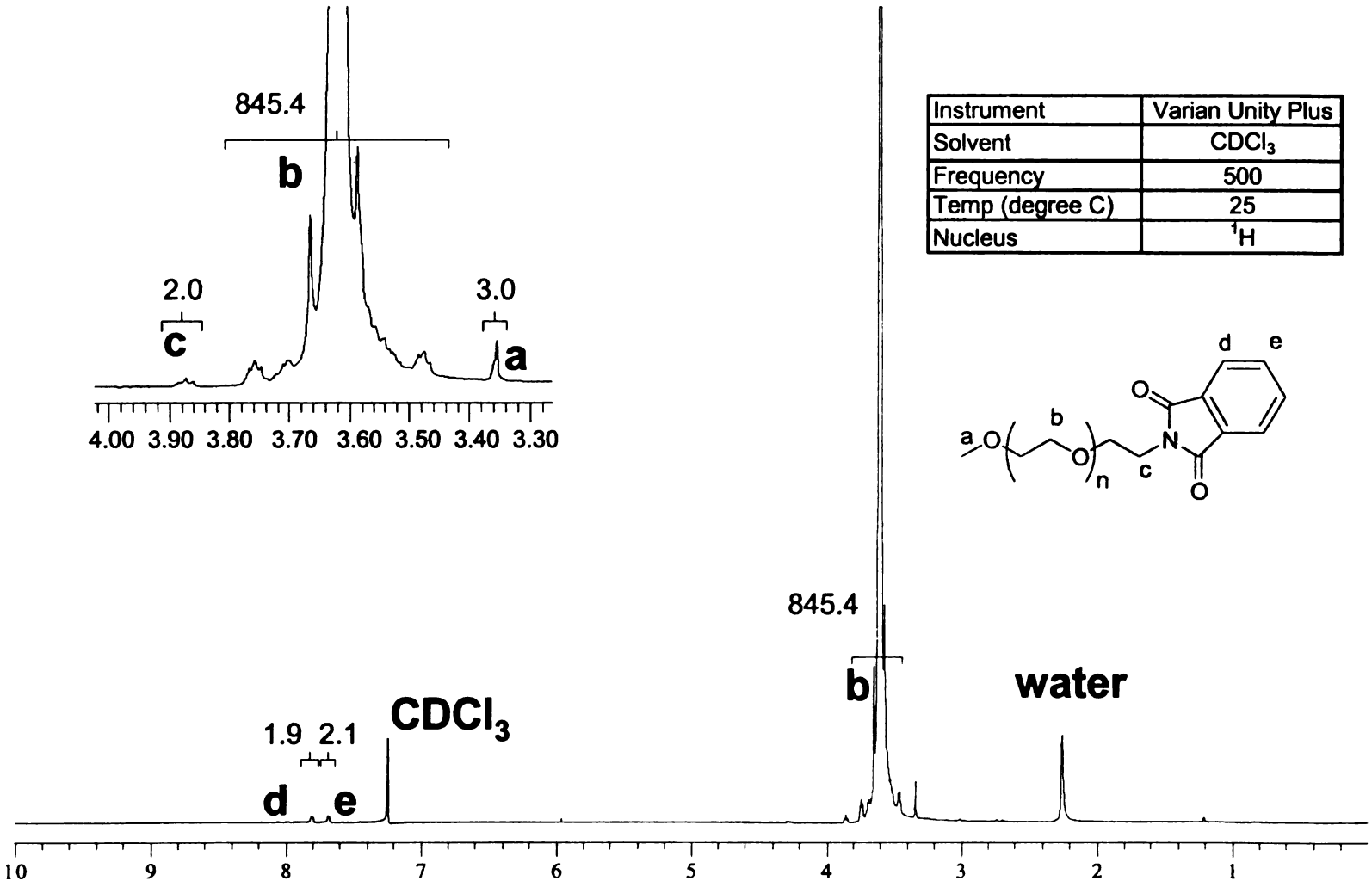

Figure C.34. ^{1}H NMR PEO 9 kDa phth

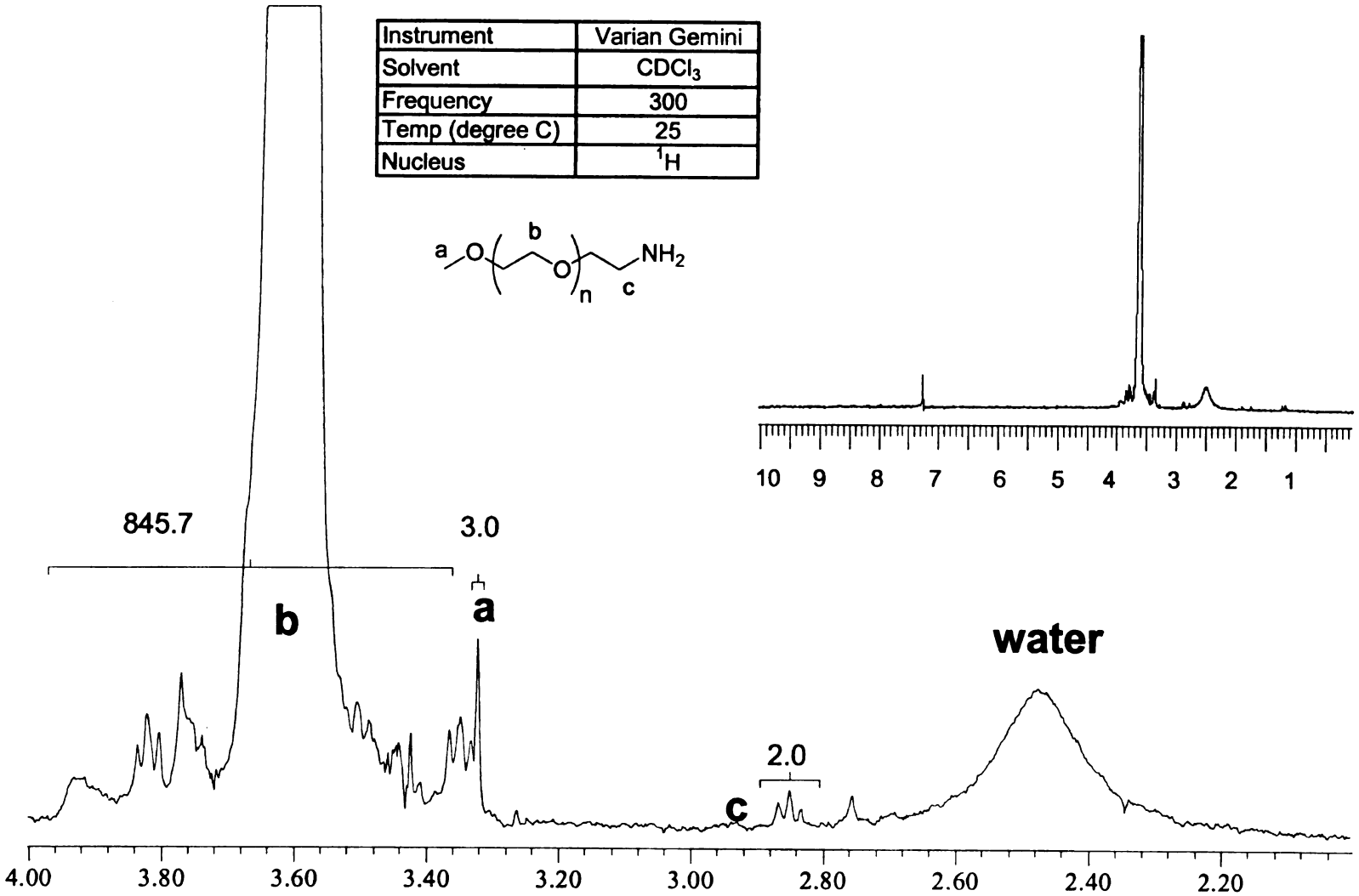

Figure C.35. ^{1}H NMR PEO 9 kDa NH_2

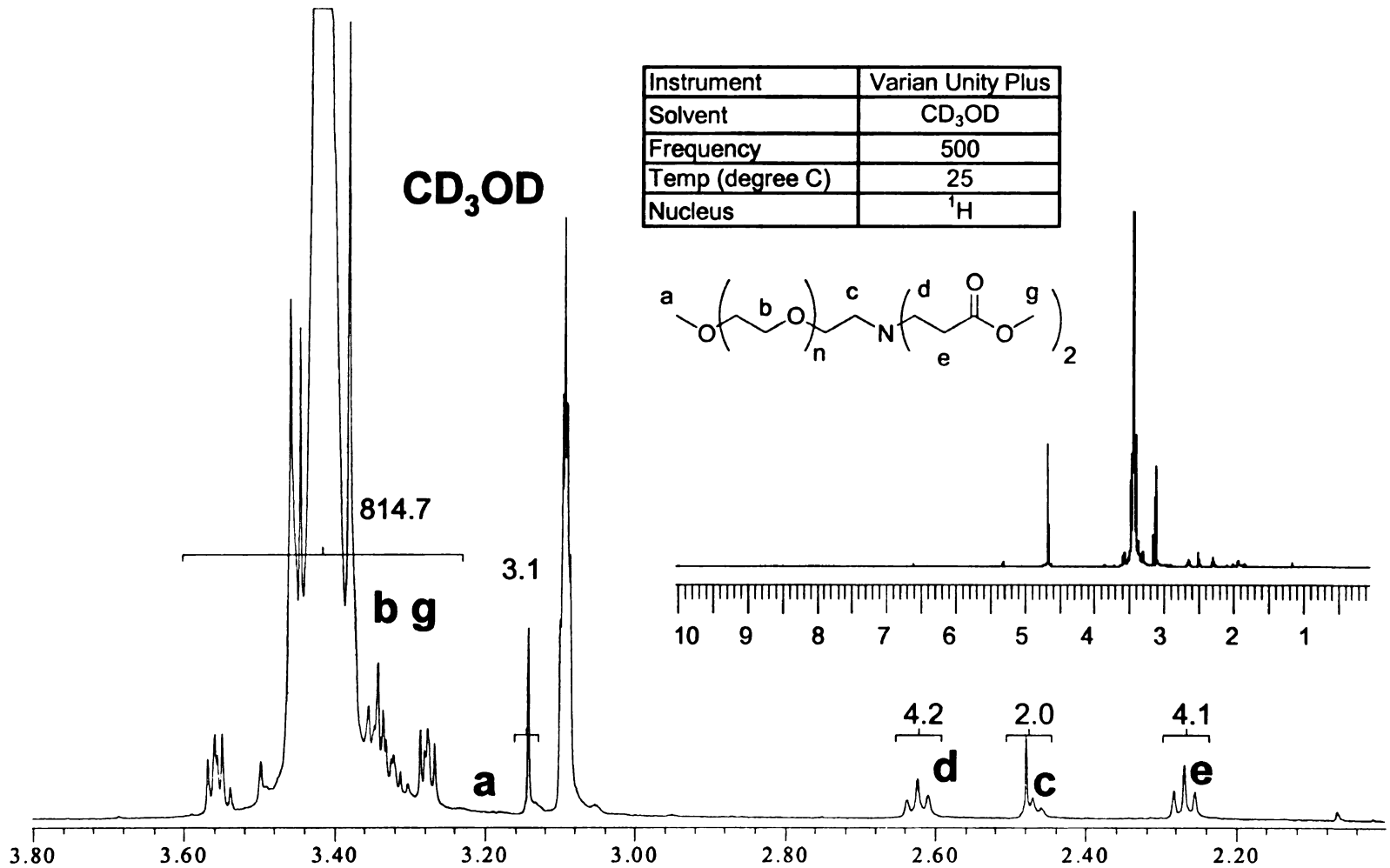

Figure C.36. ^{1}H NMR PEO 9 kDa G0.5

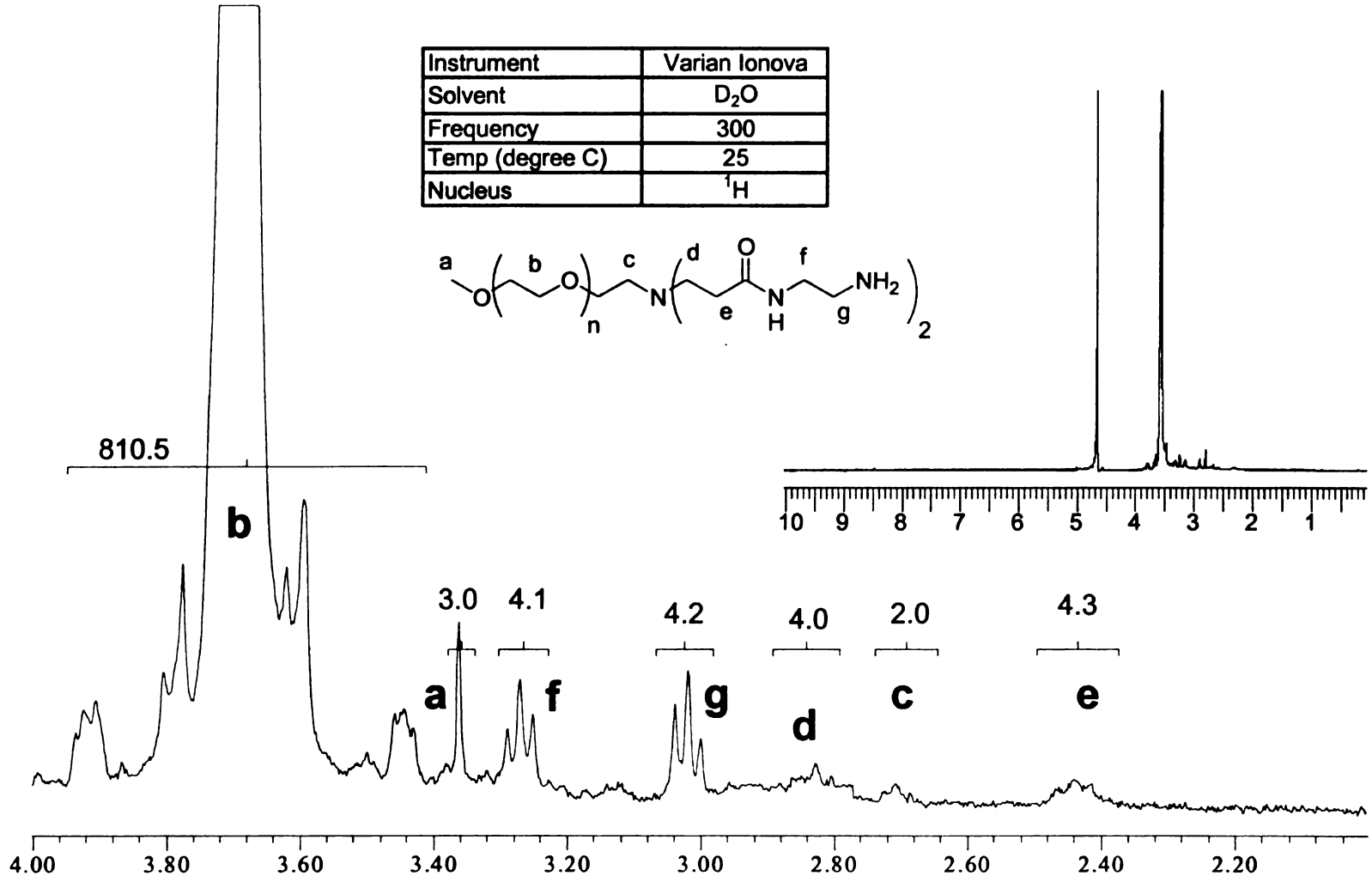

Figure C.37. ^{1}H NMR PEO 9 kDa G1.0

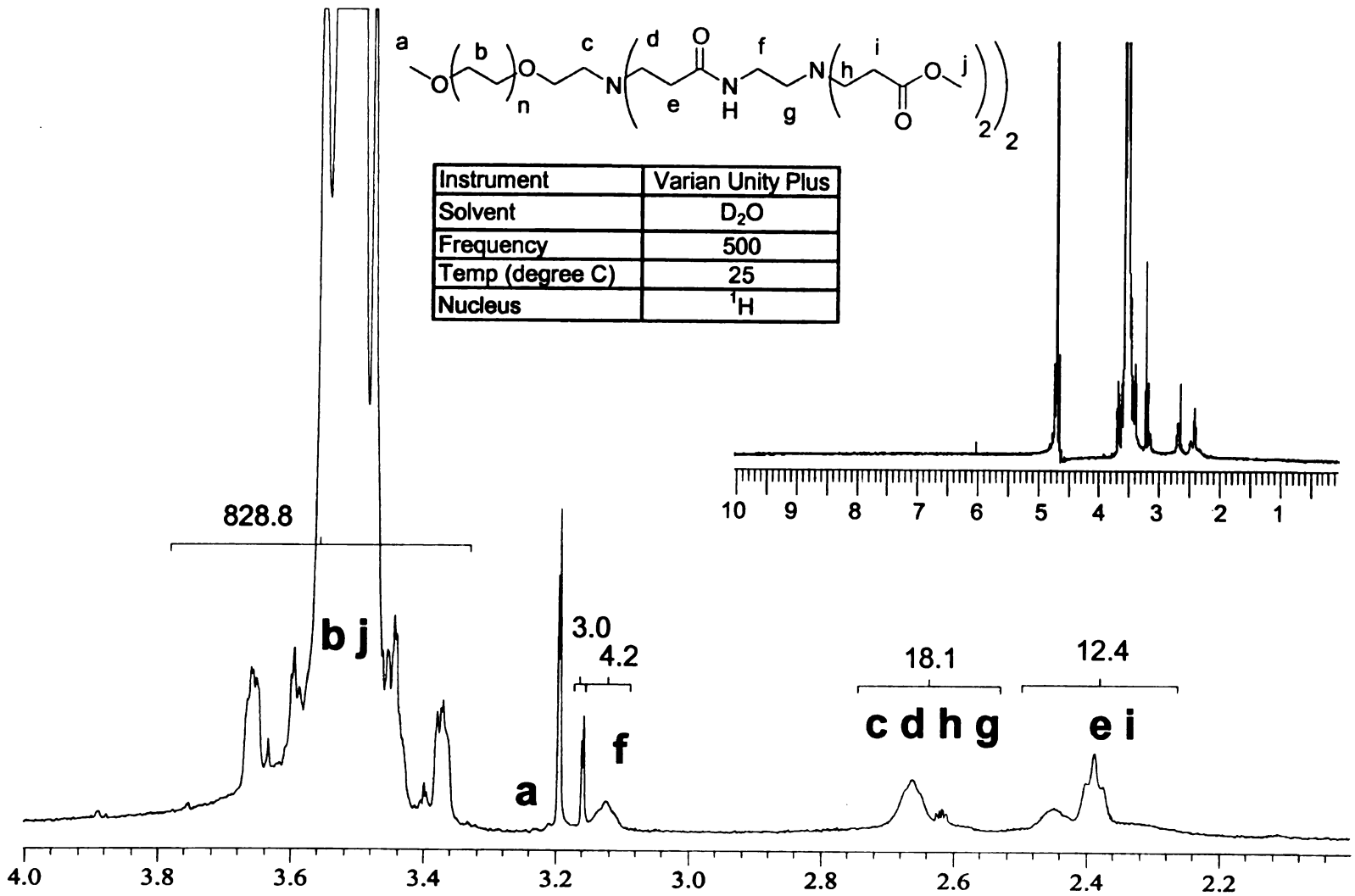

Figure C.38. ^{1}H NMR PEO 9 kDa G1.5

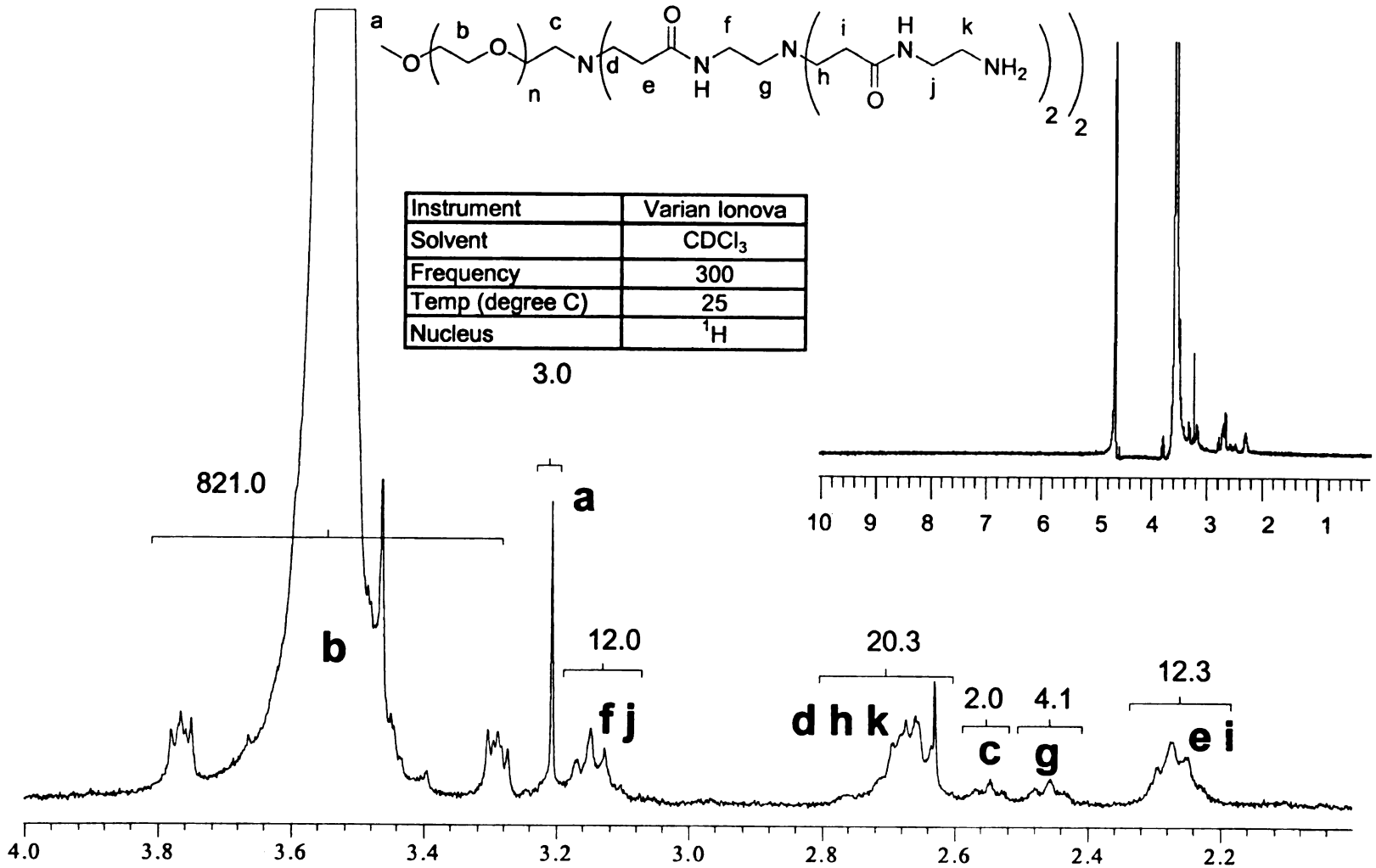

Figure C.39. ^{1}H NMR PEO 9 kDa G2.0

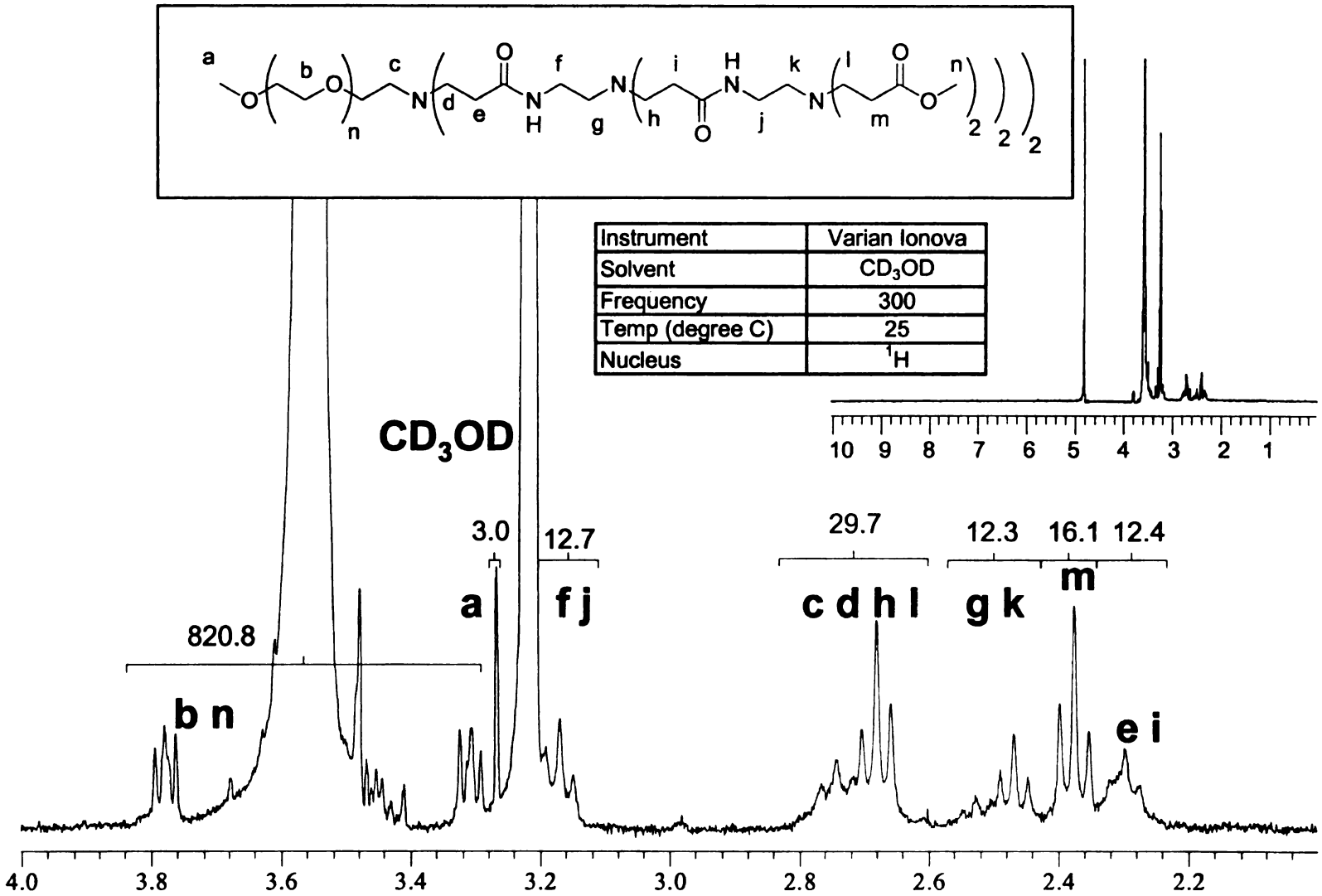

Figure C.40. ^{1}H NMR PEO 9 kDa G2.5

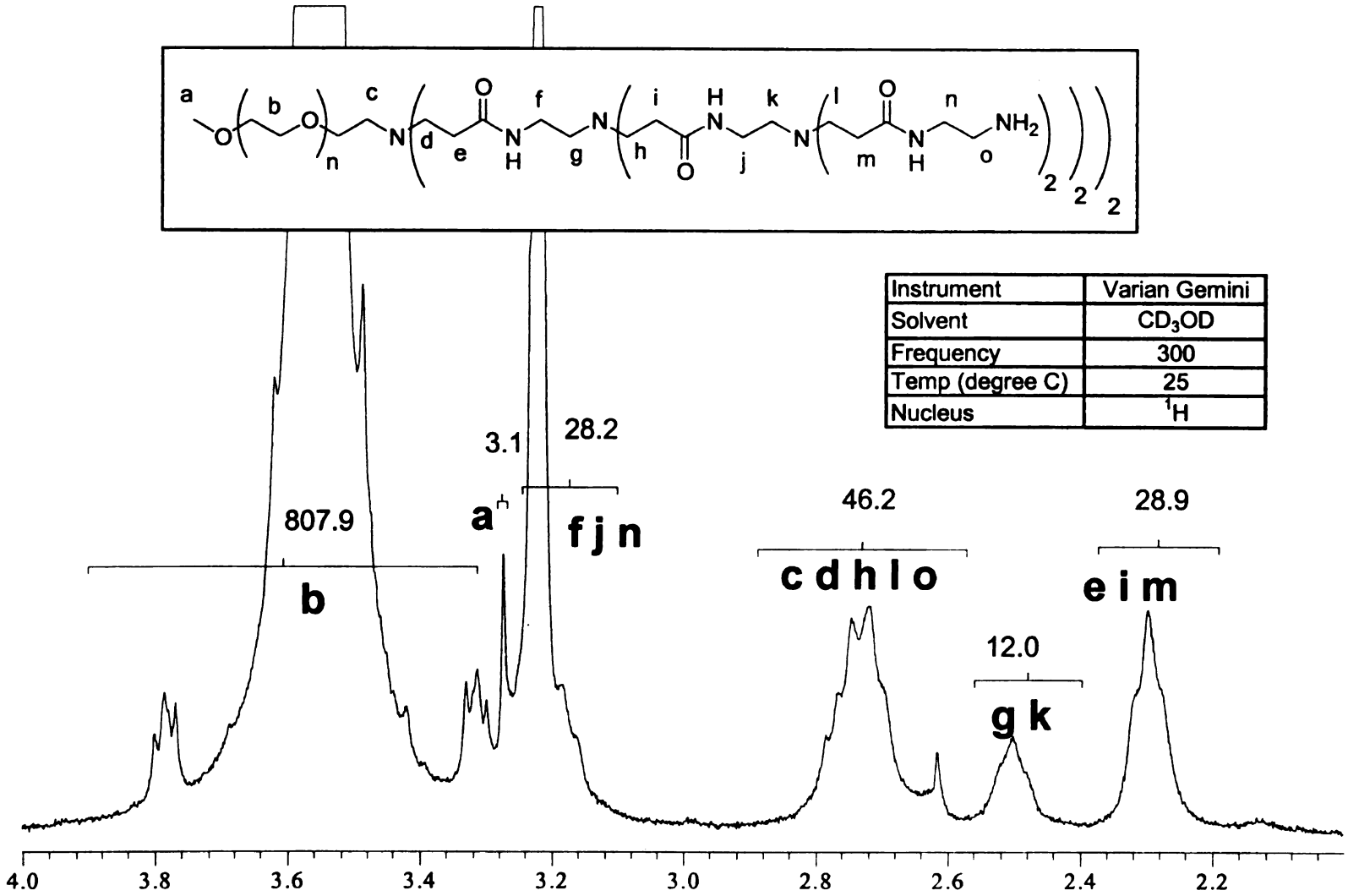

Figure C.41. ^{1}H NMR PEO 9 kDa G3.0

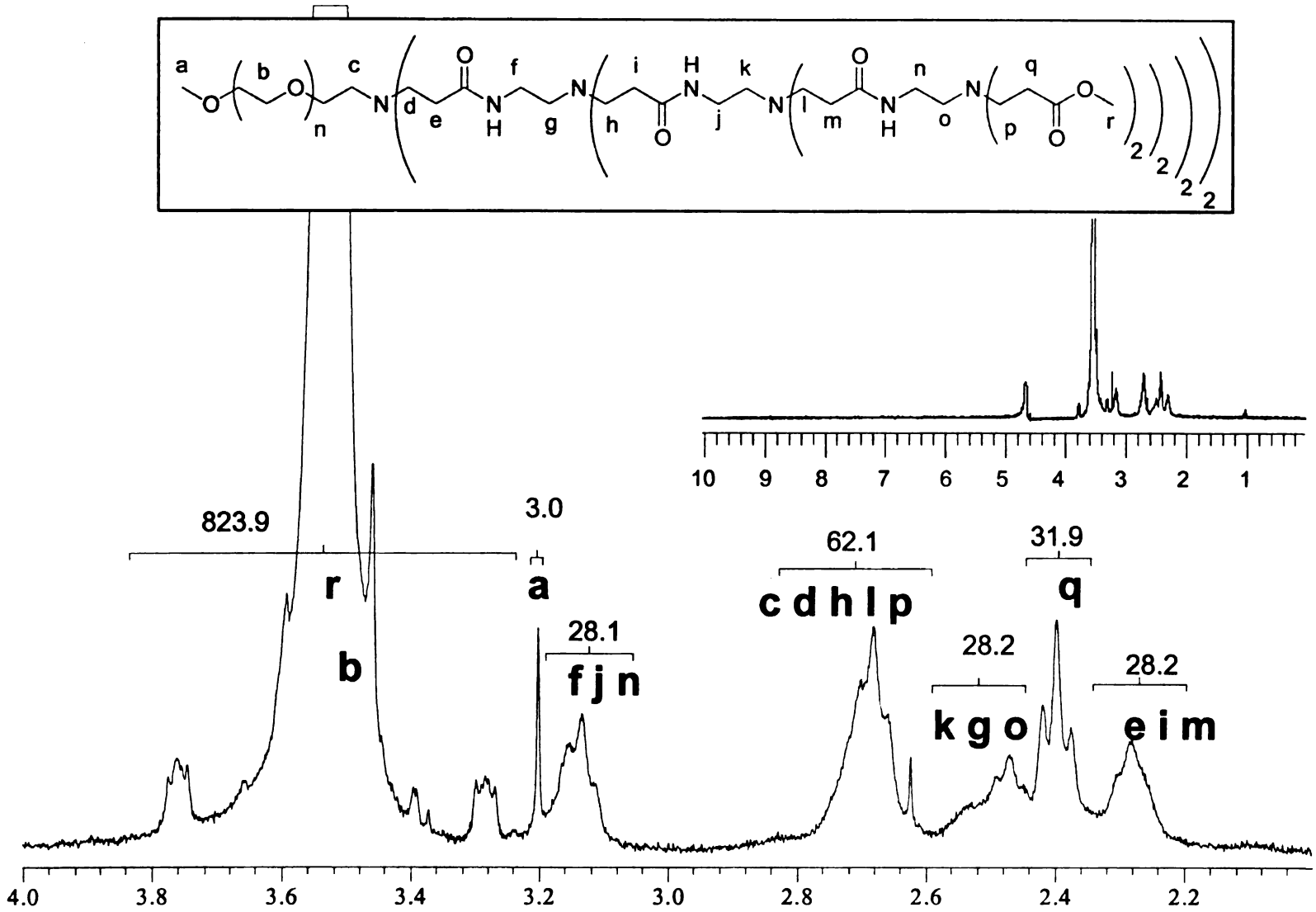

Figure C.42. ^{1}H NMR PEO 9 kDa G3.5

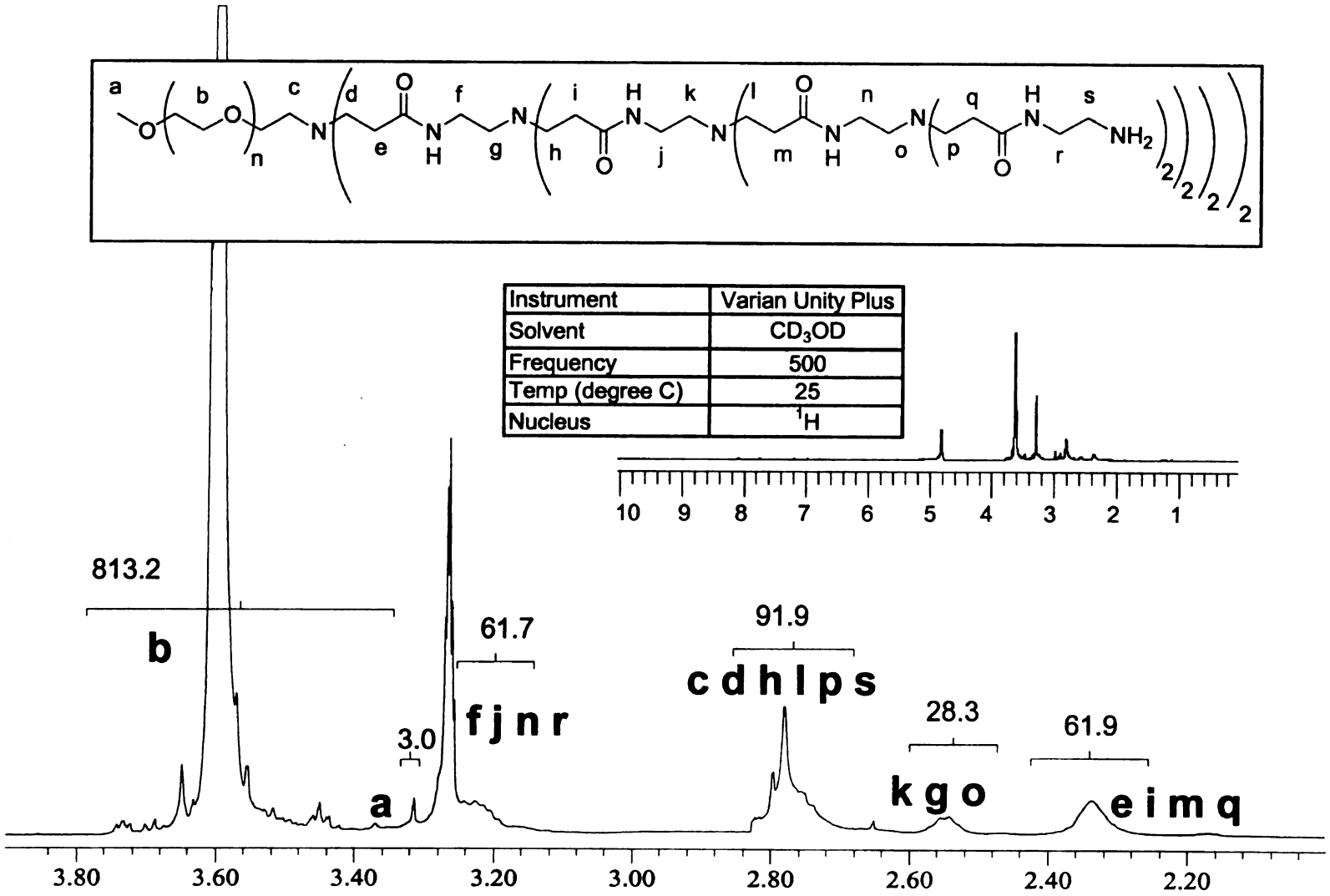

Figure C.43. ^{1}H NMR PEO 9 kDa G4.0

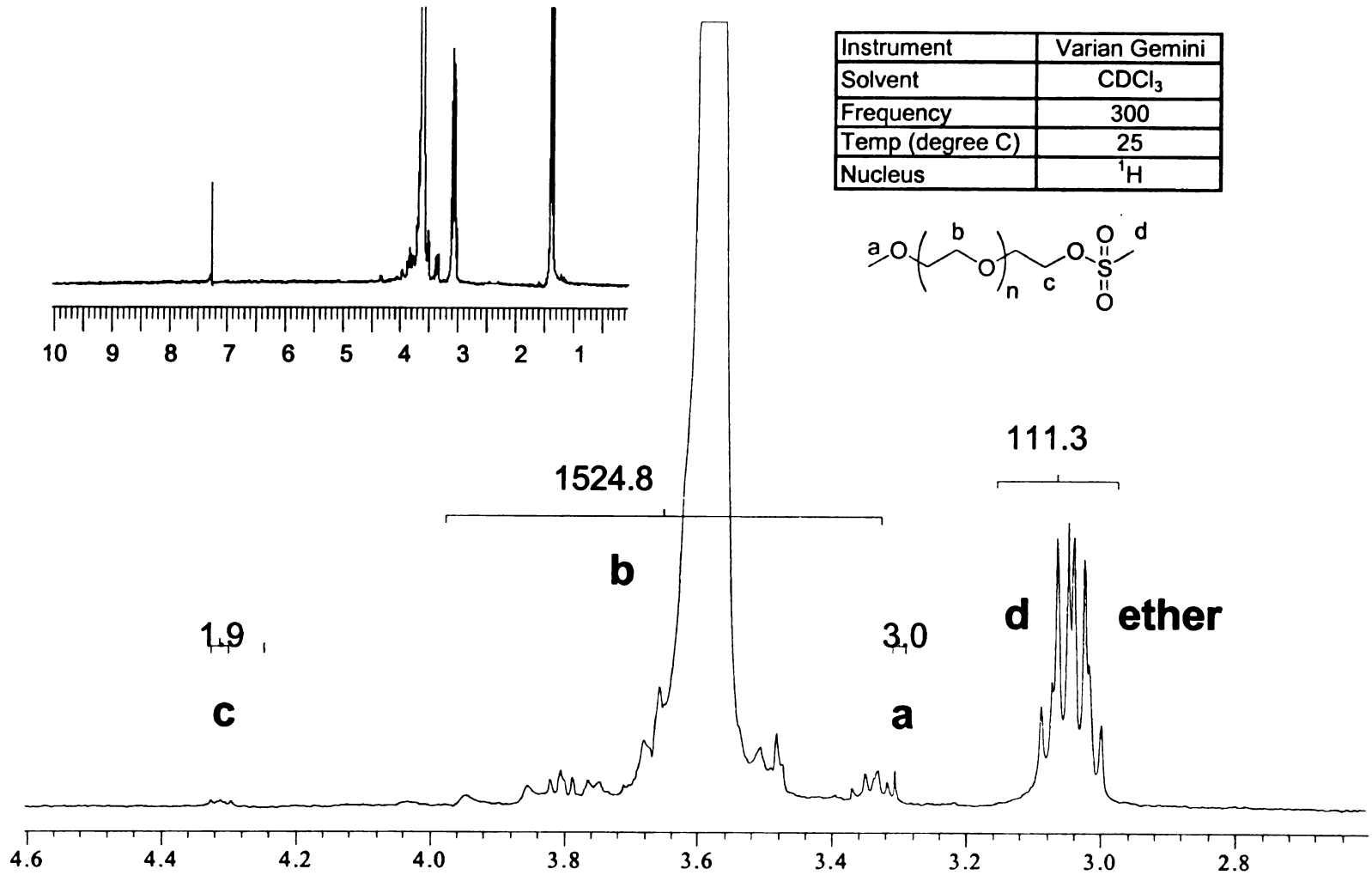

Figure C.44. ^{1}H NMR PEO 20 kDa OMs

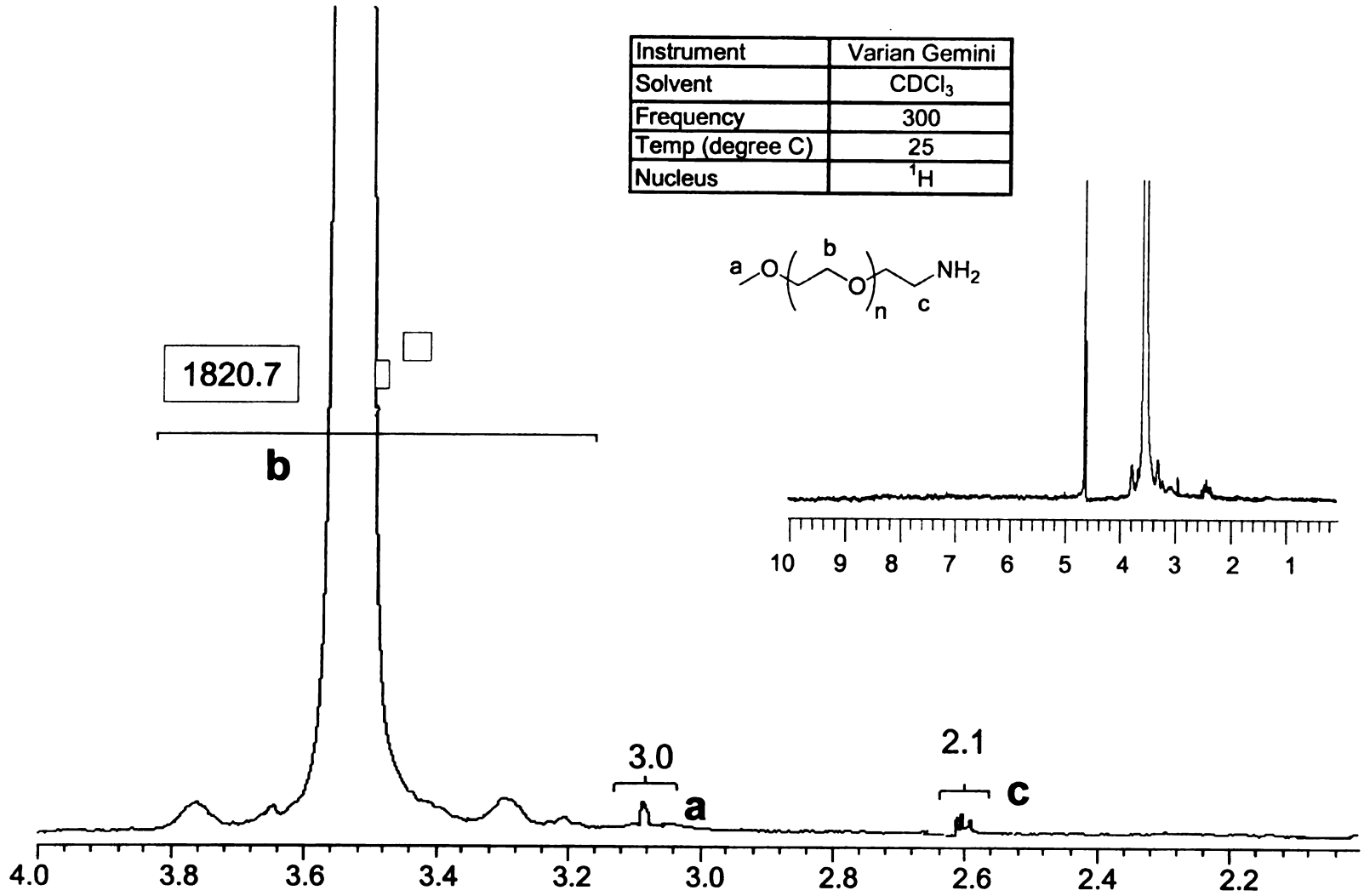

Figure C.45. ^{1}H NMR PEO 20 kDa NH_2

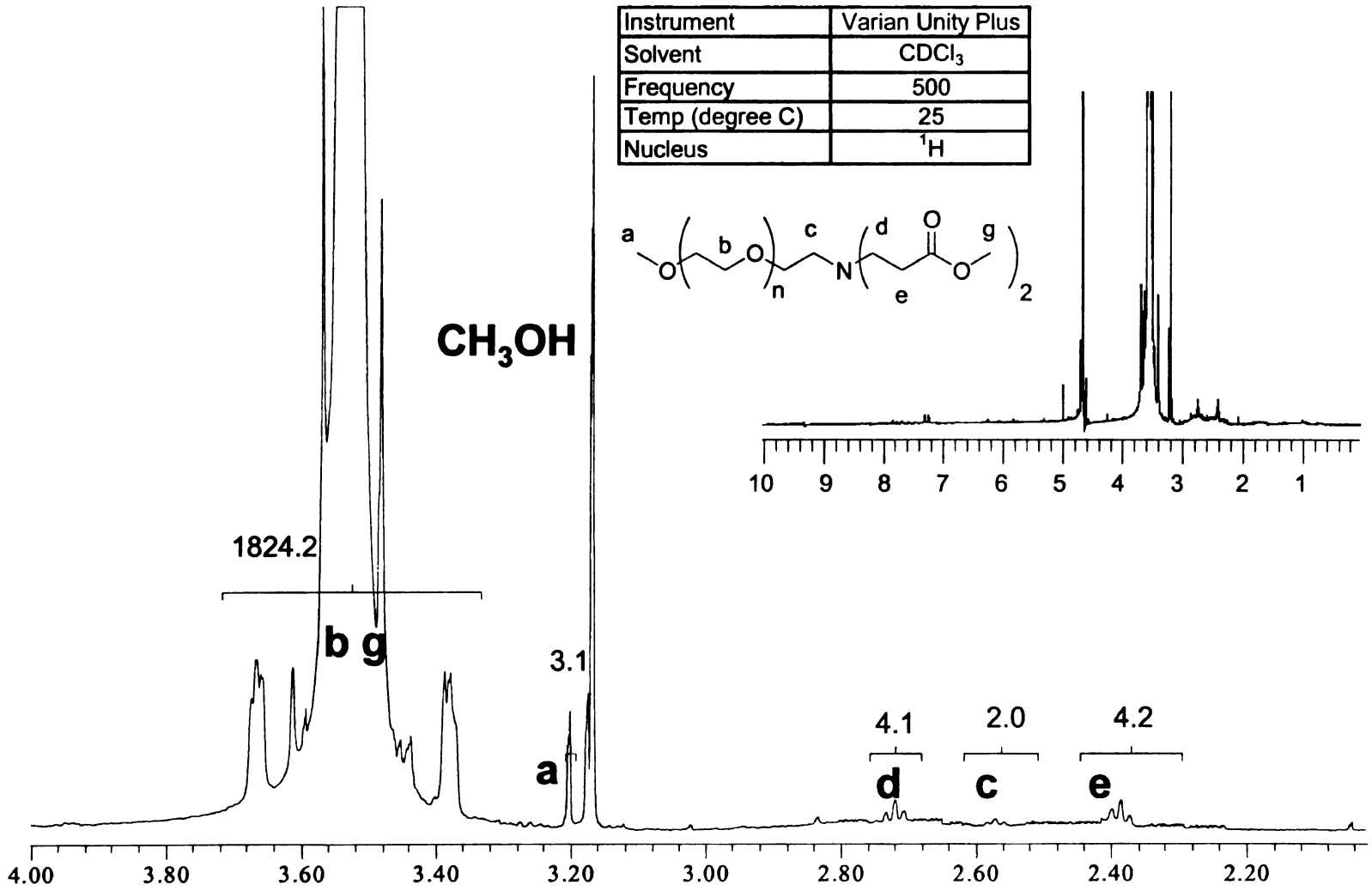

Figure C.46. ^{1}H NMR PEO 20 kDa G0.5

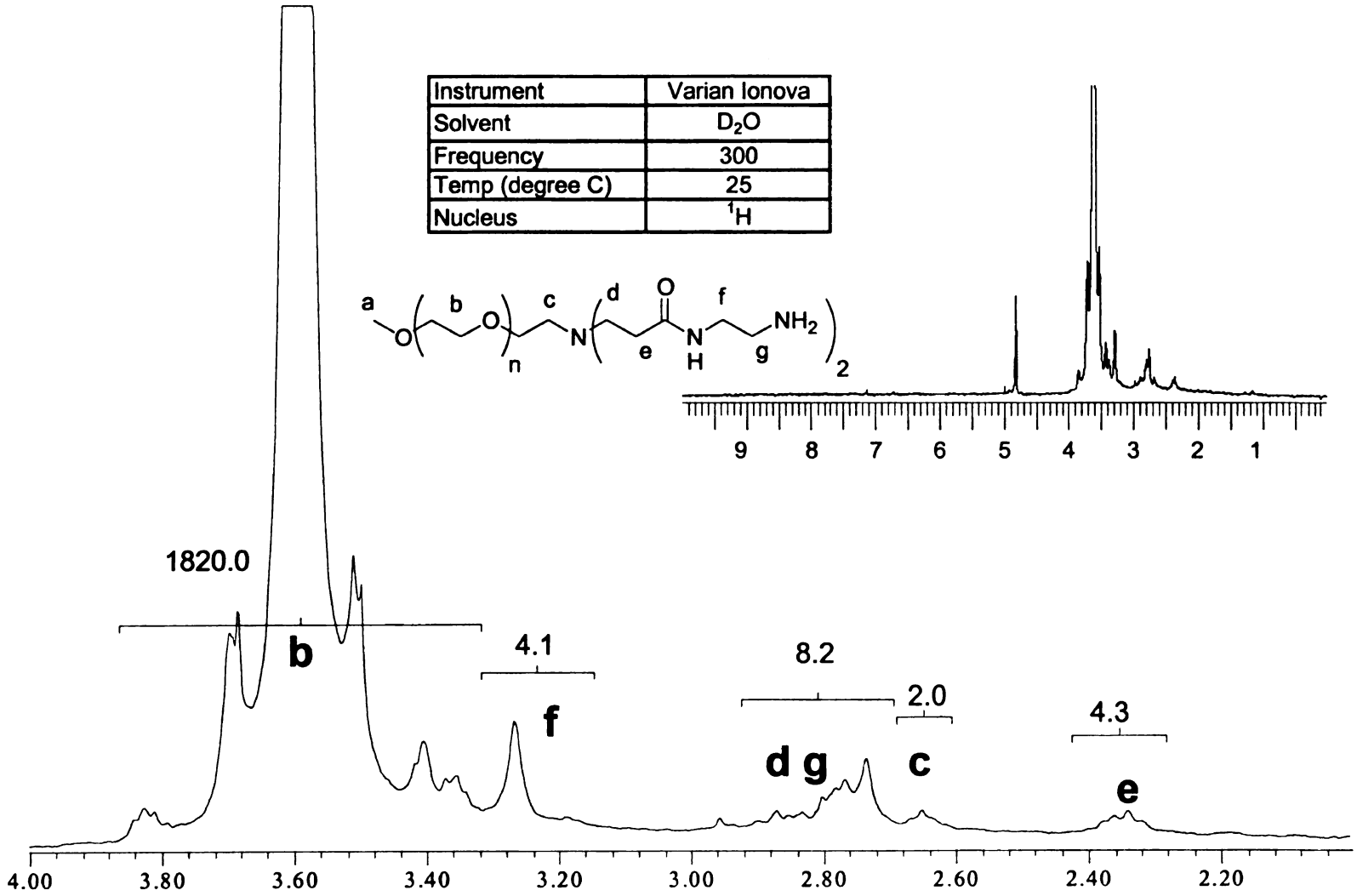

Figure C.47. ^1H NMR PEO 20 kDa G1.0

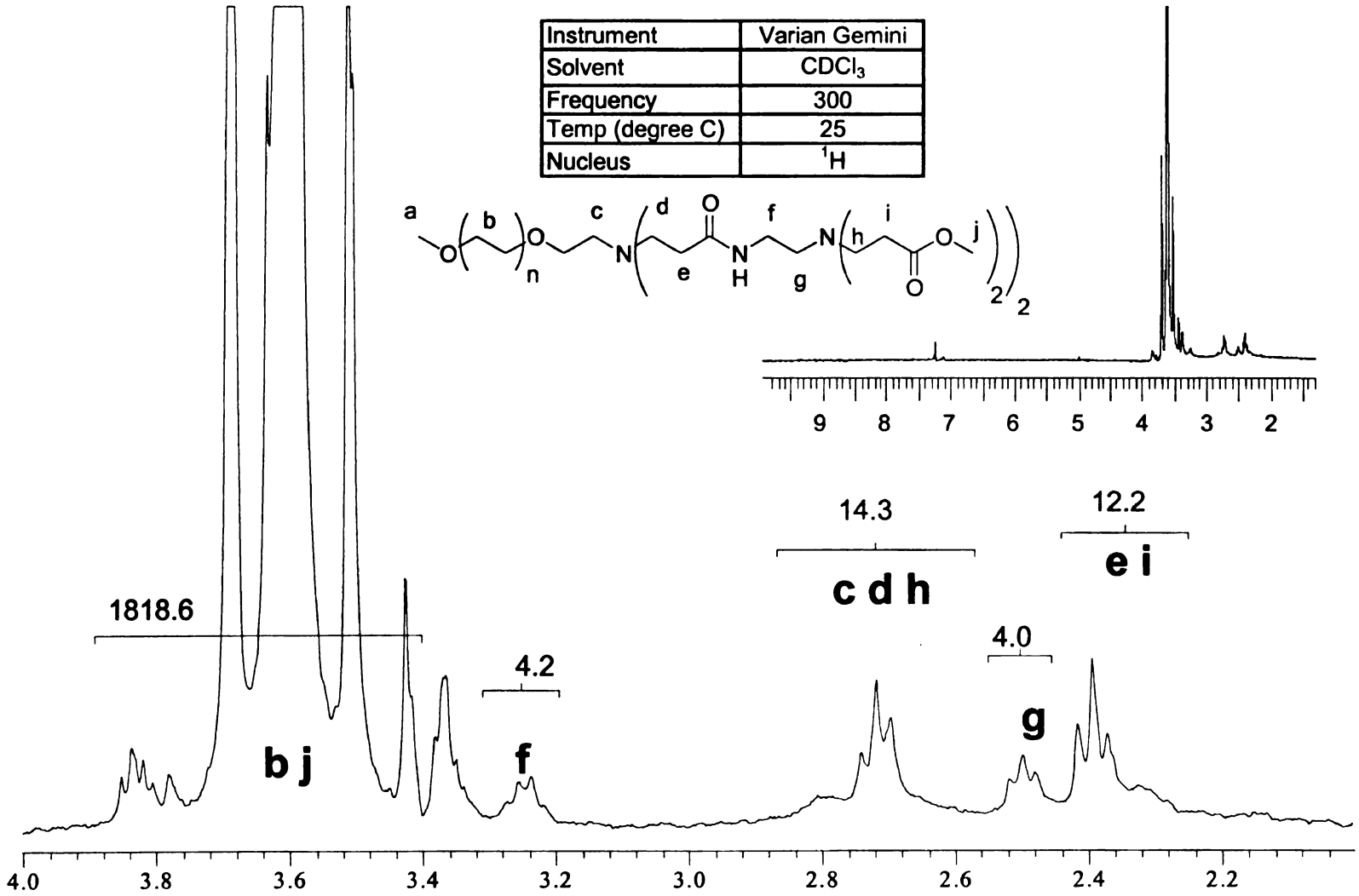

Figure C.48. ^{1}H NMR PEO 20 kDa G1.5

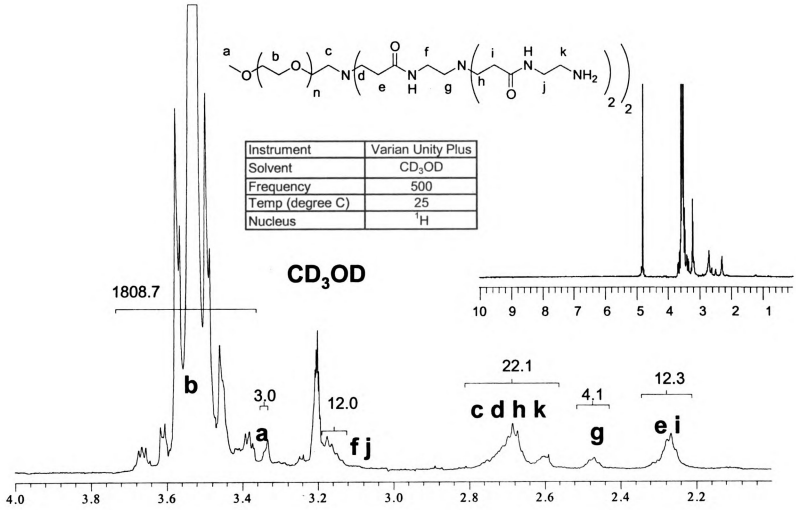

Figure C.49. ^{1}H NMR PEO 20 kDa G2.0

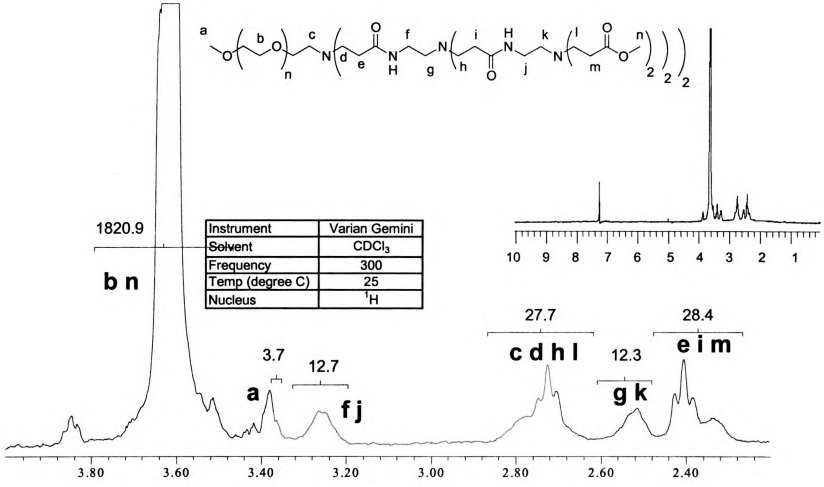

Figure C.50. ^{1}H NMR PEO 20 kDa G2.5

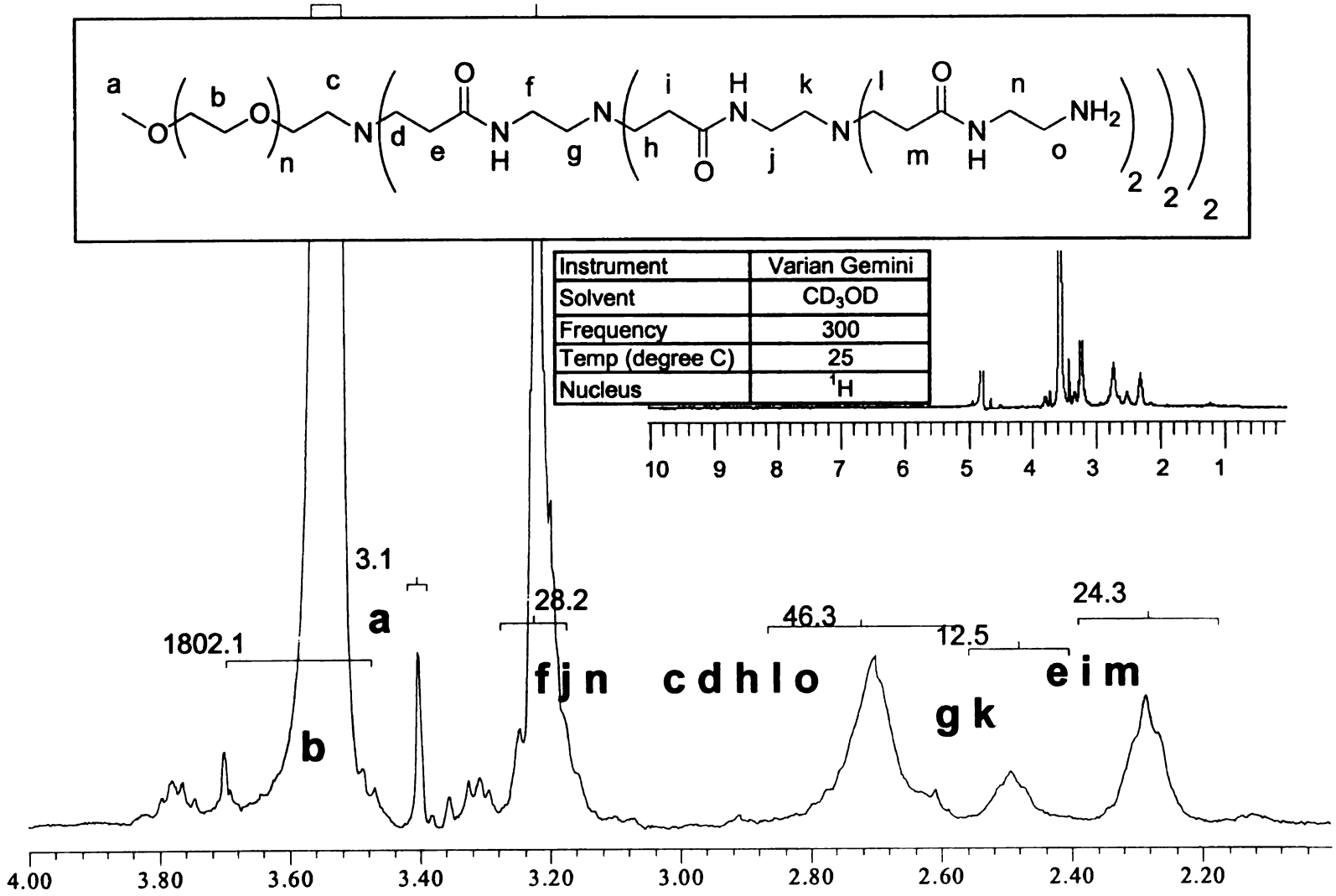

Figure C.51. ^{1}H NMR PEO 20 kDa G3.0

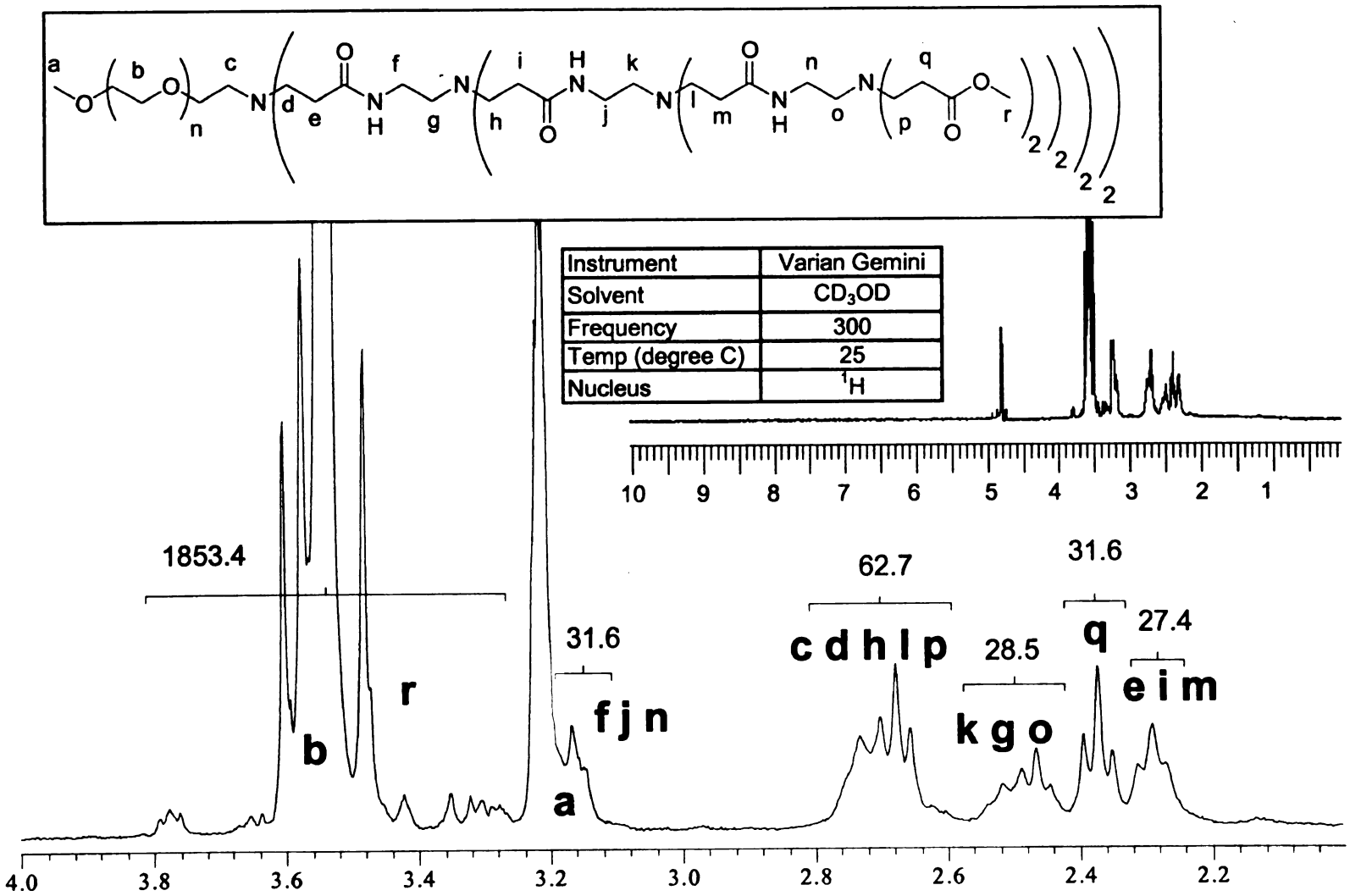

Figure C.52. ^{1}H NMR PEO 20 kDa G3.5

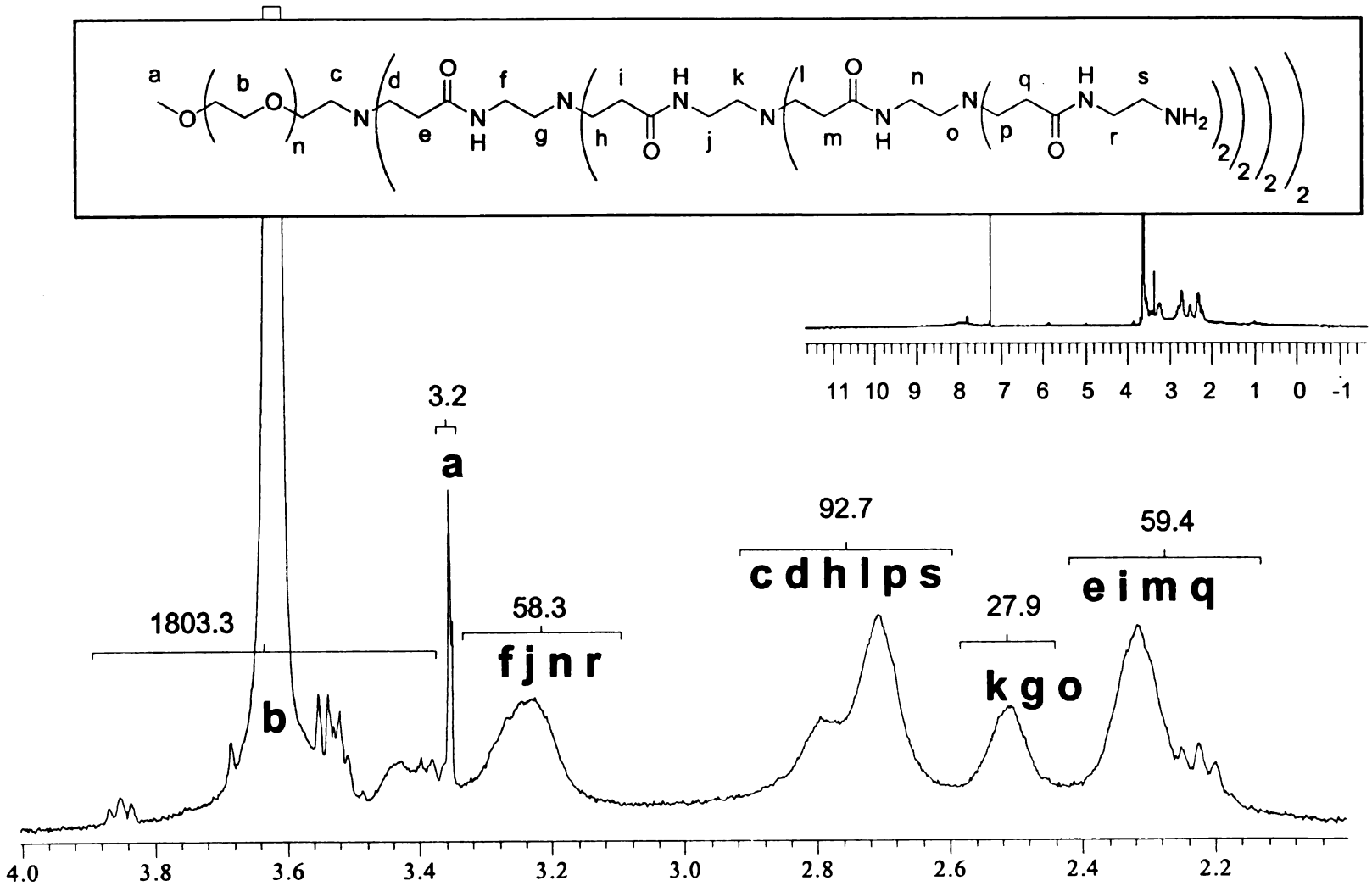

Figure C.53. ^{1}H NMR PEO 20 kDa G4.0

MICHIGAN STATE UNIVERSITY LIBRARIES
3 1293 02845 3433